PUBLICATIONS

A. Publications in peer-reviewed international journals from thesis work

1. **Madhubala, D.**, Patra, A., Islam, T., Saikia, K., Khan, M. R., Ahmed, S. A., ... & Mukherjee, A. K. (2023). Snake venom nerve growth factor-inspired designing of novel peptide therapeutics for the prevention of PT-induced apoptosis, neurodegeneration, and alteration of metabolic pathway genes in the rat pheochromocytoma PC-12 cell. **Free Radical Biology and Medicine** 197, 23-45. **IF- 8.101**
2. **Madhubala, D.**, Saikia, K., Patra, A., Mahato, R., Fernandes, P.A., Kumar, A., Khan, M. R., and Mukherjee, A. K. (2023). Snake venom-inspired novel peptides protect Caenorhabditis elegans against PT-induced Parkinson's pathology (**Revised Manuscript communicated**).
3. **Madhubala, D**., Patra, A., Khan, M. R., & Mukherjee, A. K. (2024). Phytomedicine for neurodegenerative diseases: The road ahead. Phytotherapy Research. **IF- 6.1**
4. **Madhubala, D**., Mahato, R., Khan, M. R., Bala, A., & Mukherjee, A. K. (2024). Neurotrophin peptidomimetics for the treatment of neurodegenerative diseases. Drug Discovery Today, 104156. **IF- 6.5**

B. Manuscript under preparation

Madhubala, D., Khan, M. R., Mukherjee, A. K. (2023). The snake-venom-inspired custom peptide (HNP) downregulates cel-miR-8207-3p and cel-miR-57-3p for neuroprotection against paraquat-induced toxicity in *C. elegans*.

C. Filed Indian Patent:

1. **Indian Patent** on "Neuritogenic Peptides and Neuroprotective Composition Comprising Such Peptides" Patent application no. 202231054298 (Under examination).

D. Presented at National and International conferences

1. **Madhubala, D.,** and Mukherjee, A. K. (2022) "Transcriptomic and functional proteomics analyses to unveil the common and unique pathway(s) of

neuritogenesis induced by Russell's viper venom nerve growth factor in rat pheochromocytoma neuronal cells" at the **national symposium on Snake and Scorpion Envenomation and Therapy: National and International Perspectives,** IASST, Guwahati, 16th July, 2022.

2. **Madhubala, D.,** Patra, A., and Mukherjee, A. K. (2022) "Reversal of PT-Induced Apoptosis, Neurodegeneration, and Alteration of Metabolic Pathway Genes in the Rat Pheochromocytoma PC-12 Cell by CPs Developed from the Nerve Growth Factors from Snake Venoms" at the **14th Annual Meeting of the Proteomics Society, India and International Conference on Proteins & Proteomics (PSI-ICPP 2022),** CSIR-Indian Institute of Chemical Biology, Kolkata, 03-05, November, 2022.
3. **Madhubala, D.,** Mahato., Rosy., Patra, A., and Mukherjee, A. K. (2024) **Two-day symposium on "From Venom Pharmacology to Drug Discovery: National and International Perspective (Snake-Symp-2024)** organized by IASST on 9th -10th Feb 2024.

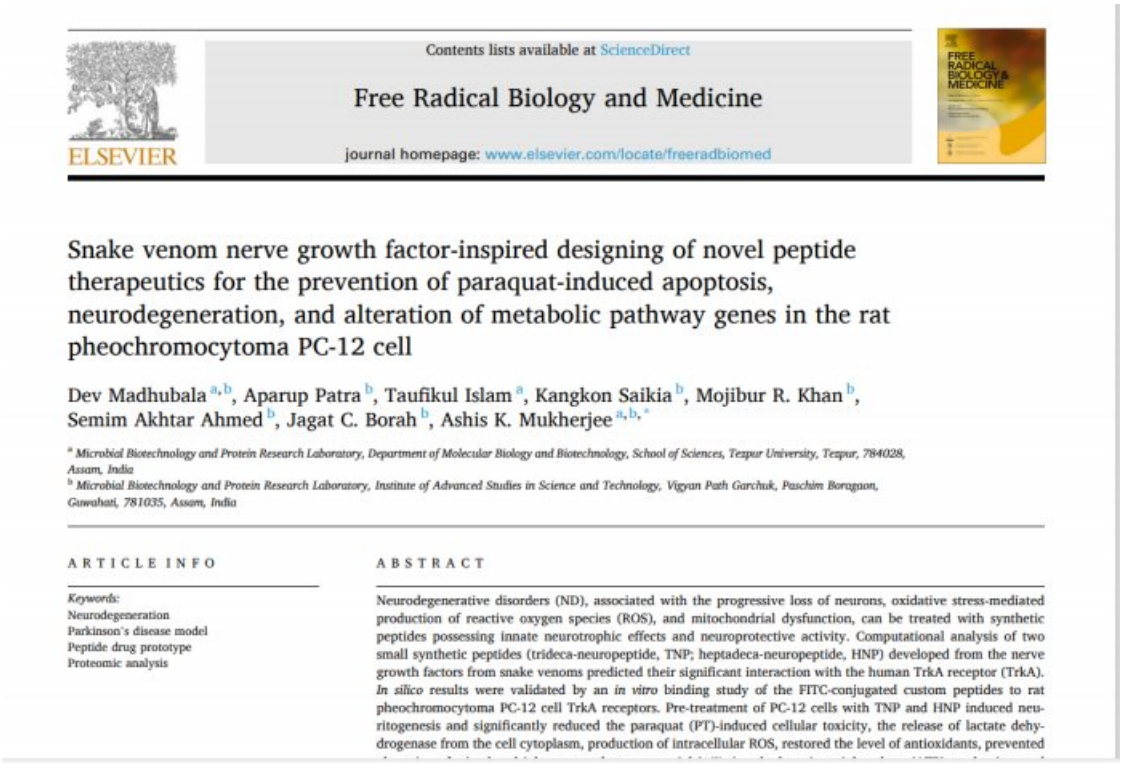

Contents lists available at ScienceDirect

Free Radical Biology and Medicine

journal homepage: www.elsevier.com/locate/freeradbiomed

Snake venom nerve growth factor-inspired designing of novel peptide therapeutics for the prevention of paraquat-induced apoptosis, neurodegeneration, and alteration of metabolic pathway genes in the rat pheochromocytoma PC-12 cell

Dev Madhubala [a,b], Aparup Patra [b], Taufikul Islam [a], Kangkon Saikia [b], Mojibur R. Khan [b], Semim Akhtar Ahmed [b], Jagat C. Borah [b], Ashis K. Mukherjee [a,b,*]

[a] Microbial Biotechnology and Protein Research Laboratory, Department of Molecular Biology and Biotechnology, School of Sciences, Tezpur University, Tezpur, 784028, Assam, India
[b] Microbial Biotechnology and Protein Research Laboratory, Institute of Advanced Studies in Science and Technology, Vigyan Path Garchuk, Paschim Boragaon, Guwahati, 781035, Assam, India

ARTICLE INFO

Keywords:
Neurodegeneration
Parkinson's disease model
Peptide drug prototype
Proteomic analysis

ABSTRACT

Neurodegenerative disorders (ND), associated with the progressive loss of neurons, oxidative stress-mediated production of reactive oxygen species (ROS), and mitochondrial dysfunction, can be treated with synthetic peptides possessing innate neurotrophic effects and neuroprotective activity. Computational analysis of two small synthetic peptides (trideca-neuropeptide, TNP; heptadeca-neuropeptide, HNP) developed from the nerve growth factors from snake venoms predicted their significant interaction with the human TrkA receptor (TrkA). *In silico* results were validated by an *in vitro* binding study of the FITC-conjugated custom peptides to rat pheochromocytoma PC-12 cell TrkA receptors. Pre-treatment of PC-12 cells with TNP and HNP induced neuritogenesis and significantly reduced the paraquat (PT)-induced cellular toxicity, the release of lactate dehydrogenase from the cell cytoplasm, production of intracellular ROS, restored the level of antioxidants, prevented

Received: 6 December 2023 | Revised: 14 February 2024 | Accepted: 10 March 2024
DOI: 10.1002/ptr.8192

REVIEW

WILEY

Phytomedicine for neurodegenerative diseases: The road ahead

Dev Madhubala[1,2] | Aparup Patra[2] | Mojibur R. Khan[2] | Ashis K. Mukherjee[1,2]

[1]Microbial Biotechnology and Protein Research Laboratory, Department of Molecular Biology and Biotechnology, Tezpur University, Tezpur, Assam, India
[2]Division of Life Sciences, Institute of Advanced Study in Science and Technology, Guwahati, Assam, India

Correspondence
Ashis K. Mukherjee, Division of Life Sciences, Institute of Advanced Study in Science and Technology, Vigyan Path, Garchuk, Paschim Boragaon, Guwahati, Assam, 781035, India.
Email: akm@tezu.ernet.in; ashmukh@yahoo.co.uk

Funding information
IASST; Science and Engineering Research Board, Grant/Award Number: EMR/2017/001829

Abstract

Neurodegenerative disorders (NDs) are among the most common causes of death across the globe. NDs are characterized by progressive damage to CNS neurons, leading to defects in specific brain functions such as memory, cognition, and movement. The most common NDs are Parkinson's, Alzheimer's, Huntington's, and amyotrophic lateral sclerosis (ALS). Despite extensive research, no therapeutics or medications against NDs have been proven to be effective. The current treatment of NDs involving symptom-based targeting of the disease pathogenesis has certain limitations, such as drug resistance, adverse side effects, poor blood–brain barrier permeability, and poor bioavailability of drugs. Some studies have shown that plant-derived natural compounds hold tremendous promise for treating and preventing NDs. Therefore, the primary objective of this review article is to critically analyze the properties and potency of some of the most studied phytomedicines, such as quercetin, curcumin, epigallocatechin gallate (EGCG), apigenin, and cannabinoids, and highlight their advantages and limitations for developing next-generation alternative treatments against NDs. Further extensive research on pre-clinical and clinical studies for developing plant-based drugs against NDs from bench to bedside

Drug Discovery Today • Volume 29, Number 11 • October 2024 REVIEWS

ELSEVIER

KEYNOTE (GREEN)

Neurotrophin peptidomimetics for the treatment of neurodegenerative diseases

Dev Madhubala[1,2,4], Rosy Mahato[2,3,4], Mojibur R. Khan[2,3], Asis Bala[2,3], Ashis K. Mukherjee[1,2,3,*]

[1] Microbial Biotechnology and Protein Research Laboratory, Department of Molecular Biology and Biotechnology, Tezpur University, Tezpur 784028, Assam, India
[2] Division of Life Sciences, Institute of Advanced Study in Science and Technology, Vigyan Path, Paschim Boragaon, Garchuk, Guwahati 781035, Assam, India
[3] Faculty of Science, Academy of Scientific and Innovative Research (AcSIR), Ghaziabad 201002, Uttar Pradesh, India

Dev Madhubala earned BSc (biotechnology) in 2015 from St. Xavier College, Ranchi University, Ranchi, India, and MSc (life science specialization in biochemistry) in 2017 from Central University of Punjab, Bathinda, Punjab, India. Currently she is enrolled in the PhD program in the Department of Molecular Biology and Biotechnology, at Tezpur University. Her research interest is snake venom nerve growth factor-derived peptide therapeutics in preventing neurodegenerative diseases.

Rosy Mahato earned BSc (zoology) in 2018 from Pragjyotish College, Gauhati University, Assam, India, and MSc (zoology specialization in entomology) in 2021 from Dakshin Kamrup College, Gauhati University, Assam, India. Currently, she is enrolled in the PhD program in Microbial Biotechnology and Protein Research Laboratory under Life Sciences

Neurotrophins, such as nerve growth factor and brain-derived neurotrophic factor, play an essential role in the

APPENDIX

Appendix Table A1 Comparison of the fold changes in differential expression of proteins in paraquat-treated *C. elegans* determined by proteomic analysis.

(a) List of upregulated proteins in paraquat-treated worms compared to untreated (control) worms and their downregulation in worms pre-treated with peptide HNP.				
Accession No	**Paraquat treatment (fold change in expression compared to control)**	**HNP pre-treatment (fold change in expression compared to control)**	**Pathway name**	**Description**
sp|P19974|CYC21_CAEEL	1.72	0.70	Apoptotic pathway	Cytochrome c 2.1 OS=*Caenorhabditis elegans* OX=6239 GN=cyc-2.1 PE=1 SV=2
G5EC98|G5EC98_CAEEL	1.62	0.60	De novo pyrimidine ribonucleotides biosynthesis	CTP synthase OS=*Caenorhabditis elegans* OX=6239 GN=ctps-1 PE=1 SV=1
sp|O17071|PRS10_CAEEL	1.39	0.98	Ubiquitin proteasome pathway	Probable 26S proteasome regulatory subunit 10B OS=*Caenorhabditis elegans* OX=6239 GN=rpt-4 PE=1 SV=2
sp|G5EEI4|ASP1_CAEEL	2.07	0.40	Programmed cell death	Aspartic protease 1 OS=*Caenorhabditis elegans* OX=6239 GN=asp-1 PE=1 SV=1
Q965Q1|Q965Q1_CAEEL	1.64	0.59	Stress response	10 kDa heat shock protein, mitochondrial OS=*Caenorhabditis elegans* OX=6239 GN=CELE_Y22D7AL.10 PE=1 SV=1
P34707 (SKN1_CAEEL)	1.29	0.75	Neuronal cell death/ MAPK pathway	Protein skinhead-1 OS=*Caenorhabditis elegans* OX=6239
O61667 (EGL1_CAEEL)	1.97	0.54	Programmed cell death	Programmed cell death activator egl-1 OS=*Caenorhabditis elegans* OX=6239
(b) List of downregulated proteins in paraquat-treated worms compared to untreated (control) worms and their upregulation in worms pre-treated with peptide HNP.				

Accession No.	**Paraquat treatment (fold change in expression compared to control)**	**HNP pre-treatment, (fold change in expression compared to control)**	**Pathway name**	**Description**
sp|P46561|ATPB_CAEEL	0.72	1.49	ATP synthesis	ATP synthase subunit beta, mitochondrial OS=*Caenorhabditis elegans* OX=6239 GN=atp-2 PE=1 SV=2
sp|Q18688|HSP90_CAEEL	0.76	1.93	Stress response pathway	Heat shock protein 90 OS=*Caenorhabditis elegans* OX=6239 GN=daf-21 PE=1 SV=1
Q23682 (GCY5_CAEEL)	0.70	1.73	Chemosensory pathway	Receptor-type guanylate cyclase gcy-5 OS=*Caenorhabditis elegans* OX=6239
A8XL75 (A8XL75_CAEBR)	0.75	2.93	Chemosensory pathway	Protein CBR-SRE-4 OS=*Caenorhabditis elegans* OX=6239
sp|P98080|UCR1_CAEEL	0.74	1.56	ATP synthesis	Cytochrome b-c1 complex subunit 1, mitochondrial OS=*Caenorhabditis elegans* OX=6239 GN=ucr-1 PE=3 SV=2
sp|P11141|HSP6_CAEEL	0.71	1.35	Stress response pathway	Heat shock protein hsp-6 OS=*Caenorhabditis elegans* OX=6239 GN=hsp-6 PE=1 SV=2
sp|Q05036|HS110_CAEEL	0.70	1.38	Stress response pathway	Heat shock protein 110 OS=*Caenorhabditis elegans* OX=6239 GN=hsp-110 PE=3 SV=1
sp|Q18115|PSMD1_CAEEL	0.78	1.54	Ubiquitin proteasome pathway	26S proteasome non-ATPase regulatory subunit 1 OS=*Caenorhabditis elegans* OX=6239 GN=rpn-2 PE=3 SV=4
O45445 (O45445_CAEEL)	0.78	2.0	Innate immune response	C-type lectin OS=*Caenorhabditis elegans* OX=6239
sp|P02513|HSP17_CAEEL	0.71	1.65	Stress response pathway	Heat shock protein Hsp-16.48/Hsp-16.49 OS=*Caenorhabditis elegans* OX=6239 GN=hsp-16.48 PE=2 SV=1
sp|P10299|GSTP1_CAEEL	1.19	1.36	Antioxidant pathway	Glutathione S-transferase P OS=*Caenorhabditis elegans* OX=6239 GN=gst-1 PE=1 SV=1

sp|Q09607|GST36_CAEEL	0.71	2.20	Antioxidant pathway	Probable glutathione S-transferase gst-36 OS=*Caenorhabditis elegans* OX=6239 GN=gst-36 PE=3 SV=2
sp|P34697|SODC_CAEEL	0.54	1.38	Antioxidant pathway	Superoxide dismutase [Cu-Zn] OS=*Caenorhabditis elegans* OX=6239 GN=sod-1 PE=1 SV=2
sp|P49632|RL40_CAEEL	0.52	1.40	Ubiquitin proteasome pathway	Ubiquitin-60S ribosomal protein L40 OS=*Caenorhabditis elegans* OX=6239 GN=ubq-2 PE=3 SV=2
Q21233|Q21233_CAEEL	0.62	1.44	Electron transport chain	NADH dehydrogenase [ubiquinone] 1 alpha subcomplex subunit 10, mitochondrial OS=*Caenorhabditis elegans* OX=6239 GN=nuo-4 PE=1 SV=1
Q17512|Q17512_CAEEL	0.76	1.65	Electron transport chain	NADH Ubiquinone oxidoreductase Fe-S protein OS=*Caenorhabditis elegans* OX=6239 GN=nduf-11 PE=1 SV=1
Q03561 (NLP36_CAEEL)	0.60	1.66	Neuronal development	Neuropeptide-like peptide 36 OS=*Caenorhabditis elegans* OX=6239
Q86NC2|Q86NC2_CAEEL	0.75	1.42	Electron transport chain	NADH dehydrogenase [ubiquinone] iron-sulfur protein 3, mitochondrial OS=*Caenorhabditis elegans* OX=6239 GN=nuo-2 PE=1 SV=1
Q93727 (SPTF1_CAEEL)	0.73	1.55	Neuronal differentiation	C2H2-type domain-containing protein OS=*Caenorhabditis elegans* OX=6239
Q93934|Q93934_CAEEL	0.79	1.65	Autophagy	Adenosine kinase OS=*Caenorhabditis elegans* OX=6239 GN=adk-1 PE=1 SV=1
Q9U329|Q9U329_CAEEL	0.74	1.65	Oxidative phosphorylation	Cytochrome c oxidase subunit 4 OS=*Caenorhabditis elegans* OX=6239 GN=cox-4 PE=1 SV=1

(c) List of commonly expressed proteins between paraquat-treated worms and peptide HNP pre-treatment worms		
Accession No	**Pathway name**	**Description**
Q966C7|Q966C7_CAEEL	Pentose phosphate pathway	Transaldolase OS=*Caenorhabditis elegans* OX=6239 GN=tald-1 PE=1 SV=1
sp|H2KYQ5|GYG1_CAEEL	Glycogen biosynthesis	Glycogenin-1 OS=*Caenorhabditis elegans* OX=6239 GN=gyg-1 PE=1 SV=1
sp|H2KYE0|NRA4_CAEEL	Neuronal development	Nicotinic receptor-associated protein 4 OS=*Caenorhabditis elegans* OX=6239 GN=nra-4 PE=1 SV=1
Q9N5S7|Q9N5S7_CAEEL	Antioxidant pathway	Thioredoxin Domain Containing protein homolog OS=*Caenorhabditis elegans* OX=6239 GN=txdc-12.2 PE=1 SV=1
sp|Q9N4X8|GSTPA_CAEEL	Antioxidant pathway	Glutathione S-transferase P 10 OS=*Caenorhabditis elegans* OX=6239 GN=gst-10 PE=1 SV=3
G5EC71|G5EC71_CAEEL	Antioxidant pathway	Glutathione S-Transferase OS=*Caenorhabditis elegans* OX=6239 GN=gst-20 PE=1 SV=1
Q09590|Q09590_CAEEL	Oxidoreductase	NADPH--cytochrome P450 reductase OS=*Caenorhabditis elegans* OX=6239 GN=emb-8 PE=1 SV=1
sp|Q11190|ETFD_CAEEL	Electron transport chain	Electron transfer flavoprotein-ubiquinone oxidoreductase, mitochondrial OS=*Caenorhabditis elegans* OX=6239 GN=let-721 PE=3 SV=2
sp|G5ECU1|SKR1_CAEEL	Neurogenesis	Skp1-related protein OS=*Caenorhabditis elegans* OX=6239 GN=skr-1 PE=1 SV=1

Appendix Table A2 Predicted downstream targets of miRNA in PNGF and PHNP group of *C. elegans*

Downstream mRNA targets of miRNAs in PNGF and PHNP group of *C.elegans*	**Panther protein class**
ZK688	Ion channel
K10D3	Transmembrane signal receptor
fust-1	RNA metabolism protein
F52F10	Acyltransferase
F09B12	Apolipoprotein
C48E7	DNA-directed RNA polymerase
ZK688	Glycosyltransferase
F44E5	Hsp70 family chaperone
K07H8	RNA splicing factor
camt-1	DNA-binding transcription factor
T24H10	Chaperone
T06D8	Peroxidase
F54D1	Ion channel
F35G2	Hydrolase
F01G4	DNA helicase
F21D5	Mutase
W03C9	Small gtpase
C08G9	Protease inhibitor
F41C3	Lipase
C52E4	RNA processing factor

C48E7	Basic leucine zipper transcription factor
B0336	G-protein
C06E7	G-protein coupled receptor
Y71F9AL	Isomerase
F42A10	Metalloprotease
Y74C9A	Methyltransferase
F59F4	Oxidoreductase
F42A10	Methyltransferase
C48E7	Ion channel
C16A3	Oxidoreductase
T26A5	Oxidoreductase
T27F7	Glycosyltransferase
Y71F9AL	Protein phosphatase
B0303	Methyltransferase
F26B1	Transporter
C06A8	Transmembrane signal receptor
T22B11	Transferase
R12E2	Scaffold/adaptor protein
ndk-1	Kinase
F33G12	Membrane traffic protein
K10D3	General transcription factor
R151	Hsp90 family chaperone
C06E1	Transmembrane signal receptor

paqr-1	G-protein coupled receptor
B0336	Scaffold/adaptor protein
C06E1	Oxidase
F42A10	Translation elongation factor
B0393	Ribosomal protein
C25F6	Dehydrogenase
F26B1	Transmembrane signal receptor
sqv-7	Secondary carrier transporter
C16A3	Transcription cofactor
C03C10	Reductase
C53A3	Phosphatase
C06E1	Transferase
T23G7	RNA metabolism protein
F21F3	Protein modifying enzyme
C05C10	Phosphatase
T10B10	Glycosyltransferase
C52E4	Cysteine protease
C16A3	Zinc finger transcription factor
R107	Intercellular signal molecule
hpo-8	Dehydratase
ZK686	C2H2 zinc finger transcription factor
C15H9	G-protein coupled receptor
F58H1	Glycosidase

C03C10	Non-receptor serine/threonine protein kinase
K11H3	Ion channel
C34F6	Ubiquitin-protein ligase
C05D11	Oxidoreductase
F29B9	Ubiquitin-protein ligase
B0252	Transmembrane signal receptor
R12E2	Transferase
F09B12	Phospholipase
nstp-2	Secondary carrier transporter
pkg-2	Non-receptor serine/threonine protein kinase
R151	DNA metabolism protein
AH9	Exoribonuclease
F40E10	Calcium-binding protein
F59F4	Chaperone
C18E9	Primary active transporter
F28H6	Transaminase
W06H8	G-protein coupled receptor
R12E2	Structural protein
C56G2	Non-receptor serine/threonine protein kinase
F41C3	Ligase
C06E1	C2H2 zinc finger transcription factor
F21C10	Structural protein
C33A11	Scaffold/adaptor protein

C25F6	Non-receptor tyrosine-protein kinase
B0336	Ribosomal protein
D1081	Small GTPase
C03C10	Non-receptor serine/threonine protein kinase
C18E9	Extracellular matrix protein
ZK686	Glycosyltransferase
C16A3	Ribosomal protein
F35G2	Protein modifying enzyme
F22D3	Cysteine protease
ZK686	RNA helicase
Y71F9AL	DNA metabolism protein
F46G10	Basic helix-loop-helix transcription factor
F55A11	Acyltransferase
F26A3	RNA metabolism protein
F26A3	Lipase
C34F6	Transferase
T06D8	Lyase
K11H3	Transporter
R107	Dehydratase
guk-1	Kinase
C28H8	Microtubule binding motor protein
F58H1	Peptide hormone
T05G5	Non-receptor serine/threonine protein kinase

B0393	Gtpase-activating protein
F42H10	Esterase
erfa-3	Translation factor
ZK470	Transporter
C05D11	Protein-binding activity modulator
C15H9	G-protein coupled receptor
T10B10	Metalloprotease
C03C10	Scaffold/adaptor protein
sams-3	Nucleotidyltransferase
C16A3	RNA metabolism protein
F28H6	Actin or actin-binding cytoskeletal protein
C28H8	RNA helicase
R05D3	Oxidoreductase
R12E2	Gap junction
T05H10	Endodeoxyribonuclease
ZK686	RNA processing factor
C37H5	Hsp70 family chaperone
C16A3	Protein phosphatase
K07B1	Oxygenase
R05D3	Histone modifying enzyme
F21F3	Oxygenase
B0303	Ribosomal protein
T23G7	DNA-binding transcription factor

K11H3	Ribosomal protein
dmsr-7	Transmembrane signal receptor
Y71F9AL	Actin and actin related protein
F01G4	DNA metabolism protein
mvk-1	Carbohydrate kinase
nkb-3	Primary active transporter
C06A8	Ubiquitin-protein ligase
F13H6	Hydrolase
C05D11	Isomerase
C05C10	Phosphatase
R06C1	Histone modifying enzyme
R107	Transferase
R12E2	Ribosomal protein
F22H10	Non-receptor serine/threonine protein kinase
acp-6	Phosphatase
F56D2	Scaffold/adaptor protein
F37B12	Ligase
B0041	Ribosomal protein
K08D12	Protease
B0393	Extracellular matrix structural protein
R12E2	Gap junction
C56G2	Protease inhibitor
Y71F9AL	Non-receptor serine/threonine protein kinase

R12E2	Translation initiation factor
F36D4	Membrane traffic protein
C14C10	Mitochondrial carrier protein
T26A5	DNA metabolism protein
F26A3	Ion channel
K08D12	Gtpase-activating protein
T10B10	Membrane trafficking regulatory protein
F47D12	Scaffold/adaptor protein
F21F3	Transporter
kcnl-2	Voltage-gated ion channel
C05D11	Ribosomal protein
egg-6	Scaffold/adaptor protein
C15H9	Dehydrogenase
asns-2	Ligase
F55A11	SNARE protein
T12G3	Ribosomal protein
F10D7	Oxidoreductase
F02A9	Ligase
K03A11	Homeodomain transcription factor
acs-22	Secondary carrier transporter
T13C2	Protein phosphatase
C15H9	Hydrolase
T06D8	Chaperone

C34F6	Dehydrogenase
F21D5	Endoribonuclease
ZC190	Membrane trafficking regulatory protein
idhb-1	Dehydrogenase
T28D9	Ion channel
K07B1	Secondary carrier transporter
ZK484	Phosphatase
Y71F9AL	RNA methyltransferase
Y74C9A	Peroxidase
R151	Ribosomal protein
AH9	G-protein coupled receptor
C05D11	Membrane traffic protein
F10D7	Secondary carrier transporter
C28H8	Membrane trafficking regulatory protein
R151	Primary active transporter
D1081	Small gtpase
F10D7	G-protein coupled receptor
R148	Structural protein
C48E7	Structural protein
C29H12	Non-receptor serine/threonine protein kinase
T05H10	Cysteine protease
K07H8	Chaperone
F59F4	Acyltransferase

Y71F9AL	Microtubule binding motor protein
B0303	Acyltransferase
K07H8	Acetyltransferase
C56G2	RNA methyltransferase
F21C10	Transmembrane signal receptor
C46C11	Cytoskeletal protein
R05D3	ATP synthase
C48E7	Acyltransferase
C10E2	Transporter
C56G2	Transferase
C05C10	Transferase
ZK484	Protein phosphatase
ZC395.10	Chaperone
F13H6	Transmembrane signal receptor
R12E2	Protein phosphatase
C16A3	RNA metabolism protein
C29H12	Aminoacyl-trna synthetase
T06D8	Protease
F21D5	Ribosomal protein
T24H10	General transcription factor
B0303	Membrane trafficking regulatory protein
F29B9	Oxidoreductase
R05D3	RNA processing factor

K02E10	Non-receptor serine/threonine protein kinase
C48E7	RNA metabolism protein
R151	Chaperone
F55A11	Ubiquitin-protein ligase
F56D2	Ubiquitin-protein ligase
ZK688	Hydrolase
C52E4	Protease
F26B1	Winged helix/forkhead transcription factor
AH9	G-protein coupled receptor
Y71F9AL	Vesicle coat protein
T26A5	Glycosyltransferase
F54D1	RNA splicing factor
F56D2	Ubiquitin-protein ligase
F40E10	HMG box transcription factor
R05D3	Microtubule binding motor protein
C06E1	RNA helicase
F02A9	Endoribonuclease
F22F7	Transferase
T26A5	Microtubule or microtubule-binding cytoskeletal protein
F29B9	Protein modifying enzyme
F40E10	Metalloprotease
C05D11	Metalloprotease

F55A11	Membrane traffic protein
T27F7	Membrane traffic protein
F09B12	Non-receptor serine/threonine protein kinase
C34F6	Cysteine protease
T05G5	Hydratase
T05G5	Basic helix-loop-helix transcription factor
F41D9	Transporter
B0393	Apolipoprotein
T10B10	Ion channel
R04E5	Ion channel
F29B9	Ribosomal protein
F09B12	Protein modifying enzyme
T24H10	Microtubule or microtubule-binding cytoskeletal protein
T24B8	Basic helix-loop-helix transcription factor
T24B8	Membrane traffic protein
C18E9	Oxidoreductase
sqv-5	Glycosyltransferase
T26A5	ATP-binding cassette (ABC) transporter
F21D5	RNA metabolism protein
W06H8	Oxidoreductase
C05D11	Growth factor

F26F12	Chromatin/chromatin-binding, or -regulatory protein
B0252	Phosphodiesteras
F21F3	Ligand-gated ion channel
C05D11	Endoribonuclease
C06A8	Scaffold/adaptor protein
R151	Phosphatase
F41D9	Gtpase-activating protein
R05D3	Transmembrane signal receptor
ZC449	Dehydratase
R06C1	Acyltransferase
F26B1	Protein phosphatase
T06D8	Phosphatase
F21C10	Transmembrane signal receptor
F56D2	Ubiquitin-protein ligase
F46G10	Histone modifying enzyme
F41C3	Serine protease
C18E9	Calmodulin-related
F21F3	Non-receptor serine/threonine protein kinase
F40E10	Transporter
B0336	General transcription factor

Contents lists available at ScienceDirect

Free Radical Biology and Medicine

journal homepage: www.elsevier.com/locate/freeradbiomed

Snake venom nerve growth factor-inspired designing of novel peptide therapeutics for the prevention of paraquat-induced apoptosis, neurodegeneration, and alteration of metabolic pathway genes in the rat pheochromocytoma PC-12 cell

Dev Madhubala [a,b], Aparup Patra [b], Taufikul Islam [a], Kangkon Saikia [b], Mojibur R. Khan [b], Semim Akhtar Ahmed [b], Jagat C. Borah [b], Ashis K. Mukherjee [a,b,*]

[a] *Microbial Biotechnology and Protein Research Laboratory, Department of Molecular Biology and Biotechnology, School of Sciences, Tezpur University, Tezpur, 784028, Assam, India*

[b] *Microbial Biotechnology and Protein Research Laboratory, Institute of Advanced Studies in Science and Technology, Vigyan Path Garchuk, Paschim Boragaon, Guwahati, 781035, Assam, India*

ARTICLE INFO

Keywords:
Neurodegeneration
Parkinson's disease model
Peptide drug prototype
Proteomic analysis

ABSTRACT

Neurodegenerative disorders (ND), associated with the progressive loss of neurons, oxidative stress-mediated production of reactive oxygen species (ROS), and mitochondrial dysfunction, can be treated with synthetic peptides possessing innate neurotrophic effects and neuroprotective activity. Computational analysis of two small synthetic peptides (trideca-neuropeptide, TNP; heptadeca-neuropeptide, HNP) developed from the nerve growth factors from snake venoms predicted their significant interaction with the human TrkA receptor (TrkA). *In silico* results were validated by an *in vitro* binding study of the FITC-conjugated custom peptides to rat pheochromocytoma PC-12 cell TrkA receptors. Pre-treatment of PC-12 cells with TNP and HNP induced neuritogenesis and significantly reduced the paraquat (PT)-induced cellular toxicity, the release of lactate dehydrogenase from the cell cytoplasm, production of intracellular ROS, restored the level of antioxidants, prevented alteration of mitochondrial transmembrane potential ($\Delta\Psi m$) and adenosine triphosphate (ATP) production, and inhibited cellular apoptosis. These peptides lack *in vitro* cytotoxicity, haemolytic activity, and platelet-modulating properties and do not interfere with the blood coagulation system. Functional proteomic analyses demonstrated the reversal of PT-induced upregulated and downregulated metabolic pathway genes in PC-12 cells that were pre-treated with HNP and revealed the metabolic pathways regulated by HNP to induce neuritogenesis and confer protection against PT-induced neuronal damage in PC-12. The quantitative RT-PCR analysis confirmed that the PT-induced increased and decreased expression of critical pro-apoptotic and anti-apoptotic genes had been restored in the PC-12 cells pre-treated with the custom peptides. A network gene expression profile was proposed to elucidate the molecular interactions among the regulatory proteins for HNP to salvage the PT-induced damage. Taken together, our results show how the peptides can rescue PT-induced oxidative stress, mitochondrial dysfunction, and cellular death and suggest new opportunities for developing neuroprotective drugs.

1. Introduction

Neurodegeneration, an age-related disorder, occurs as a progressive loss of neurons or from the neuronal failure to transmit signals [1]. Parkinson's disease (PD) is the second most common neurodegenerative disorder after Alzheimer's disease (AD) [2,3]. PD is characterized by α-synuclein aggregation and progressive dopaminergic (DAergic) neuronal degeneration in the substantia nigra leading to impaired motor control, rigidity, tremors, postural instability, and slow movement of the patient [4–6]. Studies have reported that in the nigrostriatal system, axons become damaged before the degeneration of dopaminergic neurons, which results in the loss of synaptic communications [7]. Although PD is primarily an age-related neurological disorder, it is often

* Corresponding author. Institute of Advanced Studies in Science and Technology, Vigyan Path Garchuk, Paschim Boragaon, Guwahati, 781035, Assam, India.
E-mail address: akm@tezu.ernet.in (A.K. Mukherjee).

https://doi.org/10.1016/j.freeradbiomed.2023.01.019
Received 27 October 2022; Received in revised form 3 January 2023; Accepted 16 January 2023

Abbreviations

AD	Alzheimer's disease
ANOVA	one-way analysis of variance
ATCC	American Type Culture Collection
ATP	adenosine triphosphate
BBB	blood-brain barrier
CD	circular dichroism
CID	collision-induced dissociation
DAPI	4′,6-diamidino-2-phenylindole
DCF	2′,7′-dichlorodihydrofluorescein
DMEM	Dulbecco's Modified Eagle Medium
DMSO	dimethyl sulfoxide
DTT	dithiothreitol
ESI	electrospray ionization
FBS	fetal bovine serum
FITC	fluorescein isothiocyanate
H2DCFDA	2′,7′-dichlorofluorescein-diacetate
HD	Huntington's disease
HNP	heptadeca-neuropeptide
L6	rat myoblast or myogenic cells
LDH	lactate dehydrogenase
MAPK	mitogen-activated protein kinase
MDA-MB-231	human breast adenocarcinoma cells
MCF-7	Michigan Cancer Foundation-7
MEM	Eagle's Minimum Essential Medium
MM-GBSA	molecular mechanics/generalized born surface area
MMP	mitochondrial membrane potential
MTT	3-(4,5-Dimethylthiazol-2-yl)-2,5-diphenyltetrazolium bromide
NCCS	National Centre for Cell Science
ND	Neurodegenerative disorders
NGF	nerve growth factor
p75NTR	p75 neurotrophin receptor
PBS	phosphate buffered saline
PC-12	adrenal pheochromocytoma cell line
PD	Parkinson's disease
PDB	Protein Data Bank
PI	propidium iodide
PI3K/Akt	phosphatidylinositol 3-kinase stimulation of protein kinase B signaling pathways
PPI	protein-protein interaction
PPP	platelet-poor plasma
PRP	platelet-rich plasma
PT	paraquat
qRT-PCR	quantitative reverse transcription-polymerase chain reaction
RESPA	reversible reference system propagator algorithms
RMSD	root mean square deviation
ROS	reactive oxygen species
RT	rotenone
SD	standard deviation
SV NGF	snake venom nerve growth factor
TIP3P	three-points water model
TNP	trideca-neuropeptide
TrkA	tropomyosin receptor kinase A receptor
UHPLC-MS/MS	ultra-performance liquid chromatography-tandem mass spectrometer

associated with exposure to toxic components of pesticides such as paraquat (PT) and rotenone (RT) that affect the mitochondrial respiratory chain and cause mitochondrial membrane depolarization, with an increase in oxidative stress and subsequent cell death [8–10]. Consequently, PT has been used extensively to induce PD in model organisms to investigate the *in vivo* mechanism of PT-induced neurodegeneration and the possible prevention by the therapeutic agents [11–14].

The effective treatment against PD is administration of levodopa (a dopamine precursor), which is enzymatically catalyzed to active dopamine in the brain by dopamine carboxylase [15]. Further, prolonged use of dopamine agonists like pramipexole (Mirapex), rotigotine (Neupro), and ropinirole (Requip) [15], tends to reduce their efficacy and lead to several adverse effects [6,16]. Thus, an urgent need exists to discover alternative drugs that can improve the management and prevention of PD [16].

Neurotrophins, a group of endogenous soluble proteins, are defined as growth factors that profoundly influence the development of the nervous system of vertebrates. In 1954, nerve growth factor (NGF) was discovered in mouse sarcomas 180 and 37 as a neurotrophic factor important for survival and maintenance of the nervous system [17,18]. Subsequently, several studies highlighted the functional importance of NGFs purified from diverse sources including snake venom [19–21]. To elicit neuritogenesis, NGF binds to two common NGF receptors, the p75 neurotrophin receptor (p^{75NTR}) and the tropomyosin receptor kinase A (TrkA) receptor [20–22], with low affinity (Kd = 10^{-9} M) and medium to high affinity (Kd = 10^{-10} M to 10^{-11} M), respectively [23,24]. Binding of neurotrophins to Trk receptor generates its dimerization followed by auto phosphorylation of intracellular tyrosine residues guiding to the activation of cascades of events through two adaptor proteins viz. Src and Shc. The cellular signaling pathways activates the Ras-induced mitogen-activated protein kinase (MAPK) pathway, phosphatidyl inositol 3-kinase (PI3K) stimulation of protein kinase B (Akt), and phospholipase Cγ(PLCγ)-dependent production of inositol 1,4,5-triphosphate (IP3), and diacylglycerol (DAG) [25,26]. The p^{75NTR} emerges to be the principal component in mediating the pro-neurotrophin signalling (converting precursors to mature neurotrophins) and also an antagonistic mode to Trk receptor [27]. The neurotrophins and Trk interaction results in cell survival, whereas the interaction of p^{75NTR} with neurotrophins precursor leads to cell death by apoptosis [28].

Due to the prominent role of neurotrophin NGF in neuronal development, the systemic administration of such exogenous molecules has been proposed as treatment for various neurodegenerative diseases such as AD and PD [29–31]. Nevertheless, despite its high therapeutic potential, the therapeutic application of native NGF is limited by its poor pharmacological properties, marginal permeability across the blood-brain barrier (BBB), short half-life, activation of multiple receptors, and pleiotropic effects [25,32,33]. The search for small NGF-like molecules that can overcome such limitations is underway.

Snake venoms are a mixture of peptides and proteins with various biological and therapeutic roles [34,35]. NGF, a low molecular mass (17–20 kDa for glycosylated NGF and 7–13 kDa for non-glycosylated NGF) non-enzymatic protein present in snake venom in a comparatively low proportion, has been isolated and characterized [20,21,36,37]. Apart from the conventional NGF, the non-conventional NGF from Indian cobra (*Naja naja*) venom has also been characterized [21]. The conventional and non-conventional snake venom NGFs (SV NGF) that target neurotrophin TrkA receptors [20,21,38] might be clinically applied as a drug prototype in treating neurodegeneration, including PD [39]. Their structural stability, small size, and target sensitivity make them powerful tools to conquer the limitations in using endogenous neurotrophins as therapeutic agents [20,21,39]. Furthermore, the non-enzymatic proteins of SV origin might be improved to elevate resistance to enzymatic degradation, potency, bioavailability, and permeability to the BBB [33,39–41]. Nevertheless, purification of NGFs from snake venom is a costly and tedious job and the scarcity of venom is

another hurdle to purifying a sufficient quantity of NGF. Therefore, we hypothesize that synthetic custom peptides derived from the TrkA receptor binding region of the SV NGFs [20,21,38] might also induce the same neurotrophic effect as their parent molecules and might act as bioactive drugs.

By computational analysis, we designed two custom peptides inspired from snake venom neurotrophin molecules [20,21,38]. The neurotrophic potency of the synthetic peptides was assessed in a rat pheochromocytoma cell line (PC-12), and we determined their therapeutic potency to inhibit PT-induced toxicity, involving oxidative stress, mitochondrial dysfunction, and apoptotic cell death. We advocate those future therapeutic applications of these peptides for preventing and treating neurological disorders such as PD and AD holds good promise.

2. Materials and methods

2.1. Materials and reagents

Custom peptides trideca-neuropeptide (TNP) and heptadeca-neuropeptide (HNP) and fluorescein isothiocyanate (FITC)-conjugated peptides were synthesized by S Biochem, Thrissur, Kerala, India. Mouse 2.5-S-nerve growth factor (NGF) was obtained from Sigma Aldrich, USA (N6009), USA. Dulbecco's Modified Eagle Medium (DMEM), Eagle's Minimum Essential Medium (MEM), trypsin, and heat-inactivated fetal bovine serum (FBS) was purchased from Gibco™ (USA). The rat adrenal phaeochromocytoma (PC-12) cell line (initial passage number 8) (CRL-1721™) was procured from the American Type Culture Collection (ATCC), USA. Rat myoblast or myogenic cells (L6) (initial passage number 18), human breast adenocarcinoma cells (MDA-MB-231) (initial passage number 16), and Michigan Cancer Foundation-7 (MCF7) cells were obtained from the National Centre for Cell Science (NCCS), Pune, India. The specification sheets provided by NCCS and ATCC stated the authenticity for the microbial contamination-free cell lines that we procured from them. During the experimental plan, each cell line was subjected to 5–6 or more passages. All chemicals were of analytical grade from Sigma, Merck, HiMedia, Invitrogen, and Thermo Fisher Scientific USA. The Annexin V-FITC/propidium iodide (PI) apoptosis detection kit (CST, 6592) and *anti*-TrkA antibodies were procured from Cell Signaling Technology, USA (CST, 2505S), and the MitoProbeTM JC-1 assay kit (Catalog No.M34152), and the CyQUANT™ LDH cytotoxicity assay kit (Catalog No. C20300) was purchased from Invitrogen, USA.

2.2. Predicting the binding affinity of synthetic peptides to different domains of human TrkA receptors by in silico analysis

The cheminformatic parameters such as mass, isoelectric point, net charge, hydrophobicity, etc. of the peptides were computed using the PepDraw server [42]. The peptide sequences were converted to PDB structures, and their dynamics and conformations were studied using molecular dynamic simulations for 100 ns. Simulations were carried out in GROMACS v2022.2 with the CHARMM36 (v 2021) force field. The periodic boundary was set as a dodecahedron with a 1.5 Å buffer region. Peptide structures were first minimized in a vacuum using 5000 steps of the steepest descent algorithm. The system was solvated using the transferable intermolecular potential with a three-points water model (TIP3P), and 0.15 M sodium chloride ions were added till neutralized. The system was equilibrated using NVT (canonical) and NPT (isobaric-isothermal) ensembles in 300 K and 1.0133 bar. Temperature coupling was done using the v-rescale (Berendsen) method and pressure coupling was done using c-rescale [43] and integrated using a leap frog algorithm. Before the production MD run, the position restraints were released following three NPT equilibration runs. The trajectory was studied for root mean square deviation (RMSD), radius of gyration, hydrogen bonding, secondary structure of the peptides, and thermodynamic properties. From the trajectory frames, an average structure of the peptide was derived in a PDB format and used in the subsequent analysis.

A molecular docking study was conducted to predict the binding affinity of custom peptides with the TrkA receptor. Crystal structures of human TrkA (UniProtKB - P04629) domains were obtained from Protein Data Bank (PDB) with entry viz. 2IFG (extracellular domain), and 5JFX (cytoplasmic domain). The structures were prepared using the protein preparation wizard of the Schrodinger suite (Schrodinger Inc. USA). Briefly, water and hetero atoms were removed, and missing residues and side chains were filled and corrected for alternate positions of the residues. The docking was carried out using a peptide dock module with the molecular mechanics/generalized born surface area (MM-GBSA) scoring method. The receptor grid was generated from centroid residues so that the grid box could occupy the whole protein domain and the peptide sequences were then added individually to output the ten best poses for each domain.

Molecular dynamic simulations were carried out using Schrodinger Desmond (Academic version, v.2022). The simulation system was comprised of the docked peptide complex, solvent, and salts. The TIP3P water model was used as a solvent within an orthorhombic boundary condition with a 10 Å buffer region. NaCl (0.15 M) was added to the system, which was neutralized using the required number of Na^+ or Cl^- ions. The system was equilibrated with NVT and NPT ensembles at 300 K and 1 bar. The reversible reference system propagator algorithms (RESPA) were used as an integrator (at 2 fs time-steps) of Newtonian dynamics with a column cut-off radius of 1.5 Å. A Nose Hoover chain thermostat and Martyna Tobias Klein barostat were used with isotropic coupling at 1 ps and 2 ps relaxation times. Relaxation of the system was done using the default, which provided a relaxation protocol followed by a production MD run for 300 ns. The energy and trajectory were recorded at every 0.5 ps and analyzed using the simulation interaction diagram module of Schrodinger Maestro. The binding free energies of the simulation trajectory complexes were calculated using the MM-GBSA method.

2.3. Solid-phase synthesis and biophysical characterization of the custom peptides

The solid-phase peptide synthesis was done using Fmoc protocols for the esterification of amino acid to the wang resin followed by a coupling reaction [39]. The peptide was then detached from the resin and isolated using cold diethyl ether. The purity and molecular mass of the peptides were ascertained by mass spectrometry analysis in a single quadrupole mass spectrometer (Shimadzu LC-MS 2020, Japan) via positive electrospray ionization (ESI). The biophysical properties of the peptides were then calculated in an online peptide property calculator (https://pepcalc.com/). The secondary structures of the peptides were also determined by circular dichroism (CD) spectroscopy (Jasco J715 spectropolarimeter, Japan) following our previously described procedure [44]. CDPRO CLUSTER software was used to determine the secondary structures of the peptides.

2.4. Cell growth and maintenance

Mammalian cells, viz. PC-12, L6, and MDA-MB-231 were grown and maintained with a complete medium comprising of DMEM containing 1% antibiotic solution (GIBCO™) and 10% heat-inactivated FBS (GIBCO™) and in 75 cm^2 tissue culture flasks at 37 °C in a humidified incubator with 5% CO_2. MCF-7 cells were maintained in MEM containing 10% FBS and 0.01 mg/mL insulin. The cells were re-suspended in medium every 2–3 days and sub-cultured after reaching confluence [20,21,38].

2.5. Assessing the binding of FITC-conjugated custom peptides to TrkA receptor-expressing mammalian cells

Custom peptides were synthesized by S Biochem, Thrissur, Kerala,

India following the previously described protocol with slight modifications [20]. Briefly, fresh FITC reagent was prepared (1 mg/mL) in DMSO, was added to the resin, and incubated in the dark for 2 h at 4 °C. The resin was washed with dimethylformide; then standard peptide cleavage protocol was performed. Spectrofluorometric interactions between the FITC-conjugated peptide and TrkA receptors were determined in mammalian cells expressing TrkA receptors, such as PC-12, MCF7, and MDA-MB-231 cells, and in non-TrkA receptor-expressing L6 cells (negative control) following the procedures that were previously described [20,21,38]. The PC-12, MCF7, MDA-MB-231, and L6 cells (1×10^4 cells per well in 96-well plates) were incubated with the FITC-conjugated peptides (2 μg/mL) at different time intervals (from 0 to 360 min) at 37 °C in a humidified incubator with 5% CO_2 (in triplicates). Cells were washed with 1X phosphate buffered saline (PBS), pH 7.4 for three times, and then fixed in 4% formaldehyde-PBS solution (pH 7.2) for 15 min at room temperature (~23 °C). The fluorescence intensities were recorded at 519 nm (λem~519 nm; [excitation wavelength was 488 nm (λex ~488 nm)] using a multimode plate reader (Varioskan Flash, Thermo Scientific, USA). The fluorescence intensity of cells treated with 0.1% dimethyl sulfoxide (DMSO) was used as a baseline, to which other values were compared.

Similarly, the PC-12 cells (1×10^4 cells) were incubated with graded concentrations (40 nM–800 nM) of FITC-conjugated peptides at 37 °C in a humidified incubator with 5% CO_2 (in triplicates). The fluorescence intensities were recorded at 519 nm using a multimode plate reader (Varioskan Flash, Thermo Scientific, USA). A hyperbola curve was plotted for change in λ_{max} ($\Delta\ \lambda_{max}$) against the concentrations (nM) of custom peptides with PC-12 cells expressing TrkA receptor and the equilibrium dissociation constant (K_d) value was determined using GraphPad Prism 8.1.1 software.

In an another study, the interaction between FITC-conjugated peptide and TrkA receptors was confirmed by fluorescence microscopic image analysis in MCF7, and MDA-MB-231 cells, and in non-TrkA receptor-expressing L6 cells (negative control) as previously described [21]. The cells were incubated with FITC-peptides with MCF7, MDA-MB-231, and L6 (negative control) cells with or without TrkA receptor inhibitor K252a (100 nM) for 120 min (TNP) and 30 min (HNP) at 37 °C in CO_2 incubator. After incubation, cells were washed with 1X PBS (pH 7.4) and fixed with 4% formaldehyde, then the cells were mounted on a cover slip and photographed under a fluorescent microscope (Olympus IX 83, Japan) at 40× magnification attached with a CCD camera.

2.6. Assessing the in vitro cell cytotoxicity of the custom peptides

For the cell viability assay, MCF7 cells, PC-12 cells, and myoblast cells isolated from L6 cells (0.1×10^5) were grown in 96-well plates at 37 °C, 5% CO2, as described by us [45]. Different concentrations of the custom peptides (500 ng/mL to 2 μg/mL) were then added to the wells (in triplicates) and cell viability was assessed after 24 h of incubation by the 3-(4,5-Dimethylthiazol-2-yl)-2,5-diphenyltetrazolium bromide (MTT)-based method. The release of lactate dehydrogenase (LDH) from the treated cells was compared to control cells. The custom peptide-induced cytotoxicity, if any, was expressed as percent cell viability, which was determined by the viability percentage of control cells (control cells were considered to be 100% viable) and LDH released from the triton-X-treated cells (considered to be 100% enzyme release) [45]. Cellular LDH release was measured using the CYQUANT™ LDH cytotoxicity assay kit (Invitrogen, C20300) according to the instruction manual [46].

2.7. In vitro effect of custom peptides on the mammalian haematological system

For the plasma clotting assay, goat blood was collected from a slaughterhouse in 3.8% trisodium citrate (9:1). The citrated blood was centrifuged at 4300 rpm for 15 min at 4 °C. The yellowish supernatant (the platelet-poor plasma, PPP) was used within 4 h to determine the plasma clotting activity [44,47]. One unit of pro-coagulant (or anticoagulant) activity was defined as a decrease (or increase) of 1 s in the clotting time of the PPP that was incubated with test samples (5 μg/mL), in comparison to the control PPP (1X PBS, pH 7.4).

The hemolytic activity of goat blood erythrocytes was assayed as described previously [44,47]. Two millilitres of a 5% red blood cells suspension (goat blood) were incubated with each custom peptide (1 μg/mL)/1X PBS (negative control)/Triton X-100 (20 μL) (positive control) at 37 °C for 3 h. The reaction mixture was then centrifuged at 4000 rpm for 10 min and 200 μL of the supernatant was put into a 96-well microtiter plate. The absorbance at 540 nm was measured and the percent hemolytic activity was calculated as stated previously [44,47].

Platelet-rich plasma (PRP) was isolated from citrated goat blood as described previously [44,47]. For assessing the platelet aggregation/de-aggregation properties of the custom peptides, the peptides (TNP, HNP, 1 μg/mL) were mixed with the PRP and the absorbance at 540 nm was measured for 30 min at 30 s intervals in a spectrophotometer (Multiskan GO, Thermo Scientific, USA). Percent aggregation/de-aggregation of the platelets was calculated for the treated samples in comparison to the control.

2.8. Assessing the neuritogenesis properties of custom peptides in PC-12 cells and the effects of chemical inhibitors on their neuritogenesis potency

For the neurite outgrowth bioassay, PC-12 cells were used as an *in vitro* model [20,21,38,39]. PC-12 cells are clonal cells that are derived from stem cells of rat pheochromocytoma expressing TrkA receptors and $p75^{NTR}$, and thus, are recommended as a useful model system for neuronal differentiation [20,21,38,48]. The neuritogenesis assay was adopted from our previous study [20,21,38]. Cells (1.0×10^5 cells/well) were seeded in six-well plates (in triplicates) and kept overnight at 37 °C in an incubator maintained with 5% CO_2 to allow the cells to adhere to the surface. The next day, the complete medium (DMEM) containing 100 ng/mL mouse 2.5S-NGF (positive control)/custom peptide (12.5 ng/mL to 100 ng/mL)/1X PBS, pH 7.4 (negative control) was added to the wells and the plates were incubated at 37 °C in 5% CO_2 for 14 days. The old media was replenished with fresh media at intervals of 72 h. Neurite outgrowth of the PC-12 cells was visualized under a phase-contrast microscope (Olympus IX 83, Japan) at 20× magnification. The percentage of neurite-bearing cells and the average neurite length (in μm) were determined using MOTIC IMAGE PLUS 3.0 software. Cells were considered to be differentiated if they had at least one neurite with a length equal to or greater than the diameter of the cell body [20,21,38,39].

Cells were pre-incubated with a chemical inhibitor, such as TrkA receptor inhibitor K252a (100 nM)/inhibitor of phosphatidylinositol 3-kinase (PI3K) stimulation of protein kinase B (Akt) signaling pathways (PI3K/AKT), pathway LY294002 (30 nM)/inhibitor of mitogen-activated protein kinase (MAPK), pathway U0126 (10 nM), or *anti*-TrkA, TrkB, and *anti*-TrkC antibody (1:1000 in DMEM) for 1 h. Cells were then treated with or without the addition of 100 ng/mL (~71 nM) custom peptide/mouse 2.5 S-NGF (positive control, 100 ng/mL)/1X PBS (control), incubated for 14 days as above, and the average length of neurite outgrowth and the percentage of neurite-bearing cells were determined [20,21,38,39].

2.9. Assessing the protective role of custom peptides against the PT-induced cytotoxicity in PC-12 cells

The cytotoxicity assay was performed as previously described [20,21,38,45]. In brief, PC-12 cells at a density of 1×10^4 cells/well were placed in a 96-well plate and then incubated in 5% CO_2 to facilitate the attachment of the cells to the well. The cells were treated with various concentrations (1–30 mM) of PT or growth medium (control), and

incubated at 37 °C in 5% CO_2 for 24 h. After 24 h, PT-induced cytotoxicity was determined by the MTT-based cytotoxicity assay [45]. A standard curve was generated from each concentration of paraquat, and the IC_{50} values were calculated from the regression analysis of growth curves of PC-12 cells in presence of PT. The protective role of TNP and HNP against PT-induced cytotoxicity (IC_{50} value was determined as 10 mM) was determined by the MTT-based cytotoxicity assay [45]. Cells were pre-incubated/post-treated/co-treated with custom peptides (HNP/TNP)/mouse 2.5S-NGF (positive control) in an increasing concentration-dependent (12.5, 25, 100, 250 and 500 ng/mL; equivalent to 18 nM–357 nM) and time-dependent (0.5, 1, 2, 4, and 6 h) manner. The percent cell viability for each group was calculated after 24 h of PT incubation and each experiment was repeated three times.

Assessing the protective role of custom peptides and their optimum dosages against the PT-induced cytotoxicity in PC-12 cells was also confirmed by quantitating the release of marker enzyme LDH from the treated cells. PC-12 cells were dispensed into a 96-well plate at a density of 1×10^4 cells/well. Cells were pre-treated with different concentrations (25, 100, 250, and 500 ng/mL; equivalent to 36 nM–357 nM) of custom peptide HNP/TNP/NGF (100 ng/mL) as a positive control/control (Triton X-treated) for 1 h (optimum time derived from the previous experiment) and followed by 10 mM PT (IC_{50} value) treatment for 24 h (in triplicates).

2.10. Flow cytometry analysis to determine PT-induced apoptotic cell death and its protection by custom peptides

Apoptotic and necrotic cells were determined by Annexin-V binding and PI uptake studies. Annexin V has a high affinity for phosphatidylserine, which is translocated from the internal to the external surface of the cell membrane when PC-12 cells undergo apoptosis. Necrotic cells absorb PI as a result of the higher permeability of their damaged cell walls.

Briefly, PC-12 cells were seeded on a 24-well culture plate, pre-treated with 100 ng/mL (~71 nM) custom peptide (HNP and TNP) for 1 h, which was followed by the PT (10 mM) treatment for 24 h before being harvested. Cells were washed three times using PBS and centrifuged at 1200 rpm for 5 min, with the concentration being adjusted to 1×10^5 cells/well [49]. Pellets were re-suspended in the 1X binding buffer, following the instructions of the manufacturer, and then incubated for 5 min with Annexin V-FITC and PI at 4 °C in proportions mentioned in the Annexin V-FITC early apoptosis kit (Cell Signaling Technology, CST-6592). Fluorescence intensity was analyzed with flow cytometry (BD-FACS-Melody, USA, Melody multi-color analyzer cum high-speed cell sorter). Normal cells without any treatment were used as a control for fluorescence compensation adjustment to reduce the spectral overlap and establish the location of the cross gate.

2.11. Determination of the effect of custom peptides in inhibiting the reactive oxygen species (ROS) production in PT-treated PC-12 cells by spectrofluorometric assay and flow cytometry analysis

The ROS level in the PC-12 cells post-PT treatment was determined using the fluorogenic probe 2′,7′-dichlorofluorescein-diacetate (H_2DCFDA) according to the procedure of Mukherjee et al. (2015) [45,50]. Briefly, PC-12 cells (1×10^6) at 70% confluence were cultured in 24-well plates and kept overnight. Cells were pre-treated with different concentrations of custom peptides (12.5 ng/mL to 500 ng/mL, equivalent to 18 nM–357 nM)/Vitamin C (10 μg/mL, positive control)/PBS for 1 h, followed by treatment with PT (10 mM) for 12 h. Media was aspired out and cells were then washed with PBS and incubated with 10 μM H_2DCFDA in the dark for 30 min at 37 °C. The cells were then washed twice with 200 μL PBS and incubated with 1% Triton X-100 (170 μL). The reaction was stopped by adding DMSO (130 μL). Cells were scraped and transferred to the black plate. Absorbance was measured at excitation and emission wavelengths of 480 and 530 nm, respectively, using a microplate reader (in triplicates). The ROS production by PT-treated cells was considered 100% (baseline), to which other activities were compared.

In another set of experiments, intracellular ROS levels generated post-PT exposure in PC-12 cells were measured by flow cytometry (BD-FACS-Melody, USA) analysis using H_2DCFDA, according to the procedure described by Mukherjee et al. (2015) [45]. Briefly, PC-12 cells were pre-treated with custom peptides (HNP and TNP) at different concentrations (12.5 ng/mL to 500 ng/mL, equivalent to 18 nM–357 nM) and Vitamin C (10000 ng/mL as the positive control) for 1 h, which was followed by PT incubation for 12 h. The adherent and non-adherent cells were collected and washed twice with PBS (pH 7.4). The cells were then incubated with 10 μM H_2DCFDA at 37 °C for 30 min in the dark, which was followed by washing twice with chilled PBS. The fluorescence intensities of 2′,7′-dichlorodihydrofluorescein (DCF) produced by intracellular ROS were analyzed by flow cytometry with excitation and emission at 480 and 530 nm, respectively.

2.12. Determination of the effect of custom peptides on reducing the PT-induced depolarization of mitochondrial membrane potential

Changes in the mitochondrial transmembrane potential were determined with the Mito Probe™ JC-1 assay kit (Invitrogen, USA, Catalog number M34152) protocol. PC-12 cells were pre-treated with 100 ng/mL (~71 nM) of a custom peptide (HNP/TNP) for 1 h, which was followed by the PT (10 mM) treatment for 10 h at 37 °C, in 5% CO_2 (in triplicates). After the treatment, cells were washed three times and incubated with 1 μg/mL JC-1 dye and incubated at 37 °C in a humidified CO_2 incubator for 4 h. The PC-12 cells were then washed three times and images were captured at excitation and emission wavelengths of 490 nm and 530 nm, respectively to see the green fluorescence JC-1 monomers. For the red fluorescence J-aggregates, excitation and emission wavelengths were set at 525 nm and 590 nm, respectively under a confocal microscope (TCS SPE, Leica, Wetzlar, Germany). The fluorescence intensities were measured using Image J software. Changes in the mitochondrial transmembrane potential were also analyzed by flow cytometry with the same JC-1 dye, as described in the previous section (Section 2.11). For flow cytometry analysis carbonyl cyanide m-chlorophenyl hydrazone (CCCP, mitochondrial uncoupler) was used as a positive control.

2.13. Determination of the effect of custom peptides on the restoration of PT-induced cellular and nuclear morphological changes in PC-12 cells

To study the cellular and nuclear morphological changes induced by PT, 1 mL of 1×10^6 PC-12 cells was seeded in a 24-well plate and allowed to adhere overnight at 37 °C. PT-induced nuclear damage in the PC-12 cells was observed by 4′,6-diamidino-2-phenylindole (DAPI) staining [45,51]. Briefly, after the above-mentioned pre-treatment with custom peptides (100 ng/mL, equivalent to ~71 nM), the cells were collected, washed in PBS, and then fixed in 1% formaldehyde (in PBS) for 30 min at room temperature. After washing with 1X PBS, the cells were suspended in DMEM media and incubated with 5 μL of DAPI (1 μg/mL) for 30 min at 37 °C. The cells were then washed with PBS, placed onto a glass slide, and observed under a fluorescence microscope at 40× magnification. The percentage of dead cells was calculated in four randomly selected microscopic fields and the changes in cellular and nuclear morphology were compared to the untreated cells (control).

2.14. DPPH free radical scavenging activity of custom peptides in in vitro condition

DPPH radical-scavenging activity of custom peptides was measured as described by Ref. [52]. Briefly, in a 96-well plate, 100 μL peptide sample (25 ng/mL – 250 ng/mL)/vitamin C (10000 ng/mL, or 10 μg/mL, positive control) was uniformly mixed with 100 μL of 0.2 mM

DPPH radical solution (dissolved with 95% ethanol) and incubated at room temperature for 30 min. Instantly, the absorbance of the solution was measured at 517 nm by a microplate reader (Varioskan Flash, Thermo Scientific, USA). The percentage of DPPH free radical-scavenging activity was determined as follows:

$$DPPH\ radical\ scavenging\ activity\ (\%) = \left[1 - \frac{A1 - A2}{A0}\right] * 100$$

where A0 signifies the absorbance of 95% ethanol (100 μL) (v/v) mixed with DPPH radical solution (100 μL) at 517 nm; A1 shows the absorbance of the peptide (100 μL) with DPPH radical solution (100 μL), A2 denotes the absorbance of peptide solution (100 μL) with 95% ethanol (100 μL). This experiment was performed in triplicates to ensure reproducibility.

2.15. Quantitative reverse transcription-polymerase chain reaction (qRT-PCR) analysis to determine the expression levels of pro- and anti-apoptotic genes in the PT-treated PC-12 cells and the effect of pre-treatment of custom peptides

The procedure for qRT-PCR analysis of stress-related gene expression was adopted from our previous studies [53,54]. PC-12 cells were subjected to different treatments at 37 °C: (a) 1X PBS (control) treated PC-12 cells (CT); (b) 10 mM PT (PT) treatment for 12 h; (c) pre-treatment with 100 ng/mL (~71 nM) custom peptide (TNP or HNP) or mouse 2.5S-NGF (positive control) (NGF) for 1 h followed by 10 mM PT treatment (PTNP, PHNP, and PNGF) for 12 h. Total RNA was isolated with a pure link RNA mini kit (Invitrogen, USA; Cat- 12183018A), and the purity and concentration (A260/A280) of the RNA were measured using a Nanodrop 2000C spectrophotometer (Thermo Scientific, USA). Reverse transcription was performed from 1 μg of the total RNA using a verso cDNA synthesis kit (Thermo Scientific, USA; Cat: AB-1453/A) according to the manufacturer's protocol. The reaction was performed at 42 °C for 30 min and ended by incubation at 85 °C for 5 min. The qRT-PCR was done with SYBR Green (Bio-Rad, USA) to quantify the expression of pro-apoptotic genes, such as caspase-3, B-cell lymphoma 2 (bcl-2), and heat shock protein function (hsp-70) (in triplicates) in a CFX96 Touch Real-Time PCR detection system (Bio-RAD, USA). The sequence of primers that were used in this experiment [55–58] is shown in Supplementary Table S1.

2.16. Quantitative proteomic analysis comparing the expression of global proteins for PC-12 cells exposed to PT and cells pre-treated with custom peptides followed by the PT treatment

Quantitative proteomics was used to identify and categorize proteins transformed by PT and compare their restoration by custom peptides in pre-treated PC-12 cells [38]. To compare the differential expression of cellular proteins, PC-12 cells were subjected to the following treatments (at 37 °C): (a) 1X PBS (control)-treated PC-12 cells (CT); (b) 10 mM PT (PT) treatment for 1 h; (c) pre-treatment with 100 ng/mL (~71 nM) custom peptide for 1 h followed by 10 mM PT treatment (PHNP) for 24 h; and (d) treatment with 100 ng/mL (~71 nM) of custom peptide (HNP) for 1 h. Differentially treated PC-12 cells were collected and lysed separately in an RIPA buffer containing proteinase K inhibitor for 30 min on ice. The tissue lysate was sonicated and centrifuged at 13,000 rpm for 20 min at 4 °C, and the protein concentration was estimated [59]. Briefly, 30 μg of the protein from the treated PC-12 cells was subjected to reduction with 10 mM dithiothreitol (DTT) and alkylation with 50 mM iodoacetamide (in the dark), which was followed by incubation with sequencing-grade trypsin (50 ng/μL in 25 mM ammonium bicarbonate comprising 10% acetonitrile) for 18 h at 37 °C [20,21,34,38,60]. The digested peptides were desalted and concentrated using ZipTip (Millipore, USA), and then re-suspended in 20 μL of 0.1% (v/v) formic acid in 2% acetonitrile. The 1 μL samples were exposed to nano-ultra-performance liquid chromatography-tandem mass spectrometer (UHPLC-MS/MS) analysis. ESI (nano-spray) was used as the ion source, collision-induced dissociation (y and b ions) was used as the fragmentation mode, FT-ICR/Orbitrap was used as the MS scan mode, with an MS/MS scan range of 500–2000 m/z being used as the linear ion trap. For the collision-induced dissociation (CID) MS/MS analysis, double or triple-charged ions were selected.

For the data analysis, MS data protein were identified, quantitated, and analyzed using the Peak studio from the Sequest HT database search engine with a 1% false discovery rate (FDR) and two missed cleavage cut-off standards. The database search consisted of all entries from the *Rattus norvegicus* (Taxonomy ID: 10116) UniProt reference proteome database. Total protein level analysis was executed using 10 parts per million precursor ion tolerance. The product-ion tolerance used for the data evaluation was 0.05 Da. Oxidation of methionine residues (+15.995 Da) was kept as a variable amendment, whereas cysteine carbamidomethylation (+57.021 Da) was kept as a static modification. Peptide spectra matches (PSMs) were adjusted to have an FDR of 0.01. Relative abundances were calculated from the spectral intensity of the respective protein, and the fold change values of the relative abundances were also calculated. Protein-protein interaction (PPI) network analysis was carried out with Cytoscape 3.9.1.

2.17. Statistical analysis

All data was denoted as mean ± standard deviation (SD) of independent triplicates. Significant differences between test and control values were analyzed with Student's t-test in Sigma Plot 11.0 for Windows (version 10.0). The significance of differences was analyzed for more than two groups with a one-way analysis of variance (ANOVA) in GraphPad Prism software. A p-value ≤ 0.05 was considered to be statistically significant.

3. Results

3.1. In silico analysis and biophysical characterization of TrkA receptor-binding custom peptides

The sequence and biophysical properties of the TrkA receptor-binding custom peptides (TNP and HNP) are summarized in Supplementary Table S2. Different domains of human TrkA were obtained from the PDB structures (Fig. 1A). Domain-3 of TrkA was characterized as an NGF-binding domain site (in humans) (Fig. 1A). Molecular docking revealed a high-affinity binding that formed a complex between the peptides (TNP and HNP) and TrkA domain-3 (Fig. 1B–C). Glide docking scores were found to be −9.35 (TNP) and −5.54 (HNP), and similarly, the MMGBSA binding energies (docked complex) were found to be −77.77 (TNP) and −68.03 (HNP) kcal/mol (Table 1).

The stability of the docked domain-3 with the TNP/HNP complex was studied using molecular dynamic simulations for 300 ns. In all cases, the RMSD of the TrkA domain-3 backbone was found to be stable over the simulation trajectory. For TNP, the first 25–50 ns of simulation showed a higher degree of variation in RMSD with a stable complex being formed afterwards (Fig. 2A). Unlike the molecular docking results, the molecular dynamic simulations predicted a stable complex of HNP with domain-3 of TrkA (Fig. 2B), and the average MMGBSA binding energy of TNP and HNP were −93.652 and −106.998 kcal/mol, respectively.

TNP interacted with five different amino acid residues of TrkA domain-3, and the interaction was stable up to 87% of the simulation time (Fig. 3A). The major TrkA domain-3 residues Arg^{273}, Ser^{277}, and Val^{198} participated in the interaction with Asp^{3}, Gly^{11}, and Gly^{12} TNP residues, respectively, and Glu^{275} of domain-3 interacted with Arg^{4}, Cys^{5}, and Ser^{6} of TNP (Fig. 3A). Nevertheless, HNP demonstrated the highest degree of stable interaction (i.e., up to 62% of the time) with seven different amino acid residues of TrkA domain-3 (Fig. 3B). The

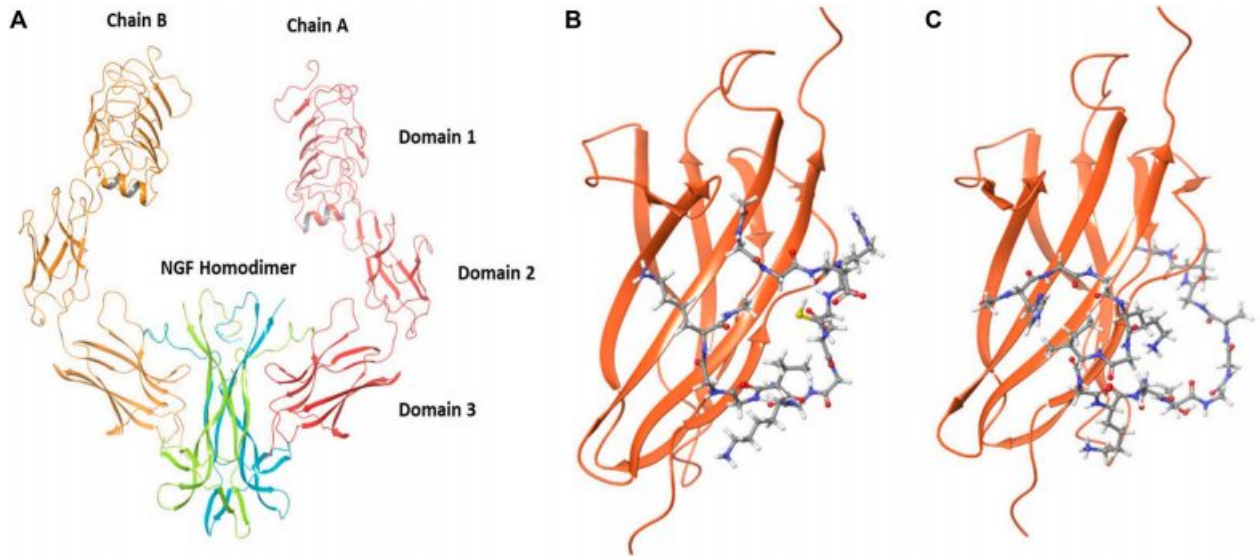

Fig. 1. The *in silico* analysis of **(A)** Human TrkA receptor Chain A and B in complex with human NGF homodimer (PDB ID- 2IFG). The 3D model shows the interaction of TrkA with **(B)** TNP, and **(C)** HNP to form a ligand-receptor complex. The ball and stick structure represent peptide structure, and string model corresponds to TrkA receptor domain-3.

Table 1
Glide scores and molecular mechanics/generalized born surface area (MM/GBSA) binding energy of custom peptides with domain 3 of NTRKA.

Custom peptide	Glide docking score	MMGBSA binding energy (ΔG) (kcal/mol)	MMGBSA binding energy (ΔG) after simulation (kcal/mol)
TNP	−9.35	−77.77	−93.65
HNP	−5.54	−68.33	−106.99

major TrkA domain-3 residue Ser^{371} interacted with His^{1}, Gly^{2}, and Lys^{8} residues of HNP. Leu^{290} of domain-3 interacted with Gly^{13} and Gly^{15} of TNP and the other domain-3 residues (Ala^{363}, Ala^{370}, Ser^{373}, His^{291}, and Ser^{304}) participated in the interaction with HNP residues Ile^{6}, Ile^{6}, Thr^{11}, Ala^{14}, and Val^{16}, respectively (Fig. 3B).

HPLC chromatograms showed the purity of the synthetic peptides (single peaks within 8–12 min of retention time) (Supplementary Figs S1 A-B). The ESI-mass spectrometry analysis also suggested the purity of the peptide preparations (Supplementary Figs S1 C-D). The CD spectrum of custom peptide TNP revealed that it was composed of α-helices (37.6%), random coils (30.9%), and turns (31.5%) with a characteristic minimum absorbance at 210 nm (Supplementary Fig. S2 A). The analysis of the CD spectrum of custom peptide HNP revealed that it was mainly composed of turns (100%) with characteristic maximum absorbances at 202 and 224 nm (Supplementary Fig. S2 B).

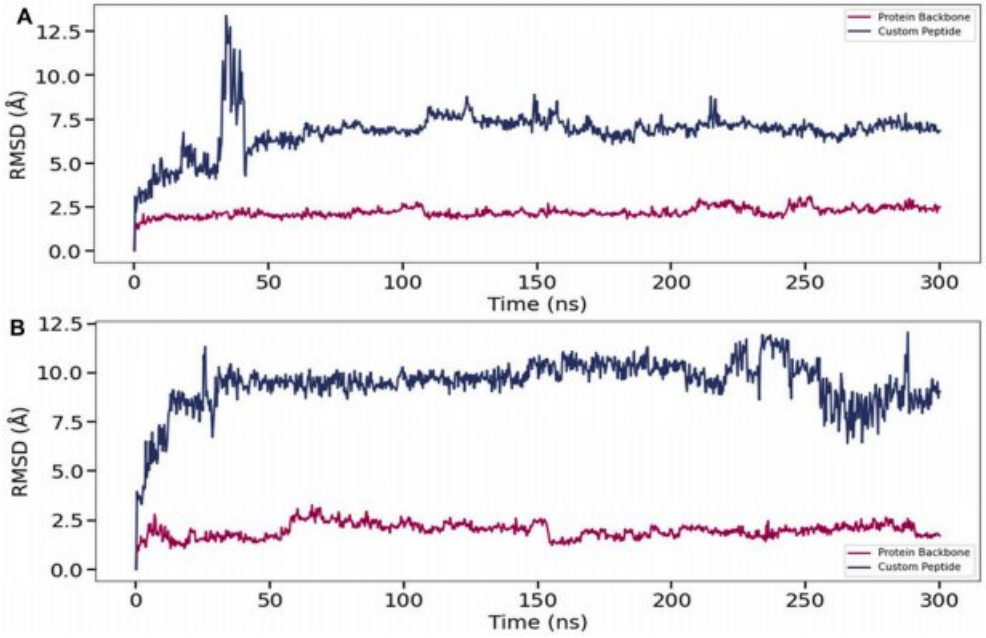

Fig. 2. Molecular dynamic simulation of domain-3 backbone and custom peptides **(A)** TNP, **(B)** HNP shown in an RMSD (root mean square deviation) plot throughout the simulation trajectory for 300 ns.

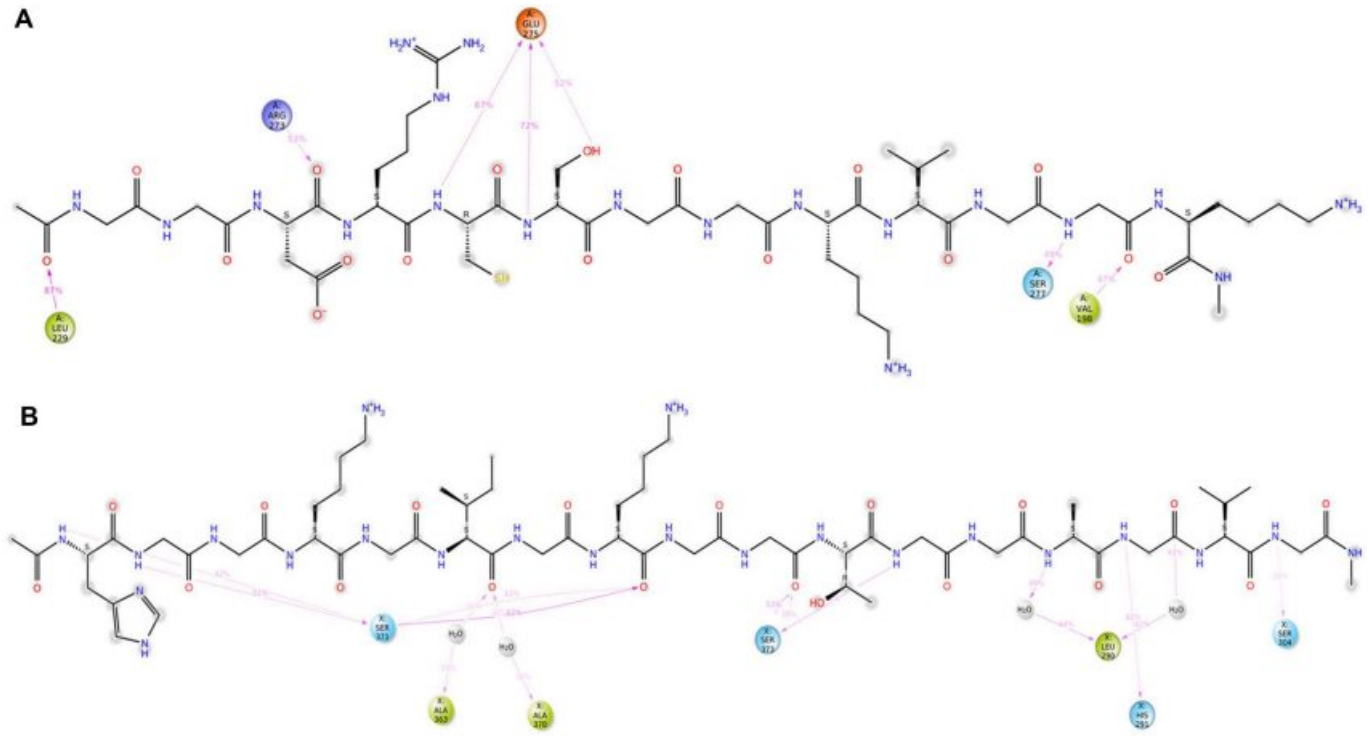

Fig. 3. Schematic diagram depicting the interaction of custom peptides **(A)** TNP **(B)** HNP with domain-3 of the TrkA receptor. The percentage of interaction is shown in the figure recorded over the simulation time of 300ns.

3.2. The FITC-conjugated custom peptides showed exclusive binding to mammalian cells expressing the TrkA receptor but not to cells with TrkB or TrkC receptors

The spectrofluorometric analysis of FITC-custom peptides showed a significant binding in a time-dependent manner to the TrkA receptor expressed in MCF7, MDA-MB-231, and PC-12 cells but not to L6 cells (devoid of extracellular TrkA receptors) (Fig. 4A). The fluorescence intensity was found to be significantly higher (3–30-fold increase) in HNP and TNP-treated samples compared to the control L6 cells. In any case, the binding efficacy of the HNP peptide was significantly higher ($p \leq 0.05$) for MCF7 and PC-12 cells, compared to those of the TNP peptide. For the MDA-MB-231 cells, no significant difference was seen between the two peptides up to 60 min of incubation, though HNP had a higher binding efficacy in the incubations of 120, 240, and 360 min (Fig. 4A).

The FITC-conjugated peptides also showed a significant increase ($p \leq 0.05$) in binding efficacies to PC-12 cells in a concentration-dependent manner (from 50 to 1000 ng/mL, equivalent to 40–800 nM) (Fig. 4B). The binding affinity of TNP and HNP towards the PC-12 cell line was expressed in K_d value and found to be 1.03×10^{-11} and 0.80×10^{-11} M, respectively (Fig. 4C).

The binding of FITC-custom peptide to MCF-7 (Fig. 4D), and MDA-MB-231 (Fig. 4E) cells expressing TrkA receptor was evident by fluorescence microscopic analysis; however, no fluorescence signal was detected in L6 cells (Fig. 4F).

3.3. Custom peptide-induced neurite outgrowth and differentiation of PC-12 cells

The TNP and HNP custom peptides did not demonstrate *in vitro* cell cytotoxicity (Fig. 5A–B and Supplementary Fig. S3) and showed negligible haemolytic, platelet-modulating, and plasma-clotting activities (Supplementary Table S3). Phase-contrast microscopic images of neurite outgrowth in PC-12 cells 14 days post-treatment with custom peptides are shown in Fig. 6A–H. The average neurite length (μm) is represented by the box and whisker plot, which shows the variation for the different concentrations (12.5–100 ng/mL, equivalent to 18–71 nM) of peptide (TNP and HNP), compared to mouse 2.5S NGF (Positive control) (Fig. 6I). Both HNP and TNP and mouse 2.5S-NGF induced neurite outgrowth and differentiation in PC-12 cells to different extents (Fig. 6I–J). The custom peptides showed significant neurite outgrowth at a minimum concentration of 50 ng/mL (equivalent to 36 nM). The average neurite length, and the percentage of differentiated cells, was significantly higher ($p \leq 0.05$) for TNP and HNP at the same concentration (100 ng/mL, equivalent to 71 nM), compared to mouse 2.5S-NGF (positive control); however, no significant difference was seen between the TNP and HNP peptides.

3.4. Chemical inhibition of TrkA receptor (K252a), PI3K/AKT (LY294002), and MAPK/ERK (U0126) pathways inhibited neuritogenesis induced by the custom peptides in PC-12 cells

The percentage of cell differentiation was examined for PC-12 cells treated with custom peptides that were pre-incubated with or without chemical inhibitors, after 14 days of incubation. The results show that the potency of the custom peptides in inducing neurite outgrowth and cell differentiation activities were significantly inhibited ($p \leq 0.05$) by the three chemical inhibitors (K252a, LY294002, and U0126) (Fig. 7A). The inhibition in the differentiation of PC-12 cells by peptides (100 ng/mL, equivalent to ~71 nM) in presence or absent of chemical inhibitor was ranked in descending order from: MAPK/ERK (U0126) pathway inhibitors (15–16% decrease) > PI3K/AKT (LY294002) (12–13% decrease) > TrkA receptor inhibitor (K252a) (9–10% decrease) when compared to neurite outgrowth and cell differentiation activities of custom peptides without inhibitor. These findings corroborate well with our earlier findings with NGFs from Indian Russell's viper and Indian cobra venoms [20,21,38].

The blocking of the TrkA receptor significantly inhibited ($p \leq 0.05$) differentiation of PC-12 cells by TNP and HNP, while blocking of the TrkB and TrkC receptors with their respective antibodies did not affect

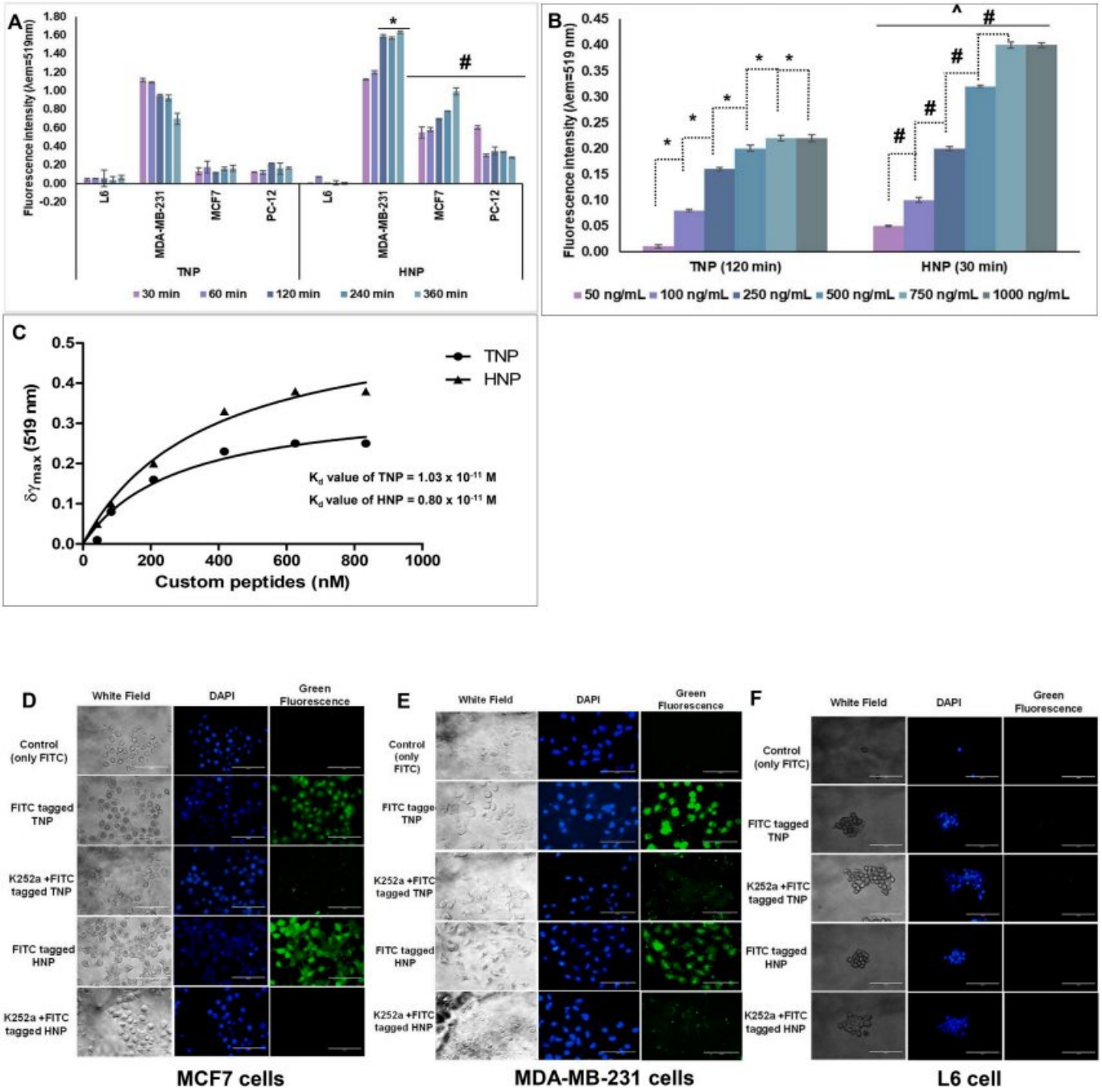

Fig. 4. Fluorescence analysis to determine the **(A)** time-dependent binding (30 min–360 min) of custom peptides (100 ng/mL, ~71 nM) with the TrkA receptor of cells. L6 cells (non-TrkA expressing cells) taken as control. Significance of difference in the binding of TNP (for 120 min–360 min) with respect to HNP for MDA-MB-231, $^{*}p \leq 0.05$. Significance of difference in the binding of TNP (for 30 min–360 min) with respect to HNP for MCF7 and PC-12 cell line, $^{\#}p \leq 0.05$. **(B)** Binding of custom peptides with cell surface TrkA receptor of PC-12 cells in an increasing concentration of custom peptides (50 ng/mL to 1000 ng/ml, equivalent to 40–800 nM). Significance of difference in the binding between different concentration for TNP $^{*}p < 0.05$ and for HNP $^{\#}p < 0.05$. Significance of difference in the binding of TNP with respect to HNP, $\hat{}p < 0.05$. **(C)** A hyperbola curve was plotted for change in λ_{max} ($\Delta\lambda$max) against the concentrations (nM) of custom peptide with TrkA receptor expressing PC-12 cells (1 x 10^4 cells) and K_d value was determined using GraphPad Prism 8.1.1 software. The binding of FITC-custom peptide (100 ng/mL) with **(D)** MCF7, **(E)** MDA-MB-231, and **(F)** L6 cells was observed under fluorescence. The binding of custom peptides was also shown in presence or absence of chemical inhibitor of TrkA receptor (K252a). Magnification was 40X. Values are mean ± SD of triplicate determinations.

differentiation of the PC-12 cells (Fig. 7B). Thus, the peptides appear to bind exclusively to TrkA receptors.

3.5. *Pre-treatment of PC-12 cells with custom peptides enhanced their cell survival against PT-induced cell death*

Pre-treatment of PC-12 cells with TNP and HNP (100 ng/mL, ~71 nM) demonstrated a significant 27–30% increase ($p \leq 0.05$) in their percent cell viability against PT (10 mM, IC_{50})-induced cell death, compared PC-12 cells that had only been treated with PT (Fig. 8A). The protection offered by the custom peptides against PT-induced cell death was significantly higher (10–13%) ($p \leq 0.05$) compared to that of mouse 2.5S-NGF (positive control). Moreover, post-treatment of PT-treated cells with TNP or HNP or co-treatment with TNP or HNP with PT did

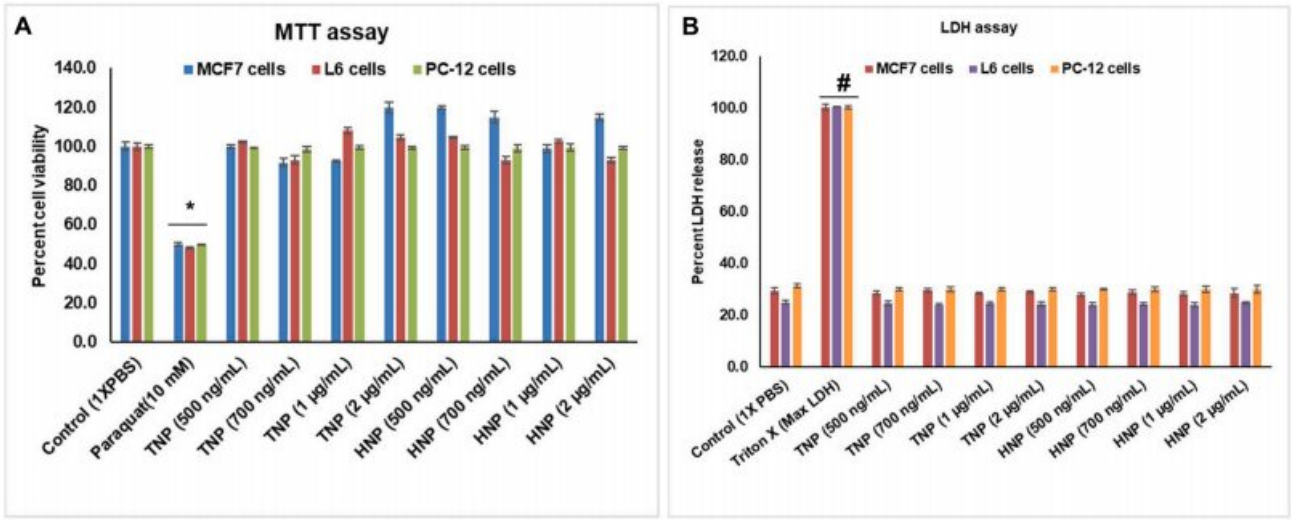

Fig. 5. Concentration-dependent *in vitro* cytotoxicity of synthetic peptides (TNP and HNP) and PT (10 mM, positive control) against mammalian cells. The cells were incubated with progressive concentrations of custom peptides (500 ng/mL to 2 µg/mL) with mammalian cells (MCF7, PC-12, and L6 cells) at 37 °C in a CO_2 incubator for 24 h. Determination of cytotoxicity by **(A)** MTT assay **(B)** LDH release assay. Significance of difference in the cell viability by MTT assay for paraquat treated cells with respected TNP and HNP treated cells, $^{*}p \leq 0.05$. Significance of difference in the cell viability by LDH release assay for Triton-X treated cells with respect to TNP and HNP treated cells, $^{\#}p \leq 0.05$. Values are mean ± SD of triplicate determinations.

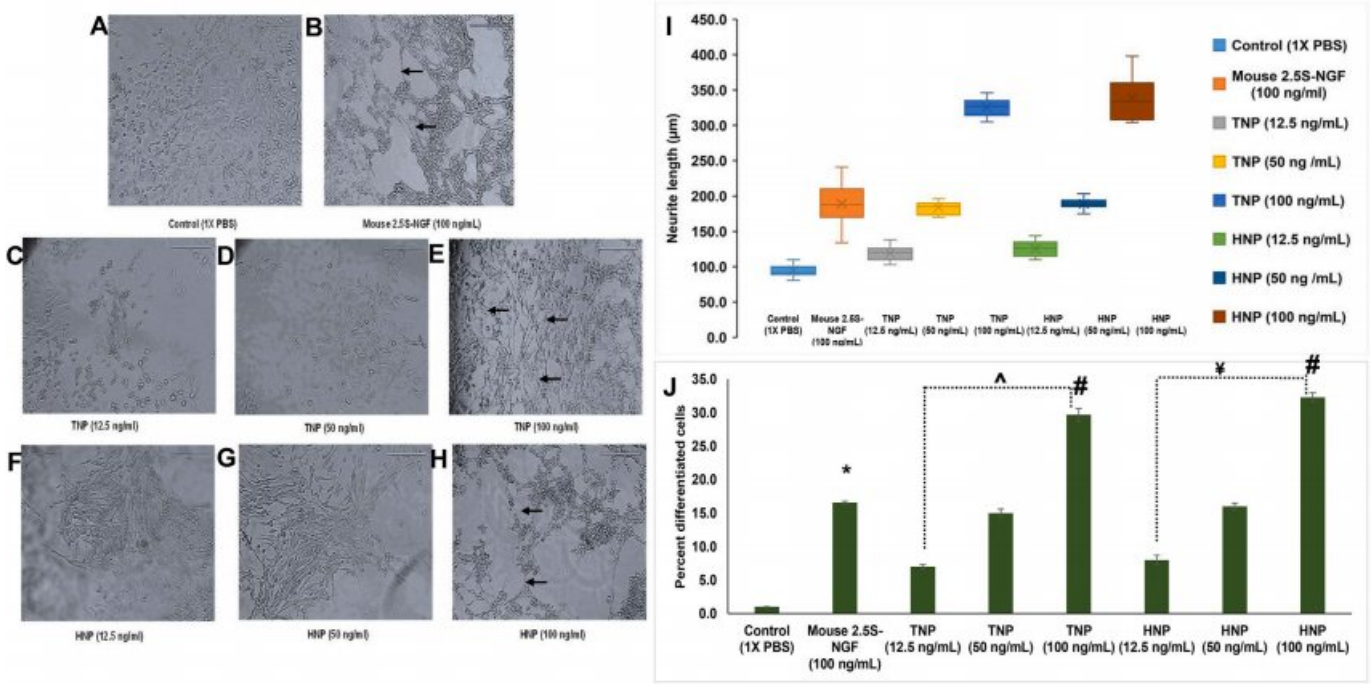

Fig. 6. Concentration-dependent (12.5–100 ng/mL) determination of neurite outgrowth in rat pheochromocytoma (PC-12) cells treated with custom peptides (TNP & HNP) post 14 days of incubation at 37 °C, 5% CO_2. The cells were observed under a phase-contrast microscope at 20× magnification. The appearance of neurite outgrowth from PC-12 cells is indicated by black arrows. **(A)** 1X PBS (control) treated cells, **(B)** mouse 2.5S-NGF treated cells, **(C–E)** TNP-treated cells with different concentrations (12.5–100 ng/mL), **(F–H)** HNP-treated cells with different concentrations (12.5–100 ng/mL). **(I)** Box and whisker plots represent average neurite outgrowth per cell (in µm). **(J)** Bar graph showing the percentage of differentiated cells (total number of cells showing neurite outgrowth) in custom peptide and mouse 2.5 S-NGF-treated PC-12 cells. The neurite length was determined using MOTIC IMAGE PLUS 3.0 software. Significance of difference in the controls with respect to mouse 2.5S-NGF, $^{*}p \leq 0.05$. Significance of difference in mouse 2.5S-NGF with respect to TNP and HNP (at the concentration 100 ng/mL), $^{\#}p \leq 0.05$. Significance of difference in different concentration for TNP, $^{\wedge}p \leq 0.05$ and for HNP, $^{¥}p \leq 0.05$. Values are mean ± SD of triplicate determinations.

not restore the cell viability against PT-induced toxicity (Fig. 8B–C). HNP/TNP at a concentration of 100 ng/mL (~71 nM) for a 1-h pre-incubation showed the optimum protection (up to 80–85% cell viability) against PT-induced (10 mM) cell toxicity (Fig. 9A–B).

The protective potential of the custom peptides was also confirmed by the inhibition of PT-induced release of LDH from PC-12 cells. The maximum release (considered as 100%) of LDH enzyme was observed in control (Triton X-treated) PC-12 cells. The only PT -treated PC-12 cells showed 50% release of LDH enzyme. Pre-treatment with the custom peptides (100 ng/mL, ~71 nM) demonstrated a significant decrease (28–29%) ($p \leq 0.05$) in the release of the marker enzyme (LDH), compared to that released from PT-treated PC-12 cells (Fig. 9C). The

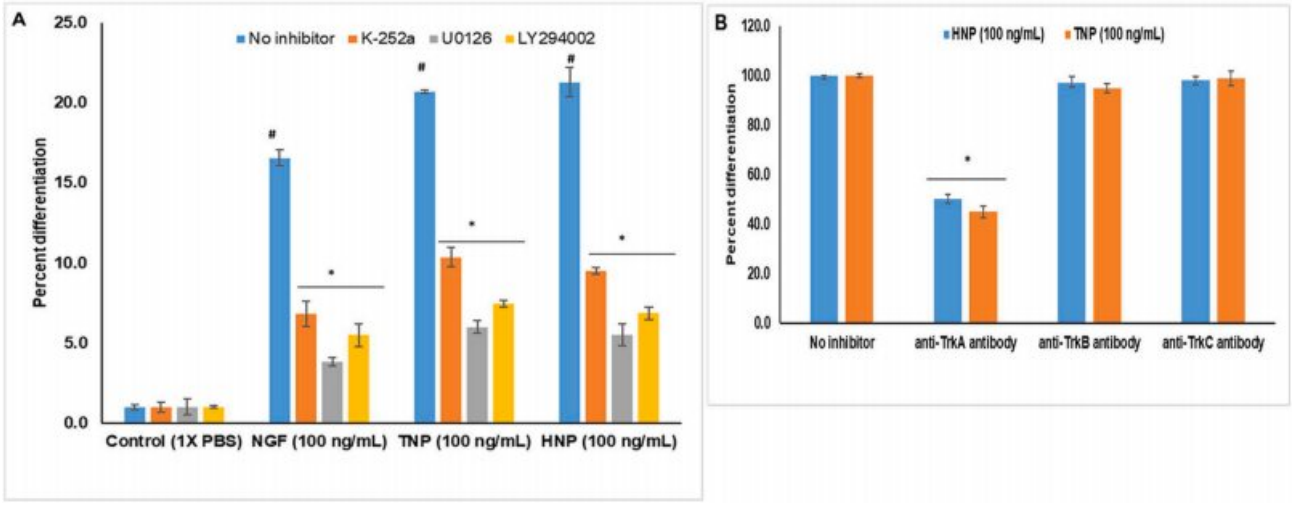

Fig. 7. (A) Effect of small synthetic inhibitors of major signaling pathways on neuritogenesis potency of custom peptides (TNP, and HNP, 100 ng/mL equivalent to 71 nM), and NGF (positive control, 100 ng/mL) in PC-12 cells. Significance of difference in the percent differentiation of control cells compared to NGF, TNP, and HNP when no inhibitor was added, $^{\#}p \leq 0.05$. Significance of difference in the percent cell differentiation between with inhibitors (K-252a, U0126, and LY294002) and without inhibitors, $^{\#}p \leq 0.05$ **(B)** Effect of *anti*-TrkA, TrkB, TrkC antibody (1:1000) on neuritogenesis potency of custom peptides (TNP, and HNP, 100 ng/mL equivalent to 71 nM), and NGF (positive control) in PC-12 cells. Significance of difference in the percent cell differentiation between with *anti*-TrkA antibody and without inhibitors, $^{*}p \leq 0.05$. Values are mean ± SD of triplicate determinations.

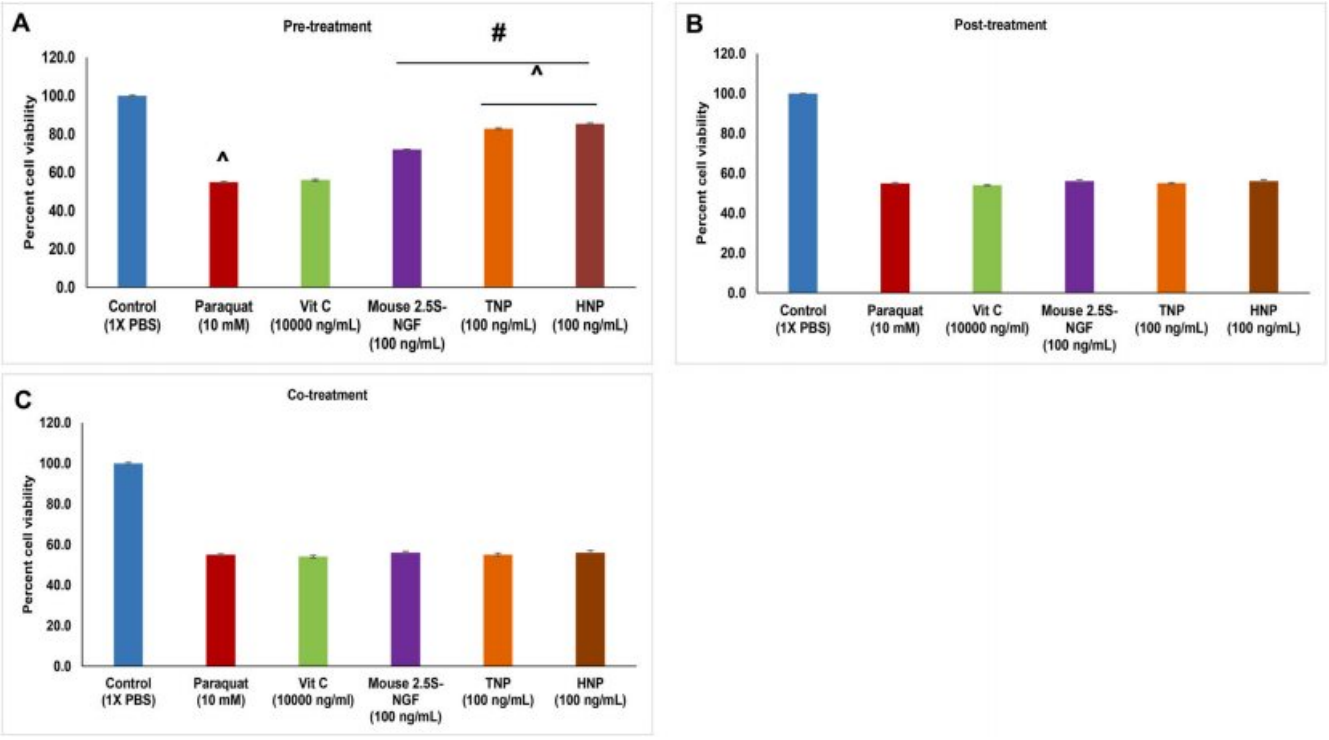

Fig. 8. Determination of the protective effects of custom peptides against PT-induced cell death. The viability of PC-12 cells was determined by MTT assay. **(A)** Pre-treatment of cells with custom peptides (100 ng/mL, ~71 nM) or vitamin C (10000 ng/mL) for 4 h followed by PT treatment for 24 h at 37 °C in a CO_2 incubator. $^{*}p \leq 0.05$, a significant difference between untreated (control) and PT-treated cells; $^{\#}p \leq 0.05$, a significant difference between PT-treated cells with respect to mouse 2.5S-NGF and custom peptide pre-treated PC-12 cells. $\hat{}p \leq 0.05$, a significant difference of mouse 2.5S-NGF treated cells with respect to the peptide (TNP and HNP) treated cells. **(B)** Treatment of cells with PT for 24 h followed by treatment with custom peptide for 4 h. There is no significant difference in the cell viability in PT-treated cells with respect to mouse 2.5S-NGF, Vit C, and peptide post-treatment. **(C)** The cells were simultaneously treated with custom peptides and PT for 24 h followed by an assay of cell viability. There is no significant difference in the cell viability in PT-treated cells with respect to mouse 2.5S-NGF, Vit C, and peptide co-treatment. Values are mean ± SD of triplicate determinations.

custom peptides showed 13–14% decrease in the release of LDH enzyme, compared to that of mouse 2.5S-NGF (positive control) (Fig. 9C). Mouse 2.5S-NGF (100 ng/mL, positive control) was less effective in protecting the PT-induced cell death, according to the results from both the MTT-based cell cytotoxicity assay (Fig. 9A–B) and the LDH release assay (Fig. 9C), when comparing the same concentrations of HNP and TNP.

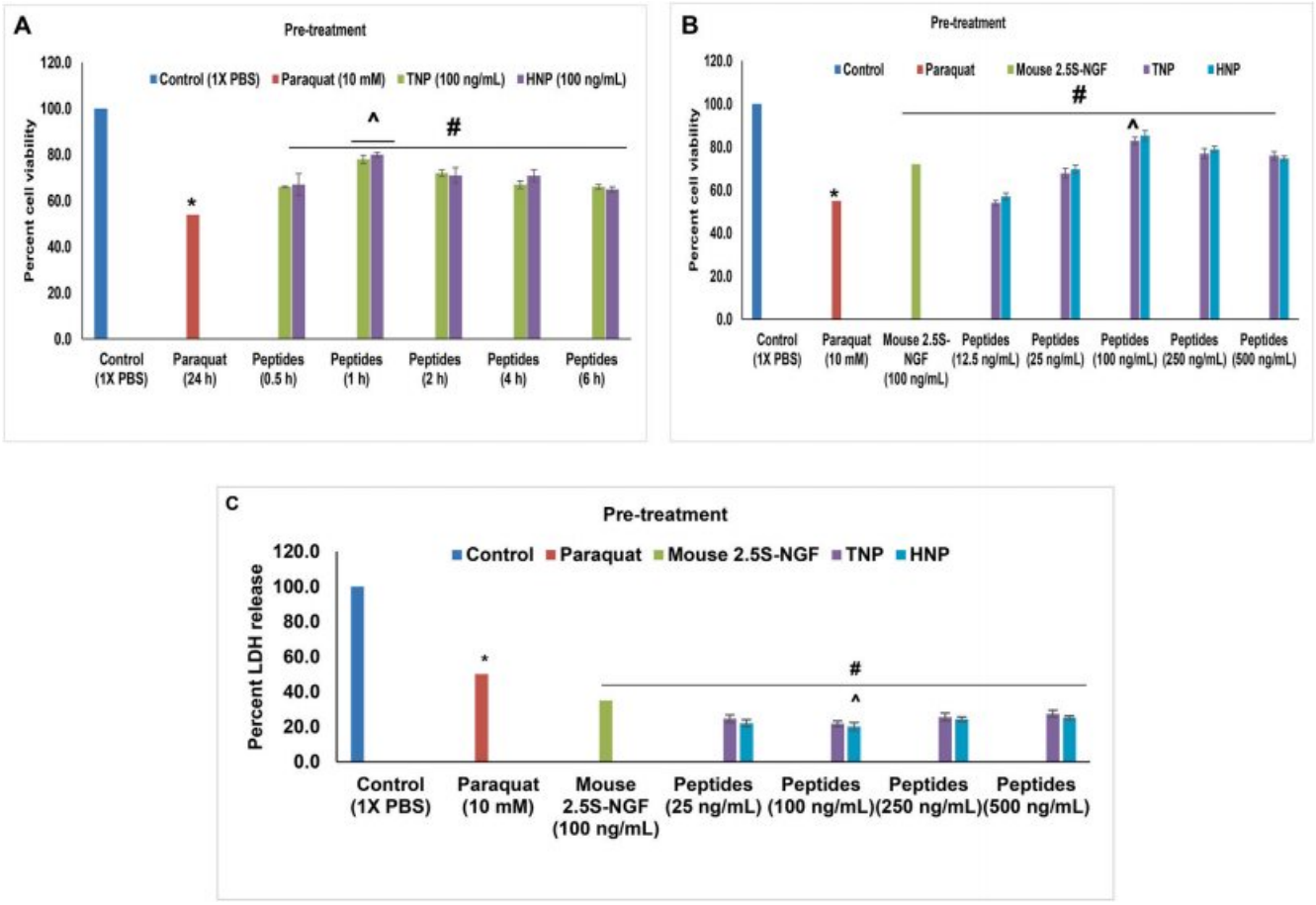

Fig. 9. Determination of the optimum time and doses of peptide for neuroprotective activity against PT-induced toxicity. Time and dose-dependent neuroprotective activity was determined by MTT and LDH assay in PC-12 cells. **(A)** Pre-treatment of cells with custom peptides (100 ng/mL, ~71 nM) at a different time interval (0.5 h–6 h) followed by PT treatment for 24 h at 37 °C in a CO_2 incubator. *$p \leq 0.05$, a significant difference between untreated (control) and PT-treated cells; $^{\#}p \leq 0.05$, a significant difference of PT-treated cells with respect to custom peptide (TNP and HNP) pre-treated PC-12 cells for different time interval (0.5–6 h). Significance of difference in the percent cell viability of custom peptide pre-treated cells incubated for 1 h with respect to 0.5–6 h $\hat{}p \leq 0.05$. **(B)** Pre-treatment of cells with different concentrations of custom peptides (12.5 ng/mL to 500 ng/mL) for 1 h (optimum time) followed by PT treatment for 24 h at 37 °C in a CO_2 incubator **(C)** LDH release assay to determine the protective effects of custom peptides on the LDH release of PT-induced PC-12 cell cytotoxicity when pre-treated with different concentrations of custom peptides (25 ng/mL to 500 ng/mL) for 1 h for 24 h at 37 °C in a CO_2 incubator. *$p \leq 0.05$, a significant difference between untreated (control) and PT-treated cells; $^{\#}p \leq 0.05$, a significant difference of PT-treated cells with respect to custom peptide (TNP and HNP) pre-treated PC-12 cells for different time interval (0.5–6 h). Significance of difference in the percent cell viability of custom peptide pre-treated cells at the dose of 100 ng/mL of with respect to 12.5–500 ng/mL, $\hat{}p \leq 0.05$. Values are mean ± SD of triplicate determinations.

3.6. Inhibition of PT-induced ROS production in PC-12 cells

The custom peptides TNP and HNP demonstrated increased antioxidant activity in an increasing concentration-dependent manner up to 100 ng/mL (Fig. 10A). The custom peptide-mediated reduction in intracellular ROS generation in PC-12 cells was determined by flow cytometry analysis (Fig. 10B–E). The data shows a significant increase ($p \leq 0.05$) in intracellular ROS production (2.1-fold-change) in PT-treated PC-12 cells compared to control PC-12 cells. Nevertheless, pre-treatment of PC-12 cells with 100 ng/mL (~71 nM) of TNP or HNP significantly diminished (1.6–1.8-fold-change) the ROS production (Fig. 10E). HNP, compared to TNP, showed superior potency (0.23-fold decrease compared to the custom peptide TNP; $p \leq 0.05$) in inhibiting the PT-induced ROS generation (Fig. 10B–E).

Spectrofluorometric analysis also validated the custom peptide-mediated reduction in intracellular ROS generation in PC-12 cells. PT treatment (10 mM) resulted in a 2-fold increase in ROS production compared to control PC-12 cells (Supplementary Fig. S4. A significant decrease ($p \leq 0.05$) in ROS levels with increasing concentration of peptides was observed in PC-12 cells pre-treated with HNP or TNP (up to 100 ng/mL, equivalent to 71 nM), compared to PT-treated PC-12 cells (Supplementary Fig. S4). Nevertheless, above this concentration, the PT-induced ROS production could not be decreased by the peptides (Supplementary Fig. S4). The custom peptides at a concentration of 100 ng/mL (~71 nM) demonstrated superior inhibition (0.6–0.8-fold decrease) ($p \leq 0.05$) of the PT-induced ROS generation, compared to that offered by Vitamin C (positive control) (0.3-fold decrease) at a higher concentration (10000 ng/mL).

3.7. Inhibition of PT-induced depolarization of mitochondrial membrane in PC-12 cells

JC-1 staining was used to study whether or not the custom peptides could restore the loss of mitochondrial membrane potential (MMP) triggered by PT in PC-12 cells. JC-1 signals red fluorescence in non-apoptotic cells as it forms an aggregate when it penetrates into non-apoptotic cells, but it signals green fluorescence as the monomeric form in apoptotic cells. The red/green fluorescence ratio was quantified from confocal images to show the change in MMP (Fig. 11A–B). The fluorescence intensity of the red/green ratio was significantly reduced ($p \leq 0.05$) by 90% in PT-treated cells, compared to control (1XPBS) PC-12 cells (Fig. 11B). The fluorescence intensity of the red/green ratio was

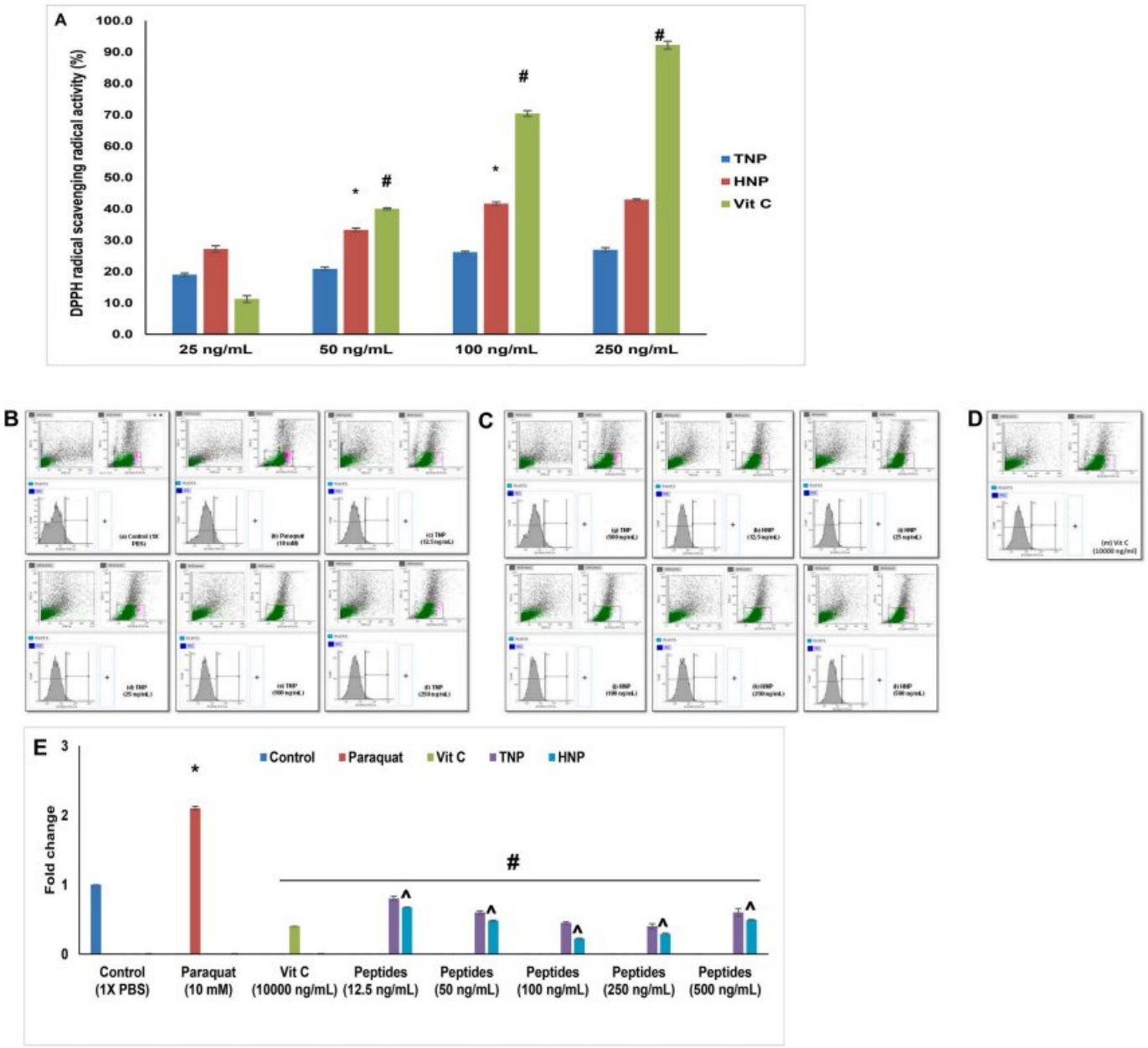

Fig. 10. Determination of PT-induced intracellular ROS generation and its reversal by pre-treatment with custom peptide (12.5 ng/mL to 500 ng/mL) and vit C (positive control, 10000 ng/mL) for 1 h followed by the PT treatment for 24 h at 37 °C in a CO_2 incubator. The ROS generation was determined by using an H_2DCFDA fluorescence probe and expressed as fold change value with respect to the control (1x PBS). **(A)** Determination of *in vitro* concentration-dependent (25–250 ng/mL) DPPH radical-scavenging activity of custom peptides. *$p < 0.05$ significant difference between different concentrations of custom peptide HNP; $^{\#}p < 0.05$ significant difference between the different concentrations of vit C. **(B–D)** Flow cytometric determination of intracellular ROS. **(E)** Bar graph representing quantitative analysis of the intracellular ROS generation (expressed by fold change value with respect to control) determined by flow cytometry analysis. *$p \leq 0.05$, a significant difference between untreated (control) and PT-treated cells; $^{\#}p \leq 0.05$, a significant difference of PT-treated cells with respect to custom peptides (TNP and HNP) and vit C pre-treated cells. Significance of difference in the fold change value in between TNP and HNP at the dose of 12.5–100 ng/mL, $^{\wedge}p \leq 0.05$. Values are mean ± SD of triplicate determinations.

significantly restored ($p \leq 0.05$) by 60–65% when PC-12 cells were pre-treated for 1 h with the TNP or HNP custom peptides and then followed by PT-treatment (Fig. 11A–B). This data suggests that pre-treatment with TNP/HNP increases the cell resistance against PT-induced mitochondrial membrane depolarization. Moreover, HNP showed a significantly higher (0.4-fold increase) inhibition ($p \leq 0.05$) of MMP, when compared to TNP.

MMP was also quantified by flow cytometry analysis using JC-1 staining. Red fluorescence is high when MMP is high, and green fluorescence is high when MMP is low. The PT-treated (10 mM) PC-12 cells showed an increase of 50% in green fluorescence, compared to the untreated PC-12 cells, indicating a disrupted MMP. Custom peptide pre-treatment (100 ng/mL, ~71 nM) resulted in a significant 40–45% increase ($p \leq 0.05$) in the intensity of red fluorescence, when compared to the PC-12 cells that were only PT-treated (Fig. 11C–D). The data showed a significant increase ($p \leq 0.05$) in mitochondrial membrane depolarization in the PT-treated PC-12 cells (2-fold decrease in red/green fluorescence) compared to the control PC-12 cells. Nevertheless, pre-treating PC-12 cells with TNP or HNP restored (1.3–1.7-fold increase in the red/green fluorescence) the PT-induced mitochondrial membrane depolarization, and HNP showed a significantly ($p \leq 0.05$) higher (0.4-fold) activity compared to TNP (Fig. 11C–D).

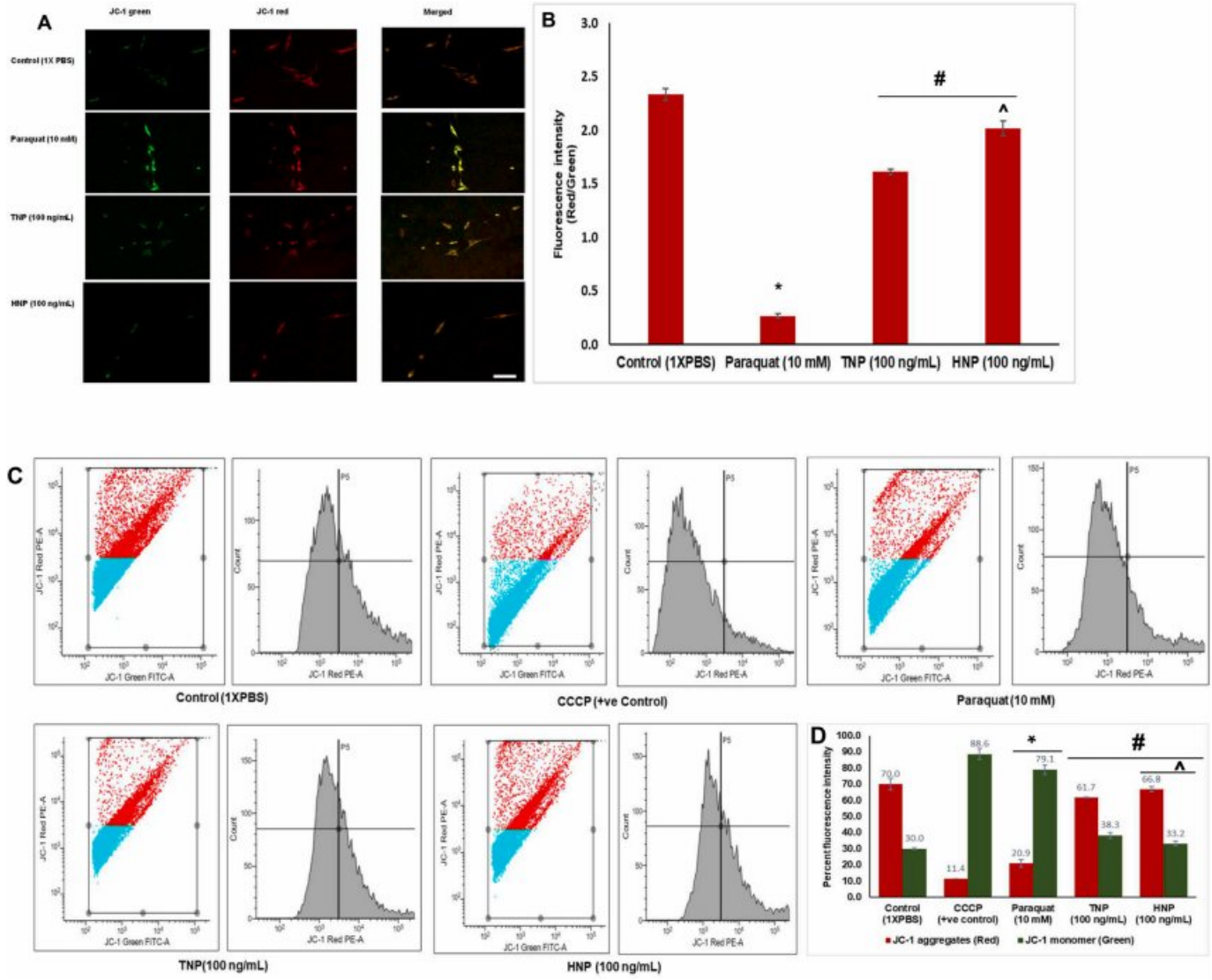

Fig. 11. Reversal of PT-induced disruption of mitochondrial membrane potential (MMP) of PC-12 cells pre-treated with custom peptides (100 ng/mL, ~71 nM) for 1 h followed by the PT treatment for 24 h at 37 °C in a CO_2 incubator. The PT-treated (10 mM) PC-12 cells pre-treated with or without custom peptide (~71 nM) were observed for the measurement of the ratio of red/green fluorescence intensity by JC-1 staining. **(A)** Confocal images of PC-12 cells stained with JC-1 dye to measure the MMP micrographed at the magnification of 40X. JC-1 red fluorescence represents normal MMP, whereas JC-1 green fluorescence indicates damaged MMP. The scale bar indicates the length as 20 μm. **(B)** Bar diagram representing the ratio of red/green fluorescence intensity quantified using Image J software. **(C)** The fluorescence signal intensity of JC-1 monomer and JC-1 aggregates was determined by flow cytometry analysis. Carbonyl cyanide m-chlorophenyl hydrazone (CCCP) is a mitochondrial uncoupling agent that depolarises the mitochondria taken as a positive control. **(D)** Bar graph representing quantitate analysis of the red and green fluorescence intensity detected by the flow cytometry. *$p \leq 0.05$, a significant difference between untreated (control) and PT-treated cells; $^{\#}p \leq 0.05$, a significant difference of PT-treated cells with respect to custom peptides (TNP and HNP) pre-treated cells. Significance of difference in fluorescence intensity between TNP and HNP, $^{\wedge}p \leq 0.05$. Values are mean ± SD of triplicate determinations. (For interpretation of the references to color in this figure legend, the reader is referred to the Web version of this article.)

3.8. Restoration of PT-induced cellular and nuclear morphological changes and apoptotic cells by the custom peptide pre-treated PC-12 cells

The anti-apoptotic potential of custom peptides (100 ng/mL, ~71 nM) against PT-induced (10 mM) apoptotic cell death was determined by flow cytometry analysis (Fig. 12A–B). PT (10 mM) induced a significant increase ($p \leq 0.05$) (10–11%) in apoptotic cell death, compared to untreated (control) PC-12 cells (Fig. 12A–B). HNP and TNP; however, at a concentration of 100 ng/mL (~71 nM) significantly inhibited ($p \leq 0.05$) apoptotic and necrotic cell death (by 5–7%), when compared to PC-12 cells that had only been PT-treated (Fig. 12A–B), and like previous analyses, HNP showed 3.3%increase in activity than TNP.

Confocal image analysis revealed a decrease in the population of PT-treated PC-12 cells, compared to untreated (control) PC-12 cells (Supplementary Fig. S5A). Induction of cell death by PT in the PC-12 cells was evident from the cell morphology (DAPI staining), shrunken nuclei, membrane blebbing, and secondary cellular necrosis (Supplementary Fig. S5A). The percent of cell death characterized by cellular and nuclear morphological changes increased by 21% when cells were treated with PT, but the pre-treatment with custom peptides significantly reduced ($p \leq 0.05$) the degree of cell death (4.6–7.9%). HNP showed a higher activity compared to TNP (Supplementary Fig. S5B).

3.9. Custom peptide pre-treatment restored the paraquat-induced upregulated and downregulated pro- and anti-apoptotic genes to delay paraquat-induced programmed cell death in PC-12 cells

The qRT-PCR analysis demonstrated a 1.5 to 2-fold-change increase

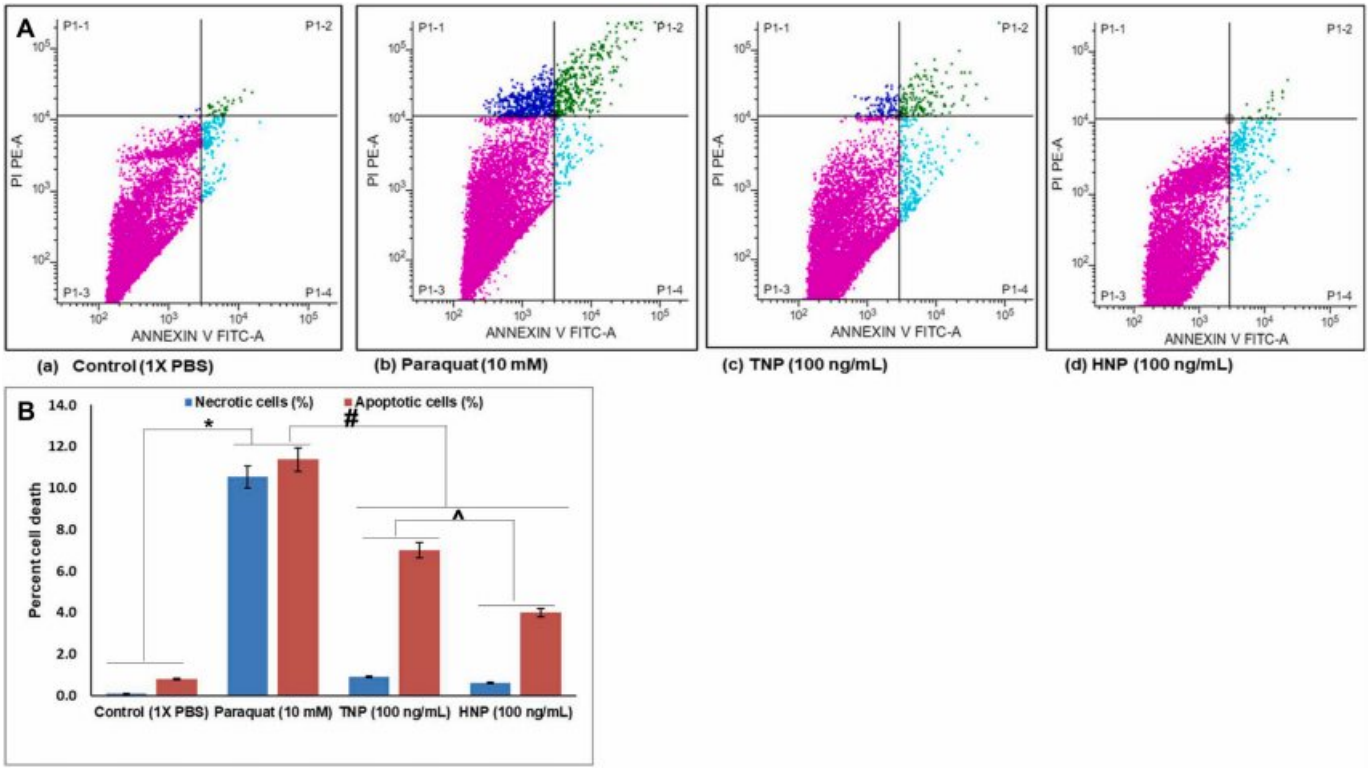

Fig. 12. Effects of the custom peptide (100 ng/mL) on inhibition of PT-induced apoptosis in PC-12 cells pre-treated with custom peptides (100 ng/mL, ~71 nM) for 1 h followed by the PT treatment for 24 h at 37 °C in a CO_2 incubator. **(A)** The fluorescence intensity of Annexin V-FITC and Propidium iodide (PI) was determined by flow cytometry. **(B)** The bar graph represents a quantitative analysis of the percent cell death determined by flow cytometry analysis. *$p \leq 0.05$, a significant difference between untreated (control) and PT-treated cells; $^{\#}p \leq 0.05$, a significant difference of PT-treated cells with respect to custom peptides (TNP and HNP) pre-treated cells. Significance of difference in percent cell death between TNP and HNP, $\hat{}p \leq 0.05$. Values are mean ± SD of triplicate determinations.

($p \leq 0.05$) in the expression of proapoptotic genes (cyt-C, bax, bid), and 3.4–3.5-fold change increase in the expression of heat shock gene-70 (hsp-70), and caspase-3 gene (a hallmark of apoptosis) in the PT group compared to the CT group of cells (Fig. 13). The pre-treatment of cells with mouse 2.5S-NGF (positive control) and TNP or HNP resulted in a significant downregulation ($p \leq 0.05$) or restoration of the expression of the genes that had been upregulated by PT treatment alone (Fig. 13). The qRT-PCR analyses showed 0.3-fold decrease in the expression of anti-apoptotic genes (bcl-2) in the PT group compared to the CT group of cells. Further, pre-treatment with TNP or HNP, and mouse 2.5S-NGF (positive control) restored the downregulated anti-apoptotic (bcl-2) genes in the PT group of cells (Fig. 13).

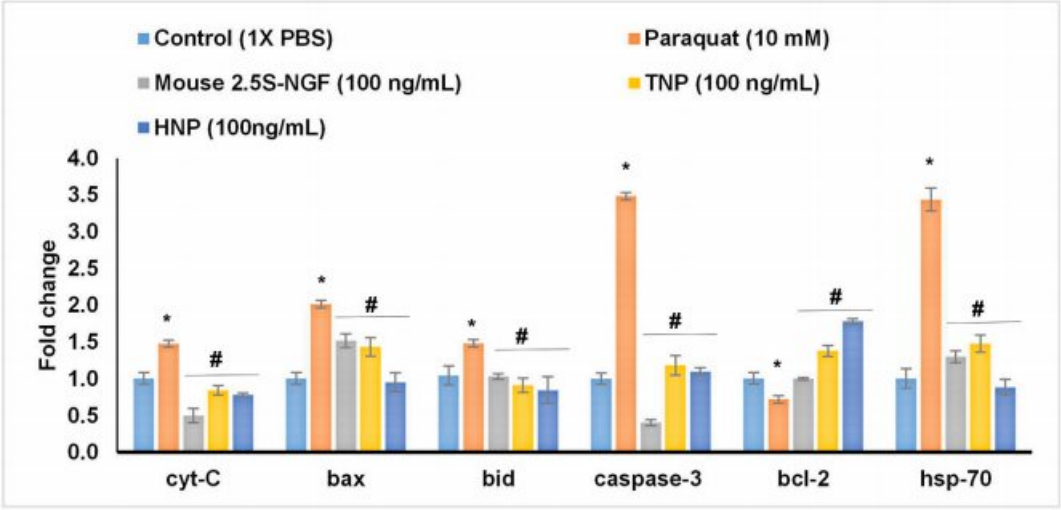

Fig. 13. The qRT-PCR analysis to show the expression of key pro-/anti-apoptotic genes in PC-12 cells post-treatment with paraquat (10 mM) for 12 h, and comparison with the custom peptides (100 ng/mL, ~71 nM)/mouse 2.5S-NGF (positive control, 100 ng/mL) pre-treatment for 1 h followed by the PT treatment for 12 h at 37 °C in a CO_2 incubator. The expression of mRNA was normalized using the house-keeping gene gapdh. *$p \leq 0.05$, a significant difference between untreated (control) and PT-treated cells; $^{\#}p \leq 0.05$, a significant difference of PT-treated cells with respect to custom peptides (TNP and HNP)/mouse 2.5S-NGF pre-treated cells. Values are mean ± SD of triplicate determinations.

3.10. Comparing the differential expression of cellular proteins in the PT-treated PC-12 cells and the cells pre-treated with custom peptides by quantitative mass spectrometry

LC-MS/MS analysis unambiguously identified 207 non-redundant proteins from the four groups of PC-12 cells (PT, PHNP, CT, and HNP). Based on their intracellular locations and biological processes, the proteins were classified into nine distinct categories, among which three major cellular proteins were present in high relative abundances compared to the other proteins (Table 2).

The quantitative analysis showed differential expression of proteins in the PT group of PC-12 cells versus the CT group. A total of 130 intracellular proteins were identified in the PT group (Fig. 14A), of which 118 proteins were differentially regulated compared to those in the CT group (Fig. 14A). Among the 118 identified proteins, the PT-induced altered expression of 27 proteins was restored in PC-12 cells that had been pre-treated with HNP (Fig. 14A). Notably, six intracellular proteins were regulated differently in the PHNP and PT groups (Fig. 14A). Two proteins (keratin type 1 and type 2 cytoskeletal proteins) were uniquely expressed in the PHNP group.

Intracellular proteins in the PHNP group were also compared in the PT and CT groups to identify differentially expressed proteins involved in apoptosis (60 kDa heat shock protein (hsp-60), cytochrome C (cycs), Heat shock cognate 71 kDa (hspa8), the electron transport chain (cytochrome *c* oxidase subunit 5A; cox5a), cytochrome *b-c*1 complex subunit 2 (uqcrc2) stress response (heat shock protein (hsp 90-beta), antioxidant function (peroxiredoxin-4 (prdx-4), glutamate dehydrogenase 1 (glud-1), Wnt signaling (actin, (actc1), signal transduction (cytoskeleton-associated protein 4, (ckap4), the innate immune response annexin A2 (anaxa2), collagen biosynthesis (collagen-binding protein (serpinh1), and phagocytosis (cathepsin B (ctsb). PT treatment of the PC-12 cells caused the upregulation of some proteins involved in these pathways (Table 3A), and their expression was restored in the PHNP treatment group. Their fold-change values are mentioned in Table 3A. In contrast, some proteins involved in neuronal development and ATP synthesis pathways were downregulated (Table 3B), though their expression was restored in the PHNP group (Table 3B). When comparing the expression of intracellular proteins in the HNP to the CT group of cells, 14 proteins were found to be uniquely expressed in the former group (Fig. 14B). Therefore, the proteomic analyses provide evidence of uniquely expressed proteins and their associated metabolic pathways in PC-12 cells treated with HNP, in comparison to untreated cells (Table 4).

The PPI network revealed the functional significance of the intracellular proteins and their involvement in particular pathways (Fig. 15). The cellular pathways governed by the 27 differentially regulated proteins in the CT, PT, and PHNP groups of PC-12 cells were curated manually and the interaction network was established to highlight the interconnected pathways (Fig. 14).

Based on the information on the neuritogenesis potency of the custom peptides, inhibition of downstream signaling pathways by specific inhibitors (MAPK-ERK, PI3K/AKT pathways), the neuroprotective potential of custom peptides (via different mechanisms such as inhibition of ROS generation, restoration of MMP, anti-apoptotic/necrotic potential), and the differential expression of proteins (determined by quantitative mass spectrometry analysis) involved in neuroprotective activities, the mechanism of action of HNP against PT-induced neuroprotective activity is shown in Fig. 16.

4. Discussion

Neuronal differentiation is a vital physiological phenomenon, often associated with intellectual development in children and age-related neurodegenerative diseases such as PD, AD, and Huntington's disease (HD) [61]. Proposing a large neurotrophin polypeptide or a protein molecule as a drug candidate has several disadvantages including its undesired pleiotropic effect, short half-life, proteolytic degradation, and poor pharmacokinetics [33,62–64]. Therefore, in recent years, the development of small, peptide-based drugs has gained momentum and opened new avenues of research to overcome the limitations of parent molecules [65]. In any case, the peptide-based drugs must show improved neuroprotective effects, synaptic and neuronal plasticity, neuritogenesis, better pharmacokinetics than their larger, parent neurotrophin molecules, and easy penetration to cells via the BBB [33,39,65,66]. In this study, two small, water-soluble custom peptides (TNP and HNP, with masses of 1.2 kDa and 1.4 kDa, respectively) were designed from snake venom neurotrophin molecules to be developed as possible neuroprotective drug prototypes with improved neuritogenesis potency, compared to mouse 2.5S-NGF (positive control) for the restoration of neurons that have been degenerated by toxic chemicals.

Several studies have demonstrated that computational analysis (docking) is a powerful tool for identifying novel compounds of therapeutic interest with high probability and which can forecast ligand-target interactions at the molecular level with high efficiency [20,21,38,50,67,68]. The computational study can assist in screening many compounds (ligands) against specific targets (i.e., a receptor) to identify compounds that can bind efficiently with the target, though *in silico* findings must be confirmed by *in vitro* and *in vivo* studies [20,21,38,50,67,68]. The *in silico* analysis demonstrated that domain-3 of the TrkA receptor extracellular domain is the only region that binds with NGF and forms the NGF/TrkA domain-3 complex. Subsequently, the complex induces TrkA dimerization and transduces a signal to activate MAPK and the PI3K/Akt signaling pathways [69]. The docking analysis also demonstrated that, like human NGF molecules, the TNP and HNP custom peptides show high-affinity binding only with domain-3 of the human TrkA receptor. The binding site for the custom peptides was also shown to differ from that of the human NGF-TrkA binding site.

Since TrkA dimerization is important for activation of the signal transduction mechanism, dimerization of the TrkA receptors after binding to custom peptides needs to be explored. The docking scores of the docked complex (custom peptide and TrkA domain-3) indicate higher binding affinities of TNP towards the TrkA domain-3, compared to that of HNP. Since binding affinity does not always correlate with the stability of the binding, the stability of binding should also be evaluated by a molecular dynamic simulation study and computational analyses. In this study, our findings predicted that HNP (compared to TNP) would form a more stable complex with the TrkA receptor. Differences in the binding affinities and stability of the custom peptides and TrkA receptors can be attributed to the electrostatic interactions (hydrogen bonds) between the charged molecules of the HNP/TrkA domain-3 complex [20,21,38].

Since the custom peptides were designed to mimic the TrkA binding region of the snake venom neurotrophin molecule, the *in silico* analysis convincingly showed that the high-affinity binding of HNP or TNP to the TrkA receptor is primarily essential for inducing neuritogenesis. The spectrofluorometric binding assay showed high-affinity binding (low K_d value in picomolar range) to the TrkA receptor expressed in mammalian cell lines (PC-12, MDA-MB-231, MCF7) but not in L6 cells, which lack TrkA receptors, which was further validated by fluorescence microscopic study. In the presence of a chemical inhibitor of the TrkA receptor (K252a), no binding was observed under a fluorescence microscope, confirming that the custom peptides bind with the TrkA receptor exclusively. These *in vitro* binding studies also validated the results of the *in silico* analysis. Further, studies have shown the Kd value of binding of mammalian NGF to TrKA receptor is also 1×10^{-11} M [23,24], indicating HNP and TNP are of equivalent potency with binding to the same receptor.

Because the *in silico* and *in vitro* binding of ligands to receptors does not necessarily assure their desired therapeutic effect, we also evaluated the neuritogenesis potency of these peptides in PC-12 cells, which is considered to be appropriate *in vitro* model for neuronal differentiation, development, and neurological diseases [20,21,38,49,70]. PC-12 cell

Table 2
The quantitative proteomics data shows the relative abundance of the intracellular proteins in the different treatment groups. The relative abundance of the proteins was calculated by MS2 based spectral count method. For comparison of differential expression of the cellular proteins, the PC-12 cells were subjected to the following treatments at 37 °C: (a) 1X PBS (control) treated PC-12 cells (CT), (b) 10 mM paraquat (PT) treatment for 24 h, (c) pre-treatment with 100 ng/mL (~71 nM) custom peptide for 1 h followed by 10 mM paraquat treatment (PHNP) for 24 h, and (d) treatment with 100 ng/mL (~71 nM) of custom peptide (HNP) for 1 h.

Accession No	Relative abundance of 1X PBS (control) treated PC-12 cells (CT)	Relative abundance of PC-12 cells pre-treated with 100 ng/mL (~71 nM) custom peptide for 1 h followed by 10 mM paraquat treatment (PHNP) for 24 h	Relative abundance of PC-12 cells treated with 10 mM paraquat (PT) for 24 h	Relative abundance of PC-12 cells treated with 100 ng/mL (~71 nM) of custom peptide (HNP) for 1 h
Antioxidant/Stress response				
P06761| BIP_RAT	0.51	0.93	3.08	0.63
P63018| HSP7C_RAT	0.51	0.80	2.51	0.62
Q07936| ANXA2_RAT	0.51	0.62	2.51	0.58
Q66HD0| ENPL_RAT	0.51	0.97	2.76	0.67
P34058| HS90B_RAT	0.51	1.02	2.51	0.60
P48679| LMNA_RAT	0.51	0.88	2.92	0.60
Q00715| H2B1_RAT	0.51	0.75	4.18	0.72
Q9Z0V5| PRDX4_RAT	0.51	0.99	2.51	0.67
Binding protein				
tr|G3V6P7| G3V6P7_RAT	0.68	0.79	2.51	0.72
P68035| ACTC_RAT	0.51	0.88	2.76	0.73
tr|Q5RJR9| Q5RJR9_RAT	0.51	0.68	2.51	0.49
P13832| MRLCA_RAT	0.51	0.87	3.34	0.67
P62804|H4_RAT	0.51	0.85	3.01	0.53
P00507| AATM_RAT	0.51	0.99	2.51	0.49
Apoptotic protein				
P63039| CH60_RAT	0.51	0.92	2.51	0.63
P62630| EF1A1_RAT	0.51	0.62	2.51	0.80
P11240| COX5A_RAT	0.51	0.99	2.51	0.49
P62898| Cycs_RAT	0.51	0.99	2.51	0.50
P00787| CATB_RAT	0.51	0.99	2.51	0.48
Mitochondrial protein				
P10860| DHE3_RAT	0.51	0.90	2.51	0.49
P04636| MDHM_RAT	0.51	0.83	2.51	0.49
P32551| QCR2_RAT	0.51	0.99	2.51	0.49
P00507| AATM_RAT	0.51	0.99	2.51	0.49
ATP synthesis				
P10719| ATPB_RAT	0.51	2.73	0.90	3.61
P15999| ATPA_RAT	0.51	2.92	0.91	3.63
Neuronal development				
Q9JLT0| MYH10_RAT	0.51	2.51	0.69	3.57
P18418| CALR_RAT	0.51	2.51	0.79	3.69
P31000| VIME_RAT	0.51	3.01	0.93	
Innate immune response				
P07150| ANXA1_RAT	0.51	0.75	2.51	0.69
P11598| PDIA3_RAT	0.51	0.81	2.51	0.49
Structural protein				
	0.51	0.76	2.51	0.63

(*continued on next page*)

Table 2 (*continued*)

Accession No	Relative abundance of 1X PBS (control) treated PC-12 cells (CT)	Relative abundance of PC-12 cells pre-treated with 100 ng/mL (~71 nM) custom peptide for 1 h followed by 10 mM paraquat treatment (PHNP) for 24 h	Relative abundance of PC-12 cells treated with 10 mM paraquat (PT) for 24 h	Relative abundance of PC-12 cells treated with 100 ng/mL (~71 nM) of custom peptide (HNP) for 1 h
Q64119|MYL6_RAT				
Endoplasmic reticulum protein				
tr|D3ZH41|D3ZH41_RAT	0.51	0.80	2.51	0.49

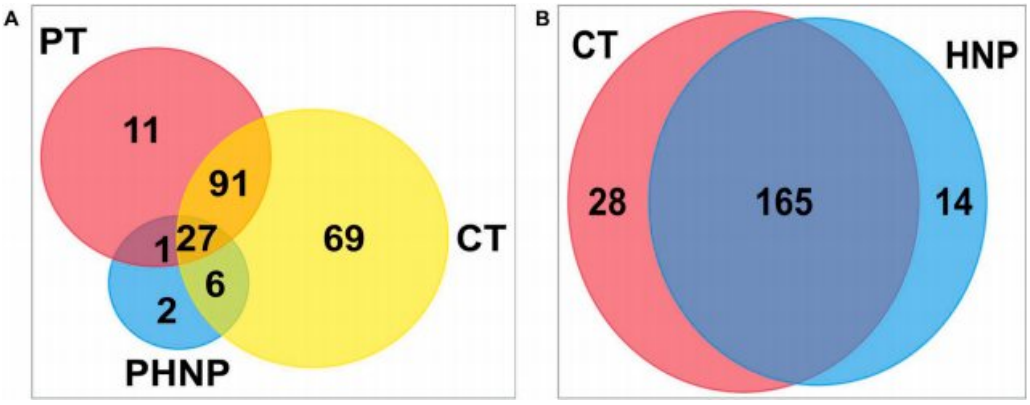

Fig. 14. (A) Venn diagram showing the common intracellular proteins among untreated (control) (CT), PT (PT) treated, and HNP pre-treated followed by PT-treated (PHNP) groups of PC-12 cells determined by LC/MS-MS analysis. **(B)** Venn diagram showing common intracellular proteins among untreated (control) (CT) and only HNP-treated PC-12 cells determined by LC/MS-MS analysis.

lines have advantages in being derived from neural crest cells with similar structures and functions, and they are easy to grow and maintain [70]. The induction of neuritogenesis is generally initiated after 4–6 h of incubation with NGF [71]; however; optimum neurite length and differentiation of PC-12 cells observed after 14 days of incubation with snake venom NGFs [20,21] TNP and HNP in this study showed the same result.

In evaluating the neuronal outgrowth-inducing properties of the custom peptides in PC-12 neuronal cells, we found that, as predicted, both peptides significantly increased the neurite length and percent differentiation of PC-12 cells measured simultaneously point, in comparison to the effect of mouse 2.5S-NGF treatment alone. No significant difference was observed between the two peptides. In previous studies, however, the neuritogenesis potency of TNP and HNP has been shown to surpass the potency of SV NGF in PC-12 cells [20,21,38] or natural polyphenols such as curcumin and resveratrol [72]. Compared to synthetic tripeptide (p-BTX-I) synthesized from *Bothrops atrox* venom [40], TNP and HNP were almost equal in their neuritogenesis potency. The reported differences in neuritogenesis potency may be due to the different experimental conditions (i.e., doses, incubation time, etc.). As mentioned, mammalian NGF and snake venom NGF-induced TrkA dimerization activates MAPK and PI3K/AKT pathway-dependent neuritogenesis [20,21,38,69]. The selective inhibition of the MAPK and PI3K/AKT pathways by U0126 and LY294002 inhibitors, respectively, provides convincing evidence of the similarity of the custom peptides to snake venom NGF molecules [20,21,38,39]. The custom peptides we developed also activate the MAPK and PI3K/AKT signalling pathways for neuronal survival and differentiation in PC-12 cells [20,21,25,26,38]. In this study, we also reported that the custom peptides lacked cytotoxicity against different cell types and did not interfere with the mammalian blood coagulation cascade, indicating a lack of side effects based on *in vitro* experiments.

A plethora of studies have reported that the pathogenesis of PD is related to oxidative stress, resulting from a homeostatic imbalance in pro-oxidant and antioxidant genes that leads to the production of excessive ROS (free radicals), which ultimately triggers apoptotic cell death [73,74]. Some non-selective herbicides (such as PT) that are frequently used by farmers in agricultural practice, cause neurotoxicity and mitochondrial toxicity, and can lead to the development of PD-like pathologies [13,75]. This study showed the neuroprotective potency of custom peptides TNP and HNP (pre-treatment conditions) in PC-12 cells by 15–20%. Further, their neuroprotective potency at a low concentration (100 ng/mL) and less incubation time (1 h) suggest that these custom peptides may have a higher effect at low concentrations compared to other natural compounds [73,77–79]. Our data also showed that both custom peptides possess similar neuroprotective effects but surpass the neuroprotective activity of mouse 2.5S-NGF (positive control) when tested at the same experimental conditions.

The antioxidant system against ROS is in dynamic balance under normal circumstances. PT induces an increase in ROS production, the oxidative stress response, mitochondrial membrane potential, induction of apoptosis, and a reduced proliferation of PC-12 cells [76,77]. Studies have already reported that natural compounds such as naringin, curcumin, resveratrol, silymarin, pirfenidone, quercetin, selenium, bacosides, and Vitamin C have a significant therapeutic potential for treating PT-induced toxicity [72,78–80]. Like these natural compounds, the custom peptides that we tested in this study have profound neuroprotective activity, and we aimed to investigate their mechanism of action. In accordance with the findings from previous studies [77], we showed that PT-treatment increases ROS production, and the custom peptide pre-treatment significantly attenuated the PT-induced ROS production, at a concentration (100 ng/mL, equivalent to 71 nM) that was 1000-times less than that of Vitamin C (positive control, 10000 ng/mL). Although Vitamin C in this study showed appreciable antioxidant activity, it did not offer protection against PT-induced neurotoxicity. This suggests that antioxidant property alone may not be sufficient to offer protection against PT-induced neuronal damage and justifies the therapeutic application of the custom peptides under study. Additional quantitative proteomic analyses demonstrated the upregulation (fold-change increase) of antioxidant proteins such as heat shock protein 90

Table 3
Comparison of the fold changes in differential expression of proteins in PT-treated PC-12 cells determined by proteomic analysis.

(A) List of up-regulated proteins in PT-treated PC-12 cells compared to untreated (control) PC-12 cells, and their downregulation in cells pre-treated with HNP.

Accession	PT treatment (fold change with respect to control)	HNP pre-treatment, (fold change with respect to control)	Pathway name	Description
P06761|BIP_RAT	6.00	1.81	Apoptosis signaling pathway	Endoplasmic reticulum chaperone BiP OS=*Rattus norvegicus* OX = 10116 GN = Hspa5 PE = 1 SV = 1
P63018|HSP7C_RAT	4.87	1.56	Apoptosis signaling pathway	Heat shock cognate 71 kDa protein OS=*Rattus norvegicus* OX = 10116 GN = Hspa8 PE = 1 SV = 1
Q07936|ANXA2_RAT	4.87	1.21	Antioxidant pathway	Annexin A2 OS=*Rattus norvegicus* OX = 10116 GN = Anxa2 PE = 1 SV = 2
Q66HD0|ENPL_RAT	5.36	1.88	Stress response pathway	Endoplasmin OS=*Rattus norvegicus* OX = 10116 GN = Hsp90b1 PE = 1 SV = 2
P34058|HS90B_RAT	4.87	1.99	Stress response pathway	Heat shock protein HSP 90-beta OS=*Rattus norvegicus* OX = 10116 GN = Hsp90ab1 PE = 1 SV = 4
P48679|LMNA_RAT	5.68	1.71	Apoptosis signaling pathway	Prelamin-A/C OS=*Rattus norvegicus* OX = 10116 GN = Lmna PE = 1 SV = 1
Q00715|H2B1_RAT	8.12	1.46	Stress response pathway	Histone H2B type 1 OS=*Rattus norvegicus* OX = 10116 PE = 1 SV = 2
Q9Z0V5|PRDX4_RAT	4.87	1.93	Stress response pathway	Peroxiredoxin-4 OS=*Rattus norvegicus* OX = 10116 GN = Prdx4 PE = 2 SV = 1
tr|G3V6P7|G3V6P7_RAT	3.69	1.16	Phagocytosis	Myosin, heavy polypeptide 9, non-muscle OS=*Rattus norvegicus* OX = 10116 GN = Myh9 PE = 1 SV = 1
P68035|ACTC_RAT	5.36	1.81	Wnt signalling pathway	Actin, alpha cardiac muscle 1 OS=*Rattus norvegicus* OX = 10116 GN = Actc1 PE = 2 SV = 1
tr|Q5RJR9|Q5RJR9_RAT	4.87	1.71	Collagen biosynthesis	Collagen-binding protein OS=*Rattus norvegicus* OX = 10116 GN = Serpinh1 PE = 1 SV = 1
P13832|MRLCA_RAT	6.50	1.33	Cell cycle	Myosin regulatory light chain RLC-A OS=*Rattus norvegicus* OX = 10116 GN = Rlc-a PE = 2 SV = 2
P62804|H4_RAT	5.85	1.69	Transcription regulation	Histone H4 OS=*Rattus norvegicus* OX = 10116 GN = H4c2 PE = 1 SV = 2
P00507|AATM_RAT	4.87	1.65	Asparagine and aspartate biosynthesis	Aspartate aminotransferase, mitochondrial OS=*Rattus norvegicus* OX = 10116 GN = Got2 PE = 1 SV = 2
P63039|CH60_RAT	4.87	1.78	Apoptosis signaling pathway	60 kDa heat shock protein, mitochondrial OS=*Rattus norvegicus* OX = 10116 GN = Hspd1 PE = 1 SV = 1
P62630|EF1A1_RAT	4.87	1.21	Protein biosynthesis	Elongation factor 1-alpha 1 OS=*Rattus norvegicus* OX = 10116 GN = Eef1a1 PE = 2 SV = 1
P11240|COX5A_RAT	4.87	1.93	Electron transport chain	Cytochrome *c* oxidase subunit 5A, mitochondrial OS=*Rattus norvegicus* OX = 10116 GN = Cox5a PE = 1 SV = 1
P62898|Cycs_RAT	4.87	1.93	Apoptosis signaling pathway	Cytochrome *c* OS=*Rattus norvegicus* OX = 10116 GN = Cycs PE = 3 SV = 1
P00787|CATB_RAT	4.87	1.93	Phagocytosis	Cathepsin B OS=*Rattus norvegicus* OX = 10116 GN = Ctsb PE = 1 SV = 2
P10860|DHE3_RAT	4.87	1.75	Antioxidant	Glutamate dehydrogenase 1, mitochondrial OS=*Rattus norvegicus* OX = 10116 GN = Glud1 PE = 1 SV = 2
P04636|MDHM_RAT	4.87	1.61	Pyruvate metabolism	Malate dehydrogenase, mitochondrial OS=*Rattus norvegicus* OX = 10116 GN = Mdh2 PE = 1 SV = 2
P32551|QCR2_RAT	4.87	1.93	Electron transport chain	Cytochrome *b-c*1 complex subunit 2, mitochondrial OS=*Rattus norvegicus* OX = 10116 GN = Uqcrc2 PE = 1 SV = 2
P07150|ANXA1_RAT	4.87	1.45	Innate immune response	Annexin A1 OS=*Rattus norvegicus* OX = 10116 GN = Anxa1 PE = 1 SV = 2
P11598|PDIA3_RAT	4.87	1.58	Vitamin D metabolism	Protein disulfide-isomerase A3 OS=*Rattus norvegicus* OX = 10116 GN = Pdia3 PE = 1 SV = 2
Q64119|MYL6_RAT	4.87	1.48	Motor function	Myosin light polypeptide 6 OS=*Rattus norvegicus* OX = 10116 GN = Myl6 PE = 1 SV = 3
tr|D3ZH41|D3ZH41_RAT	4.87	1.55	Signal transduction	Cytoskeleton-associated protein 4 OS=*Rattus norvegicus* OX = 10116 GN = Ckap4 PE = 1 SV = 2

(B) List of down-regulated proteins in PT treated PC-12 cells compared to untreated (control) PC-12 cells and their upregulation in cells pre-treated with HNP.

Accession	**Paraquat treatment (fold change with respect to control)**	**HG17 pre-treatment, (fold change with respect to control)**	**Pathway name**	**Description**
P10719|ATPB_RAT	1.76	3.02	ATP synthesis	ATP synthase subunit beta, mitochondrial OS=*Rattus norvegicus* OX = 10116 GN = Atp5f1b PE = 1 SV = 2
P15999|ATPA_RAT	1.77	3.22	ATP synthesis	ATP synthase subunit alpha, mitochondrial OS=*Rattus norvegicus* OX = 10116 GN = Atp5f1a PE = 1 SV = 2
Q9JLT0|MYH10_RAT	1.34	3.63	Neuronal development	Myosin-10 OS=*Rattus norvegicus* OX = 10116 GN = Myh10 PE = 1 SV = 1
P18418|CALR_RAT	1.54	3.17	Neuronal development	Calreticulin OS=*Rattus norvegicus* OX = 10116 GN = Calr PE = 1 SV = 1
P31000|VIME_RAT	1.05	5.85	Neuronal development	Vimentin OS=*Rattus norvegicus* OX = 10116 GN = Vim PE = 1 SV = 2
O08878|GPER1_RAT	1.20	3.40	Neuritogenesis	G-protein coupled estrogen receptor 1 OS=*Rattus norvegicus* OX = 10116 GN = Gper1 (Cmkrl2, Gper, Gpr30, Gpr41) SV = 2

Table 4
List of the uniquely expressed metabolic pathways in PC-12 cells treated with HNP when compared to untreated PC-12 cells. These pathways are determined by quantitative proteomic analyses.

Mapped IDs	Pathway name	Protein
RAT|RGD = 71000|UniProtKB = Q9JLT0, RAT|RGD = 1565476| UniProtKB = Q6P9V9	Cytoskeletal regulation by Rho GTPase	Tuba1b, Plec
RAT|RGD = 2451|UniProtKB = P62898, RAT|RGD = 621379| UniProtKB = Q06647, RAT| RGD = 68374|UniProtKB = P10888	ATP synthesis	Cycs, Cox4i1, Atp5
RAT|RGD = 71000|UniProtKB = Q9JLT0	Nicotinic acetylcholine receptor signalling pathway	Myh10
RAT|RGD = 71000|UniProtKB = Q9JLT0	Inflammation mediated by chemokine and cytokine signalling pathway	Myh10
RAT|RGD = 1565476|UniProtKB = Q6P9V9	Gonadotropin-releasing hormone receptor pathway	Tuba1b
RAT|RGD = 71006|UniProtKB = Q63692, RAT|RGD = 1305960| UniProtKB = Q498E0	Stress response antioxidant pathway	Txndc12, Plec

(hsp90), peroxiredoxin (prdx4), and glutamate dehydrogenase (glud1) in PT-treated PC-12 cells. These genes are reported to play an important role in the oxidative deamination and reduction of free radicals [81,82]. The increased ROS production in the PT group was validated by the upregulation of antioxidant proteins, and the activity of the custom peptides to attenuate the ROS production was confirmed by the down-regulation of the same proteins in the PHNP group.

Mitochondrial dysfunction is another crucial phenomenon involved in the pathogenesis of PD, which is caused by oxidative stress [74,83]. Oxidative stress eventually leads to the loss of MMP, which results in the release of cytochrome C (pro-apoptotic protein) from the mitochondria and activation of the caspase cascade that induces cellular apoptosis [76,77,84,85]. Studies have shown that preventing the mitochondrial dysfunction may be a therapeutic strategy for avoiding cell death [86]. In this study, we showed that pre-treatment of PC-12 cells with custom peptides significantly restored the depolarization of PT-induced MMP, which points to the neuroprotective property of custom peptides to maintain mitochondrial health and balance the expression of apoptotic proteins.

Due to the high energy demand of neuronal cells, they can be vulnerable to extensive mitochondrial damage, which can lead to nerve cell injury and death [86]. Different cellular pathways are involved in maintaining mitochondrial homeostasis and integrity, like the rapid translation of mitochondrial protein, pathways involved in autophagy, energy (ATP) production via oxidative phosphorylation, amino acid synthesis, fat metabolism, and other biochemical pathways [74,87]. Together, these pathways maintain mitochondrial homeostasis by replacing defective mitochondria with new organelles that subsequently prevent neurodegeneration and show neuroprotective effects [88]. The proteomic analyses indicated that HNP pre-treatment restored the PT-induced upregulated genes and proteins involved in mitochondrial stress response pathways, such as glutamate dehydrogenase 1 (glud1) and glutamic-oxaloacetic transaminase (got2) involved in the mitochondrial redox balance [82,89]. To help maintain cellular integrity, HNP pre-treatment restored the upregulation of pro-apoptotic proteins in the PT group, such as cytochrome C (cyt-C), heat shock protein 60 (hspd1, GO:0043065), heat shock protein 70 (hspa5, GO:1903265). These proteins are reported to participate in the mitogen-activated protein kinase (p38/MAPK) signaling pathways, which are coupled to the oxidative stress response [90]. The global proteomic studies of snake venom NGF treated PC-12 cells had revealed about the oxidative stress-mediated apoptosis [20,21,38]. Moreover, the release of mitochondrial cyt-C into the cytoplasm in response to pro-apoptotic signals

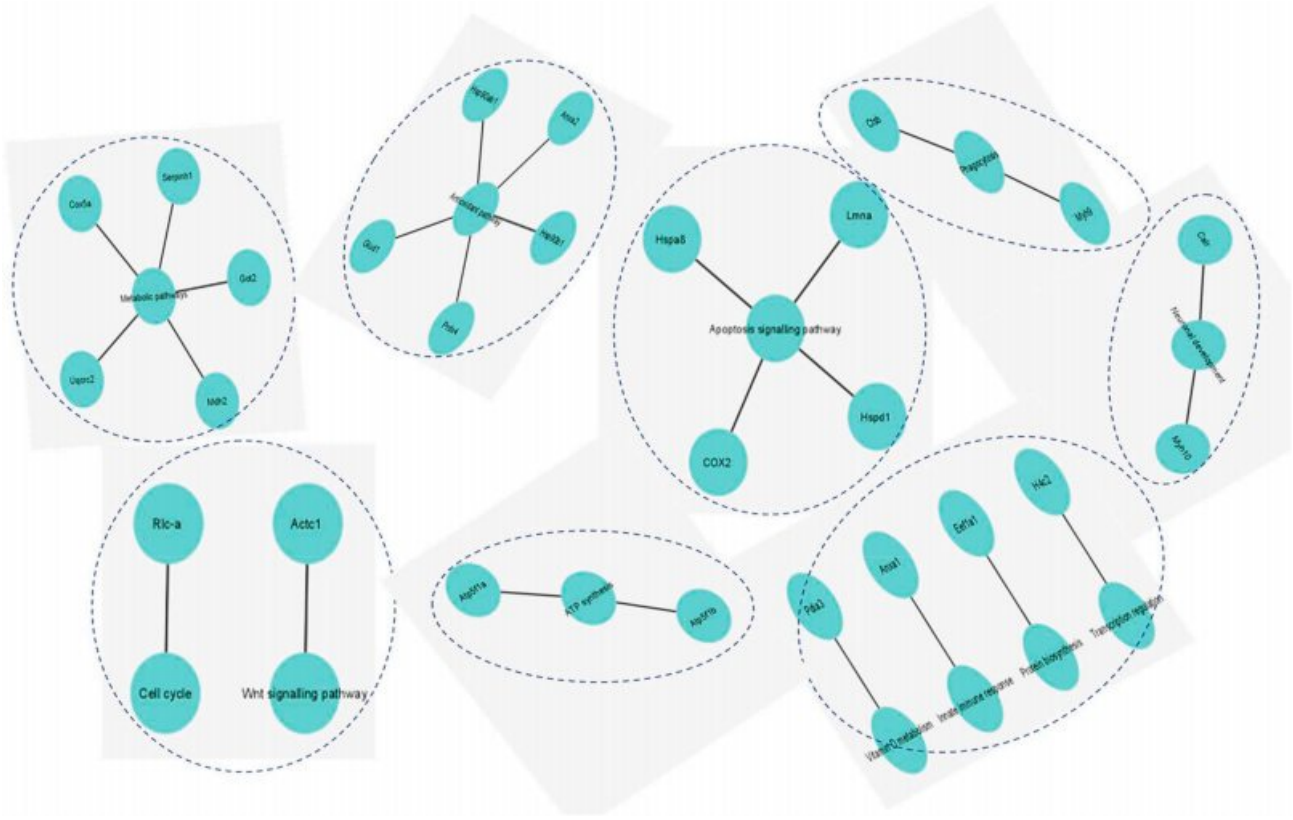

Fig. 15. Molecular network of HNP-mediated neuroprotection drawn in Cytoscape (version 3.9.1). The molecular network shows the multiple pathways which are interconnected to each other and involved in the HNP-mediated neuroprotection. The protein involved in the pathways were determined by LC/MS-MS analysis.

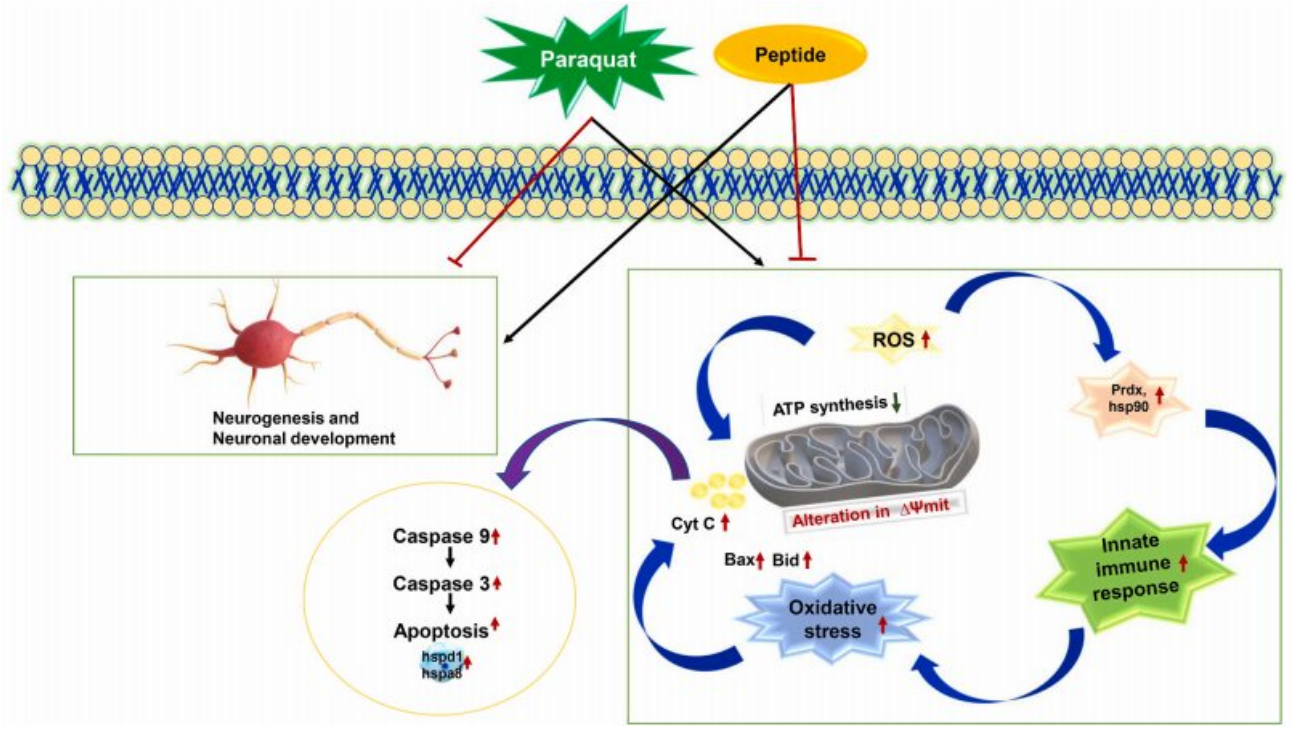

Fig. 16. The proposed neuroprotection mechanism of custom peptides against PT-induced neurotoxicity in PC-12 cells.

(bax, bid) and the activation of caspase-3 (cas-3) leads to apoptotic cell death [3,45,53]. In this study, the qRT-PCR analysis showed the downregulation of anti-apoptotic gene (bcl-2) expression and the upregulation of pro-apoptotic genes (cyt-C, bax, bid, hsp-70, and cas-3) in PT-treated PC-12 cells, which triggered cell death. The custom peptide pre-treatment restored the gene expression of the pro-/anti-apoptotic genes suggesting the therapeutic potency of the peptides to prevent PT-induced premature apoptosis in PC-12 cells.

The PT group of cells also showed upregulation of genes involved in detoxification (myh9 and ctsb) [91,92], the TCA cycle (cox5a and uqcrc2) [93,94] and the innate immune response (anxa1) [95], which were downregulated in the PHNP group of cells. As mentioned before, more energy is required to maintain mitochondria against oxidative stress, so the upregulation of these proteins is essential for the neuroprotective effect [86]. Our findings also suggest the upregulation of proteins involved in energy production by ATP synthesis via oxidative phosphorylation, such as the ATP synthase F1 subunit beta, alpha (atp5f1b and atp5f1a) [96] in HNP pre-treated cells, compared to the PT group of cells. In addition, HNP pre-treatment showed a neuroprotective effect by counteracting the PT-induced downregulation of proteins directly or indirectly involved in neural development (myh10 and vim) and neuritogenesis [97] (gper1, cmkrl2, gper, gpr30, and gpr41) [97] (GO:0007399, GO:0019228).

A molecular network was constructed to show the multiple pathways that are interconnected and involved in HNP-mediated neuroprotection. Based on our experimental results, an overall neuroprotective mechanism was proposed for the action of the custom peptides against PT-induced neuronal damage (Fig. 16).

5. Conclusion

Developing safe and effective neuroprotective drugs is still a challenge. In this study, we showed that our designed custom peptides, derived from snake venom neurotrophin molecules, can protect PC-12 cells from PT-induced neurotoxicity. The custom peptides counteract PT-induced neurotoxicity by thwarting excessive ROS production, oxidative stress, MMP, and premature apoptotic death. Our findings provide a greater understanding of the altered expression of proteins involved in the neurodegeneration pathways in the PT-induced PD model of PC-12 cells and how the expression of our custom peptides can be used in treatments. Our findings provide a fundamental basis for developing new agents that specifically target neurodegenerative diseases, especially PD, and encourage future, in-depth investigations through *in vivo*, pharmacokinetic, and pharmacodynamic studies for the successful development of safe drug prototypes.

Acknowledgments

The authors thank C-CAMP, NCBS, Bangalore, for LC-MS/MS analysis, Dr. S. S. Ghosh, and Ms. M. Saha, IIT, Guwahati for CD analysis. DM received SRF from the SERB project, and AP received a postdoctoral fellowship from IASST. This work was funded by the Science and Engineering Research Board, New Delhi (EMR/2017/001829) and partially contributed from the core research grant of IASST to AKM.

Appendix A. Supplementary data

Supplementary data to this article can be found online at https://doi.org/10.1016/j.freeradbiomed.2023.01.019.

References

[1] M.F. Schmidt, Z.Y. Gan, D. Komander, G. Dewson, Ubiquitin signalling in neurodegeneration: mechanisms and therapeutic opportunities, Cell Death Differ. 28 (2) (2021) 570–590.
[2] C.-W. Tsai, R.-T. Tsai, S.-P. Liu, C.-S. Chen, M.-C. Tsai, S.-H. Chien, H.-S. Hung, S.-Z. Lin, W.-C. Shyu, R.-H. Fu, Neuroprotective effects of betulin in pharmacological and transgenic *Caenorhabditis elegans* models of Parkinson's disease, Cell Transplant. 26 (12) (2017) 1903–1918.
[3] P. Sanphui, S.K. Pramanik, N. Chatterjee, P. Moorthi, B. Banerji, S.C. Biswas, Efficacy of cyclin dependent kinase 4 inhibitors as potent neuroprotective agents against insults relevant to Alzheimer's disease, PLoS One 8 (11) (2013), e78842.
[4] C. Blauwendraat, M.A. Nalls, A.B. Singleton, The genetic architecture of Parkinson's disease, Lancet Neurol. 19 (2) (2020) 170–178.
[5] P. Chalorak, T. Sanguanphun, T. Limboonreung, K. Meemon, Neurorescue effects of frondoside A and ginsenoside Rg3 in C. elegans model of Parkinson's disease, Molecules 26 (16) (2021) 4843.

[6] T. Long, Q. Wu, J. Wei, Y. Tang, Y.-N. He, C.-L. He, X. Chen, L. Yu, C.-L. Yu, B.Y.-K. Law, Ferulic acid exerts neuroprotective effects via autophagy induction in *C. elegans* and cellular models of Parkinson's disease, Oxid. Med. Cell. Longev. (2022) 2022.

[7] P. Tagliaferro, R.E. Burke, Retrograde axonal degeneration in Parkinson disease, J. Parkinsons Dis. 6 (1) (2016) 1–15.

[8] J. Lotharius, K.L. O'Malley, The parkinsonism-inducing drug 1-methyl-4-phenylpyridinium triggers intracellular dopamine oxidation: a novel mechanism of toxicity, J. Biol. Chem. 275 (49) (2000) 38581–38588.

[9] H.M. Cochemé, M.P. Murphy, Complex I is the major site of mitochondrial superoxide production by paraquat, J. Biol. Chem. 283 (4) (2008) 1786–1798.

[10] A. Ray, B. Martinez, L. Berkowitz, G. Caldwell, K. Caldwell, Mitochondrial dysfunction, oxidative stress, and neurodegeneration elicited by a bacterial metabolite in a *C. elegans* Parkinson's model, Cell Death Dis. 5 (1) (2014) e984, e984.

[11] C.P. Gonzalez-Hunt, M.C. Leung, R.K. Bodhicharla, M.G. McKeever, A.E. Arrant, K. M. Margillo, I.T. Ryde, D.D. Cyr, S.G. Kosmaczewski, M. Hammarlund, Exposure to mitochondrial genotoxins and dopaminergic neurodegeneration in Caenorhabditis elegans, PLoS One 9 (12) (2014), e114459.

[12] B. Dilberger, S. Baumanns, F. Schmitt, T. Schmiedl, M. Hardt, U. Wenzel, G. P. Eckert, Mitochondrial oxidative stress impairs energy metabolism and reduces stress resistance and longevity of C. elegans, Oxid. Med. Cell. Longev. 2019 (2019) 1–14.

[13] S. Bora, G.S.H. Vardhan, N. Deka, L. Khataniar, D. Gogoi, A. Baruah, Paraquat exposure over generation affects lifespan and reproduction through mitochondrial disruption in C. elegans, Toxicology 447 (2021), 152632.

[14] M. Lu, L. Tan, X.-G. Zhou, Z.-L. Yang, Q. Zhu, J.-N. Chen, H.-R. Luo, G.-S. Wu, Tectochrysin increases stress resistance and extends the lifespan of Caenorhabditis elegans via FOXO/DAF-16, Biogerontology 21 (5) (2020) 669–682.

[15] S. Cerri, F. Blandini, An update on the use of non-ergot dopamine agonists for the treatment of Parkinson's disease, Expet Opin. Pharmacother. 21 (18) (2020) 2279–2291.

[16] J. Jankovic, W. Poewe, Therapies in Parkinson's disease, Curr. Opin. Neurol. 25 (4) (2012) 433–447.

[17] S. Cohen, R. Levi-Montalcini, V. Hamburger, A nerve growth-stimulating factor isolated from sarcom as 37 and 180, Proc. Natl. Acad. Sci. USA 40 (10) (1954) 1014–1018.

[18] R. Levi-Montalcini, The nerve growth factor 35 years later, Science 237 (4819) (1987) 1154–1162.

[19] T. Saatov, G. Artykbaeva, I. Yalalova, A. Mamadjanov, Isolation and purification of the nerve growth factor from the murine submaxillary salivary glands simple method for isolation the NGF peptide, Annal. Roman. Soc. Cell Biol. 25 (6) (2021) 17161–17167.

[20] T. Islam, M. Majumder, A. Bidkar, S.S. Ghosh, R. Mukhopadhyay, Y. Utkin, A. K. Mukherjee, Nerve growth factor from Indian Russell's viper venom (RVV-NGFa) shows high affinity binding to TrkA receptor expressed in breast cancer cells: application of fluorescence labeled RVV-NGFa in the clinical diagnosis of breast cancer, Biochimie 176 (2020) 31–44.

[21] T. Islam, M. Majumder, B. Kalita, A. Bhattacharjee, R. Mukhopadhyay, A. K. Mukherjee, Transcriptomic, proteomic, and biochemical analyses reveal a novel neuritogenesis mechanism of *Naja naja* venom α-elapitoxin post binding to TrkA receptor of rat pheochromocytoma cells, J. Neurochem. 155 (6) (2020) 612–637.

[22] M.V. Chao, B.L. Hempstead, p75 and Trk: a two-receptor system, Trends Neurosci. 18 (7) (1995) 321–326.

[23] R. Klein, S. Jing, V. Nanduri, E. O'Rourke, M. Barbacid, The trk proto-oncogene encodes a receptor for nerve growth factor, Cell 65 (1) (1991) 189–197.

[24] M. Benedetti, A. Levi, M.V. Chao, Differential expression of nerve growth factor receptors leads to altered binding affinity and neurotrophin responsiveness, Proc. Natl. Acad. Sci. USA 90 (16) (1993) 7859–7863.

[25] S.D. Skaper, The biology of neurotrophins, signalling pathways, and functional peptide mimetics of neurotrophins and their receptors, CNS Neurol. Disord. - Drug Targets 7 (1) (2008) 46–62.

[26] L.F. Reichardt, Neurotrophin-regulated signalling pathways, Phil. Trans. Biol. Sci. 361 (1473) (2006) 1545–1564.

[27] P. Lu, L. Jones, M. Tuszynski, BDNF-expressing marrow stromal cells support extensive axonal growth at sites of spinal cord injury, Exp. Neurol. 191 (2) (2005) 344–360.

[28] F.S. Lee, A.H. Kim, G. Khursigara, M.V. Chao, The uniqueness of being a neurotrophin receptor, Curr. Opin. Neurobiol. 11 (3) (2001) 281–286.

[29] J.M. Fletcher, R.A. Hughes, Modified low molecular weight cyclic peptides as mimetics of BDNF with improved potency, proteolytic stability and transmembrane passage in vitro, Bioorg. Med. Chem. 17 (7) (2009) 2695–2702.

[30] A.C. Mondal, M. Fatima, Direct and indirect evidences of BDNF and NGF as key modulators in depression: role of antidepressants treatment, Int. J. Neurosci. 129 (3) (2019) 283–296.

[31] G. Eftimiadi, M. Soligo, L. Manni, D. Di Giuda, M.L. Calcagni, A. Chiaretti, Topical delivery of nerve growth factor for treatment of ocular and brain disorders, Neural Regenerate. Res. 16 (9) (2021) 1740.

[32] S.C. Apfel, Nerve growth factor for the treatment of diabetic neuropathy: what went wrong, what went right, and what does the future hold? Int. Rev. Neurobiol. 50 (2002) 393–413.

[33] T.A. Gudasheva, P. Povarnina, A.V. Tarasiuk, S.B. Seredenin, The low molecular weight brain-derived neurotrophic factor mimetics with antidepressant-like activity, Curr. Pharmaceut. Des. 25 (6) (2019) 729–737.

[34] B. Kalita, A. Patra, A. Das, A.K. Mukherjee, Proteomic analysis and immuno-profiling of eastern India Russell's Viper (*Daboia russelii*) venom: correlation between RVV composition and clinical manifestations post RV bite, J. Proteome Res. 17 (8) (2018) 2819–2833.

[35] H.F. Williams, B.A. Mellows, R. Mitchell, P. Sfyri, H.J. Layfield, M. Salamah, R. Vaiyapuri, H. Collins-Hooper, A.B. Bicknell, A. Matsakas, Mechanisms underpinning the permanent muscle damage induced by snake venom metalloprotease, PLoS Neglected Trop. Dis. 13 (1) (2019), e0007041.

[36] V. Paalme, K. Trummal, M. Samel, K. Tõnismägi, L. Järvekülg, H. Vija, J. Subbi, J. Siigur, E. Siigur, Nerve growth factor from *Vipera lebetina* venom, Toxicon 54 (3) (2009) 329–336.

[37] K. Trummal, K. Tõnismägi, V. Paalme, L. Järvekülg, J. Siigur, E. Siigur, Molecular diversity of snake venom nerve growth factors, Toxicon 58 (4) (2011) 363–368.

[38] T. Islam, D. Madhubala, R. Mukhopadhyay, A.K. Mukherjee, Transcriptomic and functional proteomics analyses to unveil the common and unique pathway (s) of neuritogenesis induced by Russell's viper venom nerve growth factor in rat pheochromocytoma neuronal cells, Expet Rev. Proteonomics 18 (6) (2021) 463–481.

[39] C.P. Bernardes, N.A. Santos, F.M. Sisti, R.S. Ferreira, N.A. Santos-Filho, A.C. Cintra, E.M. Cilli, S.V. Sampaio, A.C. Santos, A synthetic snake-venom-based tripeptide (Glu-Val-Trp) protects PC12 cells from MPP+ toxicity by activating the NGF-signaling pathway, Peptides 104 (2018) 24–34.

[40] R.J. McCleary, R.M. Kini, Non-enzymatic proteins from snake venoms: a gold mine of pharmacological tools and drug leads, Toxicon 62 (2013) 56–74.

[41] A. Osipov, Y. Utkin, Effects of snake venom polypeptides on central nervous system, Cent. Nerv. Syst. Agents Med. Chem. 12 (4) (2012) 315–328.

[42] N. Prabha, A. Guru, R. Harikrishnan, M.K. Gatasheh, A.A. Hatamleh, A. Juliet, J. Arockiaraj, Neuroprotective and antioxidant capability of RW20 peptide from histone acetyltransferases caused by oxidative stress-induced neurotoxicity in in vivo zebrafish larval model, J. King Saud Univ. Sci. 34 (3) (2022), 101861.

[43] N.G. Wells, C.A. Smith, Prediction of Allosterically Acting Mutations Using MD Simulations and Rosetta, bioRxiv, 2022.

[44] R. Doley, G.F. King, A.K. Mukherjee, Differential hydrolysis of erythrocyte and mitochondrial membrane phospholipids by two phospholipase A2 isoenzymes (NK-PLA2-I and NK-PLA2-II) from the venom of the Indian monocled cobra *Naja kaouthia*, Arch. Biochem. Biophys. 425 (1) (2004) 1–13.

[45] A.K. Mukherjee, A.J. Saviola, P.D. Burns, S.P. Mackessy, Apoptosis induction in human breast cancer (MCF-7) cells by a novel venom L-amino acid oxidase (Rusvinoxidase) is independent of its enzymatic activity and is accompanied by caspase-7 activation and reactive oxygen species production, Apoptosis 20 (10) (2015) 1358–1372.

[46] X. Zhao, Z. Zeng, U. Gaur, J. Fang, T. Peng, S. Li, W. Zheng, Metformin protects PC12 cells and hippocampal neurons from H2O 2-induced oxidative damage through activation of AMPK pathway, J. Cell. Physiol. 234 (9) (2019) 16619–16629.

[47] B. Das, A. Patra, A.K. Mukherjee, Correlation of venom toxinome composition of Indian red scorpion (*Mesobuthus tamulus*) with clinical manifestations of scorpion stings: failure of commercial antivenom to immune-recognize the abundance of low molecular mass toxins of this venom, J. Proteome Res. 19 (4) (2020) 1847–1856.

[48] L.A. Greene, A.S. Tischler, Establishment of a noradrenergic clonal line of rat adrenal pheochromocytoma cells which respond to nerve growth factor, Proc. Natl. Acad. Sci. USA 73 (7) (1976) 2424–2428.

[49] L. Zhang, M.-N. Dong, J. Deng, C.-H. Zhang, M.-W. Liu, Resveratrol exhibits neuroprotection against paraquat-induced PC12 cells via heme oxygenase 1 upregulation by decreasing MiR-136-5p expression, Bioengineered 13 (3) (2022) 7065–7081.

[50] A. Kvetkina, E. Pislyagin, E. Menchinskaya, E. Yurchenko, R. Kalina, S. Kozlovskiy, L. Kaluzhskiy, A. Menshov, N. Kim, S. Peigneur, Kunitz-type peptides from sea anemones protect neuronal cells against Parkinson's disease inductors via inhibition of ROS production and ATP-induced P2X7 receptor activation, Int. J. Mol. Sci. 23 (9) (2022) 5115.

[51] D. Cheng, G. Wang, X. Wang, J. Tang, Q. Yu, X. Zhang, S. Wang, Neuro-protection of chlorogenic acid against Al-induced apoptosis in PC12 cells via modulation of Al metabolism and Akt/GSK-3β pathway, J. Funct.Foods 70 (2020), 103984.

[52] H. Chen, S. Wang, A. Zhou, J. Miao, J. Liu, S. Benjakul, A novel antioxidant peptide purified from defatted round scad (*Decapterus maruadsi*) protein hydrolysate extends lifespan in *Caenorhabditis elegans*, J. Funct.Foods 68 (2020), 103907.

[53] R. Thakur, S. Kini, S. Kurkalang, A. Banerjee, P. Chatterjee, A. Chanda, A. Chatterjee, D. Panda, A.K. Mukherjee, Mechanism of apoptosis induction in human breast cancer MCF-7 cell by Ruviprase, a small peptide from *Daboia russelii russelii* venom, Chem. Biol. Interact. 258 (2016) 297–304.

[54] A. Kumar, T. Joishy, S. Das, M.C. Kalita, A.K. Mukherjee, M.R. Khan, A potential probiotic *Lactobacillus plantarum* JBC5 improves longevity and healthy aging by modulating antioxidative, innate immunity and serotonin-signaling pathways in *Caenorhabditis elegans*, Antioxidants 11 (2) (2022) 268.

[55] X. Wang, W. Xu, M. Fan, T. Meng, X. Chen, Y. Jiang, D. Zhu, W. Hu, J. Gong, S. Feng, Deoxynivalenol induces apoptosis in PC12 cells via the mitochondrial pathway, Environ. Toxicol. Pharmacol. 43 (2016) 193–202.

[56] Y. Liu, X.-c. Wang, D. Hu, S.-r. Huang, Q.-s. Li, Z. Li, Y. Qu, Heat shock protein 70 protects PC12 cells against ischemia-hypoxia/reoxygenation by maintaining intracellular Ca2+ homeostasis, Neural Regenerate. Res. 11 (7) (2016) 1134.

[57] Y.J. Jang, J.H. Won, M.J. Back, Z. Fu, J.M. Jang, H.C. Ha, S. Hong, M. Chang, D. K. Kim, Paraquat induces apoptosis through a mitochondria-dependent pathway in RAW264. 7 cells, Biomol. Therap. 23 (5) (2015) 407.

[58] L. Jing, R. Gao, J. Zhang, D. Zhang, J. Shao, Z. Jia, H. Ma, Norwogonin attenuates hypoxia-induced oxidative stress and apoptosis in PC12 cells, BMC Complement Med. Therap. 21 (1) (2021) 1–12.

[59] O. Lowry, Protein estimation with the folin ciocalteau reagent, Methods Enzymol. 111 (1957) 448.
[60] A. Chanda, A.K. Mukherjee, Quantitative proteomics to reveal the composition of Southern India spectacled cobra (Naja naja) venom and its immunological cross-reactivity towards commercial antivenom, Int. J. Biol. Macromol. 160 (2020) 224–232.
[61] C.-L. Schengrund, Gangliosides: glycosphingolipids essential for normal neural development and function, Trends Biochem. Sci. 40 (7) (2015) 397–406.
[62] S. Maliartchouk, Y. Feng, L. Ivanisevic, T. Debeir, A.C. Cuello, K. Burgess, H. U. Saragovi, A designed peptidomimetic agonistic ligand of TrkA nerve growth factor receptors, Mol. Pharmacol. 57 (2) (2000) 385–391.
[63] F.M. Longo, T. Yang, J.K. Knowles, Y. Xie, L.A. Moore, S.M. Massa, Small molecule neurotrophin receptor ligands: novel strategies for targeting Alzheimer's disease mechanisms, Curr. Alzheimer Res. 4 (5) (2007) 503–506.
[64] A.M. Colangelo, M.R. Bianco, L. Vitagliano, C. Cavaliere, G. Cirillo, L. De Gioia, D. Diana, D. Colombo, C. Redaelli, L. Zaccaro, A new nerve growth factor-mimetic peptide active on neuropathic pain in rats, J. Neurosci. 28 (11) (2008) 2698–2709.
[65] M. Muttenthaler, G.F. King, D.J. Adams, P.F. Alewood, Trends in peptide drug discovery, Nat. Rev. Drug Discov. 20 (4) (2021) 309–325.
[66] F.M. Longo, S.M. Massa, Small-molecule modulation of neurotrophin receptors: a strategy for the treatment of neurological disease, Nat. Rev. Drug Discov. 12 (7) (2013) 507–525.
[67] R.R. Deshpande, A.P. Tiwari, N. Nyayanit, M. Modak, In silico molecular docking analysis for repurposing therapeutics against multiple proteins from SARS-CoV-2, Eur. J. Pharmacol. 886 (2020), 173430.
[68] I. Sarkar, G. Sen, M. Bhattacharya, S. Bhattacharyya, A. Sen, In silico inquest reveals the efficacy of Cannabis in the treatment of post-Covid-19 related neurodegeneration, J. Biomol. Struct. Dynam. (2021) 1–10.
[69] T. Wehrman, X. He, B. Raab, A. Dukipatti, H. Blau, K.C. Garcia, Structural and mechanistic insights into nerve growth factor interactions with the TrkA and p75 receptors, Neuron 53 (1) (2007) 25–38.
[70] A.K. Kalvala, V.G. Yerra, A. Kumar, LONP1 induction by SRT1720 attenuates mitochondrial dysfunction against high glucose induced neurotoxicity in PC12 cells, Toxicol. Vitro 62 (2020), 104695.
[71] L. Grumolato, E. Louiset, D. Alexandre, D. Aït-Ali, V. Turquier, A. Fournier, A. Fasolo, H. Vaudry, Y. Anouar, PACAP and NGF regulate common and distinct traits of the sympathoadrenal lineage: effects on electrical properties, gene markers and transcription factors in differentiating PC12 cells, Eur. J. Neurosci. 17 (1) (2003) 71–82.
[72] G. Bora-Tatar, H. Erdem-Yurter, Investigations of curcumin and resveratrol on neurite outgrowth: perspectives on spinal muscular atrophy, BioMed Res. Int. 2014 (2014).
[73] K.J. Barnham, C.L. Masters, A.I. Bush, Neurodegenerative diseases and oxidative stress, Nat. Rev. Drug Discov. 3 (3) (2004) 205–214.
[74] A. Areti, P. Komirishetty, M. Akuthota, R.A. Malik, A. Kumar, Melatonin prevents mitochondrial dysfunction and promotes neuroprotection by inducing autophagy during oxaliplatin-evoked peripheral neuropathy, J. Pineal Res. 62 (3) (2017), e12393.
[75] S. Bastías-Candia, J.M. Zolezzi, N.C. Inestrosa, Revisiting the paraquat-induced sporadic Parkinson's disease-like model, Mol. Neurobiol. 56 (2) (2019) 1044–1055.
[76] P.-C. Lee, Y. Bordelon, J. Bronstein, B. Ritz, Traumatic brain injury, paraquat exposure, and their relationship to Parkinson disease, Neurol. India 79 (20) (2012) 2061–2066.
[77] Z.-D. Zhang, Y.-J. Yang, Z. Qin, X.-W. Liu, S.-H. Li, L.-X. Bai, J.-Y. Li, Protective activity of aspirin eugenol ester on paraquat-induced cell damage in SH-SY5Y cells, Oxid. Med. Cell. Longev. (2021) 2021.
[78] T. Blanco-Ayala, A. Andérica-Romero, J. Pedraza-Chaverri, New insights into antioxidant strategies against paraquat toxicity, Free Radic. Res. 48 (6) (2014) 623–640.
[79] W. Jia, Q. Su, Q. Cheng, Q. Peng, A. Qiao, X. Luo, J. Zhang, Y. Wang, Neuroprotective effects of palmatine via the enhancement of antioxidant defense and small heat shock protein expression in aβ-transgenic *Caenorhabditis elegans*, Oxid. Med. Cell. Longev. 2021 (2021), 9966223.
[80] R.R. Hou, J.Z. Chen, H. Chen, X.G. Kang, M.G. Li, B.R. Wang, Neuroprotective effects of (-)-epigallocatechin-3-gallate (EGCG) on paraquat-induced apoptosis in PC12 cells, Cell Biol. Int. 32 (1) (2008) 22–30.
[81] D.-Y. Jin, H.Z. Chae, S.G. Rhee, K.-T. Jeang, Regulatory role for a novel human thioredoxin peroxidase in NF-κB activation, J. Biol. Chem. 272 (49) (1997) 30952–30961.
[82] X. Zhang, A.S. Vincent, B. Halliwell, K.P. Wong, A mechanism of sulfite neurotoxicity: direct inhibition of glutamate dehydrogenase, J. Biol. Chem. 279 (41) (2004) 43035–43045.
[83] A. Yamaguchi, K.I. Ishikawa, T. Inoshita, K. Shiba-Fukushima, S. Saiki, T. Hatano, A. Mori, Y. Oji, A. Okuzumi, Y. Li, M. Funayama, Y. Imai, N. Hattori, W. Akamatsu, Identifying therapeutic agents for amelioration of mitochondrial clearance disorder in neurons of familial Parkinson disease, Stem Cell Rep. 14 (6) (2020) 1060–1075.
[84] W. Yang, E. Tiffany-Castiglioni, Paraquat-induced apoptosis in human neuroblastoma SH-SY5Y cells: involvement of p53 and mitochondria, J. Toxicol. Environ. Health, Part A 71 (4) (2008) 289–299.
[85] M.T. Islam, Oxidative stress and mitochondrial dysfunction-linked neurodegenerative disorders, Neurol. Res. 39 (1) (2017) 73–82.
[86] M. Golpich, E. Amini, Z. Mohamed, R. Azman Ali, N. Mohamed Ibrahim, A. Ahmadiani, Mitochondrial dysfunction and biogenesis in neurodegenerative diseases: pathogenesis and treatment, CNS Neurosci. Ther. 23 (1) (2017) 5–22.
[87] D.J. Pagliarini, S.E. Calvo, B. Chang, S.A. Sheth, S.B. Vafai, S.-E. Ong, G.A. Walford, C. Sugiana, A. Boneh, W.K. Chen, A mitochondrial protein compendium elucidates complex I disease biology, Cell 134 (1) (2008) 112–123.
[88] K. Okamoto, N. Kondo-Okamoto, Mitochondria and autophagy: critical interplay between the two homeostats, Biochim. Biophys. Acta Gen. Subj. 1820 (5) (2012) 595–600.
[89] P. Guidetti, L. Amori, M.T. Sapko, E. Okuno, R. Schwarcz, Mitochondrial aspartate aminotransferase: a third kynurenate-producing enzyme in the mammalian brain, J. Neurochem. 102 (1) (2007) 103–111.
[90] Y. Song, X. Liang, Y. Hu, Y. Wang, H. Yu, K. Yang, p, p′-DDE induces mitochondria-mediated apoptosis of cultured rat Sertoli cells, Toxicology 253 (1–3) (2008) 53–61.
[91] D. Ozaslan, S. Wang, B.A. Ahmed, A.M. Kocabas, J.C. McCastlain, A. Bene, F. Kilic, Glycosyl modification facilitates homo-and hetero-oligomerization of the serotonin transporter: a specific role for sialic acid residues, J. Biol. Chem. 278 (45) (2003) 43991–44000.
[92] Y.-D. Wen, R. Sheng, L.-S. Zhang, R. Han, X. Zhang, X.-D. Zhang, F. Han, K. Fukunaga, Z.-H. Qin, Neuronal injury in rat model of permanent focal cerebral ischemia is associated with activation of autophagic and lysosomal pathways, Autophagy 4 (6) (2008) 762–769.
[93] H. Schägger, H. Noack, W. Halangk, U. Brandt, G. Von Jagow, Cytochrome-c oxidase in developing rat heart enzymic properties and amino-terminal sequences suggest identity of the fetal heart and the adult liver isoform, Eur. J. Biochem. 230 (1) (1995) 235–241.
[94] G. Sun, M.T. Kinter, V.E. Anderson, Mass spectrometric characterization of mitochondrial electron transport complexes: subunits of the rat heart ubiquinol–cytochrome c reductase, J. Mass Spectrom. 38 (5) (2003) 531–539.
[95] B.K. De, K.S. Misono, T. Lukas, B. Mroczkowski, S. Cohen, A calcium-dependent 35-kilodalton substrate for epidermal growth factor receptor/kinase isolated from normal tissue, J. Biol. Chem. 261 (29) (1986) 13784–13792.
[96] P.L. Pedersen, N. Williams, J. Hullihen, Mitochondrial ATP synthase: dramatic magnesium-induced alterations in the structure and function of the F1-ATPase moiety, Biochemistry 26 (26) (1987) 8631–8637.
[97] H. Xu, S. Qin, G. Carrasco, Y. Dai, E. Filardo, E. Prossnitz, G. Battaglia, L. Doncarlos, N. Muma, Extra-nuclear estrogen receptor GPR30 regulates serotonin function in rat hypothalamus, Neuroscience 158 (4) (2009) 1599–1607.

To study the snake venom nerve growth factor-derived custom peptides for their application in preventing Parkinson’s disease

by Dev Madhubala

Submission date: 12-Dec-2023 02:46PM (UTC+0530)
Submission ID: 2256664612
File name: ides_for_their_application_in_preventing_Parkinson_s_disease.pdf (7.42M)
Word count: 42890
Character count: 238055

ABSTRACT

ABSTRACT

Neurodegeneration, an age-related disorder, occurs as a progressive loss of neurons or from the neuronal failure to transmit signals. Neurodegenerative disorders (NDs), a group of neuronal dysfunctions, principally affect the neurons in the CNS and ultimately result in the defect of specific brain functions such as cognition, memory, and movement. The epidemiology of the NDs surges with aged people. It contributes approximately 12% of the total deaths globally. As a result, WHO has declared NDs to be the second leading cause of death worldwide. The most common NDs are Alzheimer's disease (AD), Parkinson's disease (PD), Huntington's disease (HD), and Amyotrophic lateral sclerosis (ALS). Decades of research evidenced the hallmarks of the NDs, including aberrant proteostasis, pathological protein aggregation, synaptic and neuronal network dysfunction, DNA and RNA defects, altered energy inflammation, homeostasis, and neuronal cell death. PD is the second most frequent ND, followed by AD. Despite groundbreaking research, physicians have no effective treatment or medications available to stop, slow, or prevent the ill effects of NDs.

Neurotrophins are a group of endogenous soluble proteins with similar structures and functions, which profoundly affect neuronal development in vertebrates. The neurotrophin molecules contain nerve growth factor (NGF), brain-derived neurotrophic factors (BDNF), neurotrophin 4/5 (NT-4/5), and neurotrophin-3 (NT-3). The mechanism of neuritogenesis involves binding neurotrophin molecules to the transmembrane receptors belonging to the tyrosine kinase receptor (Trk) family. After binding neurotrophin molecules to their respective Trk receptors, neurotrophins promote their dimerization and autophosphorylation of the intracellular tyrosine residues of the receptor, which activates cascades of signaling pathways. These signaling pathways resulted in neuronal proliferation, survival, and differentiation. Because of the prominent role of neurotrophin molecules in neuronal development, endogenous administration of the exogenous neurotrophin molecule (such as NGF and BDNF) can be used as the drug prototype to treat NDs. Despite the high pharmacotherapeutic potential of neurotrophin, their poor pharmacokinetic potential, inability to permeate through the blood-brain barrier (BBB), large molecular weight, adverse side effects, and short half-life have limited their therapeutic applications.

Peptide mimetics is an apparent way to challenge the disadvantages of natural peptides. To overcome the limitations associated with using endogenous neurotrophin

molecules as drug therapy, scientists have been trying since the 90s to develop low molecular weight neurotrophin mimetics with better Pharmacokinetic potency and without any adverse side effects. To date, two neurotrophin mimetics (LM11A-31 and D3) are undergoing clinical trials, two (GK-2 and 7,8-dihydroxyflavone) have completed preclinical studies, and one (GSB-106) is at the stage of advanced pharmacological studies.

Venoms are intriguing sources of unique molecules that are being enhanced in evolution and also have unique characteristics such as low molecular mass, pharmacological activity, stability and high potency, and selectivity and affinity in mammalian systems for many targets. Animal venom has, therefore, a remarkable ability to generate therapeutic agents, and several venom toxins have been clinically applied and used as templates for drug design. NGF, a prominent member of the neurotrophin family, is one of the non-enzymatic intriguing proteins found in snake venoms. The proteomic analysis from our lab has shown that venoms of India's 'Big Four' venomous snakes contain several isoforms of NGF; however, in a small proportion. Previous studies from our lab have isolated and characterized neurotrophin molecules from Indian snake venoms, which exhibit neuritogenesis potency in rat pheochromocytoma (PC-12) cells. However, drug development from a native snake venom toxin has various limitations. Low abundance of the neurotrophin molecules in the snake venom leads to the scarcity of the animal venom. The purification and characterization of the neurotrophin molecule from snake venom is costly and tedious.

Therefore, we have designed two low molecular weight peptide mimetics (trideca-neuropeptide, TNP; heptadeca-neuropeptide, HNP) inspired by the snake venom neurotrophin molecules. These two synthetic custom peptides (CPs) were elective to the TrkA receptor (TrkA) determined by computational in silico analysis. In silico results were validated by an *in vitro* binding study of the FITC-conjugated CPs to PC-12 cell TrkA receptors. Pre-treatment of PC-12 cells with TNP and HNP induced neuritogenesis and significantly reduced the paraquat (PT)-induced cellular toxicity, the release of lactate dehydrogenase from the cell cytoplasm, production of intracellular ROS, restored the level of antioxidants, prevented alteration of mitochondrial transmembrane potential ($\Delta\Psi m$) and adenosine triphosphate (ATP) production, and inhibited cellular apoptosis. These peptides lack *in vitro* cytotoxicity, hemolytic activity, and platelet-modulating properties and do not interfere with the blood coagulation system. Functional proteomic

analyses demonstrated the reversal of PT-induced upregulated and downregulated metabolic pathway genes in PC-12 cells that were pre-treated with HNP and revealed the metabolic pathways regulated by HNP to induce neuritogenesis and confer protection against PT-induced neuronal damage in PC-12. The quantitative RT-PCR analysis confirmed that the PT-induced increased and decreased expression of critical pro-apoptotic and anti-apoptotic genes had been restored in the PC-12 cells pre-treated with the CPs. A network gene expression profile was proposed to elucidate the molecular interactions among the regulatory proteins for HNP to salvage the PT-induced damage. Taken together, our results show how peptides can protect against PT-induced oxidative stress, mitochondrial dysfunction, and cellular death and suggest new opportunities for the development of neuroprotective drugs.

The *in vivo* protective mechanisms of two low molecular mass (~1.4 kDa) novel CPs against PT-induced neurodegenerative dysfunction in the *Caenorhabditis elegans* model were also deciphered. CPs prevent the PT binding to the nerve ring adjacent to the pharynx in *C. elegans* (N2 strain) by stable and high-affinity binding to the tyrosine-protein kinase receptor CAM-1, resulting in significant inhibition of PT-induced toxicity by reducing enhanced reactive oxygen species production, mitochondrial membrane depolarization, and chemosensory dysfunction. The CPs inhibited PT-induced dopaminergic (DAergic) neuron degeneration and alpha-synuclein aggregation, the hallmarks of Parkinson's Disease, in transgenic BZ555 and NL5901 strains of *C. elegans*. The qRT-PCR, transcriptomic, and functional proteomics analyses unanimously elucidated that CPs restored PT-mediated oxidative stress, apoptosis, and neuronal damage in *C. elegans* by inhibiting increased expression of the skn-1 downstream pathway genes. A network of gene expression profiles showed the molecular interactions among the regulatory proteins to salvage the PT-induced damage by the neuroprotective peptides. Further, CPs (10 mg/kg, parental route) did not show toxicity or induce inflammatory mediators in the mice model.

MicroRNAs (miRNAs) are small non-coding RNAs that control different biological processes, viz. proliferation, differentiation, development, and apoptosis through translational inhibition and mRNA degradation. In this study, we aimed to decode the role of miRNAs in the neuritogenesis and neuroprotection activity of snake-venom-inspired CP (HNP) in the model organism *C. elegans*. We compared the miRNA expression profiles of the CPs-treated *C. elegans* versus mouse 2.5S-NGF-treated ones

(positive control). This study is the first report that showed the upregulation and downregulation of miRNAs in the mouse 2.5S/HNP-treated *C. elegans*. The potential miRNAs involved in the neuroprotection against PT-induced toxicity in the *C. elegans* PD model were studied. Functional characterization of its target genes regulating the different pathways was investigated. Mir-4813-3p was highly downregulated with the PT treatment, which involves the clearance of alpha-synuclein protein, and upregulated with the HNP/mouse 2.5S-NGF treatment. Two novel miRNAs, cel-miR-57-3p and cel-miR-8207-3p, were drastically upregulated with the PT treatment and significantly downregulated when pre-treated with the HNP/mouse 2.5S-NGF, indicating their roles in the protection against PT-toxicity in *C. elegans*.

For easy understanding, this thesis is structured into the following six chapters-

Chapter I: This chapter introduces neurodegenerative disorders (NDs), the second most cause of death worldwide. This chapter also briefly introduces some clinically meaningful NDs, their pathophysiology, current treatment, and associated challenges and limitations. We have briefly discussed several mechanisms allied with neurodegeneration that are concerned with the progression and pathogenesis of NDs. This chapter also introduced neurotrophin molecule and its role in treating NDs. The aim and objectives of the present study are also described in this chapter.

Chapter II: This chapter reviews the published literature on limitations associated with the therapeutic application and delivery of neurotrophic molecules for the treatment of NDs around the globe. This chapter also reviews the advantages of neurotrophin mimetic molecules over parent neurotrophins as a drug prototype to treat NDs.

Chapter III: This chapter enlists the chemicals and consumables used in the study and the methods and protocols employed for performing various experiments.

Chapter IV, V, and VI: These chapters include results and discussions, and the content of each chapter is briefly discussed below:

Chapter IV depicts the in silico and *in vitro* binding of custom peptides (CPs) to the mammalian TrkA receptor. The binding of custom peptides does not ensure the therapeutic potential of our designed CPs; therefore, we determine the neurite outgrowth and differentiation potential of the CPs in PC-12 cells. Further, the finding suggests the neuroprotective potential of the CPs against the paraquat (PT)-induced Parkinson's disease (PD) model in PC- 12 cells by thwarting excessive ROS production, oxidative

stress, MMP, and premature apoptotic death. Moreover, this chapter provides a greater understanding of the altered expression of proteins involved in the neurodegeneration pathways in the PT-induced PD model of PC-12 cells and how the expression of our custom peptides can be used in treatments by qRT-PCR and quantitative proteomic analysis.

Chapter V: After confirming the exclusive binding of TNP and HNP to the TrkA receptor, we were puzzled to understand the binding region of custom peptides in C. elegans because it lacks Trk receptors. Therefore, this chapter confirms the binding of CPs to the tyrosine-protein kinase receptor CAM-1 receptor (TrkA receptor homolog) present at the nerve ring region of *C. elegans*. This study also focuses on the neuroprotective potential of the CPs against the PT-induced PD model of *C. elegans* by thwarting excessive ROS production, MMP, and premature apoptotic death in a higher *in vivo* wild-type N2 *C. elegans* model. Moreover, this chapter includes that CPs protect PT-induced DAergic neuron degeneration in BZ555 worms, loss of chemotaxis behavior, and diminished α-synuclein accumulation in NL5901 worms. Moreover, qRT-PCR, transcriptomics, and proteomics studies unveiled the in-depth mechanism of neuroprotective activity of custom peptides in the PT-induced PD model of *C. elegans* N2 worms.

Chapter VI: This chapter focuses on studying expression profiles of the microRNAs (miRNA) in the neurotrophic and neuroprotective potential of the CPs/Mouse 2.5S-NGF against the PT-induced PD model of *C. elegans*. The acute toxicity of CPs tested in mice models showed that the peptide is devoid of toxicity in mice.

Chapter VII: This chapter presents the conclusion of this study and visualizes the future prospective of the study's findings.

In this study, our findings provide a fundamental basis for developing new agents that specifically target neurodegenerative diseases, especially PD, and encourage future, in-depth investigations through *in vivo*, pharmacokinetic, and pharmacodynamic studies to develop safe drug prototypes.

CHAPTER I

INTRODUCTION

1.1. Neurodegenerative diseases- a concern for millions of people worldwide

Neurons play a central role in the proper functioning of the human brain [1,2]. Neural stem cells generate the majority of neurons in childhood, but with an increase in age, their numbers are progressively reduced [3]. Neurons are not immortal, but the progressive loss of neuronal structure and function, or sometimes the neuronal failure to transmit the signal, is known as neurodegeneration, which is the most common cause in the pathophysiology of different brain diseases [4,5]. Therefore, a group of diseases characterized by the degeneration of neurons are collectively known as neurodegenerative diseases (NDs) [5]. NDs principally affect neurons in the central nervous system (CNS), which is presented by the progressive loss of CNS neurons, resulting in defects in specific brain functions such as memory, cognition, and movement [6].

Acute neurodegeneration defines a pathological feature in which neurons are promptly damaged and generally die in return for a rapid traumatic incident like strokes, head injury, cerebral haemorrhage, ischemic brain damage, and traumatic brain injury [7]. Chronic neurodegeneration is a condition in which the process of neuron degeneration generally initiates slowly but gradually degrades over time resulting in the irreversible loss of a particular neuron population [6]. The example of chronic NDs are Alzheimer's disease (AD), Parkinson's disease (PD), amyotrophic lateral sclerosis (ALS), Huntington's disease (HD) [8-10].

In 2019, approximately 349 million disability-adjusted life years (DALYs) and 10 million deaths were reported globally and became the second foremost cause of death after cardiovascular disease worldwide due to NDs [11]. From 1990 to 2019, there was a 1.91% surge in the global burden of NDs, such as stroke, AD, PD, migraine, motor neuron disease, etc [11,12]. As shown in Fig 1.1, significant DALY reductions from 1990 to 2019 were reported globally in most regions of Asia, South America, the Archipelago, Malaya, and Central Africa [11,12].

NDs are categorized by their principal clinical parameter, viz. protein accumulation, movement disorders, anatomic vulnerability, and cognitive disorders [5,9]. The neuronal dysfunction and death in NDs involve various fundamental mechanisms, viz. proteotoxic stress and its associated aberrations in the ubiquitin-autophagosomal and proteasomal system, neuroinflammation, oxidative stress, and programmed cell death (Fig 1.2) [9,10,13]. Decades of research presented the evidence for hallmarks of NDs,

including aberrant proteostasis, pathological protein aggregation, synaptic and neuronal network dysfunction, DNA and RNA defects, altered energy inflammation, homeostasis, and neuronal cell death (Fig 1.3) [14].

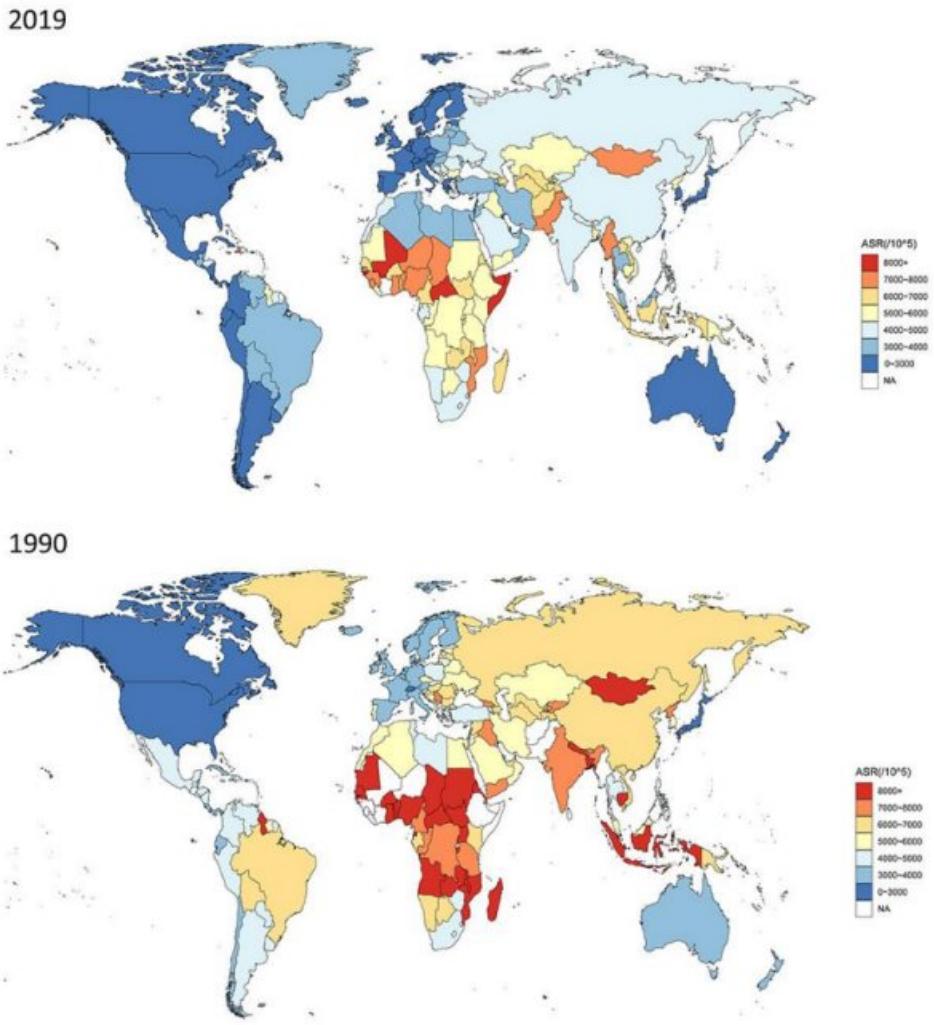

Fig 1.1 Age-standardized DALY rates of neurological disorders for both sexes and all ages among 204 countries and territories. (A) in 2019; (B) in 1990. This figure is adapted from [11].

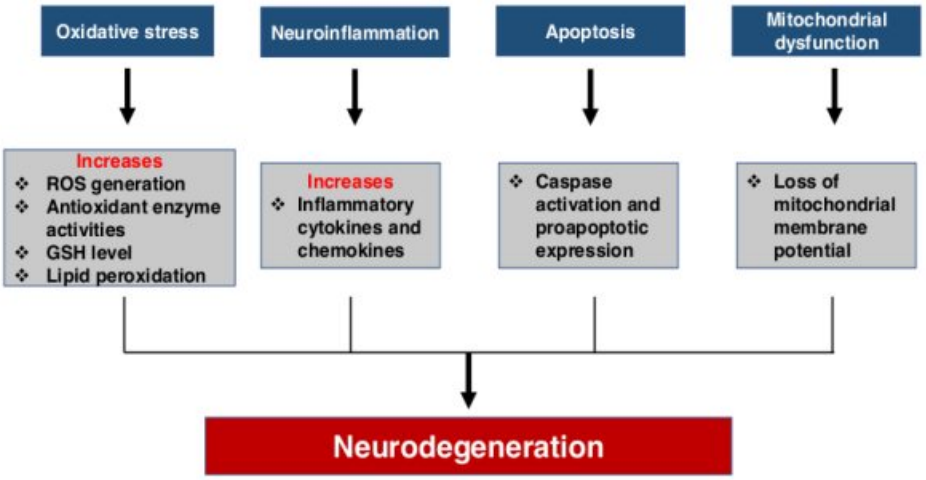

Fig 1.2 Several mechanisms allied with neurodegeneration that is concerned with the progression and pathogenesis of neurodegenerative diseases. This figure is adapted from [13].

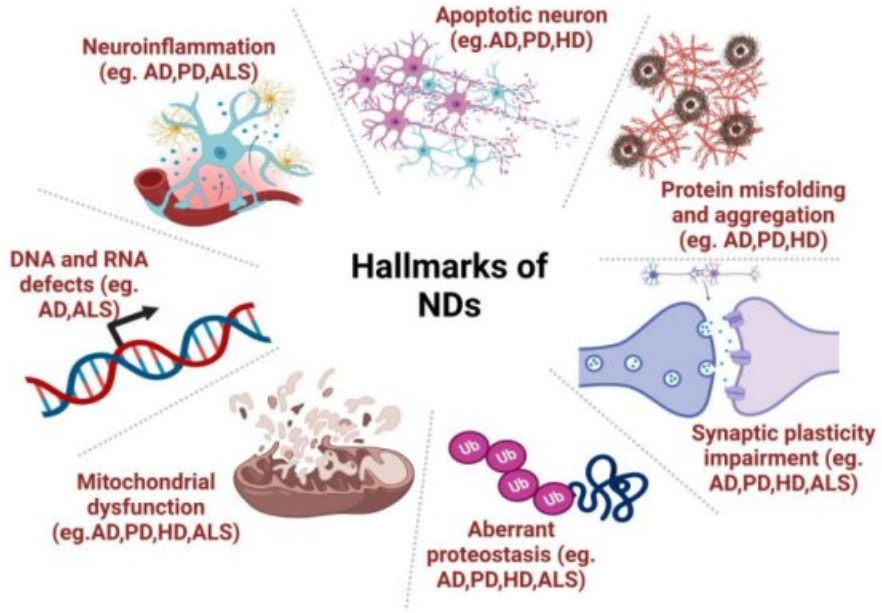

Fig 1.3 Schematic presentation of the neurodegenerative disorder hallmarks and their subcellular location. Created with BioRender.com

1.1.1. Types of neurodegenerative diseases and current treatments

In the subsequent subsection, the basic pathology and available current treatments of some of the important chronic NDs have been discussed. The pathophysiology of the above-mentioned NDs is summarized in Fig 1.4.

1.1.1.1. Alzheimer's disease: AD is described as a loss of synapse and synaptic proteins that correlates with the decline in cognitive function and the presence of neuritic plaques due to deposition of amyloid-β (Aβ) in the medial temporal lobes and neocortical structures [10]. Currently, there are approximately 50 million people suffer from AD worldwide, and this number is expected to double every five years to reach 152 million by 2050 [15]. The burden of Alzheimer's disease affects individuals, their families, and socio-economic conditions and is estimated to cost 1 trillion USD annually worldwide for treatment.

At present, there is no permanent cure for Alzheimer's disease, but there are treatments that only improve symptoms of the disease [15]. Glutamate regulators and cholinesterase inhibitors are two major classes of drugs available for the treatment of AD. Memantine [N-methyl-D-aspartate (NMDA) receptor antagonist] is the only approved glutamate regulator class of medication used to treat AD that is allied to memory and learning. In ordinary people, glutamate binds to NMDA receptors and allows excitatory glutamatergic neurotransmission, which exhibits neuronal plasticity and survival. But the accelerated activity of the NMDA receptor promotes neuronal cell death and contributes to the AD pathogenesis [16]. Cholinesterase inhibitors manage AD function by delaying the failure of acetylcholine (neurotransmitter); however, their side effects are nausea, loss of appetite, increased frequency of bowel movements, and vomiting [17]. Memantine is the only effective drug with cholinesterase inhibitors; however, the drug's efficacy is not satisfactory and is effective only in 50% of patients for a very short period. Constipation, headache, dizziness, and confusion are the side-effects of Memantine, which is a significant concern for AD treatment and management.

1.1.1.2. Parkinson's disease: PD is the second most common neurodegenerative disorder after AD that affects 2-3% of the population [18,19]. PD is characterized by α-synuclein aggregation in the brain and progressive dopaminergic (DAergic) neuronal degeneration in the substantia nigra leading to impaired motor control, rigidity, tremors, postural instability, and slow movement of the patient [20-22]. Studies have reported that in the

nigrostriatal system, axons become damaged before the degeneration of dopaminergic neurons, which results in the loss of synaptic communications [23]. The principal molecular pathogenesis of PD includes various pathways and mechanisms, viz. α-synuclein proteostasis, oxidative stress, mitochondrial dysfunction, axonal transport, and neuroinflammation [24].

Levodopa, apomorphine, monoamine oxidase type B inhibitors, and amantadine are approved by the FDA (USA) for symptomatic therapy of PD. Regrettably, since 1970, no further advanced drug has been approved for PD therapy. The primary target of these drugs is to increase the dopamine (neurotransmitter) level to improve motor symptoms of the disease [25,26]. However, long-term PD medication of these drugs reduces efficacy and leads to other adverse effects, such as motor complications [22,26].

1.1.1.3. Amyotrophic lateral sclerosis: In 1869, Jean-Martin Charcot initially explained ALS as a pure motor neuron disease, which is now known as a multisystem neurodegenerative disease with heterogeneity [27,28]. The clinical manifestation of ALS (weak focal muscle and wasting) spreads with the progression of the disease. The initial symptoms of ALS can differ between patients; most commonly, the onset of weakness in the limb muscles (also known as spinal onset), whereas there are approximately 20-30% of patients have bulbar-onset disease presenting with dysphagia (difficulty in swallowing), dysarthria (difficulty in speech), dysphonia (abnormal voice), and rare masseter weakness [29].

The incidence of ALS prevalent in Europe ranges from 2-3 cases per 1000,000 individuals [28,29]. The mechanism underlying ALS is poorly understood, although various factors such as genetic factors, oxidative stress, excitotoxicity, autoimmune response, neurofilament aggregation, impaired axonal transport, mitochondrial dysfunction, and environmental factors may be involved [13]. ALS is linked with a mutation in a gene encoding the zinc/copper dismutase-1 enzyme [13].

On account of its pathophysiology, other drugs such as ibudalist (cyclic nucleotide phosphodiesterase inhibitors), TRIUMEQ (antiretrovirals used as anti-HIV therapy), tamoxifen (antiestrogen; NCT00214110 under www.clinicaltrials.gov), retigabine (antiepileptic drugs), and mastinib (tyrosine kinase inhibitor; NCT02588677, www.clinicaltrials.gov) are currently being explored for ALS treatment. Although only two drugs, edaravone (free-radical scavenger; NCT01492686, www.clinicaltrials.gov)

and riluzole (antagonist of glutamate receptor), are prescribed to the patients; nevertheless, these drugs only slow down the disease progression but cannot cure the disease and inept at reverting associated symptoms of ALS [30].

1.1.1.4. Huntington's disease: HD is an autosomal dominant and progressive NDS. In basal ganglia, it is presented pathologically by diminished gamma-aminobutyric acid (GABA) and undue dopaminergic activity. Clinical manifestations of HD include movement dysfunction, cognitive impairment, and psychiatric abnormalities [31]. HD occurred by repeat expansion of CAG trinucleotide in the huntingtin (*htt*) gene at the chromosome 4 short arm [32]. Currently, there is no treatment for HD; the only possibility is to manage the symptoms [33,34]. The often-prescribed medication for HD treatment is tetrabenazine (depletes dopamine), aripiprazole, and olanzapine. However, they develop the risk of adverse side effects such as depression, akathisia, dizziness, parkinsonism, or fatigue [34].

The pathophysiology of the above-mentioned NDs is summarized in Fig 1.4.

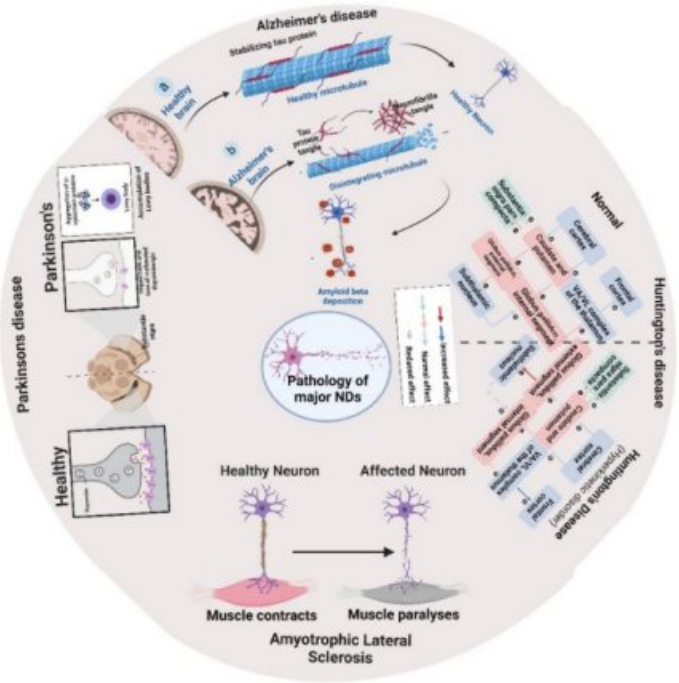

Fig 1.4 The pathophysiology of four major NDs - AD, PD, HD, and ALS. Created with BioRender.com

1.1.2. Oxidative stress and neurodegenerative disorders

Oxidative stress contributes a significant role in the aetiology of common NDs [35]. The disparity between reactive oxygen species (ROS) production and poor antioxidant defence potential results in oxidative stress causing cellular damage, system impairment, mitochondrial dysfunction, and DNA repair. These abnormalities encourage the neurodegenerative action and advancement of NDs [36]. The cellular damages include lipids, proteins, and nucleic acid damage that leads to excessive uptake of calcium (Ca^{2+}) through the mitochondrial membrane, which triggers the ROS production, deteriorates energy (ATP) production, and releases cytochrome c (cyt c, a proapoptotic factor) into the cytoplasm that causes neuronal cell death [37].

1.1.2.1. Neuroinflammation: Furthermore, neuroinflammation plays an important role in the pathophysiology of NDs [38]. Neuroinflammation, known as an inflammatory response (innate and adaptive immune system) within CNS and contributes to neurodegeneration. Microglia are the most abundant macrophage (innate immune effector cells) in the CNS and participate in homeostasis of CNS while neuronal development and ageing [39]. The nervous system in response to any pathological changes rapidly secrete different inflammatory molecules viz. chemokines, cytokines, and toxic components (glutamate, ROS, cyclooxygenase, prostaglandins, etc) [38,39]. The release of these inflammatory molecules or mediators is stimulated by astrocytes that ultimately trigger secondary inflammatory responses that encourage the survival of neurons [38].

1.1.2.2. Mitochondrial dysfunction: Mitochondria signify the energy (ATP) powerhouse and protecting guard of the cell. Mitochondria function as the site of oxidative phosphorylation, and cellular respiration, and maintain low calcium (Ca^{2+}) concentration in cytosol [37]. The consequences of mitochondrial dysfunction are dire, so it is considered a critical organelle for determining cell fate (death/survival) by controlling autophagy and apoptotic signals [37]. Activation of multiple signals (autophagic or apoptotic) stimulates mitochondrial permeability transition (MPT) that causes the release of proapoptotic proteins (cyt c) from the intermembrane space, which activates caspase for apoptosis or stimulates autophagy [37]. In the cytosol, cyt c activates a cascade of caspases (caspase 3, 6, and 7) after binding to apoptotic protease-activating

factor-1 (apaf-1) and procaspase-9 and forming apoptosome complex. The caspase activation eventually leads to apoptotic neuronal cell death [40].

1.1.2.3. Release of Cytochrome c: Rationally, the release of cyt c into the extracellular space can occur during the incidence of cell damage, there it acts as a danger-associated molecular pattern (DAMP) i.e., translocation of self-molecules in an inappropriate compartment [41]. Therefore, the anti-inflammatory/pro-inflammatory activity of cyt c depends on their location. In normal cells, cyt c is present inside the mitochondria. Emigration of cyt c into the cytosol triggers the apoptotic pathway (non-inflammatory). However, translocation of cyt c into the extracellular space induces inflammation and can be measured in the serum as a marker of severe mitochondrial damage or cell death (Fig 1.5) [40,41].

1.1.2.4. Apoptosis: Apoptosis of neuronal cells contribute to neurodegeneration, which results in NDs. Apoptosis is known as programmed cell death, which is characterized by chromatin condensation, shrinkage of the cells, and DNA fragmentation. This process is an energy-dependent mechanism that requires ATP for translation (protein synthesis) and signal activation [13]. Apoptosis can occur via two pathways, i.e., intrinsic and extrinsic pathways. In the extrinsic pathway, death ligands bind and activate death receptors, which induce death signals via a cascade of protein and protein interactions. Whereas the intrinsic pathway is triggered by the release of proapoptotic (cyt c) mediators from the intermembrane space of mitochondria through MPT and induces a caspase-dependent/caspase-independent pathway [42,43]. Targeting the aforementioned mechanism of action may hold good promise for the treatment and prevention of NDs. To deal with NDs, various probable therapeutic targets can be explored.

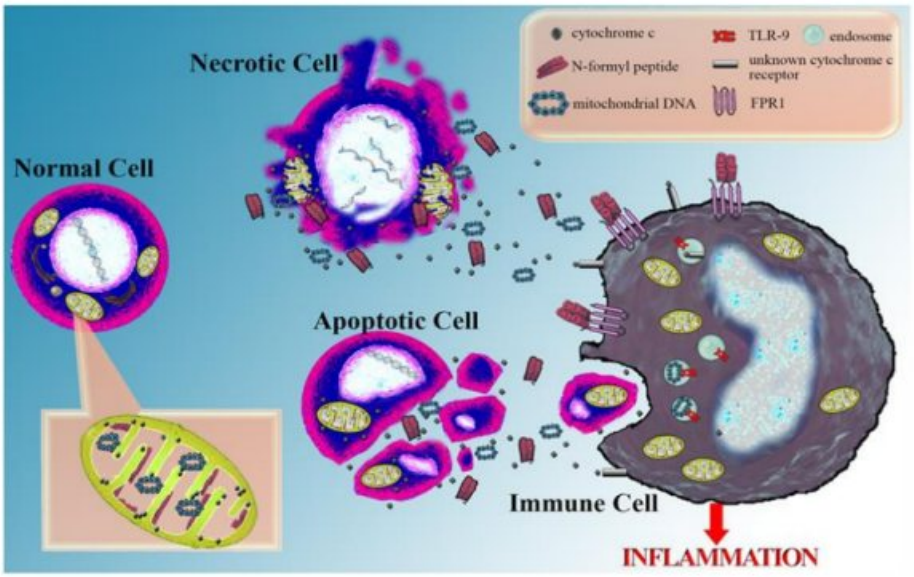

Fig 1.5 The potential cytochrome c (a marker of apoptosis) as a danger-associated molecular pattern (DAMP). This figure is adapted from Eleftheriadis et al. (2016) [40].

1.1.3. Challenges associated with current therapy

Management of NDs is disease-specific. Currently accepted strategies for the management either aim at the pathogenesis of the disease or challenge the recovery of the symptoms experienced [8]. Present therapy can potentially control the disease progression rather than eliminate the root causes of NDs. The blood-brain barrier (BBB) is one of the major concerns for successfully treating neurodegenerative diseases, where most of the drugs under clinical trials fail. The BBB is known as a diffusion barrier that thwarts the transport of ingredients into the brain, aided in maintaining the homeostasis and normal functioning of the brain. The effective intervention of NDs is restricted due to the unsuccessful delivery of adequate formulations to the brain. The poor permeability of most drugs and the advanced properties of BBB account for the lack of appropriate treatment opportunities for NDs [8].

The pharmacokinetic characteristics of systematically conducted drugs determine their efficacy [44]. In most cases, the therapeutic molecules are unfavorable for delivering to the target site. The plasma proteins in the human circulation system are the initial point of attention. Some medicinal drugs have a high affinity towards these proteins, thus restricting the extent of the drug in circulation and eventually reducing the availability of

the unbound pharmaceutical and their transportation to the brain [8,45]. Furthermore, the elimination rate of some drugs by the liver and kidney (clearance organ) is limited and releases few into the blood.

Moreover, the drug-target cell interaction confines the amount of drug absorption. Unambiguously, drug molecules can block the channels (alter the membrane potential), which affects the cell conformation. The administration and absorption of drug molecules are limited by this transient effect [46]. Small lipophilic therapeutic drug molecules with limited interactions with plasma proteins aid brain delivery [8].

The multifactorial nature of NDs promotes the search for multi-target drugs (hybrids and co-drugs), which target more than one pathophysiological symptom. This approach is promising for treating NDs [47].

1.2. Neurotrophins: Role in neurological disorders and prospects

1.2.1. Neurotrophins and their receptors

Neurotrophins are a group of endogenous soluble proteins with similar structures and functions, which profoundly affect neuronal development in vertebrates. The first neurotrophin, viz. nerve growth factor (NGF), was identified in 1951 by Levi-Montalcini and their colleagues [48]. The neurotrophins family consists of NGF [48], brain-derived neurotrophic factor (BDNF) [49], neurotrophin- 4/5 (NT-4/5) [50] and neurotrophin-3 (NT-3) [51]. Other than these neurotrophins, two neurotrophins named neurotrophin-6 (NT-6) and neurotrophin-7 (NT-7) have been discovered in teleost fish [52]. These neurotrophins are grouped based on structural similarity to the NGF, which is involved in neuronal growth, development, and maintenance [53,54].

The mechanism of neuritogenesis involves the binding of neurotrophins to transmembrane receptors belonging to the tyrosine kinase receptors family, for example, tropomyosin-related kinase A (Trk A), tropomyosin-related kinase B (Trk B), and tropomyosin-related kinase C (Trk C) [55,56]. Neurotrophins also bind to the receptor of the Tumor Necrosis Factor (TNF) superfamily, the p^{75NTR} neurotrophin receptor [55,56], and mediates pro-neurotrophin signalling (converting precursors to mature neurotrophins) [57]. NGF and NT-3 show high-affinity binding (K_d value~10^{-11} M) [58-61] with Trk A and Trk C receptors; respectively, although, brain-derived neurotrophic factor (BDNF) and neurotrophin-4/5 (NT-4/5) exclusively bind with high-affinity (K_d

value~10^{-11} M) to the Trk B receptor [58,61]. However, all the neurotrophins show low-affinity binding (K_d value~10^{-9} M) with p^{75NTR} [58,59]. Moreover, p^{75NTR} can also regulate the selective and specific binding of neurotrophins (NT) to the correct tropomyosin-related kinase (Trk) receptors [62].

1.2.2. Snake venom neurotrophins

Venoms are exciting sources of special molecules that are being enhanced in evolution and also have unique characteristics such as low molecular mass, pharmacological activity, stability, and high potency, along with selectivity and affinity in mammalian systems for many targets. Animal venoms, therefore, have a great potential to generate therapeutic agents, and many venom toxins have been applied clinically and used as templates for drug design [63].

Nerve growth factor (NGF), a prominent member of the neurotrophin family, is one of the intriguing non-enzymatic proteins found in snake venoms. The proteomic analysis has shown that venoms of all the 'Big Four' venomous snakes of India contain several isoforms of NGF; however, in a small proportion (Fig 1.6) [64-67], although its role and significance in snake venoms remain unclear [68].

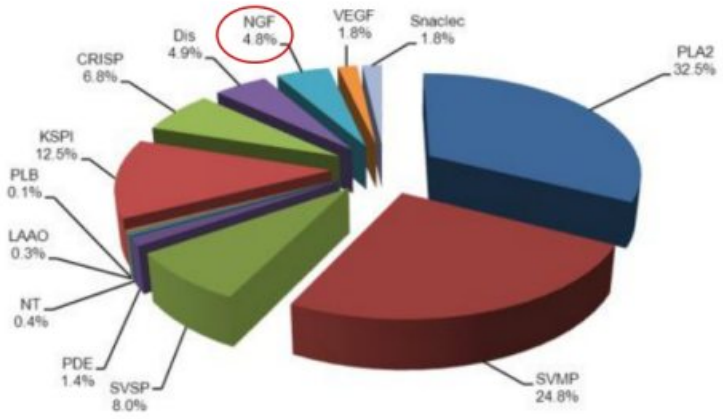

Fig 1.6 Protein family composition of western India (WI) Russell's viper venom (RVV). Nerve growth factor (NGF) constituting 4.8% of WI RVV proteome identified by tandem mass spectrometry analysis. This figure is adapted from [67].

1.2.3. Neurotrophins signalling pathways

After binding to the respective Trk receptors, neurotrophins promote their dimerization, followed by autophosphorylation of intracellular tyrosine residues of the receptor, which activates a cascade of events through two adapter proteins—Src and Shc. The Trk receptor-induced cascade of signalling pathways includes the Ras-induced Mitogen-Activated Protein Kinase (MAPK) pathway [54,69], MAPK-extracellular signal-regulated kinase (ERK) pathway [70], phosphatidyl inositol 3-kinase (PI3K) stimulation of protein kinase B (Akt) and phospholipase Cγ (PLCγ)-dependent secretion of diacylglycerol (DAG) and inositol 1,4,5-triphosphate (IP3)-mediated pathway (Fig 1.7)[54,69]. Neurotrophin and Trk interaction-induced signalling pathways resulted in neuronal proliferation, survival, and differentiation [70,71].

Notably, the p^{75NTR} can function antagonistically to the Trk receptor [57]. For example, the interaction between neurotrophin and Trk results in cell survival, whereas the binding of p^{75NTR} with neurotrophins precursor leads to neuronal cell death by apoptosis [62]. The mechanism of such cell death involves that p^{75NTR} receptor activation stimulates the c-Jun N-terminal kinase (JNK) signalling pathway, which activates the tumour suppressor (p53) protein that causes apoptosis [72,73]. The binding of the p^{75NTR} receptor by NGF or neurotrophins also stimulates the expression of the Fas ligand responsible for activating the Fas receptor resulting in apoptosis [72,73]. When the Trk A receptor is absent, the pro-apoptotic function is reported in cells where the p^{75NTR} receptor is expressed [74]. The TrkA receptor performs all the neuritogenesis functions of NGF independent of the appearance of the p^{75NTR} receptor [75,76]. p^{75NTR} receptor induces both negative and positive signals, which play a significant role in neural development and other higher-order functions viz. learning and memory (Fig 1.7).

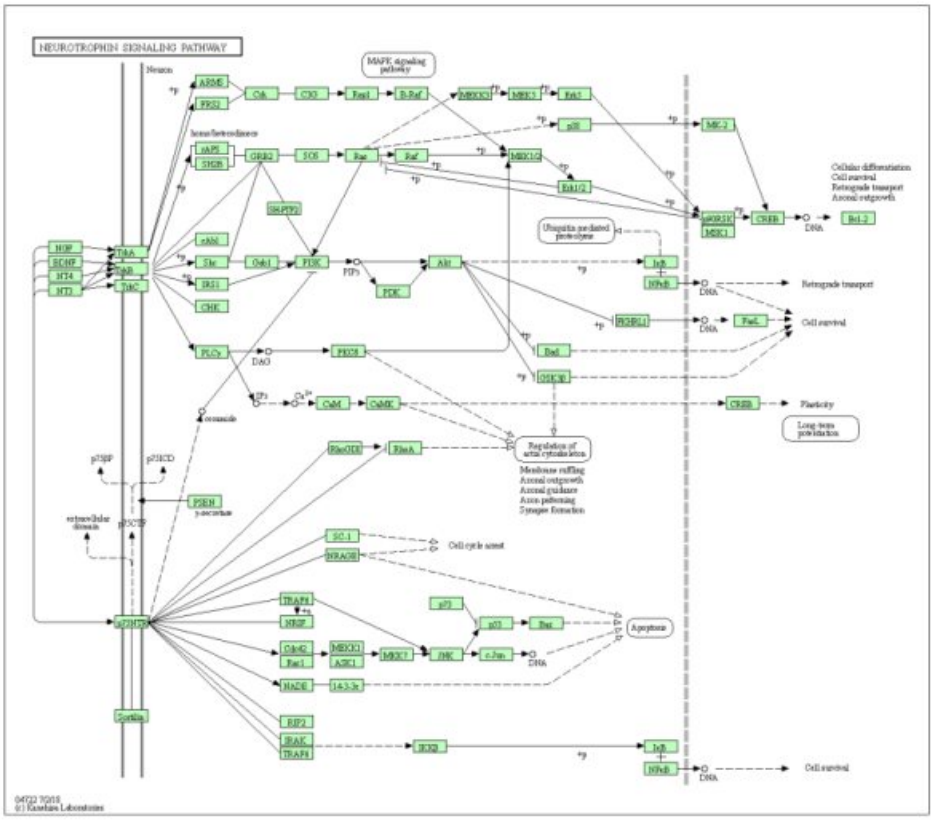

Fig 1.7 Kegg pathway. Human neurotrophin signalling pathways.

1.2.4. Neurotrophins as therapeutics in NDs

Since the discovery of NGF, the crucial role of neurotrophins to regulate numerous essential neuronal functions, such as promoting neurite regeneration, avoiding degeneration, and increasing synaptic plasticity has been elucidated by *in vitro* laboratory studies and in *in vivo* experimental models [77]. Because of their prominent effects on neuronal development by systemic administration of exogenous neurotrophin molecule proteins, NGF molecules can be used as drug prototypes to treat various NDs. Over the years, the neuroprotective effect of neurotrophic factors has been well documented, leading to the hypothesis of their therapeutic application [77-79].

1.2.5. Limitations of neurotrophins as a therapeutic in neurological diseases

Despite the high pharmacotherapeutic potential of neurotrophins, their poor pharmacological properties, marginal permeability of the blood-brain barrier, short half-life, activation of multiple receptors, and pleiotropic effects have limited their therapeutic applications [54,80]. Therefore, there is an urgent requirement to resolve these impediments for the successful therapeutic application of neurotrophins. Several strategies focusing on the better pharmacokinetics of native neurotrophins, such as - (a) systemic or intraventricular administration of neurotrophins, (b) transplantation of cells producing neurotrophins, (c) neurotrophin expression via viral vectors and cell-based delivery systems, (d) combinatorial strategy using combination of neurotrophins enhanced neuroprotection, and (e) small molecule or synthetic peptide development that binds to specific receptors or neurotrophins mimetics have been suggested [81,82].

1.3 Peptidomimetics and small molecules therapeutics

A peptidomimetic is a compound with pharmacophore similarity that mimics natural protein-fragment, peptide, or whole protein and which also possesses the ability to interact with the specific target and generate similar biological effects [83]. Peptide mimetics provide an obvious way to tackle the disadvantages of natural peptides. The molecule which mimics the biological activity of a natural peptide and has a molecular weight of less than 700 Da is referred to as peptide mimetics. Peptide mimetics also have significantly improved patient compliance and cost savings.

Moreover, peptide mimetics are less expensive to produce than natural peptides. Also, natural peptides not encountered with peptide mimetics have issues with peptide storage, stability, and immunoreactivity [84]. In recent years, peptide mimetics have emerged as a new generation of promising drugs due to the rapid screening of small molecule libraries and rational design approaches [84,85].

1.3.1 Neurotrophin's mimetics role in neurological diseases

The word ‘mimetic’ in neurotrophin mimetic is broadly used to illustrate a modulator with similar structural features of neurotrophic factor and stimulating the property of neurotrophin molecules. Mimetic group of members might act as receptor agonists [86-88] or antagonists [86,89-91]. However, some group of mimetics binds in a non-competitive manner at neurotrophin receptor to upregulate or downregulate the activity

of receptor to change the expression of different cellular proteins to induce neuritogenesis [92,93].

In recent years attention has been paid to the characterization of novel neurotrophin peptidomimetics in clinical trials of different neurological diseases due to their therapeutic approach to neuroprotective effect, synaptic and neuronal plasticity, neurogenesis, better pharmacokinetics than the parent neurotrophin [86,94,95]. Neurotrophin mimetics may trigger the change in different prospects of signalling pathways in a manner that is unique from the native neurotrophin-triggered pathways [82].

1.4. Model organism for neurobiological studies

1.4.1. Rat pheochromocytoma (PC-12) cell as an *in vitro* model

The rat pheochromocytoma cell line (PC-12 cells) is considered to be an appropriate *in vitro* model for neuronal differentiation, development, and neurological diseases [96-100]. PC-12 cell lines have advantages in being derived from neural crest cells that have similar structures and functions, and they are easy to grow and maintain [99].

1.4.2. *Caenorhabditis elegans* (*C. elegans*) as *in vivo* model

Caenorhabditis elegans, a tiny microscopic nematode, is a good choice of *in vivo* model for its wide acceptability in neuronal research to understand the development of neural lineages and neuronal differentiation. The advantages of using *C. elegans* as a model organism are its transparent body, small size, short life cycle, and prominent and well-developed nervous system; consequently, they serve as a widely-used model organism for neuronal research [101-104]. Unlike experimental rodents, they do not require any room for growth, their maintenance is easy and cost-effective, and they can save the life and high expenses of using laboratory experimental animals. A transgene strain (BZ555; Pdat-1::gfp) has dopaminergic (DAergic) neurons expressing green fluorescence protein (GFP), and has been used to study neurodegeneration.

Another *C. elegans* strain (NL5901; Punc-54:: α-synuclein:: YFP+unc-119) expressing the human α-synuclein protein tagged with yellow fluorescence protein (YFP) in the muscles (one of the critical proteins involved in PD), can easily live imaged by *a* confocal microscope. Therefore, neuronal damage caused by toxic substances and their

regeneration by a therapeutic molecule can be assessed speedily in *C. elegans* model [105-108]. Further, the genome of this worm is wholly sequenced and shows 60-80% similarity with human genes, which is an added advantage of using them as *in vivo* model organisms [109-111].

In 1993, Lee et al. reported the first miRNA, lin-4, discovered in *C. elegans*, which targets lin-14 and regulates the aging process in *C. elegans* [112]. Since then, *C. elegans* has been used as a model system for researching miRNAs related to neuronal development and their target genes [113-115]. *C. elegans* as a model system has proven several advantages, including highly conserved miRNAs during its evolution, well-known neural networks, and neuroanatomy [116]. Moreover, it is in high demand to understand the role of miRNAs in neurobiology and their dysfunction related to medical implications.

1.4.3. Micro-RNAs

MicroRNAs (miRNAs) are small non-coding RNAs with an approximate length of 22–24 nucleotides that act as transcriptional repressors primarily by binding to the 3′-untranslated region (3′-UTR) of target mRNAs [116]. Micro-RNAs regulate a range of biological functions, such as ageing, proliferation, development, differentiation, apoptosis, inflammation, immune response, and neurodegeneration [117,118] by targeting the genes involved in these processes [119]. Altered expression of miRNAs ends up in various diseases, including NDs [116-118]. Although some miRNAs, for example, miR-64, miR-81 [120], and miR-128 [121], etc., have been reported to be involved in regulating specific biological processes; however, the function of a large number of miRNAs has yet to be revealed [116].

In the field of neuroscience, accumulated evidence progressively revealed the potential of miRNA in regulating neurodevelopment, neurite outgrowth synaptic plasticity, memory process, neurodegeneration, and nervous system morphogenesis [122,123]. Numerous miRNAs are reported as biomarkers in the pathogenesis of NDs, which imparts targets for ingenious therapies [124-127]. An individual miRNA can affect multiple target genes; therefore, the entire phenotype of the disease can be improved by modifying a single miRNA. This property makes RNA molecules very captivating from therapeutic prospectives. Moreover, the identification of dysregulated miRNAs in ND or

other disease cases may help in early diagnosis or monitoring of the disease progression [127].

1.5. Gap in the study

Despite the success of mammalian NGFs in diseased animal models for treating neurogenerative disorders, their clinical trials need to look more promising as drug prototypes. The failure of applying large neurotrophin polypeptides as drugs (poor pharmacological agents) can be attributed to various reasons, such as undesired pleiotropic effect, short half-life, proteolytic degradation, and poor pharmacokinetics. To overcome the impediments associated with the isolation, purification, and therapeutic application of high molecular weight neurotrophins, research on developing low-molecular-weight mimetics of the neurotrophins possessing innate neurotrophic activity and improved pharmacokinetic role to replace the traditional neurotrophins for treating the neurodegenerative disorders has gained tremendous momentum in recent years. There is a dearth of knowledge on snake venom neurotrophins and their low-molecular-weight mimetics in treating neurological disorders.

1.6. Objectives of this study

By *in silico* analysis, our laboratory has synthesized four custom peptides from the TrkA receptor binding region of Indian Russell's viper (*Daboia russelii*) and Indian cobra (*Naja naja*) venom NGF molecules. These peptides were characterized further to develop as potential drug prototypes to treat neurodegenerative disorders. The specific objectives of the present research work are mentioned below.

1. To study the interaction of synthetic custom peptides with mammalian TrkA receptor and TrkA homolog in *C. elegans* by computational (*in silico*) analysis.

2. To study the *in vitro* mechanism of neuritogenesis and neuroprotective role, of custom peptides in pheochromocytoma of the rat adrenal medulla (PC-12) cells.

3. To study the *in vivo* neuroprotective mechanism of custom peptides in *C. elegans*.

4. To study the microRNA expression profile in custom peptides-treated cultured *C. elegans*.

CHAPTER II

REVIEW OF LITERATURE

2.1 Therapeutic role of conventional neurotrophins and neurotrophic factors (NTFs) derived from natural resources for treating neurodegenerative diseases

The therapy that can avoid the death of the neuronal cell either by inhibiting or intervening in various pathogenetic cascades that initially result in the dysfunction of the cell and eventually lead to the cell's death is defined as neuroprotection [1]. The theory of neuroprotection preserves some of the damage after administering the agent or prevents further adverse effects. Since the discovery of neurotrophins, their crucial role in regulating numerous essential neuronal functions, such as promoting neurite regeneration, preventing neuronal degeneration, and increasing synaptic plasticity, has been elucidated by various researchers both in *in vitro* laboratory studies and in *in vivo* experimental models [2-4].

Anticipating the remarkable physiological activity of NTFs in neuroprotective function and restoration of neuronal damage, they hold enormous potential to treat NDs [5]. Such examples include the reduced level of BDNF (essential for memory and learning) reported in some regions of the brain, viz. substantial nigra in PD patients [6], and reduced level of NGF noted in AD patients [7] eventually leads to a withdrawal of neuronal function and decrease the number and size of neurons. Therefore, maintaining the level of neurotrophins in the related degenerating region of the brain is a tremendous therapeutic invention. Studies have shown that systemic administration of exogenous neurotrophin molecules exerts prominent effects on neuronal development, thus suggesting they have significant therapeutic potential in the treatment of NDs malignancies, inflammations, and neuronal injury [8-11]. Some examples of the therapeutic significance of NTFs are mentioned in the following section.

2.1.1 BDNF delivery as a therapeutic target for PD and HD

Numerous reports highlight the therapeutic activity of NTFs in *in vivo* models of NDs induced by different neurotoxins (such as paraquat, acrolein, heavy metals, rotenone, etc.), which alter motor functions [7]. BDNF over-expression following BDNF gene transfection in dopamine neurons associated with D3 receptor activation, emerging as an essential strategy to restore the function of dopamine neurons in the 6-hydroxydopamine (6-OHDA)-induced rat PD model [12]. Baydyuk and Xu (2014) have established the significant contribution of the decreased level of striatal BDNF in HD pathogenesis and

highlighted BDNF-TrkB downstream signalling pathway as a probable therapeutic target for the treatment of HD pathogenesis [13].

2.1.2 NGF delivery as a therapeutic target for AD

NGF treatment has immense potential to prevent the degeneration and dysfunction of cholinergic neurons in *the in vivo* AD model [14]. Tuszynski et al. (2005) performed a phase 1 clinical trial of ex vivo NGF gene delivery with AD patients and marked the restoration in the rate of cognitive decline [15]. Other studies demonstrated the first clinical trial (Registration no: NCT01163825) with NGF delivery via implantation of encapsulated and genetically modified NGF-producing human cell line (NsG0202 implant) to the cholinergic basal forebrain of AD patients. The implants were taken off smoothly at 12 months and continual NGF secretion was observed in half of the AD patients [16]. Therefore, experimental and clinical facts confirmed that NGF can be a promising candidate for treating AD pathogenesis. NGF delivery alleviates Aβ accumulation and recovers cognitive and behavioral activity [14,17].

2.2 The challenges associated with the therapeutic application of conventional neurotrophins in treating NDs

Despite all the therapeutic potential of neurotrophins or NTFs, some studies have reported various issues and challenges related to the clinical implementation of NTFs. The most significant impediments associated with the clinical use of NTFs are their poor pharmacokinetic properties, short *in vivo* half-lives, and poor penetration via BBB [11,18]. However, the proteolytic degradation, rapid clearance mechanism (fast excretion by kidneys), and different binding sites on the peripheral tissues restrict access of the NTFs to the neuronal targets [18]. Therefore, as summarised in Fig 2.1, clinical application for neurotrophic factors has to face multiple limitations regarding pharmacokinetic features of delivery, physiochemical characteristics, and physiological aspects of the CNS compartment, [5].

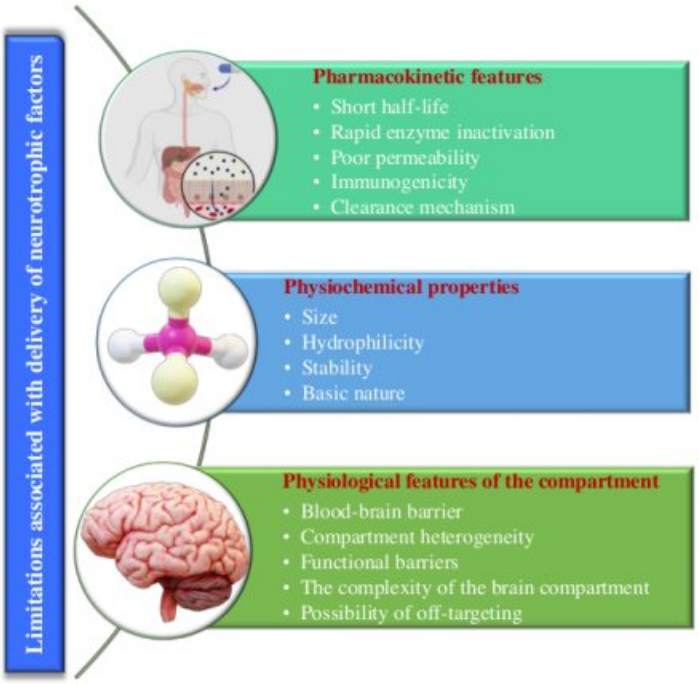

Fig 2.1 Limitations associated with the clinical application and delivery of neurotrophic factors. Created with BioRender.com.

2.3 Advantages of neurotrophin mimetic molecules over parent neurotrophins as therapeutics

There is an urgent requirement to resolve these impediments for the successful therapeutic application of neurotrophins. Several strategies focusing on the better pharmacokinetics of native neurotrophins, such as a small molecule or synthetic peptide (peptidomimetic) development that binds to specific receptors or neurotrophins mimetic have been suggested [19-21]. A peptidomimetic is a compound with pharmacophore similarity that mimics natural protein-fragment, peptide, or whole protein and which also possesses the ability to interact with the specific target and generate similar biological effects [22,23]. Peptide mimetics provides an obvious way to tackle the disadvantages of natural peptides. The molecule that mimics the biological activity of a natural peptide and has a molecular weight of less than 700 Da is referred to as a peptide mimetic. Peptide mimetics have significantly improved patient compliance and cost savings [23].

Moreover, peptide mimetics are far less expensive to produce than natural peptides. Also, natural peptides not encountered with peptide mimetics have issues with peptide storage, stability, and immunoreactivity [24]. In recent years, peptide mimetics have emerged as a new generation of promising drugs due to the rapid screening of small molecule libraries and rational design approaches [21,25].

The pharmacological benefits of peptidomimetics over protein therapeutics comprise favourable pharmacokinetic profiles, low molecular mass, absence of immunogenicity, and low cost [26,27].

2.4 Trends in the discovery of therapeutic peptide

The journey of peptide drugs started more than 100 years ago (Fig 2.2) when benzoylglycylglycine, the first dipeptide, was discovered by Theodor Curtius in 1881 [28]. Shortly, Emil Fischer (1901) synthesized the first unprotected dipeptide glycylglycine, and in 1902, he got a Nobel Prize for chemistry [28,29]. In the 1920s, since the emergence of insulin therapy, curiosity about peptide-based drugs has extensively increased [30]. du Vigneaud (1953) synthesized oxytocin as the first synthetic polypeptide that emerged as a therapeutic agent.

The commercial interest of an industrial group increased in peptide therapeutics, and peptides became more studied as an essential future for drug candidates in the 1960s. However, during that time, peptide synthesis by solution-phase method required years of effort. In 1963, the discovery of solid-phase peptide synthesis (SPPS), along with the advancement in the purification methods, gained significant focus from the pharmaceutical industry [31], and in 1984 Bruce Merrifield received the Noble Prize in Chemistry for his achievements [32]. The 1970s saw the progression in molecular biology techniques like recombinant DNA technology that facilitated the industrial-scale production of therapeutic peptides. Furthermore, human insulin was the first accepted therapeutic peptide produced in 1974 [33].

Over the last few decades, great progress in peptidomimetics technology has taken place, which has promoted researchers and industries to identify peptides of therapeutic utility, and various peptides (natural and synthetic analogues) are undergoing clinical studies [34]. Since insulin was the first accepted therapeutics, around 80 peptide therapeutics or more are available in markets for a range of diseases such as cancer, diabetes, multiple sclerosis, chronic pain, HIV infection, and osteoporosis [32].

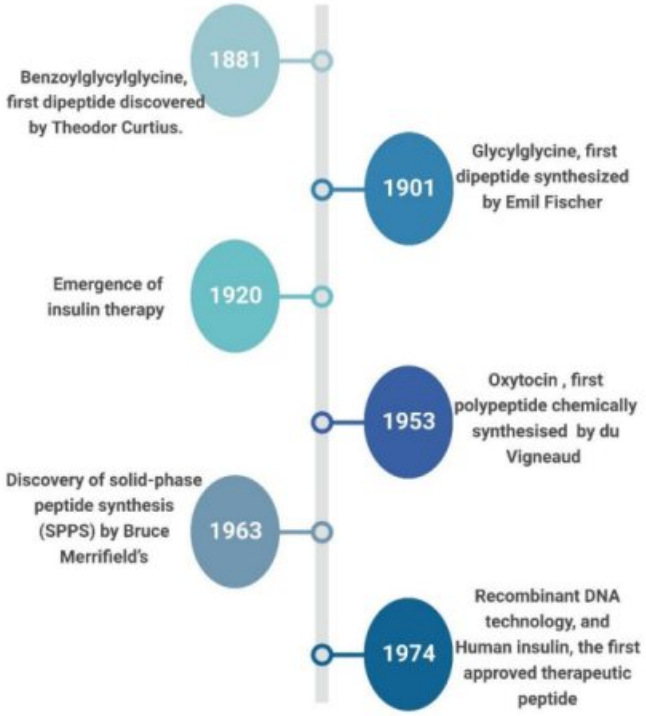

Fig 2.2 Trends in peptide therapeutic development. Created with BioRender.com

2.5 Application of peptidomimetics as drug prototypes to treat NDs

2.5.1. Peptide mimetics to NGF and TrkA receptor: Longo et al. (1990) were the first to show that NGF mimetics, which is a small cyclized dimeric peptide, P7 (KGKE amino acid residues) exerts p75NTR-dependent neurotrophic activity and inhibits neuronal death [35]. The first cyclic dimeric peptide P7 (CATDIKGAEC amino acid residue) mimetic to NGF domain was verified to trigger a neurotrophic response after binding through p^{75NTR} receptor (p^{75NTR} antagonist) and protect neurons from beta-amyloid (Aβ) induced cell death [36]. The study persistent with the site-directed mutagenesis revealed that the NGF residues Lys32, Lys34, and Lys95 are crucial for the interaction of NGF to p^{75NTR} [37].

Scientists further expanded their findings and showed that peptide P7, NGF peptidomimetic blocked amyloid β (Aβ) binding to the p^{75NTR} receptor and protected from the cell death caused by Aβ [36]. Mutagenesis studies have indicated that the NGF loop 4 domain is one of the domains crucial for the binding of TrkA; hence peptide mimetics of the NGF loop 4 domain plays a significant role in interacting with TrkA receptor

[37,38]. LeSauteur et al. (1995) reported cyclic peptide mimetics to NGF β-loop [24] inhibited the NGF-induced growth of neurite in PC-12 cells, acting as a potent 'antagonist' of TrkA receptor [39]. However, they exhibited no neurotrophic potential without NGF, implying their 'agonist' activity [39].

On the other hand, a monomeric peptide C (92-96) maintained the survivability of PC-12 and other cells when monoclonal antibodies bound the p^{75NTR} receptor, signifying a 'partial agonist profile' [40]. Cyclized dimeric peptide, C (92-97) of β-turn appears to mediate TrkA binding, is responsible for *in vitro* activation of TrkA, and encourages the survival of neuroblastoma and PC-12 cells [40]. The NGF-like neurotrophic activity demonstrated by cyclic dimeric peptide loop4 mimetics P92 induces TrkA-dependent ERK and Akt signal transduction pathways [41]. A Series of functional peptides mimetics to the C-D loop of NGF were designed to understand their bioactivity [42,43]. Another peptide mimetic to NGF named LIL4 established NGF agonist activity in PC-12 cells and a rat model of neuropathic pain [44].

Estenne-Bouhtou and team (1996) combined various NGF areas in one molecule [45]. Two β-hairpin loops, L1 and L4, were united by them to produce active peptide mimetics of NGF. It has been reported that a synthetic chimeric peptide NL4, including the NGF loop 4 hairpin motif linked to the nucleic acid binding domain, shows a potential advantage for targeted gene delivery to cells or tissue expressing TrkA receptors [46]. Peptide mimetics to two linear sequences of N-cadherin extracellular domain 1 (INPISGQ and HAVDI) act as an antagonist [47]. In contrast, a cyclic peptide N-Ac-CHAVDINGHAVDIC-NH2 consists of a tandem repeat of individual motifs. It acts as an N-cadherin agonist capable of stimulating the outgrowth of neurites in a comparable way to native N-cadherin [48].

Another TrkA selective peptide mimetic to NGF named D3 (TrkA partial agonist) is homologous to the β loop of the NGF side chain, inducing TrkA dimerization and supporting dorsal root ganglion neurons to survive [49]. Compound D3 has been found to protect root ganglion neurons from degeneration, improve memory in aged rats after the administration by intracerebroventricular minipump [40,50], and rescue short-term memory deficit [51]. Furthermore, MIM-D3, a TrkA agonist peptidomimetic, enhanced the secretion of glycoconjugate and significantly improved corneal injury in a rat with dry eye syndrome [52,53].

The design of dimeric dipeptide mimetic of NGF loop4 named GK- 2 (bis(N-succinyl-Lglutamyl-L-lysine) hexamethylenediamine) indicated therapeutic impact in *in vitro* neuronal cells and an *in vivo* rat model of neurodegenerative disorders like PD and AD, diabetes mellitus and brain ischemia with no side effects [2]. Gk-2 dimeric peptide completed the pre-clinical trials as a therapeutic drug for healing poststroke situations without adverse side effects [21,54]. In 2021, Tarasyuk et al. reported synthesizing two analogues of the peptide mimetics to NGF loop1 bis-(N-aminocaproic-glycyl-L-lysine)hexamethylenediamine (GK-6) that are bis-(N-acetyl-glycyl-L-lysine)hexamethylenediamine (GTS-611) and bis-(N-aminocaproyl-glycyl-glycine)hexamethylenediamine (GTS-613). The GTS-613 analogue of GK-6 showed neuroprotective effects in oxidative stress induced-HT-22 neuron cells *in vitro* at concentrations of 106 and 105 M, whereas GK-6 and GTS-611 induced distinction in PC-12 cells [55].

A synthetic peptide consisting of N-terminal encoding amino acid 1-14 of human NGF (hNGF 1-14) has been reported to induce TrkA-dependent cascade in PC-12 cells, comparable with native NGF [3]. Peptide derivative hNGF1-14 (TrkA agonist) triggered neuronal activity in the CNS and PNS, signifying that peptide hNGF1-14 can retain the neurotrophic potency of parent NGF [4]. The acylated form of hNGF1-14 (Ac-hNGF1-14) has prospected to show even better potency in inducing TrkA signaling that signifies the increasing stability of the peptide, which in turn might influence the ligand-receptor complex formation [4].

Previously, *in vitro*, studies have demonstrated that hNGF 1-14 mimics the whole NGF activating TrkA-dependent downstream pathways catalyzed explicitly by the Zn^{2+} and Cu^{2+} metal ions [56]. Peptide mimetics of NGF-mediated phosphorylation of cyclic AMP response element-binding protein (CREB) transcription factor ensued in the enhanced appearance of BDNF [4,57].

2.5.2. Peptide mimetics to BDNF and TrkB receptor: BDNF specifically binds to TrkB and encourages synaptic function, neuronal survival, and differentiation [58]. In recent years, research focus has intensified toward peptide mimetics to BDNF loops 2 and 4 as a therapeutic agent for treating neurodegenerative diseases like AD [20,59]. Cyclic monomeric peptides analogous to BDNF Loop 2 that may acquire BDNF-like antagonist activity had no intrinsic activity [60]; however, cyclic dimeric peptides analogous to loop

2 promoted neuron survival with lesser efficacy than native BDNF and some possessed pro-survival properties [61].

Linear, monomeric, synthetic tetra peptides (B-1 to B-5) developed from the loop 4 carboxy-terminal region of BDNF-induced TrkB phosphorylation. They (peptides B-3 and B-5) displayed a neurotrophic effect in cultured hippocampal neuronal cells [62]. Active dipeptide GSB-106 mimetics of BDNF loop 4 was designed that exhibited in oxidative stress (H_2O_2-induced) model of rat hippocampal cell line HT22 and *in vivo* neuroprotection activity in Balb/c male mice model and provided the basis for the development of anti-depressant drug under preclinical studies (https://4science.ru/project/14- N08- 12- 0086) [54,63]. Neuroprotective activity of GSB-106 was found *in vitro* neurotoxin 6-hydroxy dopamine (6-OHDA) induced-SH-SY5Y human neuroblastoma cells [64].

To explore the receptor binding role of the BDNF loop, Fletcher and Hughes designed a total of five monomeric monocyclic peptides mimetics, loop1 analogue (L1), loop 2 analogues (L2a and L2b), and loop 4 analogues (L4a and L4b) [8]. All designed peptides were discovered to inhibit BDNF neurotrophic effect; however, interestingly, one peptide mimetics of BDNF loop 4(L4a-L4b) acted as a partial BDNF-like agonist [65]. In addition, cyclized pentapeptide2 (cyclo(-D-Pro-Ala-Lys-Arg-) derived from BDNF loop 4 binding regions to p^{75NTR} showed neurotrophic activity without Trk B activation [66]. Further, it was investigated that this pentapeptide cyclo-D PAKKR promoted neuronal myelination *in vitro* dorsal root ganglion sensory neurons and *in vivo* rat model via p75NTR receptor [9,66].

The therapeutic role of cyclo-D PAKKR was further studied in experimental autoimmune neuritis (EAN), demyelinating peripheral neuropathy rat model [67]. The most bioactive peptide, tricyclic dimeric peptide 6 (TDP6), a small polycyclic peptide that mimics the BDNF region that binds TrkB to act as a TrkB agonist, significantly inhibits *in vitro* TrkB-dependent oligodendrocyte myelination [68].

Using a peptidomimetic approach, scientists developed a cyclic peptide cyclotraxin-B derived from BDNF, a highly variable region III, a TrkB inhibitor that inhibited both BDNF mediated and BDNF independent activities [69,70]. Recently, peptide mimetics of neurotrophin molecules have found use in several clinical trials [54,71]. Some small peptides function as inhibitors and mimetics of BDNF pair of loops

appropriate for therapeutic use [61,65]. BDNF tetrapeptides were identified that mimic the neurotrophic effect of BDNF in mouse hippocampal cell culture [62].

In 2010, a study described two mimicking peptides, Betrofin-3(RGI, RGIDKRHWNSQ) and Betrofin-4 (SYVRALTMDSKKRIGWR), were obtained from the loop-3 and loop-4, respectively, of BDNF, which interacted with BDNF receptors, TrkB and p75NTR to induced neurite outgrowth as well as to increase the neuron survival through MAPK and Akt pathways [72]. These pathways are also activated by native BDNF post-binding to TrkB and p^{75NTR} [59].

Zhan et al. (2013) reported a novel self-assembling nanofibre scaffold (SAPNS) named RADA16-I to uphold peripheral nerve regeneration in a sciatic nerve injury model [73]. Because peptide mimetics to BDNF alone were not sufficient to activate the receptor, scientists developed a functionalized self-assembling peptide that was produced by BDNF-derived neurotrophic peptide (RGI) to the self-assembling peptide RADA16-I C-terminal (Ac-(RAD)4-CONH2) that promoted nerve regeneration with increased re-myelination and recovered motor function [74].

2.5.3. Peptide mimetics to NT-3 and Trk-C receptor: β- turn peptidomimetics are produced to mimic the NT-3 hot spot that binds to TrkC receptor subtype and NT-3 like neurotrophic function [75-77]. A Peptidomimetics mini-library has also been designed based on the β-turn of NGF and NT-3 [78]. Some peptide mimetics elicited neuritogenesis and survival, whereas others caused either survival or neurite outgrowth [78]. This group also described the design and synthesis of bivalent TrkC peptide mimetic ligands that promoted neuritogenesis or potentiated phosphorylation of TrkC [79].

The list of neurotrophins mimetics-based treatment of NDs is summarised in Table 2.1.

Table 2.1. Peptidomimetic-based treatment of NDs with neurotrophin

Neurotrophins	Sequence	Neurodegenerative diseases (NDs)	Model	Mechanism of action	References
NGF loop 1 mimetics	IPenKGKEVCT NGF partial agonists	Neoplasia	*In vitro* Dorsal root ganglia chick embryos, mice	Encourage neuronal survival via p75 dependent mechanism	[35,39]
NGF loop 4 mimetics, P92	TDEKQ, NGF partial agonist	Neurodegenerative disease	*In vitro* Dorsal root ganglia chick embryos	TrkA-dependent ERK and Akt signaling. Promote both survival and neurotrophic activity.	[41,80]
NGF β turn	Peptidomimetic	Neurodegenerative disease, pain, neoplasia	*In vitro*		[40]
NGF mimetics containing KGA amino acid sequence	CATDIKGAEC p75NTR antagonist	Alzheimer's disease	*In vitro* p75 NTR- and p140trkA-NIH-3T3 cell and E17 foetal rat cortical neurones	Block the Aβ-mediated p75 NTR signaling and arresting the Alzheimer's disease progression	[36]
NGF loop 1 and 4 mimetics, LIL4	CTDIKGKCTGACDGKQC NGF agonist	Neuropathic pain	*In vitro* in chick dorsal root ganglia, PC-12 cells, and; *in vivo* rat model of peripheral neuropathic pain	Induced tyrosine phosphorylation of TrkA, but not TrkB, receptor and restored neuropathic behavior in a rat model of peripheral neuropathic pain	[44]

NGF mimetics, C(92-97)$_{dimer}$	Cyclized dimer C(92-97)$_{dimer}$ *N*-Ac-YCTDEKQACY	Neoplasia, pain	*In vitro* neuroblastoma and PC-12 cells	Induced TrkA dimerization, phosphorylation, and internalization	[40]
NGF loop C-D mimetics,	N-acetyl-YCTDEKQCY		*In silico*	An essential constituent of induced-fit ligand binding between the NGF C-D loop and TrkA.	[42,43]
NGF loop 4 mimetics	NL4 and NL4-10K Synthetic peptide for targeted gene delivery	Neurodegenerative disease	*in vitro* in PC-12 cells and NIH3T3 cells	Act through TrkA to trigger the same signal transduction pathways that NGF activates.	[46]
N-Cadherin mimetics	*N*-Ac-CHAVC-NH2 N-cadherin antagonists	Axonal regeneration	*In vitro* 3T3 cells		[47,48]
D3	Peptidomimetics, Trk A agonist	Neurodegenerative disease, rescue short-term memory deficit	*in vitro* PC-12 cells and; *in vivo* cognitively impaired aged rats	Induce dimerization and activation of TRK Receptor. Inhibits loss of dorsal root ganglion neurons.	[50,51]
MIM-D3	TrkA agonist	Dry eye treatment	Phase III clinical trial (https://clinicaltrials.gov/ct2/show/study/NCT03925727)	Promotes secretion of glycoconjugate from cultured conjunctival cells and improved concentration of glycoconjugates in the tear fluid of normal rats	[52,53]

GK-2 mimetics to NGF loop4	The beta-turn sequence of NGF loop 4, GK-2	Neurodegenerative disease, brain ischemia, diabetes mellitus	Pre-clinical studies *in vitro* mouse hippocampal neurons (line HT-22), primary culture of rat hippocampal neurons (HN), PC-12 cells of rat pheochromocytoma, and; *in vivo* in rats model	Crossed the blood-brain barrier without any toxic effect. Binds with TrkA receptors and specifically triggers PI3K/ Akt signaling pathway. Neuroprotective with no side effects.	[2,54]
NGF mimetic hNGF 1-14, Ac-hNGF1–14, hNGF1–15 dimer	human NGF 1–14 sequence (SSSHPIFHRGESFV-NH2); Ac-hNGF1–14 (Ac-SSS H4PIFH8RGESFV-NH2); hNGF1–15 dimer (SSS HPIFHRGESFC-S)$_2$ TrkA agonist	CNS diseases	*in vitro* PC-12 cells, Dorsal Root Ganglion Dissociated Culture and	hNGF1–14 peptide has shown full NGF-mimetic potential; Survival and differentiation of dissociated dorsal root ganglia (DRG)	[3,4,56]
BDNF loop 2 mimetic	Cyclic peptide partial BDNF-like agonist	Neurodegenerative disease	*in vitro* dorsal root ganglion sensory neurons	TrkB dimerization, Neuron survival	[61]
BDNF mimetics tetra peptides B3 and B5	Peptide B-5 (Ac-I-K-R-G-CONH2), B-3 (Ac-S-K-K-R-CONH2), BDNF partial agonist and antagonist	Neurodegenerative diseases, depression, stress,s and anxiety	*in vitro* mouse primary hippocampal neuronal culture	Increase the expression of BDNF and TrkB	[62]
BDNF loop 4 mimetics dipeptide GSB-106	GSB-106 [28], TrkB agonist	Psychiatric disorders, cerebral ischemia	Preclinical studies *in vitro* hippocampal cells of the HT22, SH-SY5Y human neuroblastoma cells and *in vivo* Balb/c male mice	Activation of TrkB-dependent pro-survival.	[54,63,64,81,82]

BDNF loop 4 mimetics Penta peptide cyclo-D PAKKR	cyclo-DPAKKR	Demyelinating diseases	*in vitro* dorsal root ganglion sensory neurons and *in a vivo* rat model	Promote NF- B pathway via a p75NTR-dependent manner. Enhances NRG1-typeIII expression in developing sciatic nerve.	[8,9,61,65-67]
BDNF mimetic multicyclic peptide TDP6	(Ac-CVPVCKGQLCE-NH_2)$_2$ dimerize by E-K amide bond TrkB agonist	Oligodendrocyte myelination	*in vitro* dorsal root ganglion sensory neurons	TrkB-dependent oligodendrocyte myelination, ERk1/2 activation	[68]
BDNF mimetic cyclic peptide cyclotraxin B [60]	CNPMGYTKEGC (Disulfide bridge: Cys1-Cys11), TrkB antagonist [60]	Brain disorders	*in vitro* Cortical neurons, PC-12cells, and *in vivo*	Allosterically alters the TrkB conformation and inhibits both BDNF-dependent and basal activities	[69,70]
Betrofin 3 and Betrofin 4 mimetics of BDNF loop 3 and 4 [23]	Betrofin 3 RGIDKRHWNSQ, Betrofin 4 (SYVRALTMDSKKRIGWR) partial agonist	Neurodegenerative diseases	*in vitro* Cortical neurons	Induce signaling Through TrkB and p75NTR-mediated Akt and MAPK pathways. Enhanced neurite outgrowth and survival	[72]
NGF loop 1 mimetics GK-6 and their analogs GTS-611 and GTS-613	bis-(N-aminocaproyl-glycyl-L-lysine) hexamethylenediamide(GK-6),bis-(N-acetyl-glycyl-Llysine)hexamethylenediamide (GTS-611) and bis-(N-	Neurodegenerative diseases	*in vitro* oxidative stress-induced HT-22 neuron cells	GTS-613 shown neuroprotective effect, GK-6 and GTS-611 induce differentiation in PC-12 cells	[55]

	aminocaproyl-glycyl-glycine)hexamethylenediamine (GTS-613)				
dimeric peptide analogs of two agonists	two agonists directed to the extracellular domain of TrkA: the peptide sequence of NGF itself, and the anti-TrkA monoclonal antibody 5C3	Neurodegenerative diseases	PC-12 cells	Binding competition, promoting TrkA phosphorylation and differentiation of cultured sensory neurons	[40]
small molecule peptidomimetics	based on β-turns of NT-3 and NGF	Neurodegenerative disease	PC-12 cells	Binding competition; promote neuron survival and/or neurite outgrowth	[78]
LM22A4	Small molecule non-peptide based on the loop 2 domain of BDNF	Traumatic brain injury	Rat model	promotes survival of hippocampal neurons in a TrkB-dependent manner	[58]
LM11A-24	Small molecule non-peptide p75NTR ligand	Neurodegenerative disease		prevents p75NTR – dependent cell death	[83]

2.6 Snake venom derived peptidomimetics as therapeutics to treat neurodegenerative disorders

In previous studies, NGFs have been isolated and characterized from *Vipera lebetina* [84,85] and *D. russellii* snake venom [85-88]. Islam et al. (2020) have isolated and characterized Nn-α-elapitoxin-1 from Indian Cobra *N. naja* venom which exhibits neuritogenesis potency (similar to other neurotrophin molecules) but no sequence similarity to conventional nerve growth factor (NGF) [89]. Venoms also contain neurotropic factors that induce sympathetic and embryonic sensory neuron differentiation and regulate neurite outgrowth from rat PC-12 cells. The PC-12 cells are clonal cells that are derived from stem cells of rat pheochromocytoma and show the phenotypic characteristics correlated with pheochromocytomas as well as their nonneoplastic counterparts; adrenal chromaffin cells [90]. In response to different neurotrophins, the cell line PC-12 is a useful model system for neuronal differentiation [91,92]. NGF facilitates the transformation of these pheochromocytoma cells into cells that develop sympathetic neuronal features [93].

Snake venom contains a mixture of peptides and proteins with various biological roles [94]. In the envenomed casualty, these biomolecules disrupt fundamental processes, leading to morbidity and death. Conversely, they also elicit signaling pathways that show advantageous effects in particular diseases. Throughout the years, convincing attempts have been made to identify new molecules from snake venom and modify them into therapeutic tools [95]. Since the development of the first peptidomimetic drug 'Captopril' derived from snake venom, numerous other toxins have been investigated as naturally active with therapeutic potential that might signify a potential alternative [96,97].

A tripeptide (p-BTX-I) derived from *Bothrops atrox* venom shows neuroprotective and neurotrophic effect at the dose of 192 µM in PC-12 cell line treated with dopaminergic neurotoxin 1mM 1-Methyl-4-phenylpyridinium iodide (MPP+), active metabolite of the putative inducer of Parkinson's disease (PD), MPTP [98]. Further studies have reported that p-BTX-I (25 μg) also shows protection against acrolein (10 μM)-induced AD model of PC-12 cells and improves bioenergetics and synaptic plasticity [99]. Therefore, synthetic peptides derived from snake venom hold considerable potential as drug candidates for treating NDs.

CHAPTER III

MATERIALS AND METHODS

3.1 Materials

3.1.1 Synthetic custom peptides

Custom peptides trideca-neuropeptide (TNP) and heptadeca-neuropeptide (HNP) and fluorescein isothiocyanate (FITC)-S Biochem, Thrissur, Kerala, India synthesized conjugated peptides. Sequences of these peptides are shown in Chapter IV.

3.1.2 Cell lines, cell culture reagents, and cell culture plastic wares

The rat adrenal phaeochromocytoma (PC-12) cell line (initial passage number 8) (CRL-1721™) was procured from the American Type Culture Collection (ATCC), USA. Rat myoblast or myogenic cells (L6) (initial passage number 18), human breast adenocarcinoma cells (MDA-MB-231) (initial passage number 16), and Michigan Cancer Foundation-7 (MCF7) cells were obtained from the National Centre for Cell Science (NCCS), Pune, India. The specification sheets provided by NCCS and ATCC stated the authenticity of the microbial contamination-free cell lines we procured from them. Each cell line was subjected to 5-6 or more passages during the experimental plan.

Dulbecco's Modified Eagle Medium (DMEM), Eagle's Minimum Essential Medium (MEM), trypsin, and heat-inactivated fetal bovine serum (FBS) were purchased from GibcoTM (USA). Cell culture accessories and sterile plastic plates were procured from Thermo Fisher Scientific, USA.

3.1.3 *Caenorhabditis elegans* strains and *Escherichia coli*

C. elegans Bristol wild-type strain N2, NL5901, BZ555, the bacterial control food *E. coli* OP50 (OP50), were purchased from Caenorhabditis Genetics Centre (CGC), University of Minnesota, USA. CAM-1(ak37) mutant strain was a kind gift from Dr. Kavita Babu, Associate Professor, Indian Institute of Science, Banglore.

3.1.4 Neurotrophic factors and fine chemicals

The nerve growth factor-2.5S from the murine submaxillary gland, fluorescein isothiocyanate (FITC), Thiazolyl blue tetrazolium bromide (for MTT assay), and protease inhibitor cocktail was procured from Sigma-Aldrich, Missouri, USA. All chemicals were of analytical grade from Sigma, Merck, HiMedia, Invitrogen, and Thermo Fisher

Scientific USA. The Annexin V-FITC / propidium iodide (PI) apoptosis detection kit was procured from Cell Signaling Technology (CST, 6592), the MitoProbeTM JC-1 assay kit and the CyQUANT™ LDH cytotoxicity assay kit was purchased from Invitrogen (M34152), from CST. RNAeasy mini kit was purchased from Invitrogen, Waltham, MA, USA, and the cDNA synthesis kit was procured from Thermo Scientific, Waltham, USA.

3.2 Methods

3.2.1 To study the interaction of synthetic Custom Peptides with mammalian TrkA receptor and TrkA homolog in *C. elegans* by computational (*in silico*) analysis.

3.2.1.1 Predicting the binding affinity of synthetic peptides to different domains of human TrkA receptors by *in silico* analysis

The peptides' cheminformatic parameters such as mass, isoelectric point, net charge, hydrophobicity, etc., were computed using the PepDraw server [1]. The peptide sequences were converted to PDB structures, and their dynamics and conformations were studied using molecular dynamic simulations for 100 ns. Simulations were carried out in GROMACS v2022.2 with the CHARMM36 (v 2021) force field. The periodic boundary was a dodecahedron with a 1.5 Å buffer region. Peptide structures were first minimized in a vacuum using 5000 steps of the steepest descent algorithm. The system was solvated using the transferable intermolecular potential with a three-point water model (TIP3P), and 0.15 M sodium chloride ions were added till neutralized. The system was equilibrated using NVT (canonical) and NPT (isobaric-isothermal) ensembles in 300 K and 1.0133 bar. Temperature coupling was done using the v-rescale (Berendsen) method, and pressure coupling was done using c-rescale [2] and integrated using a leapfrog algorithm. Before the production MD run, the position restraints were released following three NPT equilibration runs. The trajectory was studied for root mean square deviation (RMSD), radius of gyration, hydrogen bonding, secondary structure of the peptides, and thermodynamic properties. From the trajectory frames, an average structure of the peptide was derived in a PDB format and used in the subsequent analysis.

A molecular docking study was conducted to predict the binding affinity of custom peptides with the TrkA receptor. Crystal structures of human TrkA (UniProtKB - P04629) domains were obtained from Protein Data Bank (PDB) with entry viz. 2IFG (extracellular

domain), and 5JFX (cytoplasmic domain). The structures were prepared using the protein preparation wizard of the Schrodinger suite (Schrodinger Inc. USA). Briefly, water and hetero atoms were removed, and missing residues and side chains were filled and corrected for alternate positions of the residues. The docking used a peptide dock module with the molecular mechanics/generalized born surface area (MM-GBSA) scoring method. The receptor grid was generated from centroid residues so that the grid box could occupy the whole protein domain. The peptide sequences were then added individually to output the ten best poses for each domain.

Molecular dynamic simulations were conducted using Schrodinger Desmond (Academic version, v.2022). The simulation system comprised the docked peptide complex, solvent, and salts. The TIP3P water model was used as a solvent within an orthorhombic boundary condition with a 10 Å buffer region. NaCl (0.15 M) was added to the system and neutralized using the required number of Na^+ or Cl^- ions. The system was equilibrated with NVT and NPT ensembles at 300 K and 1 bar. The reversible reference system propagator algorithms (RESPA) were used as an integrator (at 2 fs time-steps) of Newtonian dynamics with a column cut-off radius of 1.5 Å. A Nose Hoover chain thermostat and Martyna Tobias Klein barostat were used with isotropic coupling at 1 ps and 2 ps relaxation times. Relaxation of the system was done using the default, which provided a relaxation protocol followed by a production MD run for 300 ns. The energy and trajectory were recorded at every 0.5 ps and analyzed using the simulation interaction diagram module of Schrodinger Maestro. The binding free energies of the simulation trajectory complexes were calculated using the MM-GBSA method.

3.2.1.2 Predicting the binding affinity of synthetic peptides to different receptors in *C. elegans* by *in silico* analysis

The custom peptides were initially developed to target the Human NTRKA. To investigate the binding of these custom peptides, a homologous *C. elegans* protein was used. Human NTRKA protein sequence was obtained from UniProt (ID: P04629), and homologous proteins in *C. elegans* were identified using BLAST search. The structural and functional information about the homologous protein found by BLAST search was retrieved from UniProt. 3D structures of different protein domains in *C. elegans* TRK (CAM-1) were manually modeled using template-based homology modeling and Alpha

Fold Prediction. Furthermore, the binding sites of these domains were predicted in PrankWeb 3 server [3]. Similarly, other proteins were selected based on the neuroprotective pathways from previous studies [4]. The proteins with available 3D structures in PDB were preferably taken. However, the unavailable 3D structures were modeled using homology modeling.

The peptides were processed by molecular dynamics simulation using our previously described method [4], and different properties, such as secondary structure and beta-hairpin loop formation, were analyzed. Subsequently, all the proteins were processed for peptide docking by adding hydrogens, filling missing side chains and residues, and restraining minimization. The peptide docking was carried out in the CABS Dock server [5]. The stability of the docked complexes was further analyzed by molecular dynamic simulation. The simulation was conducted in Schrodinger Desmond (academic version v2022) with an OPLS4 force field. The simulation system was prepared with orthorhombic boundary condition with 10 Å buffer region and solvated with TIP3P water model, followed by the addition of 0.15 M sodium chloride. The system was equilibrated at 300 K and 1 bar using NVT and NPT ensembles. Nose Hoover chain thermostat and Martyna Tobias Klein barostat were used with isotropic coupling at 1 ps and 2 ps relaxation time. The system was relaxed using default options provided by Desmond, and finally, production MD was carried out for 100 ns. The binding free energy of the complexes was calculated using the MM-GBSA method.

3.2.2 To study the *in vitro* mechanism of neuritogenesis and neuroprotective role, of custom peptides in pheochromocytoma of the rat adrenal medulla (PC-12) cells

3.2.2.1 Solid-phase synthesis and biophysical characterization of the custom peptides

The solid-phase peptide synthesis was done using Fmoc protocols for the esterification of amino acid to the wang resin followed by a coupling reaction [6]. The peptide was then detached from the resin and isolated using cold diethyl ether. The purity and molecular mass of the peptides were ascertained by mass spectrometry analysis in a single quadrupole mass spectrometer (Shimadzu LC-MS 2020, Japan) via positive electrospray ionization (ESI). The biophysical properties of the peptides were then calculated in an online peptide property calculator (https://pepcalc.com/). The secondary structures of the peptides were also determined by circular dichroism (CD) spectroscopy (Jasco J715

spectropolarimeter, Japan) following our previously described procedure [7]. CDPRO CLUSTER software was used to determine the secondary structures of the peptides.

3.2.2.2 Cell growth and maintenance

Mammalian cells, viz. PC-12, L6, and MDA-MB-231 were grown and maintained with a complete medium comprising of DMEM containing 1% antibiotic solution (GIBCO™) and 10% heat-inactivated FBS (GIBCO™) and in 75 cm^2 tissue culture flasks at 37°C in a humidified incubator with 5% CO_2. MCF-7 cells were maintained in MEM containing 10% FBS and 0.01 mg/mL insulin. The cells were re-suspended in a medium every 2-3 days and subcultured after reaching confluence [8-10].

3.2.2.3 Assessing the binding of FITC-conjugated custom peptides to TrkA receptor-expressing mammalian cells

Custom peptides were synthesized by S Biochem, Thrissur, Kerala, India, following the previously described protocol with slight modifications [8]. Fresh FITC reagent was prepared (1 mg/mL) in DMSO, added to the resin, and incubated in the dark for 2 h at 4°C. The resin was washed with dimethylformide; standard peptide cleavage protocol was followed. Spectrofluorometric interactions between the FITC-conjugated peptide and TrkA receptors were determined in mammalian cells expressing TrkA receptors, such as PC-12, MCF7, and MDA-MB-231 cells, and in non-TrkA receptor-expressing L6 cells (negative control) following the procedures that were previously described [8-10].

The PC-12, MCF7, MDA-MB-231, and L6 cells (1×10^4 cells per well in 96-well plates) were incubated with the FITC-conjugated peptides (2 μg/mL) at different time intervals (from 0 to 360 min) at 37°C in a humidified incubator with 5% CO_2 (in triplicates). Cells were washed with 1X phosphate-buffered saline (PBS), pH 7.4, three times and then fixed in 4% formaldehyde-PBS solution (pH 7.2) for 15 min at room temperature (~23°C). The fluorescence intensities were recorded at 519 nm (λem~519 nm; [excitation wavelength was 488 nm (λex ~488 nm)] using a multimode plate reader (Varioskan Flash, Thermo Scientific, USA). The fluorescence intensity of cells treated with 0.1% dimethyl sulfoxide (DMSO) was used as a baseline, to which other values were compared.

Similarly, the PC-12 cells (1×10^4 cells) were incubated with graded concentrations (40 nM to 800 nM) of FITC-conjugated peptides at 37°C in a humidified incubator with 5% CO_2 (in triplicates). The fluorescence intensities were recorded at 519 nm using a

multimode plate reader (Varioskan Flash, Thermo Scientific, USA). A hyperbola curve was plotted for change in λmax (Δ λmax) against the concentrations (nM) of custom peptides with PC-12 cells expressing TrkA receptor, and the equilibrium dissociation constant (K_d) value was determined using GraphPad Prism 8.1.1 software.

In another study, the interaction between FITC-conjugated peptide and TrkA receptors was confirmed by fluorescence microscopic image analysis in MCF7 and MDA-MB-231 cells and non-TrkA receptor-expressing L6 cells (negative control) as previously described [9]. The cells were incubated with FITC-peptides with MCF7, MDA-MB-231, and L6 (negative control) cells with or without TrkA receptor inhibitor K252a (100 nM) for 120 min (TNP) and 30 min (HNP) at 37°C in CO_2 incubator. After incubation, cells were washed with 1X PBS (pH 7.4) and fixed with 4% formaldehyde. Then, the cells were mounted on a cover slip and photographed under a fluorescent microscope (Olympus IX 83, Japan) at 40X magnification attached to a CCD camera.

3.2.2.4 Assessing the *in vitro* cell cytotoxicity of the custom peptides

For the cell viability assay, MCF7 cells, PC-12 cells, and myoblast cells isolated from L6 cells (0.1 x 10^5) were grown in 96-well plates at 37°C, 5% CO2, as described by us [11]. Different concentrations of the custom peptides (500 ng/mL to 2 μg/mL) were then added to the wells (in triplicates), and cell viability was assessed after 24 h of incubation by the 3-(4,5-Dimethylthiazol-2-yl)-2,5-diphenyltetrazolium bromide (MTT)-based method [11]. The release of lactate dehydrogenase (LDH) from the treated cells was compared to control cells. The custom peptide-induced cytotoxicity, if any, was expressed as percent cell viability, which was determined by the viability percentage of control cells (control cells were considered to be 100% viable) and LDH released from the triton-X-treated cells (assumed to be 100% enzyme release) [11]. According to the instruction manual, cellular LDH release was measured using the CYQUANT™ LDH cytotoxicity assay kit (Invitrogen, C20300) [12].

3.2.2.5 *In vitro* effect of custom peptides on the mammalian hematological system

For the plasma clotting assay, goat blood was collected from a slaughterhouse in 3.8% trisodium citrate (9:1). The citrated blood was centrifuged at 4,300 rpm for 15 min at 4°C. The yellowish supernatant (the platelet-poor plasma, PPP) was used within 4 h to determine the plasma clotting activity [7,13]. One unit of pro-coagulant (or anticoagulant)

activity was defined as a decrease (or increase) of 1 s in the clotting time of the PPP that was incubated with test samples (5 μg/mL), in comparison to the control PPP (1X PBS, pH 7.4).

The hemolytic activity of goat blood erythrocytes was assayed as described previously [7,13]. Two milliliters of a 5% red blood cells suspension (goat blood) were incubated with each custom peptide (1 μg/mL) / 1X PBS (negative control) / Triton X-100 (20 μL) (positive control) at 37°C for 3 h. The reaction mixture was centrifuged at 4,000 rpm for 10 mins, and 200 μL of the supernatant was put into a 96-well microtiter plate. The absorbance at 540 nm was measured, and the percent hemolytic activity was calculated as stated previously [7,13].

As described previously, platelet-rich plasma (PRP) was isolated from citrated goat blood [7,13]. For assessing the platelet aggregation / de-aggregation properties of the custom peptides, the peptides (TNP, HNP, 1 μg/mL) were mixed with the PRP, and the absorbance at 540 nm was measured for 30 min at 30 sec intervals in a spectrophotometer (Multiskan GO, Thermo Scientific, USA). Percent aggregation / de-aggregation of the platelets was calculated for the treated samples compared to the control.

3.2.2.6 Assessing the neuritogenesis properties of custom peptides in PC-12 cells and the effects of chemical inhibitors on their neuritogenesis potency

For the neurite outgrowth bioassay, PC-12 cells were used as an *in vitro* model [6,8-10]. PC-12 cells are clonal cells derived from stem cells of rat pheochromocytoma expressing TrkA receptors and $p75^{NTR}$, and thus, are recommended as a functional model system for neuronal differentiation [8-10,14]. Our previous study adopted the neuritogenesis assay [8-10]. Cells (1.0 x 10^5 cells/well) were seeded in six-well plates (in triplicates) and kept overnight at 37°C in an incubator with 5% CO_2 to allow the cells to adhere to the surface. The next day, the complete medium (DMEM) containing 100 ng/mL mouse 2.5S-NGF (positive control) / custom peptide (12.5 ng/mL to 100 ng/mL) / 1X PBS, pH 7.4 (negative control) was added to the wells and the plates were incubated at 37°C in 5% CO_2 for 14 days. The old media was replenished with fresh media at intervals of 72 h. Neurite outgrowth of the PC-12 cells was visualized under a phase-contrast microscope (Olympus IX 83, Japan) at 20x magnification. The percentage of neurite-bearing cells and the average neurite length (in μm) were determined using MOTIC IMAGE PLUS 3.0

software. Cells were considered to be differentiated if they had at least one neurite with a length equal to or greater than the diameter of the cell body [6,8-10].

Cells were pre-incubated with a chemical inhibitor, such as TrkA receptor inhibitor K252a (100 nM) / inhibitor of phosphatidylinositol 3-kinase (PI3K) stimulation of protein kinase B (Akt) signaling pathways (PI3K/AKT), pathway LY294002 (30 nM) / inhibitor of mitogen-activated protein kinase (MAPK), pathway U0126 (10 nM), or anti-TrkA, TrkB, and anti-TrkC antibody (1:1000 in DMEM) for 1 h. Cells were then treated with or without the addition of 100 ng/mL (~71 nM) custom peptide/mouse 2.5 S-NGF (positive control, 100 ng/mL) / 1X PBS (control), incubated for 14 days as above. The average length of neurite outgrowth and the percentage of neurite-bearing cells were determined [6,8-10].

3.2.2.7 Assessing the protective role of custom peptides against the PT-induced cytotoxicity in PC-12 cells

The cytotoxicity assay was performed as previously described [8-11]. In brief, PC-12 cells at a density of 1×10^4 cells/well were placed in a 96-well plate and then incubated in 5% CO_2 to facilitate the attachment of the cells to the well. The cells were treated with various concentrations (1- 30 mM) of PT or growth medium (control), and incubated at 37 °C in 5% CO_2 for 24 h. After 24 h, PT-induced cytotoxicity was determined by the MTT-based cytotoxicity assay [11]. A standard curve was generated from each paraquat concentration, and the IC_{50} values were calculated from the regression analysis of growth curves of PC-12 cells in the presence of PT. The protective role of TNP and HNP against PT-induced cytotoxicity (IC_{50} value was determined as 10 mM) was determined by the MTT-based cytotoxicity assay [11]. Cells were pre-incubated / post-treated / co-treated with custom peptides (HNP / TNP) / mouse 2.5S-NGF (positive control) in an increasing concentration-dependent (12.5, 25, 100, 250 and 500 ng/mL; equivalent to 18 nM to 357 nM) and time-dependent (0.5, 1, 2, 4, and 6 h) manner. The percent cell viability for each group was calculated after 24 h of PT incubation, and each experiment was repeated thrice.

Assessing the protective role of custom peptides and their optimum dosages against the PT-induced cytotoxicity in PC-12 cells was also confirmed by quantitating the release of marker enzyme LDH from the treated cells. PC-12 cells were dispensed into a 96-well

plate at a density of 1 X 10^4 cells/well. Cells were pre-treated with different concentrations (25, 100, 250, and 500 ng/mL; equivalent to 36 nM to 357 nM) of custom peptide HNP / TNP / NGF (100 ng/mL) as a positive control/control (triton X-treated) for 1 h (optimum time derived from the previous experiment) and followed by 10 mM PT (IC_{50} value) treatment for 24 h (in triplicates).

3.2.2.8 Flow cytometry analysis to determine PT-induced apoptotic cell death and its protection by custom peptides

Annexin-V binding and PI uptake studies determined apoptotic and necrotic cells. Annexin V has a high affinity for phosphatidylserine, which is translocated from the internal to the external surface of the cell membrane when PC-12 cells undergo apoptosis. Necrotic cells absorb PI due to the higher permeability of their damaged cell walls.

Briefly, PC-12 cells were seeded on a 24-well culture plate, pre-treated with 100 ng/mL (~ 71 nM) custom peptide (HNP and TNP) for 1 h, which was followed by the PT (10 mM) treatment for 24 h before being harvested. Cells were washed three times using PBS and centrifuged at 1200 rpm for 5 min, with the concentration adjusted to 1 X 10^5 cells/well [15]. Pellets were re-suspended in the 1X binding buffer, following the instructions of the manufacturer, and then incubated for 5 min with Annexin V-FITC and PI at 4°C in proportions mentioned in the Annexin V-FITC early apoptosis kit (Cell Signaling Technology, CST-6592). Fluorescence intensity was analyzed with flow cytometry (BD-FACS-Melody, USA. Melody multi-color analyzer cum high-speed cell sorter). Normal cells without any treatment were used as a control for fluorescence compensation adjustment to reduce the spectral overlap and establish the location of the cross gate.

3.2.2.9 Determination of the effect of custom peptides in inhibiting the reactive oxygen species (ROS) production in PT-treated PC-12 cells by spectrofluorometric assay and flow cytometry analysis

The ROS level in the PC-12 cells post-PT treatment was determined using the fluorogenic probe 2',7'-dichlorofluorescein-diacetate (H_2DCFDA) according to the procedure of Mukherjee et al. (2015) [11,16]. Briefly, PC-12 cells (1 X 10^6) at 70% confluence were cultured in 24-well plates and kept overnight. Cells were pre-treated with different concentrations of custom peptides (12.5 ng/mL to 500 ng/mL, equivalent to 18 nM to 357

nM) / Vitamin C (10 μg/mL, positive control) / PBS for 1 h, followed by treatment with PT (10 mM) for 12 h. Media was aspired out, cells were washed with PBS, and incubated with 10 μM H_2DCFDA in the dark for 30 min at 37°C. The cells were washed twice with 200 μL PBS and incubated with 1% Triton X-100 (170 μL). The reaction was stopped by adding DMSO (130 μL). Cells were scraped and transferred to the black plate. Absorbance was measured at excitation and emission wavelengths of 480 and 530 nm using a microplate reader (in triplicates). The ROS production by PT-treated cells was considered 100% (baseline), compared to other activities.

In another set of experiments, intracellular ROS levels generated post-PT exposure in PC-12 cells were measured by flow cytometry (BD-FACS-Melody, USA) analysis using H_2DCFDA, according to the procedure described by Mukherjee et al. (2015) [11]. Briefly, PC-12 cells were pre-treated with custom peptides (HNP and TNP) at different concentrations (12.5 ng/mL to 500 ng/mL, equivalent to 18 nM to 357 nM) and Vitamin C (10000 ng/mL as the positive control) for 1 h, which was followed by PT incubation for 12 h. The adhesive and non-adherent cells were collected and washed twice with PBS (pH 7.4). The cells were then incubated with 10 μM H_2DCFDA at 37°C for 30 min in the dark, then washed twice with chilled PBS. The fluorescence intensities of 2`,7`-dichlorodihydrofluorescein (DCF) produced by intracellular ROS were analyzed by flow cytometry with excitation and emission at 480 and 530 nm, respectively.

3.2.2.10 Determination of the effect of custom peptides on reducing the PT-induced depolarization of mitochondrial membrane potential

Changes in the mitochondrial transmembrane potential were determined with the Mito Probe™ JC-1 assay kit (Invitrogen, USA, Catalog number M34152) protocol [17]. PC-12 cells were pre-treated with 100 ng/mL (~71 nM) of a custom peptide (HNP/ TNP) for 1 h, which was followed by the PT (10 mM) treatment for 10 h at 37°C, in 5% CO_2 (in triplicates). After the treatment, cells were washed three times, incubated with 1 μg/mL JC-1 dye, and incubated at 37°C in a humidified CO_2 incubator for 4 h. The PC-12 cells were washed three times, and images were captured at excitation and emission wavelengths of 490 nm and 530 nm, respectively, to see the green fluorescence of JC-1 monomers. For the red fluorescence J-aggregates, excitation and emission wavelengths were set at 525 nm and 590 nm under a confocal microscope (TCS SPE, Leica, Wetzlar, Germany). The fluorescence intensities were measured using Image J software. Changes

in the mitochondrial transmembrane potential were also analyzed by flow cytometry with the same JC-1 dye, as described in the previous section (Section 2.11). The carbonyl cyanide m-chlorophenyl hydrazone (CCCP, mitochondrial uncoupler) was used as a positive control for flow cytometry analysis.

3.2.2.11 Determination of the effect of custom peptides on the restoration of PT-induced cellular and nuclear morphological changes in PC-12 cells

To study the cellular and nuclear morphological changes induced by PT, 1 mL of 1 X 10^6 PC-12 cells was seeded in a 24-well plate and allowed to adhere overnight at 37°C. PT-induced nuclear damage in the PC-12 cells was observed by 4′,6-diamidino-2-phenylindole (DAPI) staining [11,18]. After the pre-treatment mentioned above with custom peptides (100 ng/mL, equivalent to ~71 nM), the cells were collected, washed in PBS, and then fixed in 1% formaldehyde (in PBS) for 30 min at room temperature. After washing with 1X PBS, the cells were suspended in DMEM media and incubated with 5 µL of DAPI (1 µg/mL) for 30 min at 37°C. The cells were washed with PBS, placed onto a glass slide, and observed under a fluorescence microscope at 40X magnification. The percentage of dead cells was calculated in four randomly selected microscopic fields, and the changes in cellular and nuclear morphology were compared to the untreated cells (control).

3.2.2.12 DPPH free radical scavenging activity of custom peptides *in vitro* condition

DPPH radical-scavenging activity of custom peptides was measured [19]. Briefly, in a 96-well plate, 100 µL peptide sample (25 ng/mL – 250 ng/mL) / vitamin C (10000 ng/mL, or 10 µg/mL, positive control) was uniformly mixed with 100 µL of 0.2 mM DPPH radical solution (dissolved with 95% ethanol) and incubated at room temperature for 30 min. Instantly, the absorbance of the solution was measured at 517 nm by a microplate reader (Varioskan Flash, Thermo Scientific, USA). The percentage of DPPH free radical-scavenging activity was determined as follows:

$$DPPH\ radical\ scavenging\ activity\ (\%) = \left[1 - \frac{A1-A2}{A0}\right] * 100$$

where A0 signifies the absorbance of 95% ethanol (100 µL) (v/v) mixed with DPPH radical solution (100 µL) at 517 nm; A1 shows the absorbance of the peptide (100 µL) with DPPH radical solution (100 µL), A2 denotes the absorbance of peptide solution

(100 µL) with 95% ethanol (100 µL). This experiment was performed in triplicates to ensure reproducibility.

3.2.2.13 Quantitative reverse transcription-polymerase chain reaction (qRT-PCR) analysis to determine the expression levels of pro- and anti-apoptotic genes in the PT-treated PC-12 cells and the effect of pre-treatment of custom peptides

The procedure for qRT-PCR analysis of stress-related gene expression was adopted from our previous studies [17,20]. PC-12 cells were subjected to different treatments at 37 ºC: (a) 1X PBS (control) treated PC-12 cells (CT); (b) 10 mM PT (PT) treatment for 12 h; (c) pre-treatment with 100 ng/mL (~71 nM) custom peptide (TNP or HNP) or mouse 2.5S-NGF (positive control) (NGF) for 1 h followed by 10 mM PT treatment (PTNP, PHNP, and PNGF) for 12 h. Total RNA was isolated with a pure link RNA mini kit (Invitrogen, USA; Cat- 12183018A), and the purity and concentration (A260 / A280) of the RNA were measured using a Nanodrop 2000C spectrophotometer (Thermo Scientific, USA). Reverse transcription was performed from 1 µg of the total RNA using a verso cDNA synthesis kit (Thermo Scientific, USA; Cat: AB-1453/A) according to the manufacturer's protocol. The reaction was performed at 42 ºC for 30 min and ended by incubation at 85 ºC for 5 min. The qRT-PCR was done with SYBR Green (Bio-Rad, USA) to quantify the expression of pro-apoptotic genes, such as caspase-3, B-cell lymphoma 2 (bcl-2), and heat shock protein function (hsp-70) (in triplicates) in a CFX96 Touch Real-Time PCR detection system (Bio-RAD, USA). The relative expression of every gene was analyzed by normalizing it with the expression of the glyceraldehyde-3-phosphate dehydrogenase (GAPDH) housekeeping gene using the 2−ΔΔCt method under identical experimental conditions. The experiment was repeated three times to ensure reproducibility. The sequence of primers used in this experiment [21-24] is shown in Table 3.1.

Table 3.1 List of oligonucleotide primer sequences for the quantitative reverse transcription-polymerase chain reaction (qRT-PCR) analysis in PC-12 cells.

Gene	Orientation	Primer sequence (5'→3')	Product size (bp)	Criteria for RT PCR	References
GAPDH	Forward	GGTGAAGGTCGGTGTGAACG	232		[21]
	Reverse	CTCGCTCCTGGAAGATGGTG			

Bcl-2	Forward	TGGGATGCCTTTGTGGAACT	153	Hold at 95o C for 3 min, followed by 40 cycles of 95o C for 30 s, 58o C for 45 s, and 72o C for 30 s.	[21]
	Reverse	GCAGGTTTGTCGACCTCACT			
Bax	Forward	GGTTTCATCCAGGATCGAGA	151		[21]
	Reverse	TCCTCTGCAGCTCCATATTGC			
Bid	Forward	AGCTACACAGCTTGTGCCAT	186		[21]
	Reverse	CAGCTCGTCTTCGAGGTCTG			
HSP-70	Forward	GAGACAACCCAGGCACCCAA	223		[22]
	Reverse	CCACCCCGAGATCCCCTAAAAA			
Cytochrome-C	Forward	GAAGAAGGGAGAAAGGGCAGA	302		[24]
	Reverse	CGGGGGCTGTCCAACAAA			
Caspase-3	Forward	TGACTGGAAAGCCGAAACT	147		[24]
	Reverse	GGGTGCGGTAGAGTAAGCAT			

3.2.2.14 Quantitative proteomic analysis comparing the expression of global proteins for PC-12 cells exposed to PT and cells pre-treated with custom peptides followed by the PT treatment

Quantitative proteomics was used to identify and categorize PT-transformed proteins and compare their restoration by custom peptides in pre-treated PC-12 cells [10]. For comparing the differential expression of cellular proteins in treated and control cells, PC-12 cells were subjected to the following treatments (at 37°C):

(a) 1X PBS (control)-treated PC-12 cells (CT); (b) 10 mM PT (PT) treatment for 1 h; (c) pre-treatment with 100 ng/mL (~71 nM) custom peptide for 1 h followed by 10 mM PT treatment (PHNP) for 24 h; and (d) treatment with 100 ng/mL (~71 nM) of custom peptide (HNP) for 1 h. Differentially treated PC-12 cells were collected and lysed separately in an RIPA buffer containing proteinase K inhibitor for 30 min on ice.

The tissue lysate was sonicated and centrifuged at 13,000 rpm for 20 min at 4°C, and the protein concentration was estimated [25]. Briefly, 30 μg of the protein from the treated PC-12 cells was subjected to reduction with 10 mM dithiothreitol (DTT) and alkylation with 50 mM iodoacetamide (in the dark), which was followed by incubation with sequencing-grade trypsin (50 ng/µL in 25 mM ammonium bicarbonate comprising 10%

acetonitrile) for 18 h at 37°C [8-10,26,27]. The digested peptides were desalted and concentrated using ZipTip (Millipore, USA), and then re-suspended in 20 μL of 0.1% (v/v) formic acid in 2% acetonitrile. The 1 μL samples were exposed to nano-ultra-performance liquid chromatography-tandem mass spectrometer (UHPLC-MS/MS) analysis. ESI (nano-spray) was used as the ion source, collision-induced dissociation (y and b ions) was used as the fragmentation mode, FT-ICR/Orbitrap was used as the MS scan mode, with an MS/MS scan range of 500 to 2000 m/z being used as the linear ion trap. Double or triple-charged ions were selected for the collision-induced dissociation (CID) MS/MS analysis.

For the data analysis, MS data protein was identified, quantitated, and analyzed using the Peak studio from the Sequest HT database search engine with a 1% false discovery rate (FDR) and two missed cleavage cut-off standards. The database search comprised all entries from the *Rattus norvegicus* (Taxonomy ID: 10116) UniProt reference proteome database. Total protein level analysis was executed using 10 parts per million precursor ion tolerance. The product-ion tolerance used for the data evaluation was 0.05 Da. Oxidation of methionine residues (+15.995 Da) was kept as a variable amendment, whereas cysteine carbamidomethylation (+57.021 Da) was kept as a static modification. Peptide spectra match (PSMs) were adjusted to have an FDR of 0.01. Relative abundances were calculated from the spectral intensity of the respective protein, and the fold change values of the relative abundances were also calculated. Protein-protein interaction (PPI) network analysis was carried out with Cytoscape 3.9.1 (download freely available at https://cytoscape.org/download.html).

3.2.3 To study the *in vivo* neuroprotective mechanism of custom peptides in *C. elegans*

3.2.3.1 Maintenance of *C. elegans* strain

Wild-type Bristol strain N2 was used as an *in vivo* model for determining PT-induced oxidative stress and its reversal by the custom peptides. The transgenic BZ555 (Pdat-1::gfp) strain of *C. elegans* has DAergic neurons expressing GFP, which was used for studying PT-induced neurodegeneration and protection by the custom peptide. A Transgenic NL5901 strain of *C. elegans* (Punc-54:: α-synuclein:: YFP+unc-119; expressing human α-synuclein protein tagged YFP in the muscles) was used to measure

the deposition of toxic α-synuclein protein after custom peptides treatment. *C. elegans* (N2), BZ555, CAM-1(ak37), and NL5901 strains were grown on nematode growth medium (NGM) plates at 20 °C in a bio-incubator, and *E. coli* strain OP50 was provided as a food source.

Synchronization was performed using the standard procedure of the alkaline hypochlorite method described previously [28] with some modifications. The NGM plates with adequate eggs were washed with M9 buffer and collected into a 15 mL conical centrifuge tube. A mixture of sodium hypochlorite (1 mL) and 5 N NaOH (0.5 mL) was added to the 15 mL tube containing worms in 3.5 mL M9 buffer. The tubes were then agitated for 2 min and centrifuged at 7500 rpm at room temperature to settle the eggs. The supernatant was discarded, and the pellet was washed two times with M9 buffer. Then 0.1 mL of M9 buffer was added to the pellet, transferred to the unseeded NGM plate, and incubated at 20°C after adding *E. coli* OP50 to the NGM plate.

3.2.3.2 Determination of *in vivo* binding of FITC-conjugated custom peptides to *C. elegans* (CAM-1 mutant and N2 strains)

The peptides were conjugated with FITC following the procedure Islam et al. described (2020) [8]. The binding assay was performed with the synchronized wild-type L4 larvae of N2 worms and CAM-1 mutant; 10 worms for each treatment were then collected in a 1.5 mL tube and washed multiple times with M9 buffer to remove the *E. coli* contamination. The N2 worms were then treated with FITC-conjugated peptides (TNP and HNP) for 1 to 4 h and the CAM-1 mutant worm for 2 h at room temperature, followed by washing the worms with M9 buffer (to remove adherent *E. coli*) and transferred onto 3% (w/v) agarose pads on a glass slide for confocal microscopy study (TCS SPE, Leica, Wetzlar, Germany). The excitation wavelength was set at 488 nm (λex ~488 nm), and the emission fluorescence signal was recorded at 519 nm (λem~519 nm) to detect the binding of peptides to *C. elegans*. The image was then quantified using Image J software.

The following experiment determined whether the peptide binds to a site where PT binds. The worms were divided into different groups:

1. Only FITC (50 μg/mL) treated N2 worms for 2 h.
2. Only custom peptide (HNP, 50 μg/mL) treated N2 worms for 2 h.

3. FITC-conjugated custom peptide (HNP, 50 μg/mL) pre-treated N2 worms for 2 h, followed by PT (10 mM) treatment for 1 h.
4. PT (10 mM) treatment for 1 h followed by FITC-conjugated custom peptide (HNP, 50 μg/mL) treatment for 2 h in N2 worms.
5. FITC-conjugated custom peptide co-treated N2 worms with different concentrations of PT (5 mM, 7.5 mM, 10 mM) were observed under a confocal microscope.
6. FITC-conjugated peptides (50 μg/mL) treated with CAM-1 mutant strain for 2 h. The signals were recorded at an excitation (λex) and emission wavelength (λem) of ~498 nm and ~519 nm respectively and quantified using Image J software.

3.2.3.3 Assessment of the protective role of custom peptides against PT-induced toxicity in *C. elegans* (N2 and CAM-1 mutant strain)

Custom peptides' *in vivo* protective activity was determined against the PT-induced oxidative stress in the *C. elegans* N2 and CAM-1 mutant strain [29]. Synchronized L4-stage adult N2 worms were pre-incubated with different concentrations (12.5 to 100 μg/mL; equivalent to 9.6 to 76.9 μM) and CAM-1 mutant with 50 μg/mL of custom peptides (HNP / TNP) for 2 h at 20 °C. The mouse 2.5S-NGF (50 μg/mL), vitamin C (100 μg/mL), and quercetin (50 μg/mL) were -incubated for 24 h at 20 °C (positive controls).

In another set of experiments, N2 worms were pre-incubated with custom peptides and quercetin (50 μg/mL, positive control) for 2, 12, and 24. For 24 h of pre-incubation study, the custom peptides were added at 12 h of pre-incubation. The pre-treated worms were then transferred into the wells of 96-well plates (20 worms per well in triplicates; approximately 60 individuals for each group). The worms were provided with *E. coli* OP50 (as a food source) and treated with 10 mM PT for 24 h [17,30], whereas, in control wells, 1X PBS was added. 'Worms' percentage (%) survival was scored visually using a stereo-zoom microscope after 24 h. Worms that did not show movement after light exposure and gentle tapping were considered dead.

In another set of experiments, the N2 worms were treated with 10 mM PT for 1 h, followed by post-treatment with various concentrations (12.5 μg/mL to 100 μg/mL; equivalent to 9.6 to 76.9 μM) of custom peptide (HNP / TNP) and vitamin C (100 μg/mL)

/quercetin (50 μg/mL, positive control)/ mouse 2.5 S NGF (50 μg/mL)/ NGM buffer with OP50 (control) for 2 h and 24 h respectively at 20 °C. The survival of N2 worms was determined, as stated above. This experiment was performed in triplicate to ensure reproducibility.

3.2.3.4 PT-induced loss of chemotaxis behavior in *C. elegans* and its restoration by treatment with custom peptides

The chemotaxis/memory learning assay was done as described by [31] with slight alterations. Synchronized wild-type N2 strain of *C. elegans* (L4 stage) was subjected to the following treatment conditions at 20 °C:

(i) untreated (control), (ii) 10 mM PT-treatment for 1 h, (iii) PT (10 mM)-treatment for 1 h followed by treatment with custom peptides HNP and TNP (50 μg/mL ~38 μM) for 2 h/ vitamin C (100 μg/mL) for 24 h, (iv) custom peptide (HNP / TNP, 50 μg/mL) pre-treatment for 2 h/ vitamin C(100 μg/mL) pre-treatment for 24 h followed by PT (10 mM) treatment for 1 h, and (v) treatment with only custom peptides (50 μg/mL) for 2 h.

The concentration and incubation time of the custom peptides used in this experiment were determined from the previous experiments (described in sections 4.3 and 4.4). The treated and untreated (control) worms were then collected in 60 mm NGM plates, and their chemotaxis behavior was determined below [31].

The plates were divided into two halves; one side was marked as "attractant" (A), and the other half was marked as "control" (C). For this experiment, 0.1% benzaldehyde dissolved in 100% ethanol was considered an odorant for the test sample, and 100% ethanol was an odorant for the control sample. On the "A" side, 2.5 µL of 0.5 M sodium azide containing 2.5 µL of odorant was added, whereas 2.5 µL of 100% ethanol containing 2.5 µL sodium azide was added on the opposite "C" side (Fig 3.1). Immediately after the addition, 20 worms were transferred to the center of the plate. This experiment was performed in triplicates to ensure reproducibility. The assay plates were then scored for the number of worms in each quadrant after 1 h. The CI was calculated as follows:

Number of worms at the "A" quadrant ---------- (T)

Number of worms at the "C" quadrant ---------- (C)

Total number of worms taken on the plate ---------- (N)

Therefore, $CI = (T - C)/N$

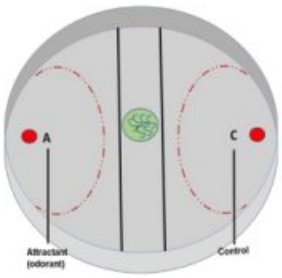

Fig 3.1 The schematic diagram represents the experimental design of the chemotaxis assay to calculate the chemotaxis index (CI).

3.2.3.5 Determination of the effect of custom peptides in inhibiting the ROS production in PT-treated *C. elegans*

The ROS level in *C. elegans* (N2 and CAM-1 mutant) post-PT treatment was determined using the fluorescent probe chloromethyl '2',7'-dichlorofluorescein-diacetate (CM-H_2DCFDA) by following the procedure of Kumar et al. [17]. Briefly, the N2 worms were synchronized, as stated above. Worms were washed and re-suspended in 1X PBS containing 50 μg/mL peptide (HNP / TNP). The mouse 2.5-S NGF (50 μg/mL) and vitamin C (100 μg/mL) were positive controls. The worms were then shaken on a tube rotator (ROTOSPINTM, Tarson, India) for 2 h with custom peptides and 24 h with positive controls at 50 rpm, washed with 1X PBS, and further re-suspended in PBS containing PT (10 mM) /1X PBS (control) and incubated for 1 h at 23 °C. The worms were washed with PBS and re-suspended in 200 μL PBS. The worms were freeze-cracked and sonicated for 10 s. The worm lysate was then kept on ice for 30 minutes, centrifuged at 13,500 rpm for 30 minutes, and the supernatant was transferred to another tube.

After protein estimation (Pierce™ BCA Protein Assay Kit), 25 µg of protein from each group was taken and made up the final volume of 50 µL with 1X PBS. For determining the PT-induced ROS generation, 50 µL protein extract containing 25 µg of each group was mixed with 100 µL of 50 µM of CM-H_2DCFDA in PBS and incubated for 4 h at 37 °C. Finally, fluorescence was measured in a multimode fluorescence plate reader

(excitation at 485 nm and emission at 535 nm). A hundred worms per treatment group were used to measure ROS production. This experiment was performed in triplicates to ensure reproducibility.

The confocal microscopic analysis also quantified the *in vivo* cytoplasmic ROS level in another set of experiments. For this experiment, ten worms of each wild type and CAM-1 mutant strain were divided into three groups. They were treated as–(i) worms pre-treated with peptides (50 µg/mL) for 2 h and mouse NGF (50 µg/mL)/ vitamin C (100 µg/mL, positive control) for 24 h followed by PT (10 mM) treatment for 1 h, and (ii) only PT (10 mM) treated worms for 1 h, and (iii) worms incubated with 1X PBS (control) for 3 h. Each group of N2 and CAM-1 mutant worm was then incubated with 50 µM of CM-H_2DCFDA at 37°C for 4 h, visualized under a confocal microscope (TCS SPE, Leica, Wetzlar, Germany). Images were photographed at 40X with a CCD camera, and the fluorescence intensity was determined and quantitated using Image J software. The experiments were carried out in triplicates to ensure reproducibility.

3.2.3.6 Determination of the effect of custom peptides on reducing the PT-induced depolarization of mitochondrial membrane potential

Mitoprobe JC-1 assay kit (Invitrogen) was used to monitor mitochondrial transmembrane potential using the Mito Probe™ JC-1 Assay Kit protocol. The L4-stage young adult of each N2 and CAM-1 mutant worm were divided into three groups- (i) pre-incubated with 50 μg/mL peptides for 2 h and vitamin C for 24 h, mixed well by shaking on a tube rotator for 2 h at 50 rpm followed by the treatment with PT (10 mM) for 1 h at 20 °C, (ii) 1X PBS (control) treated worms for 3 h, (iii) only PT (10 mM) treated worms for 1h at 20 °C. After the treatment, worms were washed three times, incubated with 1 µg/mL JC-1 dye, and incubated at room temperature for 4 h. The experiments were repeated in triplicates to ensure reproducibility. The worms were washed three times, and the images were captured at excitation and emission wavelengths of 490 nm and 530 nm, respectively, for green fluorescence JC-1 monomers and at excitation and emission wavelengths of 525 nm and 590 nm for red fluorescence J-aggregates under a confocal microscope. The fluorescence intensity was measured using Image J software.

3.2.3.7 Quantitative analysis of the effect of custom peptides on PT-induced dopaminergic (DAergic) neurodegeneration

The transgenic BZ555 (P^{dat-1}::gfp) strain of *C. elegans* has specifically DAergic neurons expressing GFP, to which PT could induce degeneration [32,33]. Briefly, the L4 stage nematode of the BZ555 strain was washed with PBS and collected in a 1.5 mL centrifuge tube containing M9 buffer. The worms were treated under four different conditions- (i) 1X PBS (control), (ii) 10 mM PT-treated worms for 1 h, (iii) PT (10 mM)-treatment for 1 h followed by treatment with custom peptide (HNP / TNP, 50 μg/mL) for 2 h, and (iv) custom peptides treatment for 2 h and vitamin C (100 μg/mL) for 24 h followed by PT (10 mM) treatment for 1 h. The worms were observed under a confocal microscope and photographed, and the fluorescent images were then analyzed using Image J software. The experiment was repeated three times to ensure reproducibility.

3.2.3.8 Quantitative analysis of the effect of custom peptides on preventing the α-synuclein accumulation in the NL5901 strain of *C. elegans*

NL5901 worms were used to observe the aggregation of the α-synuclein protein after being treated with custom peptides (50 μg/mL), as stated previously [34]. Briefly, synchronized L4 stage nematodes were incubated with 50 μg/mL custom peptides for 12 h and 100 μg/mL vitamin C for 24 h at 20 °C. After treatment, worms were washed two times with M9 buffer and transferred onto a 3 % agarose pad slide containing 100 mM sodium azide. The fluorescence intensity of the accumulated α-synuclein was observed under a microscope, and the live worms were also observed under a confocal microscope. The fluorescent and confocal images were photographed and analyzed using Image J software. The experiment was repeated three times to ensure reproducibility.

3.2.3.9 Quantitative reverse transcription-polymerase chain reaction (qRT-PCR) analysis to determine the effect of pre-treatment of *C. elegans* with custom peptides on the PT-induced stress-related gene expression

The procedure for qRT-PCR analysis of stress-related gene expression is adopted from our previous studies [17,20]. Approximately 400-500 L4-stage adult worms were collected in a 1.5 mL centrifuge tube and washed multiple times to remove the adhering bacteria. Further, the worms were centrifuged, the supernatant was aspirated, and the pellet was re-suspended in 1 mL of 1X PBS containing 50 μg/mL peptide (HNP / TNP)

and 100 μg/mL vitamin C (positive control) and shaken on a tube rotator for 2 h and 24 h respectively at 50 rpm. The worms (pellet) were then washed, and the pellet was re-suspended in 1 mL of 1X PBS containing 10 mM PT and incubated for 1 h at 20 °C. Then, the worms were washed, total RNA was isolated using an RNA isolation kit (Invitrogen, USA), and RNA quality was determined by measuring absorbance at 260/280 nm in a nanodrop spectrophotometer. The cDNA was described from mRNA as described previously [4]. The sequence of the primers used for qRT-PCR [17] is shown in Table 3.2. The relative expression of every gene was analyzed by normalizing it with the expression of the *act-1* housekeeping gene using the $2^{-\Delta\Delta Ct}$ method under identical experimental conditions. The experiment was repeated three times to ensure reproducibility.

Table 3.2: List of oligonucleotide primer sets used for qRT-PCR analysis in *C. elegans*.

Sequence name	Sequence	No. of Bases
sek-1_F	GCCGATGGAAAGTGGTTTTA	20
sek-1_R	TAAACGGCATCGCCAATAAT	20
pmk-1_F	CCGACTCCACGAGAAGGATA	20
pmk-1_R	AGCGAGTACATTCAGCAGCA	20
skn-1b_F	CTCTCTTCTGGCATCCTCTACCA	23
skn-1b_R	CCGACTCCACGAGAAGGATA	20
pmk-1_F	AGCGAGTACATTCAGCAGCA	20
pmk-1_R	TTCTTGGATTCTTCTTCTTGTTCGT	25
act-1_F	GCTGGACGTGATCTTACTGATTACC	25
act-1_R	GTAGCAGAGCTTCTCCTTGATGTC	24
sod-1_F	CGTAGGCGATCTAGGAAATGTG	22
sod-1_R	AACAACCATAGATCGGCCAACG	22
sod-3_F	TTCAAAGGAGCTGATGGACACT	22
sod-3_R	AAGTGGGACCATTCCTTCCAA	21
trx-1_F	TCCAACACTTTTTGACGCAG	20
trx-1_R	CAAGATGATGCCGACTTTCA	20

ser-1_F	AAGAGCCAGTCGCCAGAAC	19
ser-1_R	GTGGTTGATGCCTCTGTCGT	20
hsp-16.1_F	GCAGAGGCTCTCCATCTGAA	20
hsp-16.1_R	GCTTGAACTGCGAGACATTG	20
hsp-16.2_F	CTATTTCCGTCCAGCTCAAC	20
hsp-16.2_R	TTTGTTCAACGGGCGCTTGC	20
hsp-60_F	CTATGGGCCCAAAAGGAAGAAACGTG	26
hsp-60_R	GGATTTCGCGACGGTGACTCCGTCC	25
hsp-70_F	GAAAGGTTGAAATCCTCGCGAACTC	25
hsp-70_R	TCCGGATTACGAGCGGCTTGATCTT	25
ctl-1_F	CGGATACCGTACTCGTGATGA	21
ctl-1_R	CCAAACAGCCACCCAAATCA	20
ctl-2_F	TCCGTGACCCTATCCACTTC	20
ctl-2_R	TGGGATCCGTATCCATTCAT	20
gst-4_F	GATGCTCGTGCTCTTGCTG	19
gst-4_R	CCGAATTGTTCTCCATCGAC	20
gst-6_F	GGACAAGACTTCGAGGACAAC	21
gst-6_R	AACTGACGAGCCAAGTAACG	20
gst-10_F	AAGAGATTGTGCAGACTGGAG	21
gst-10_R	AGAACATGTCGAGGAAGGTTG	21
ced-3_F	ACGGGAGATCGTGAAAGC	18
ced-3_R	AGAGTTGGCGGATGAAGG	18
ced-4_F	AGTCACTCGCAATGGCTCT	19
ced-4_R	GCTGATGAACGACGGAAT	18
ced-9_F	AAAGGCACAGAGCCCACC	18
ced-9_R	CGTTCCCATAACTCGCATC	19

3.2.3.10 Transcriptomic analysis to study the gene expression in *C. elegans* when treated with PT vs. pre-treatment with custom peptides followed by treatment with PT

Synchronized L4 stage wild-type N2 strain of *C. elegans* was subjected to the following treatments at 20 °C: (a) CT group, (b) PT group, (c) PHNP, (d) HNP group. Total RNA extraction was done from the treatments of C. *elegans* using the Trizol Method [10]. Extracted RNA was subjected to DNase treatment per manufacturer protocol using New England Biolabs (NEB) (Cat# M0303L kit). The concentration and quality of RNA were measured using a Qubit fluorometer. Further, the quality of preparation was also examined by checking the RNA integrity number (RIN) using BioAnalyser from Agilent. The samples with RIN value ≥ 7 were subjected to the RNA library preparation.

Per the manufacturer's protocol, transcriptomic mRNA libraries were prepared using NEB (cat# E7770L kit) as previously described [35]. The libraries were subjected to quantification using Qubit and Bioanalyser from Agilent. Sequencing done on an Illumina 150 bp PE platform was outsourced (Biokart India Pvt Ltd, Banglore, India).

The quality of reads obtained from the libraries was assessed using Fastqc (v0.11.8), followed by eliminating adapters / inferior-quality reads using Trim Galore (v 0.6.7). Trinity (v v2.13.2) was used for *de novo* transcriptome assembly. The redundancy of the primary assembly was removed and validated using cd-hit and RNA-Seq by Expectation-Maximization (RSEM), respectively.

The validated transcripts are subjected to Gene Ontology (GO) analysis, a Database for Annotation, Visualization, and Integrated Discovery (DAVID), and respective databases. Raw read count files were obtained by using tools viz RSEM (v v1.3.3) / Spliced Transcripts Alignment to a Reference (STAR) (v v2.7.10a) or Salmon (v v1.6.0)/ Binary Alignment Map (BAM) & Sequence Alignment Map (SAM) (v v1.14)/ Picard (v v2.18.7). For a comparative analysis, the Interactive Gene Expression Analysis Kit for Microarray & RNA-seq Data (iGEAK) (v1.0a) tool was used, which is an R (v3.3.2) and JavaScript-based open-source desktop application with the Shiny platform. Further, Voom /edgeR/limma analysis was performed to analyze differentially expressed genes (DEG). The data generation and analysis were performed at Biokart India Pvt Ltd, Bangalore, India.

3.2.3.11 Quantitative proteomics analysis to compare the expression of global proteins between *C. elegans* pre-treated with custom peptides followed by PT and *C. elegans* treated only with PT

For comparison of differential expression of the cellular proteins, the worms were subjected to the following treatments at room temperature: (a) CT group (untreated), (b) PT group (treated with PT), (c) PHNP group (pre-treated with HNP for 2h followed by PT treatment for 1h, and (d) HNP group (only HNP treatment. Approximately 400-500 L4-stage adult worms from each group were collected in a 1.5 mL centrifuge tube and washed multiple times to remove the adhering bacteria. Further, the worms were centrifuged, the supernatant was aspirated, and the pellet was re-suspended in 1 mL of 1X PBS. The proteins were extracted separately from the above-mentioned treated groups using RIPA lysis buffer containing proteinase K inhibitor for 30 min on ice, followed by sonication and centrifugation.

The extracted proteins were quantified, and 30 μg of the protein from each treatment group was subjected to ESI LC/MS-MS analysis as described in our previous study [10]. Briefly, the proteins are reduced (10 mM DTT) and alkylated (50 mM iodoacetamide), followed by subjected to digestion with sequencing-grade trypsin for 18 h at 37 °C. The tryptic-digested peptides were desalted, concentrated, and subject to nano-UHPLC, followed by LC/MS-MS analysis. For ionization and fragmentation nano spray electrospray positive ionization (ESI) and collision-induced dissociation were used, respectively. MS and MS/MS scans (ranging from 500 to 2000 m/z) were carried out in FT-ICR/Orbitrap and linear ion trap, respectively. Only double or triple-charged ions were selected for collision-induced dissociation (CID) MS/MS analysis.

The raw data obtained from MS/MS analysis was analyzed in Peak studio, and the parameter for identifying proteins was adopted from our previous study[4]. The relative abundances were calculated from the spectral intensity of the respective protein, and fold change values of the relative abundances were also calculated.

3.2.4 Study the micro-RNA expression profile in mouse 2.5 S-NGF and custom peptides-treated *C. elegans*

3.2.4.1 Sequencing of miRNA to study the global miRNA expression profile and comparison between the PT group and PHNP group of *C. elegans*

Synchronized L4 stage wild-type N2 strain of *C. elegans* was subjected to the following treatments at 20 °C: (a) 1X PBS treated worms (CT group), (b) 10 mM paraquat treatment for 1 h (PT group), (c) 50 μg/mL custom peptide (HNP) pre-treatment for 2 h followed

by 10 mM paraquat incubation for 1 h (PHNP group), (d) treatment with 50 μg/mL custom peptide HNP for 2 h (HNP group), (e) 50 μg/mL mouse 2.5 S-NGF pre-treatment for 2 h followed by 10 mM paraquat incubation for 1 h (PHNGF group), (f) treatment with 50 μg/mL mouse 2.5 S-NGF for 2 h (NGF group).

Total RNA extraction and quantification was done using RNeasy Plant Mini Kit (Qiagen) as described in section 3.2.3.10. Extracted RNA was subjected to DNase treatment per manufacturer protocol using New England Biolabs (NEB) (Cat# M0303L kit). The concentration and quality of RNA were measured using a Qubit fluorometer. Further, the RNA quality was also analyzed by checking the RNA integrity number (RIN) using BioAnalyser from Agilent. The samples with RIN value ≥ 7 were subjected to the RNA library preparation.

Transcriptomic mRNA libraries were prepared using QIAseq miRNA Library Kit, as per the manufacturer's protocol, where the qualified RNA is subjected to either poly-A capture or ribodepletion. This is followed by RNA fragmentation, 3' Ligation, 5' Ligation, cDNA Cleanup, adapter, barcode ligation, size selection, and amplification. These libraries were subjected to quantification using Qubit and Bioanalyser from Agilent. Sequencing done on an Illumina 150 bp PE platform was outsourced (Biokart India Pvt Ltd, Banglore, India).

Total reads generated from the libraries were subjected to quality control using Fastqc (v0.11.8), followed by removing adapters / low-quality reads using Trim Galore (v 0.6.7). The de novo transcriptome assembly is performed by Trinity (v v2.13.2). The primary assembly is subjected to redundancy removal and validation using cd-hit and RNA-Seq by Expectation-Maximization (RSEM). The validated transcripts are subjected to Gene Ontology (GO) analysis—database for Annotation, Visualization, and Integrated Discovery (DAVID) and respective databases. RSEM (v v1.3.3) / Spliced Transcripts Alignment to a Reference (STAR) (v v2.7.10a) or Salmon (v v1.6.0)/ Binary Alignment Map (BAM) & Sequence Alignment Map (SAM) (v v1.14)/ Picard (v v2.18.7) tools were used for obtaining a raw read count file. For a comparative analysis, the Interactive Gene Expression Analysis Kit for Microarray & RNA-seq Data (iGEAK) (v1.0a) tool was used, which is an R (v3.3.2) and JavaScript-based open-source desktop application with the Shiny platform. The raw read counts were subjected to Voom /edgeR/limma analysis, and

this data was used to perform differentially expressed genes (DEG) analysis with the up and down-regulated genes. MiRTarBase predicted the target genes of miRNAs and the function of those target genes was analyzed through the Panther database. The data generation and analysis were performed at Biokart India Pvt Ltd, Bangalore, India.

3.2.4.2 Determination of acute *in vivo* toxicity and biochemical changes post-treatment of the peptides in a Swiss albino mice model

Acute *in vivo* toxicity of custom peptides was assessed in Swiss albino mice (18-20 g) following OECD guidelines. Ethical permission was approved by the animal ethics committee of IASST (IASST/IAEC/2022/10). For *in vivo* toxicity evaluation, custom peptides (TNP: HNP, 1:1 w/w) were dissolved in 0.2 mL of 1X PBS (pH-7.4) and injected intravenously (10 mg/kg body weight, *i.v.*) into the Swiss albino mice (n=6) (70). The control mice group received only 0.2 mL of 1X PBS (pH-7.4) (placebo). The treated mice were continuously monitored at intervals of 6 h up to 24 h of injection for any behavioral alteration or death. The mice were sacrificed after 24 h post-treatment of custom peptides, and blood was collected instantly by cardiac puncture. Plasma was isolated from the blood (control/treated group) by centrifuging at 4500 rpm for 20 min at 4°C, and the biochemical parameter was investigated viz. SGOT, ALKP, SGPT, BUN, glucose content, creatinine, cholesterol, bilirubin, and albumin level using BeneSphera C61 semi-automatic biochemistry analyzer.

To study possible custom peptides (1:1)-induced morphological changes, the heart, liver, brain, kidney, liver, ovary, and testis of each control and treated group of mice were dissected after 24 h of treatment. Tissues were fixed in 10% buffered formaldehyde, dehydrated, and embedded in paraffin. The slides were observed under light microscopic (Zeiss Axiolab A1) after hematoxylin-eosin (H/E) staining (70). Serum levels of proinflammatory cytokines (TNF-α, IL-6, IL-1β) were determined by a commercial immunoassay kit (Quantikine® HS Immunoassay kit, biotech R and D systems) and followed manufacturer instructions.

3.2.5 Statistical analysis

All the data were denoted as mean ± standard deviation (SD) of independent triplicates. Significant differences between the test and control were analyzed using the student's t-test in Sigma Plot 11.0 for Windows (version 10.0). The significance of difference was

examined for more than two groups using one-way variance analysis (ANOVA) in GraphPad Prism software. The p-value ≤ 0.05 was considered statistically significant. The fold change of miRNA expression was calculated by averaging the reads of the control, and each corresponding miRNA was normalized for individual treatment groups concerning the control before converting into $\log_2$ values. miRNAs without reads were removed from consequent analyses in each biological replicate.

CHAPTER IV

Neurotrophic potency and mechanism of neuroprotective action of snake venom-derived custom peptides in pheochromocytoma of the rat adrenal medulla (PC-12) cells

4.1 Results

4.1.1 The biophysical characterization to ascertain the purity of the synthesized peptides

HPLC chromatograms showed the purity of the synthetic peptides (single peaks within 8-12 min of retention time) (Figs 4.1A-B). The ESI-mass spectrometry analysis also suggested the purity of the peptide preparations (Figs 4.1C-D). The CD spectrum of custom peptide TNP revealed that it was composed of α-helices (37.6%), random coils (30.9%), and turns (31.5%) with a characteristic minimum absorbance at 210 nm (Fig 4.2A). The analysis of the CD spectrum of custom peptide HNP revealed that it was mainly composed of turns (100%) with characteristic maximum absorbances at 202 and 224 nm (Fig 4.2B).

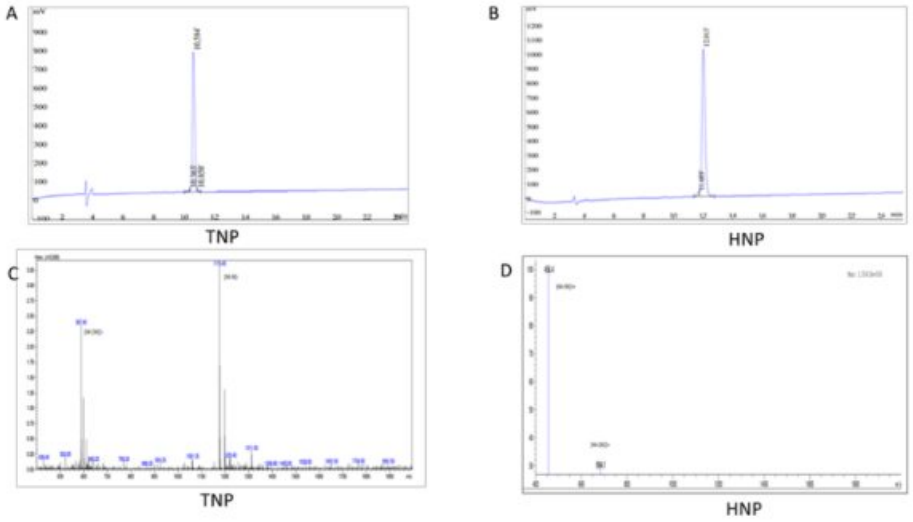

Fig 4.1 HPLC chromatogram of the custom peptide (A) TNP, (B) HNP. MS/MS spectrum of the peptide (C) TNP, and (D) HNP was analyzed by ESI LC/MS-MS.

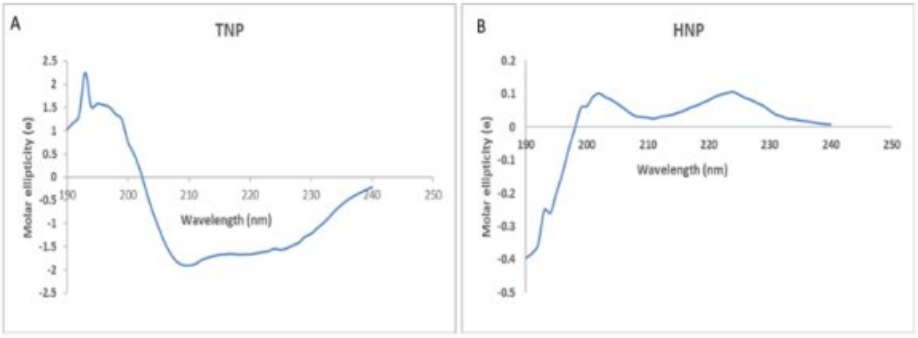

Fig 4.2 Circular dichroism (CD) spectra of custom peptides (A) TNP and (B) HNP. Custom peptides (0.3 mg/ml) were dissolved in 20 mM potassium phosphate buffer pH 7.0 and the far UV-CD spectra were recorded at room temperature (~25 °C) between 190 and 250 nm against the appropriate buffer (blank).

4.1.2 Computation analysis to predict the interaction between different domains of TrKA receptor and SV NGF-derived custom peptides

The sequence and biophysical properties of the TrkA receptor-binding custom peptides (TNP and HNP) are summarized in Table 4.1. Different domains of human TrkA were obtained from the PDB structures (Fig 4.3A). Domain-3 of TrkA was characterized as an NGF-binding domain site (in humans) (Fig 4.3A). Molecular docking revealed a high-affinity binding that formed a complex between the peptides (TNP and HNP) and TrkA domain-3 (Figs 4.3B-C). Glide docking scores were found to be -9.35 (TNP) and -5.54 (HNP), and similarly, the MMGBSA binding energies (docked complex) were found to be -77.77 (TNP) and -68.03 (HNP) kcal/mol (Table 4.2).

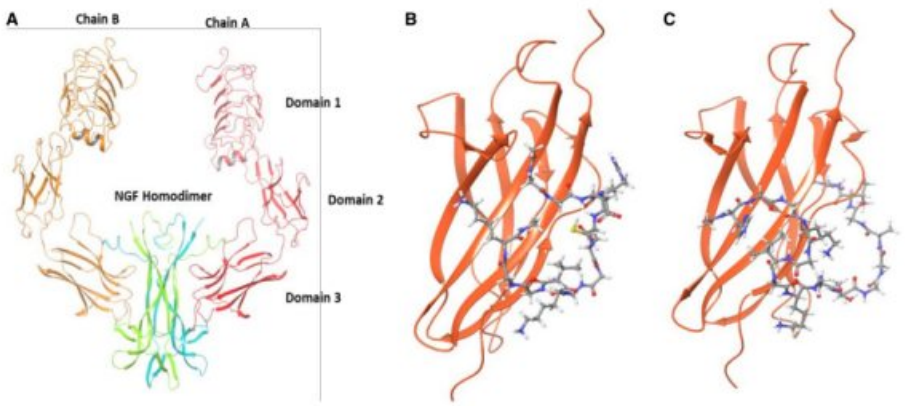

Fig. 4.3 The *in silico* analysis of (A) Human TrkA receptor Chain A and B in complex with human NGF homodimer (PDB ID- 2IFG). The 3D model shows the interaction of TrkA with (B) TNP, and (C) HNP to form a ligand-receptor complex. The ball and stick structure represent peptide structure, and the string model corresponds to TrkA receptor domain-3.

Table 4.1 The custom peptide sequences and their properties

Peptide	**Peptide sequence**	**Length (amino acid)**	**Molecular formula**	**Molecular weight (KDa)**	**Solubility**	**Extinction coefficient ($M^{-1}cm^{-1}$)**	**Isoelectric point (pH)**	**Purity (RP-HPLC analysis)**	**Hydrophobicity (Kcal * mol^{-1})**
TNP	NH_2-GGDRCSGGKVGGK-COOH	13	$C_{45}H_{80}N_{18}O_{17}S_1$	1.2	DMSO (0.1% w/v)	0	9.67	98%	+25.83
HNP	NH_2-HGGKGIGKGGTGGAGVG-COOH	17	$C_{56}H_{95}N_{21}O_{19}$	1.4	DMSO (0.1% w/v)	0	10.65	98%	+26.50

Table 4.2 Glide scores and molecular mechanics/generalized Born surface area (MM/GBSA) binding energy of custom peptides with domain 3 of human TrkA.

Custom peptide	Glide docking score	MMGBSA binding energy (ΔG) (kcal/mol)	MMGBSA binding energy (ΔG) after simulation (kcal/mol)
TNP	-9.35	-77.77	-93.65
HNP	-5.54	-68.33	-106.99

The stability of the docked domain-3 with the TNP/ HNP complex was studied using molecular dynamic simulations for 300 ns. In all cases, the RMSD of the TrkA domain-3 backbone was found to be stable over the simulation trajectory. For TNP, the first 25 - 50 ns of simulation showed a higher variation in RMSD with a stable complex forming afterward (Fig 4.4A). Unlike the molecular docking results, the molecular dynamic simulations predicted a stable complex of HNP with domain-3 of TrkA (Fig 4.4B), and the average MMGBSA binding energy of TNP and HNP were -93.652 and -106.998 kcal/mol, respectively.

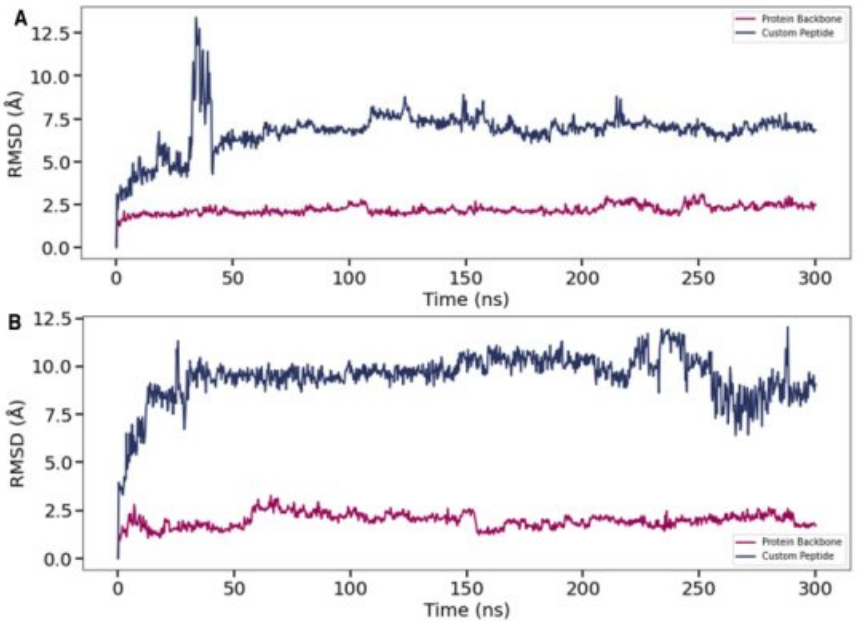

Fig 4.4 Molecular dynamic simulation of domain-3 backbone and custom peptides (A) TNP, (B) HNP shown in an RMSD (root mean square deviation) plot throughout the simulation trajectory for 300 ns.

TNP interacted with five different amino acid residues of TrkA domain-3, and the interaction was stable up to 87% of the simulation time (Fig 4.5A). The major TrkA domain-3 residues Arg273, Ser277, and Val198 participated in the interaction with Asp3, Gly11, and Gly12 TNP residues, respectively, and Glu275 of domain-3 interacted with Arg4, Cys5, and Ser6 of TNP (Fig 4.5A). Nevertheless, HNP demonstrated the highest degree of stable interaction (i.e., up to 62% of the time) with seven different amino acid residues of TrkA domain-3 (Fig 4.5B). The major TrkA domain-3 residue Ser371 interacted with His1, Gly2, and Lys8 residues of HNP. Leu290 of domain-3 interacted with Gly13 and Gly15 of TNP and the other domain-3 residues (Ala363, Ala370, Ser373, His291, and Ser304) participated in the interaction with HNP residues Ile6, Ile6, Thr11, Ala14, and Val16, respectively (Fig 4.5B).

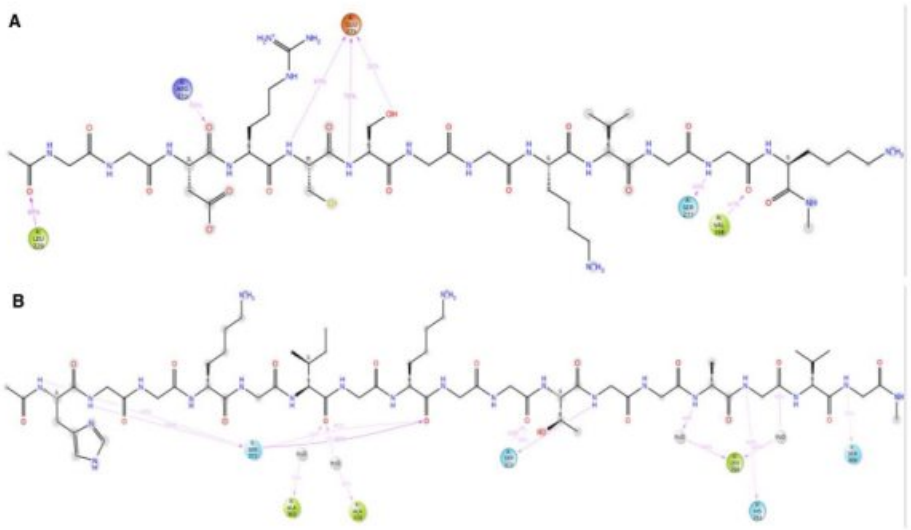

Fig 4.5 Schematic diagram depicting the interaction of custom peptides (A) TNP (B) HNP with domain-3 of the TrkA receptor. The percentage of interaction is shown in the figure recorded over the simulation time of 300ns.

4.1.3 The FITC-conjugated custom peptides showed exclusive binding to mammalian cells expressing the TrkA receptor but not to cells with TrkB or TrkC receptors

The spectrofluorometric analysis of FITC-custom peptides showed a significant binding in a time-dependent manner to the TrkA receptor expressed in MCF7, MDA-MB-231, and PC-12 cells but not to L6 cells (devoid of extracellular TrkA receptors) (Fig 4.6A). The fluorescence intensity was found to be significantly higher (3 to 30-fold increase) in HNP and TNP-treated samples compared to the control L6 cells. In any case, the binding efficacy of the HNP peptide was significantly higher ($p \leq 0.05$) for MCF7 and PC-12 cells, compared to those of the TNP peptide. For the MDA-MB-231 cells, no significant difference was seen between the two peptides up to 60 min of incubation (Fig 4.6A).

The FITC-conjugated peptides also showed a significant increase ($p \leq 0.05$) in binding efficacies to PC-12 cells in a concentration-dependent manner (from 50 to 1000 ng/mL, equivalent to 40 to 800 nM) (Fig 4.6B). The binding affinity (Kd value) of TNP and HNP towards the PC-12 cell line was determined at 1.03×10^{-11} and 0.80×10^{-11} M, respectively (Fig 4.6C).

The binding of FITC-custom peptides to MCF-7 (Fig 4.6D), and MDA-MB-231 (Fig 4.6E) cells expressing TrkA receptor was evident by fluorescence microscopic analysis; however, no fluorescence signal was detected in L6 cells post incubation with FITC-conjugated peptides (Fig 4.6F).

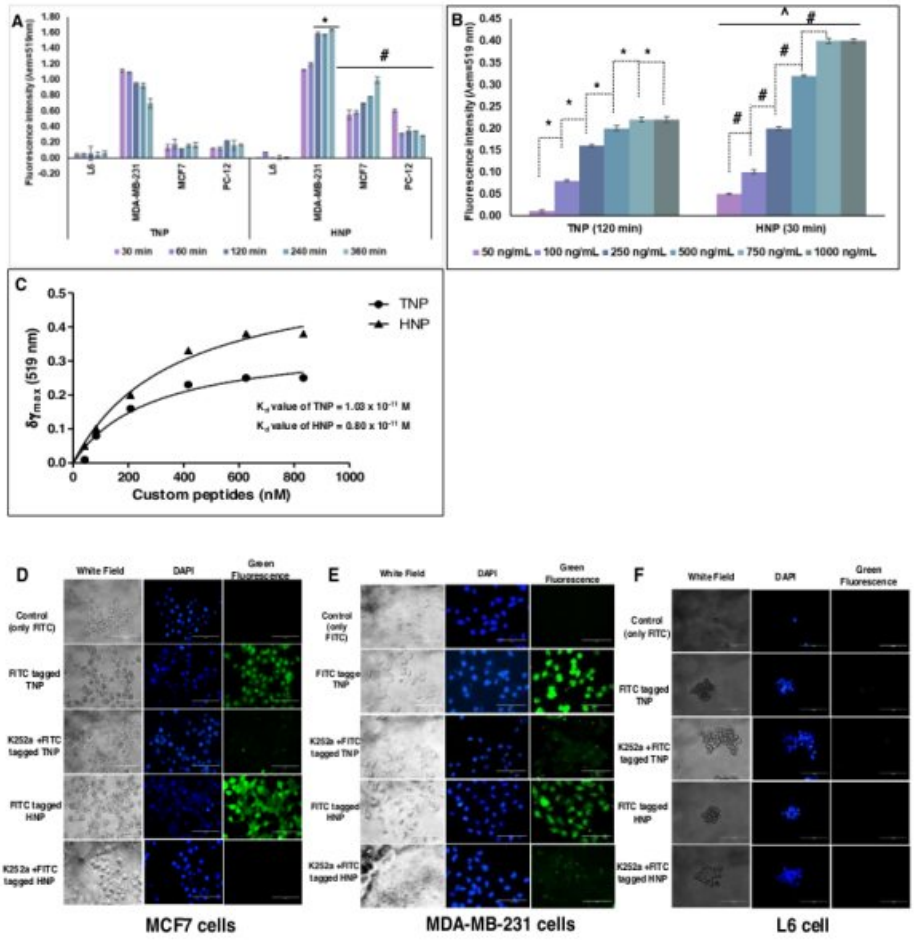

Fig 4.6 Fluorescence analysis to determine the (A) time-dependent binding (30 min to 360 min) of custom peptides (100 ng/mL, ~71nM) with the TrkA receptor of cells. L6 cells (non-TrkA expressing cells) were taken as control. Significance of difference in the binding of TNP (for 120 min to 360 min) with respect to HNP for MDA-MB-231, $^{*}p < 0.05$. Significance of difference in the binding of TNP (for 30 min to 360 min) with respect to HNP for MCF7 and PC-12 cell line, $^{\#}p < 0.05$. (B) Binding of custom peptides with cell surface TrkA receptor of PC-12 cells in an increasing concentration of custom peptides (50 ng/mL to 1000 ng/ml, equivalent to 40 to 800 nM). Significance of difference in the binding between different concentrations for TNP $^{*}p < 0.05$ and for HNP $^{\#}p < 0.05$. Significance of difference in the binding of TNP with respect to HNP, $^{\wedge}p< 0.05$. (C) A hyperbola curve was plotted for change in λmax (Δλmax) against the concentrations (nM)

of the custom peptide with TrkA receptor expressing PC-12 cells (1 x 10^4 cells) and the Kd value was determined using GraphPad Prism 8.1.1 software. The binding of FITC-custom peptide (100 ng/mL) with (D) MCF7, (E) MDA-MB-231, and (F) L6 cells was observed under fluorescence. The binding of custom peptides was also shown in the presence or absence of a chemical inhibitor of the Trk family (K252a). Magnification was 40X. Values are mean ± SD of triplicate determinations.

4.1.4 Custom peptide-induced neurite outgrowth and differentiation of PC-12 cells

The TNP and HNP did not demonstrate *in vitro* cell cytotoxicity (Figs 4.7A-B) and showed negligible haemolytic, platelet-modulating, and plasma-clotting activities (Table 4.3).

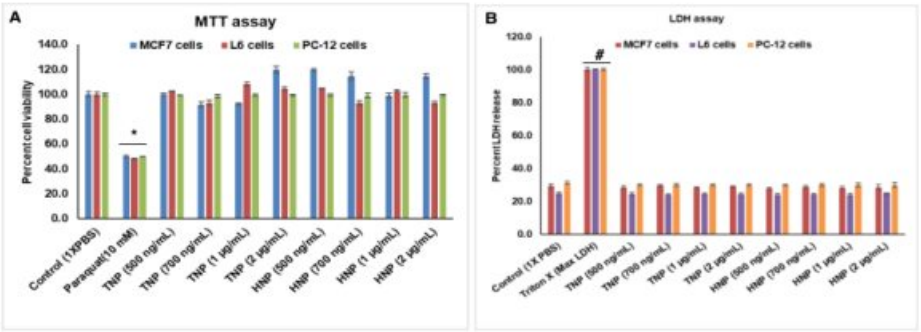

Fig 4.7 Concentration-dependent *in vitro* cytotoxicity of synthetic peptides (TNP and HNP) and PT (10 mM, positive control) against mammalian cells. The cells were incubated with progressive concentrations of custom peptides (500 ng/mL to 2 μg/mL) with mammalian cells (MCF7, PC-12, and L6 cells) at 37°C in a CO_2 incubator for 24h. Determination of cytotoxicity by (A) MTT assay, and (B) LDH release assay. Significance of difference in the cell viability by MTT assay for paraquat-treated cells with respected TNP and HNP treated cells, $^{*}p < 0.05$. Significance of difference in the cell viability by LDH release assay for Triton-X treated cells with respect to TNP and HNP treated cells, $^{\#}p < 0.05$. Values are mean ± SD of triplicate determinations.

Table 4.3 *In vitro* effect of custom peptides on mammalian blood

Custom peptides	[a]Plasma clotting activity (sec),	Coagulant (C)	[b]Platelet aggregation	[c]Indirect hemolysis

		anticoagulant (AC)	(%)	(%)
NTP	10.6 ± 0.14	C	(-) 2.9± 0.9	0.39± 0.04
HTP	5.7 ± 0.11	C	(+) 3.1± 0.7	0.33± 0.05

[a] Plasma clotting activity of custom peptide (TNP, and HNP) was assayed with 300 µL of goat platelet-poor plasma (PPP) at a dose of 5 µg/mL. The clotting time of untreated plasma was 120 sec. Values are mean ± SD of triplicate determinations. [b]Platelet aggregation property of custom peptides (TNP, and HNP) was assayed against goat platelet-rich plasma (PRP) at a dose of 1 µg/mL. (+) and (−) represent platelet aggregation and deaggregation activities, respectively. [c]The Hemolytic activity of custom peptides (TNP, and HNP) was assayed against 5% (v/v) mammalian erythrocytes at a dose of 1 µg/mL.

Phase-contrast microscopic images of neurite outgrowth in PC-12 cells 14 days post-treatment with custom peptides are shown in Figs 4.8A-H. The average neurite length (μm) is represented by the box and whisker plot, which shows the variation for the different concentrations (12.5 to 100 ng/mL, equivalent to 18 to 71 nM) of peptide (TNP and HNP), compared to mouse 2.5S NGF (Positive control) (Fig 4.8I). Both HNP and TNP and mouse 2.5S-NGF induced neurite outgrowth and differentiation in PC-12 cells to different extents (Figs 4.8I-J). The custom peptides showed significant neurite outgrowth at a minimum concentration of 50 ng/mL (equivalent to 36 nM). The average neurite length, and the percentage of differentiated cells, were significantly higher ($p \leq 0.05$) for TNP and HNP at the same concentration (100 ng/mL, equivalent to 71 nM), compared to mouse 2.5S-NGF (positive control); however, no significant difference ($p>0.05$) was observed between the TNP and HNP peptides.

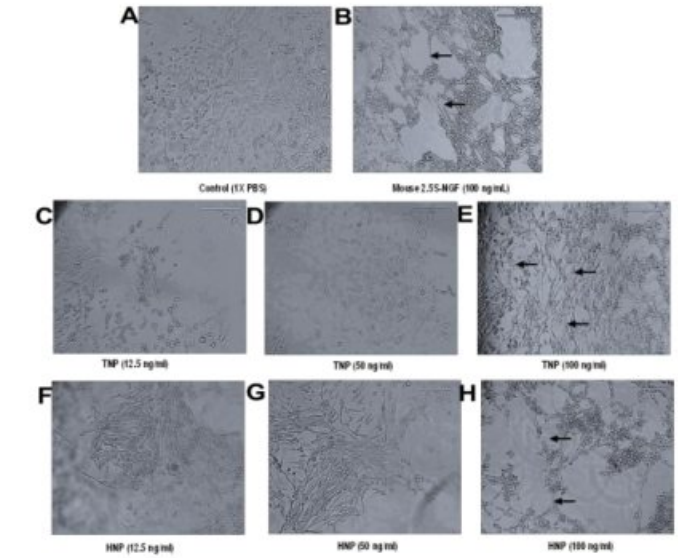
A
B
Control (1X PBS)
Mouse 2.5S-NGF (100 ng/mL)
C
D
E
TNP (12.5 ng/ml)
TNP (50 ng/ml)
TNP (100 ng/ml)
F
G
H
HNP (12.5 ng/ml)
HNP (50 ng/ml)
HNP (100 ng/ml)

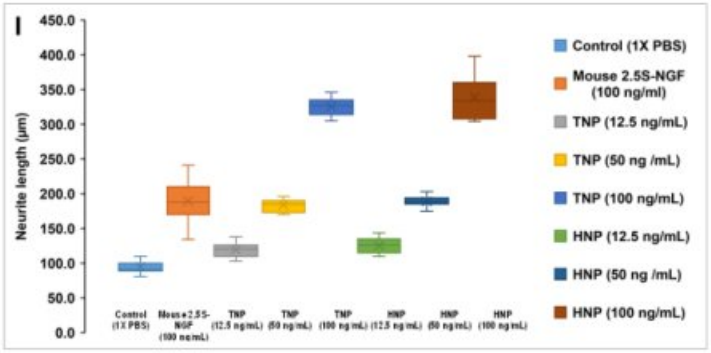
I
Neurite length (µm)
450.0
400.0
350.0
300.0
250.0
200.0
150.0
100.0
50.0
0.0
Control (1X PBS)
Mouse 2.5S-NGF (100 ng/ml)
TNP (12.5 ng/mL)
TNP (50 ng /mL)
TNP (100 ng/mL)
HNP (12.5 ng/mL)
HNP (50 ng /mL)
HNP (100 ng/mL)

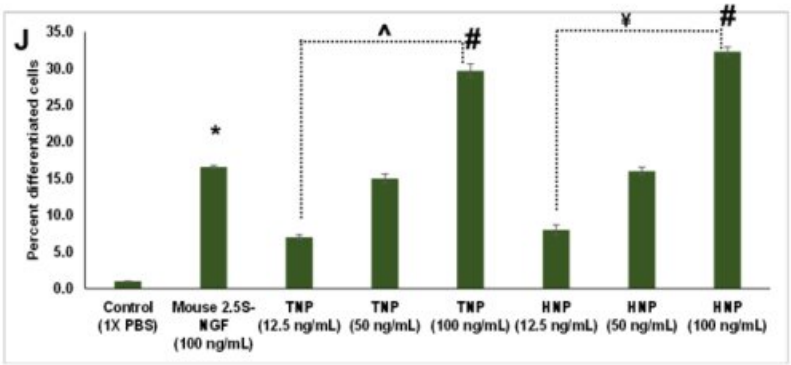
J
Percent differentiated cells
35.0
30.0
25.0
20.0
15.0
10.0
5.0
0.0
*
^
#
¥
#
Control (1X PBS)
Mouse 2.5S-NGF (100 ng/mL)
TNP (12.5 ng/mL)
TNP (50 ng/mL)
TNP (100 ng/mL)
HNP (12.5 ng/mL)
HNP (50 ng/mL)
HNP (100 ng/mL)

Fig 4.8 Concentration-dependent (12.5 to 100 ng/mL) determination of neurite outgrowth in rat pheochromocytoma (PC-12) cells treated with custom peptides (TNP & HNP) post 14 days of incubation at 37°C, 5% CO_2. The cells were observed under a phase-contrast microscope at 20x magnification. The appearance of neurite outgrowth from PC-12 cells is indicated by black arrows. (A) 1X PBS (control) treated cells, (B) mouse 2.5S-NGF treated cells, (C-E) TNP-treated cells with different concentrations (12.5 to 100 ng/mL), (F-H) HNP-treated cells with different concentrations (12.5 to 100 ng/mL). (I) Box and whisker plots represent average neurite outgrowth per cell (in μm). (J) Bar graph showing the percentage of differentiated cells (total number of cells showing neurite outgrowth) in custom peptide and mouse 2.5 S-NGF-treated PC-12 cells. The neurite length was determined using MOTIC IMAGE PLUS 3.0 software. Significance of difference in the controls with respect to mouse 2.5S-NGF, $^{*}p < 0.05$. Significance of difference in mouse 2.5S-NGF with respect to TNP and HNP (at the concentration 100 ng/mL), $^{\#}p < 0.05$. Significance of difference in different concentrations for TNP, $^{\wedge}p < 0.05$ and for HNP, $^{\Upsilon}p < 0.05$. Values are mean ± SD of triplicate determinations.

4.1.5 Chemical inhibition of TrkA receptor (K252a), PI3K/AKT (LY294002), and MAPK/ERK (U0126) pathways inhibited neuritogenesis induced by the custom peptides in PC-12 cells

The percentage of cell differentiation was examined for PC-12 cells treated with custom peptides that were pre-incubated with or without chemical inhibitors, after 14 days of incubation. The results show that the potency of the custom peptides in inducing neurite outgrowth and cell differentiation activities was significantly inhibited ($p \leq 0.05$) by the three chemical inhibitors (K252a, LY294002, and U0126) (Fig 4.9A). The inhibition in the differentiation of PC-12 cells by peptides (100 ng/mL, equivalent to ~71 nM) in the presence or absence of chemical inhibitors were ranked in descending order MAPK/ERK (U0126) pathway inhibitors (15 to 16% decrease) > PI3K/AKT (LY294002) (12 to 13 % decrease) > TrkA receptor inhibitor (K252a) (9 to 10% decrease) when compared to neurite outgrowth and cell differentiation activities of custom peptides without inhibitor. These findings corroborate well with our earlier findings with NGFs from Indian Russell's viper and Indian cobra venoms [1-3].

The blocking of the TrkA receptor significantly inhibited ($p \leq 0.05$) differentiation of PC-12 cells by TNP and HNP, while blocking of the TrkB and TrkC receptors with their

respective antibodies did not affect differentiation of the PC-12 cells (Fig 4.9B). Thus, the peptides appear to bind exclusively to TrkA receptors.

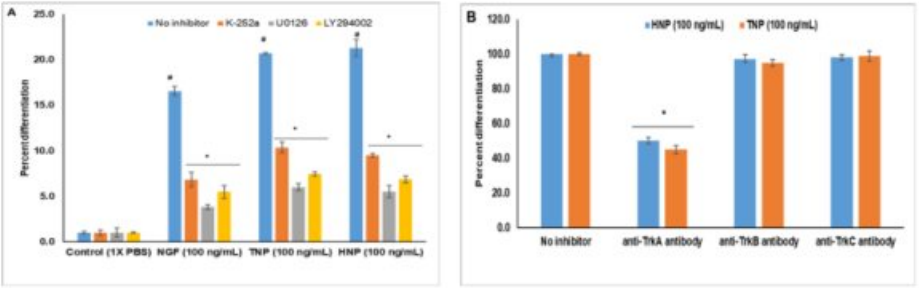

Fig 4.9 (A) Effect of small synthetic inhibitors of major signaling pathways on neuritogenesis potency of custom peptides (TNP, and HNP, 100 ng/mL equivalent to 71nM), and NGF (positive control, 100 ng/mL) in PC-12 cells. Significance of difference in the percent differentiation of control cells compared to NGF, TNP, and HNP when no inhibitor was added, $^{\#}p \leq 0.05$. Significance of difference in the percent cell differentiation between with inhibitors (K-252a, U0126, and LY294002) and without inhibitors, $^{\#}p \leq 0.05$ (B) Effect of anti-TrkA, TrkB, TrkC antibody (1:1000) on neuritogenesis potency of custom peptides (TNP, and HNP, 100 ng/mL equivalent to 71nM), and NGF (positive control) in PC-12 cells. Significance of difference in the percent cell differentiation between with anti-TrkA antibody and without inhibitors, $^{*}p \leq 0.05$. Values are mean ± SD of triplicate determinations.

4.1.6 Pre-treatment of PC-12 cells with custom peptides enhanced their cell survival against PT-induced cell death

Pre-treatment of PC-12 cells with TNP and HNP (100 ng/mL, ~71 nM) demonstrated a significant 27 to 30% increase ($p \leq 0.05$) in their percent cell viability against PT (10 mM, IC_{50})-induced cell death, compared PC-12 cells that had only been treated with PT (Fig 4.10A). The protection offered by the custom peptides against PT-induced cell death was significantly higher (10 to 13%) ($p \leq 0.05$) compared to that of mouse 2.5S-NGF (positive control). Moreover, post-treatment of PT-treated cells with TNP or HNP or co-treatment with TNP or HNP with PT did not restore the cell viability against PT-induced toxicity (Figs 4.10B-C).

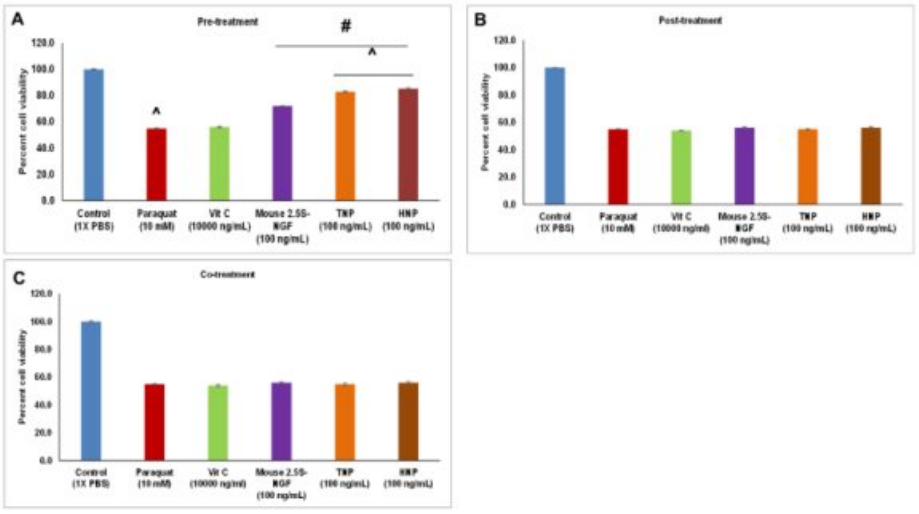

Fig 4.10 Determination of the protective effects of custom peptides against PT-induced cell death. The viability of PC-12 cells was determined by MTT assay. (A) Pre-treatment of cells with custom peptides (100 ng/mL, ~71 nM) or vitamin C (10000 ng/mL) for 4 h followed by PT treatment for 24 h at 37°C in a CO_2 incubator. $^{*}p \leq 0.05$, a significant difference between untreated (control) and PT-treated cells; $^{\#}p \leq 0.05$, a significant difference between PT-treated cells with respect to mouse 2.5S-NGF and custom peptide pre-treated PC-12 cells. $^{\wedge}p \leq 0.05$, a significant difference of mouse 2.5S-NGF treated cells with respect to the peptide (TNP and HNP) treated cells. (B) Treatment of cells with PT for 24 h followed by treatment with custom peptide for 4h. There is no significant difference in the cell viability in PT-treated cells with respect to mouse 2.5S-NGF, Vit C, and peptide post-treatment. (C) The cells were simultaneously treated with custom peptides and PT for 24 h followed by an assay of cell viability. There is no significant difference in the cell viability in PT-treated cells with respect to mouse 2.5S-NGF, Vit C, and peptide co-treatment. Values are mean ± SD of triplicate determinations.

HNP/TNP at a concentration of 100 ng/mL (~71 nM) for a one-hour pre-incubation showed the optimum protection (up to 80 to 85 % cell viability) against PT-induced (10 mM) cell toxicity (Figs 4.11A-B). The protective potential of the custom peptides was also confirmed by the inhibition of PT-induced release of LDH from PC-12 cells. The maximum release (considered as 100%) of LDH enzyme was observed in control (Triton X-treated) PC-12 cells. Only PT-treated PC-12 cells showed a 50% release

of LDH enzyme, compared to only triton-X-100 treated cells. Pre-treatment with the custom peptides (100 ng/mL, ~71 nM) demonstrated a significant decrease (28 to 29%) ($p \leq 0.05$) in the release of the marker enzyme (LDH), compared to that released from PT-treated PC-12 cells (Fig 4.11C). The custom peptides showed a 13 to 14% decrease in the release of LDH enzyme, compared to that of mouse 2.5S-NGF (positive control) (Fig 4.11C). Mouse 2.5S-NGF (100 ng/mL, positive control) was less effective in protecting the PT-induced cell death, according to the results from both the MTT-based cell cytotoxicity assay (Fig 4.11A-B) and the LDH release assay (Fig 4.11C), when comparing the same concentrations of HNP and TNP.

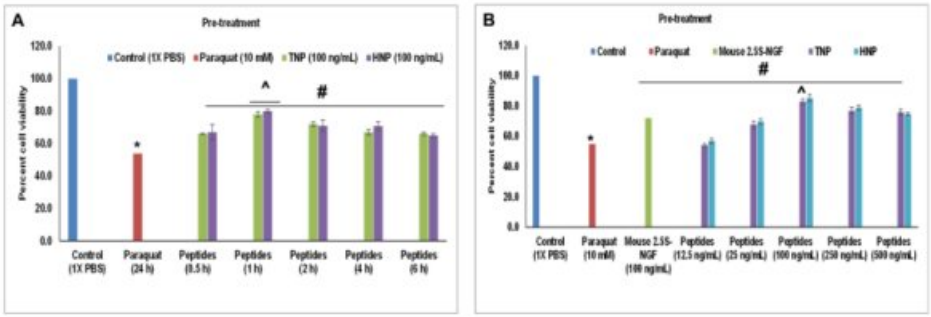

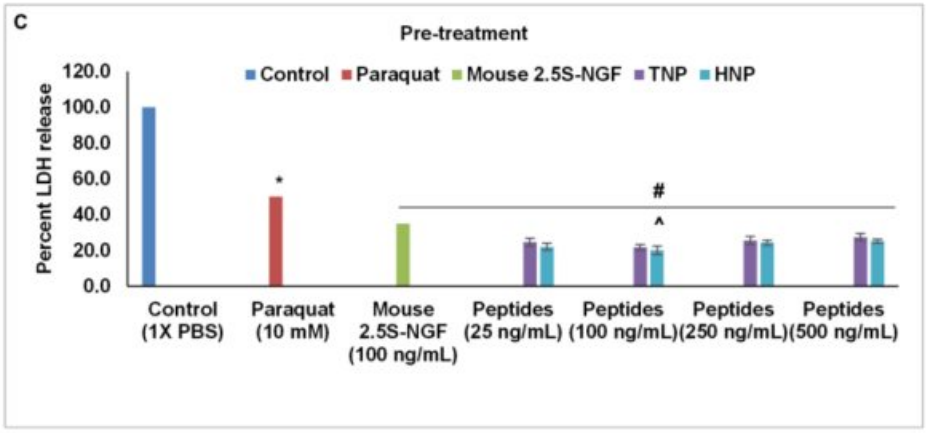

Fig 4.11. Determination of the optimum time and doses of peptide for neuroprotective activity against PT-induced toxicity. Time and dose-dependent neuroprotective activity was determined by MTT and LDH assay in PC-12 cells. (A) Pre-treatment of cells with custom peptides (100 ng/mL, ~ 71 nM) at a different time interval (0.5 h - 6 h) followed by PT treatment for 24 h at 37°C in a CO_2 incubator. $^{*}p \leq 0.05$, a significant difference

between untreated (control) and PT-treated cells; $^{\#}p \leq 0.05$, a significant difference of PT-treated cells with respect to custom peptide (TNP and HNP) pre-treated PC-12 cells for different time intervals (0.5 - 6 h). Significance of difference in the percent cell viability of custom peptide pre-treated cells incubated for 1 h with respect to 0.5-6 h, $^{\wedge}p \leq 0.05$. (B) Pre-treatment of cells with different concentrations of custom peptides (12.5 ng/mL to 500 ng/mL) for 1h (optimum time) followed by PT treatment for 24 h at 37°C in a CO_2 incubator (C) LDH release assay to determine the protective effects of custom peptides on the LDH release of PT-induced PC-12 cell cytotoxicity when pre-treated with different concentrations of custom peptides (25 ng/mL to 500 ng/mL) for 1h followed by PT treatment for 24 h at 37°C in a CO_2 incubator. $^{*}p \leq 0.05$, a significant difference between untreated (control) and PT-treated cells; $^{\#}p \leq 0.05$, a significant difference of PT-treated cells with respect to custom peptide (TNP and HNP) pre-treated PC-12 cells for different time intervals (0.5-6 h). Significance of difference in the percent cell viability of custom peptide pre-treated cells at the dose of 100 ng/mL with respect to 12.5-500 ng/mL, $^{\wedge}p \leq 0.05$. Values are mean ± SD of triplicate determinations.

4.1.7 Inhibition of PT-induced ROS production in PC-12 cells

The custom peptides TNP and HNP demonstrated increased antioxidant activity in an increasing concentration-dependent manner up to 100 ng/mL (Fig 4.12A). The custom peptide-mediated reduction in intracellular ROS generation in PC-12 cells was determined by flow cytometry analysis (Figs 4.12B-E). The data shows a significant increase ($p \leq 0.05$) in intracellular ROS production (2.1-fold-change) in PT-treated PC-12 cells compared to control PC-12 cells. Nevertheless, pre-treatment of PC-12 cells with 100 ng/mL (~71 nM) of TNP or HNP significantly diminished (1.6 to 1.8-fold-change) the ROS production (Fig 4.12E). HNP, compared to TNP, showed superior potency (0.23-fold decrease compared to the custom peptide TNP; $p \leq 0.05$) in inhibiting the PT-induced ROS generation (Figs 4.12B-E).

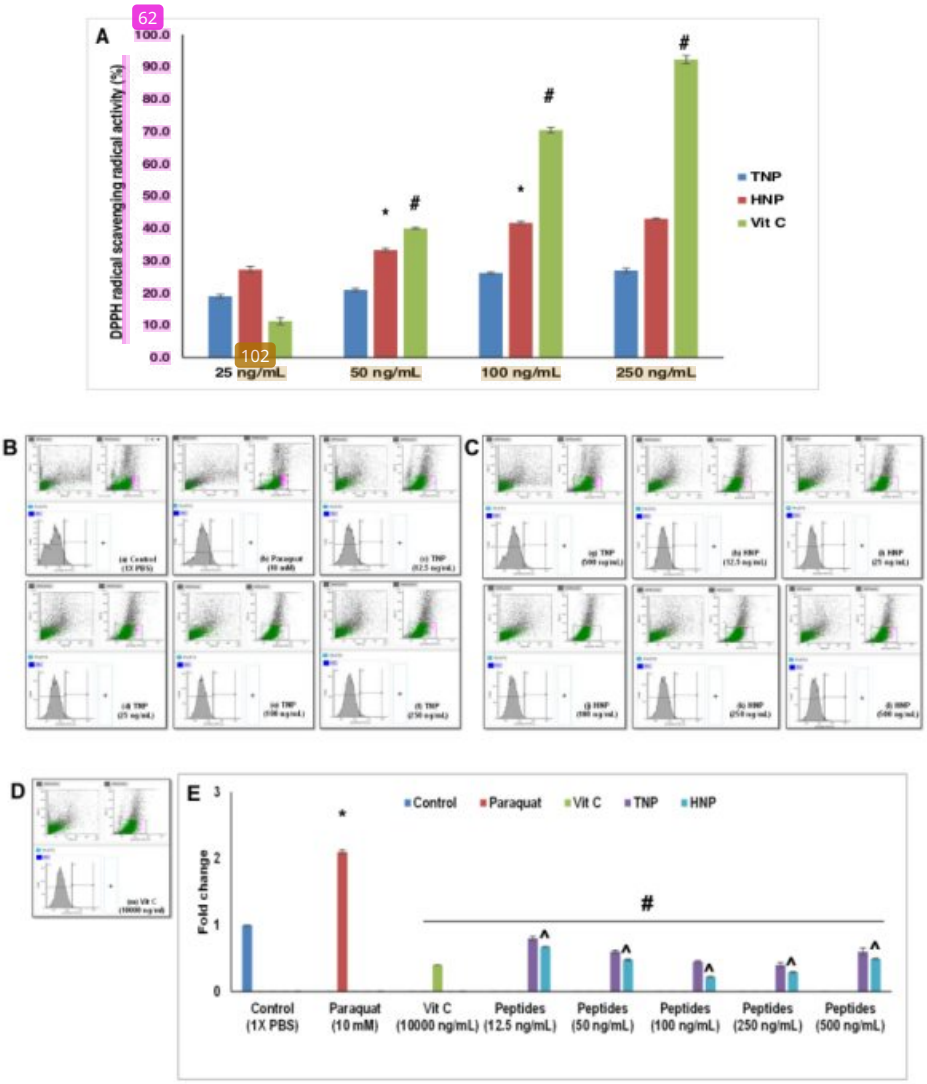

Fig 4.12 Determination of PT-induced intracellular ROS generation and its reversal by pre-treatment with custom peptide (12.5 ng/mL to 500 ng/mL) and Vitamin C (positive control, 10000 ng/mL) for 1 h followed by the PT treatment for 24 h at 37°C in a CO_2 incubator. The ROS generation was determined by using an H_2DCFDA fluorescence probe and expressed as a fold change value with respect to the control (1x PBS). (A) Determination of *in vitro* concentration-dependent (25-250 ng/mL) DPPH radical-scavenging activity of custom peptides. $^{*}p < 0.05$ significant difference between different concentrations of custom peptide HNP; $^{\#}p < 0.05$ significant difference between the

different concentrations of vit C. (B-D) Flow cytometric determination of intracellular ROS. (E) Bar graph representing quantitative analysis of the intracellular ROS generation (expressed by fold change value with respect to control) determined by flow cytometry analysis. $^{*}p \leq 0.05$, a significant difference between untreated (control) and PT-treated cells; $^{\#}p \leq 0.05$, a significant difference of PT-treated cells with respect to custom peptides (TNP and HNP) and vit C pre-treated cells. Significance of difference in the fold change value in between TNP and HNP at the dose of 12.5 to 100 ng/mL, $^{\wedge}p \leq 0.05$. Values are mean ± SD of triplicate determinations.

The spectrofluorometric analysis also validated the custom peptide-mediated reduction in intracellular ROS generation by PT in PC-12 cells. PT treatment (10 mM) resulted in a 2-fold increase in ROS production compared to control PC-12 cells (Fig 4.13). A significant decrease ($p \leq 0.05$) in ROS levels with increasing concentration of peptides was observed in PC-12 cells pre-treated with HNP or TNP (up to 100 ng/mL, equivalent to 71 nM), compared to PT-treated PC-12 cells (Fig 4.13). Nevertheless, above this concentration, the PT-induced ROS production could not be decreased by the peptides (Fig 4.13). The custom peptides at a concentration of 100 ng/mL (~71 nM) demonstrated superior inhibition (0.6 to 0.8-fold decrease) ($p \leq 0.05$) of the PT-induced ROS generation, compared to that offered by Vitamin C (positive control) (0.3-fold decrease) at a higher concentration (10000 ng/mL).

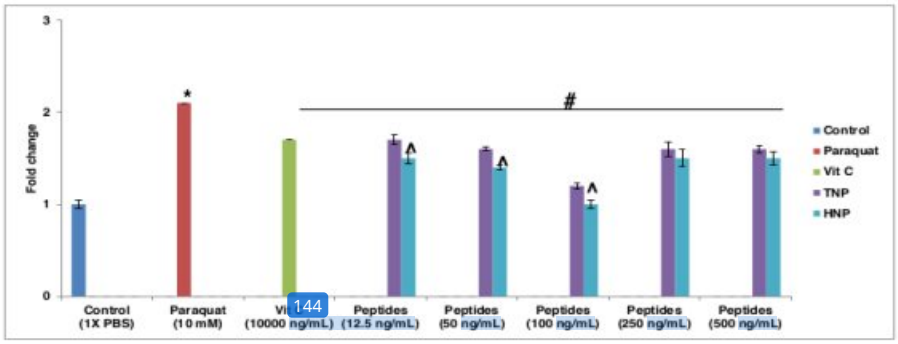

Fig 4.13 Spectrofluorometric determination of intracellular ROS. $^{*}p < 0.05$, a significant difference between untreated (control) and PT-treated cells; $^{\#}p < 0.05$, a significant difference of PT-treated cells with respect to custom peptides (TNP and HNP) and Vit C pre-treated cells. Significance of difference in the fold change value between TNP and

HNP at the dose of 12.5 to 100 ng/mL, ^p < 0.05. Values are mean ± SD of triplicate determinations.

4.1.8 Inhibition of PT-induced depolarization of mitochondrial membrane in PC-12 cells

JC-1 staining was used to study whether or not the custom peptides could restore the loss of mitochondrial membrane potential (MMP) triggered by PT in PC-12 cells. JC-1 signals red fluorescence in non-apoptotic cells as it forms an aggregate when it penetrates non-apoptotic cells, but it signals green fluorescence as the monomeric form in apoptotic cells. The red/green fluorescence ratio was quantified from confocal images to show the change in MMP (Figs 4.14A-B). The fluorescence intensity of the red/green ratio was significantly reduced ($p \leq 0.05$) by 90% in PT-treated cells, compared to control (1XPBS) PC-12 cells (Fig 4.14B). The fluorescence intensity of the red/green ratio was significantly restored ($p \leq 0.05$) by 60 to 65% when PC-12 cells were pre-treated for 1 h with the TNP or HNP custom peptides and then followed by PT-treatment (Figs 4.14A-B). This data suggests that pre-treatment with TNP/ HNP increases cell resistance against PT-induced mitochondrial membrane depolarization. Moreover, HNP showed a significantly higher (0.4-fold increase) inhibition ($p \leq 0.05$) of MMP, when compared to TNP.

MMP was also quantified by flow cytometry analysis using JC-1 staining. Red fluorescence is high when MMP is high, and green fluorescence is high when MMP is low. The PT-treated (10 mM) PC-12 cells showed an increase of 50% in green fluorescence, compared to the untreated PC-12 cells, indicating a disrupted MMP. Custom peptide pre-treatment (100 ng/mL, ~71 nM) resulted in a significant 40 to 45% increase ($p \leq 0.05$) in the intensity of red fluorescence when compared to the PC-12 cells that were only PT-treated (Figs 4.14C-D). The data showed a significant increase ($p \leq 0.05$) in mitochondrial membrane depolarisation in the PT-treated PC-12 cells (a 2-fold decrease in red/green fluorescence) compared to the control PC-12 cells. Nevertheless, pre-treating PC-12 cells with TNP or HNP restored (1.3-1.7-fold increase in the red/green fluorescence) the PT-induced mitochondrial membrane depolarization, and HNP showed a significantly ($p \leq 0.05$) higher (0.4-fold) activity compared to TNP (Figs 4.14C-D).

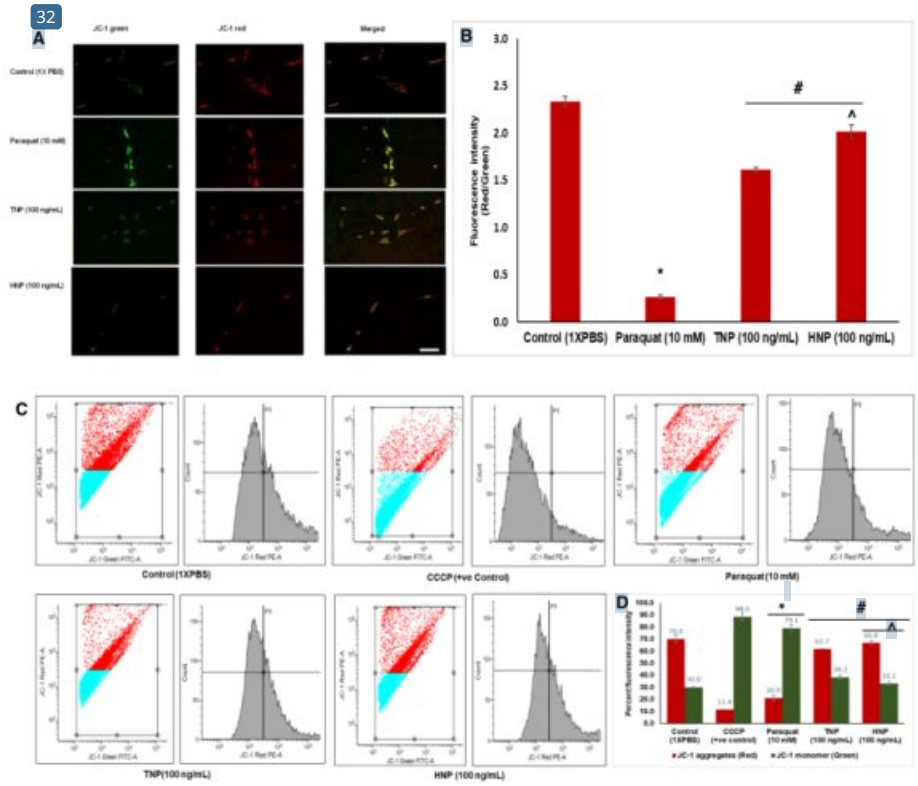

Fig 4.14 Reversal of PT-induced disruption of mitochondrial membrane potential (MMP) of PC-12 cells pre-treated with custom peptides (100 ng/mL, ~71 nM) for 1 h followed by the PT treatment for 24 h at 37°C in a CO_2 incubator. The PT-treated (10 mM) PC-12 cells pre-treated with or without custom peptide (~71 nM) were observed for the measurement of the ratio of red/green fluorescence intensity by JC-1 staining. (A) Confocal images of PC-12 cells stained with JC-1 dye to measure the MMP micrographed at the magnification of 40X. JC-1 red fluorescence represents normal MMP, whereas JC-1 green fluorescence indicates damaged MMP. The scale bar indicates the length as 20 μm. (B) Bar diagram representing the ratio of red/green fluorescence intensity quantified using Image J software. (C) The fluorescence signal intensity of JC-1 monomer and JC-1 aggregates was determined by flow cytometry analysis. Carbonyl cyanide m-chlorophenyl hydrazone (CCCP) is a mitochondrial uncoupling agent that depolarises the mitochondria taken as a positive control. (D) Bar graph representing quantitate analysis of the red and green fluorescence intensity detected by the flow cytometry. $^{*}p \leq 0.05$, a significant difference between untreated (control) and PT-treated cells; $^{\#}p \leq 0.05$, a

significant difference of PT-treated cells with respect to custom peptides (TNP and HNP) pre-treated cells. Significance of difference in fluorescence intensity between TNP and HNP, $^{\wedge}p \leq 0.05$. Values are mean ± SD of triplicate determinations.

4.1.9 Restoration of PT-induced cellular and nuclear morphological changes and apoptotic cells by the custom peptide pre-treated PC-12 cells

The anti-apoptotic potential of custom peptides (100 ng/mL, ~71 nM) against PT-induced (10 mM) apoptotic cell death was determined by flow cytometry analysis (Figs 4.15A-B). PT (10 mM) induced a significant increase ($p \leq 0.05$) (10-11%) in apoptotic cell death, compared to untreated (control) PC-12 cells (Figs 4.15A-B). HNP and TNP; however, at a concentration of 100 ng/mL (~71 nM) significantly inhibited ($p \leq 0.05$) apoptotic and necrotic cell death (by 5-7%) induced by PT, when compared to PC-12 cells that had only been PT-treated (Figs 4.15A-B), and like previous analyses, HNP showed 3.3%increase in activity than TNP.

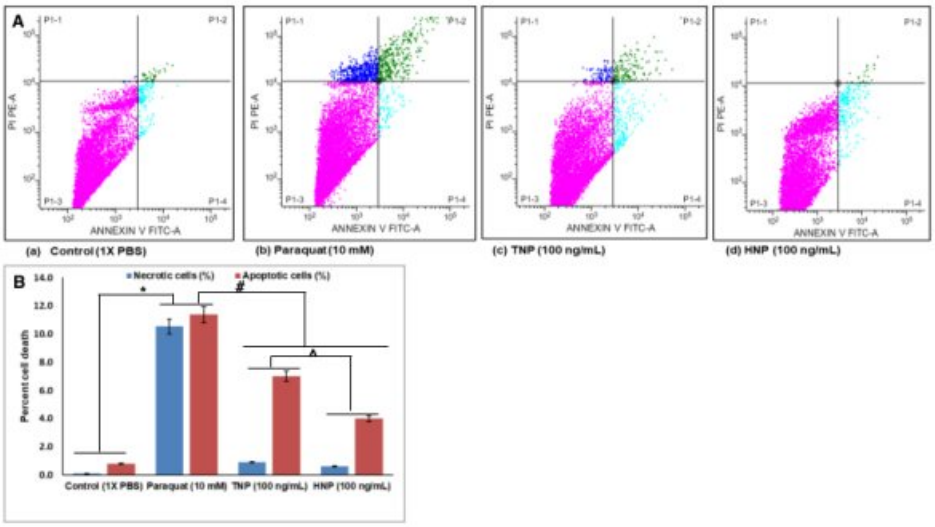

Fig 4.15 Effects of the custom peptide (100 ng/mL) on inhibition of PT-induced apoptosis in PC-12 cells pre-treated with custom peptides (100 ng/mL, ~71 nM) for 1 h followed by the PT treatment for 24 h at 37°C in a CO_2 incubator. (A) The fluorescence intensity of Annexin V-FITC and Propidium iodide (PI) was determined by flow cytometry. (B) The bar graph represents a quantitative analysis of the percent cell death determined by flow cytometry analysis. $^{*}p \leq 0.05$, a significant difference between untreated (control)

and PT-treated cells; $^{\#}p \leq 0.05$, a significant difference of PT-treated cells with respect to custom peptides (TNP and HNP) pre-treated cells. Significance of difference in percent cell death between TNP and HNP, $^{\wedge}p \leq 0.05$. Values are mean ± SD of triplicate determinations.

Confocal image analysis revealed a decrease in the population of PT-treated PC-12 cells, compared to untreated (control) PC-12 cells (Fig 4.16A). Induction of cell death by PT in the PC-12 cells was evident from the cell morphology (DAPI staining), shrunken nuclei, membrane blebbing, and secondary cellular necrosis (Fig 4.16A). The percent of cell death characterized by cellular and nuclear morphological changes increased by 21% when cells were treated with PT, but the pre-treatment with custom peptides significantly reduced ($p \leq 0.05$) the degree of cell death (4.6 - 7.9%). HNP showed a higher activity compared to TNP (Fig 4.16B).

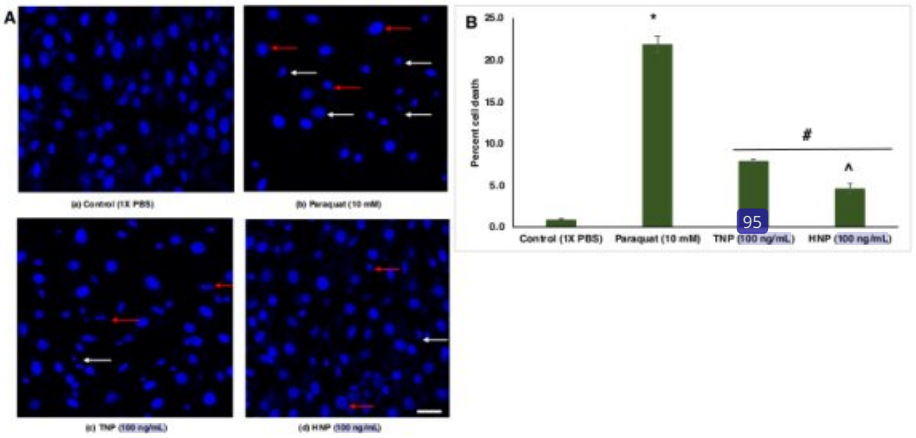

Fig 4.16 Effects of the custom peptide (100 ng/mL) on inhibition of PT-induced apoptosis in PC-12 cells pre-treated with custom peptides (100 ng/mL, ~71 nM) for 1 h followed by the PT treatment for 24 h at 37°C in a CO2 incubator. (A) Confocal microscopic analysis of changes in the cellular and nuclear morphology of PC-12 cells by DAPI staining at the magnification of 40X. The red arrows indicate cells with membrane blebbing and shrunken nuclei, and the white (solid) arrows indicate secondary cellular necrosis. The scale bar indicates the length of 20 μm. (B) The bar diagram shows the percent cell death determined from the changes in the cellular and nuclear morphology with respect to the control (1x PBS). The intensity of the DAPI staining was determined

using Image J software. *p < 0.05, a significant difference between untreated (control) and PT-treated cells; #p < 0.05, a significant difference of PT-treated cells with respect to custom peptides (TNP and HNP) pre-treated cells. Significance of difference in percent cell death between TNP and HNP, ^p < 0.05. Values are mean ± SD of triplicate determinations.

4.1.10 Custom peptide pre-treatment restored the paraquat-induced upregulated and downregulated pro- and anti-apoptotic genes to delay paraquat-induced programmed cell death in PC-12 cells

The qRT-PCR analysis demonstrated a 1.5 to 2-fold-change increase ($p \leq 0.05$) in the expression of proapoptotic genes (cyt-C, bax, bid), and a 3.4 to 3.5-fold change increase in the expression of heat shock gene-70 (hsp-70), and caspase-3 gene (a hallmark of apoptosis) in the PT group compared to the CT group of cells (Fig 4.17). The pre-treatment of cells with mouse 2.5S-NGF (positive control) and TNP or HNP resulted in a significant downregulation ($p \leq 0.05$) or restoration of the expression of the genes that had been upregulated by PT treatment alone (Fig 4.17). The qRT-PCR analyses showed a 0.3-fold decrease in the expression of anti-apoptotic genes (bcl-2) in the PT group compared to the CT group of cells. Further, pre-treatment with TNP or HNP, and mouse 2.5S-NGF (positive control) restored the downregulated anti-apoptotic (bcl-2) genes in the PT group of cells (Fig 4.17).

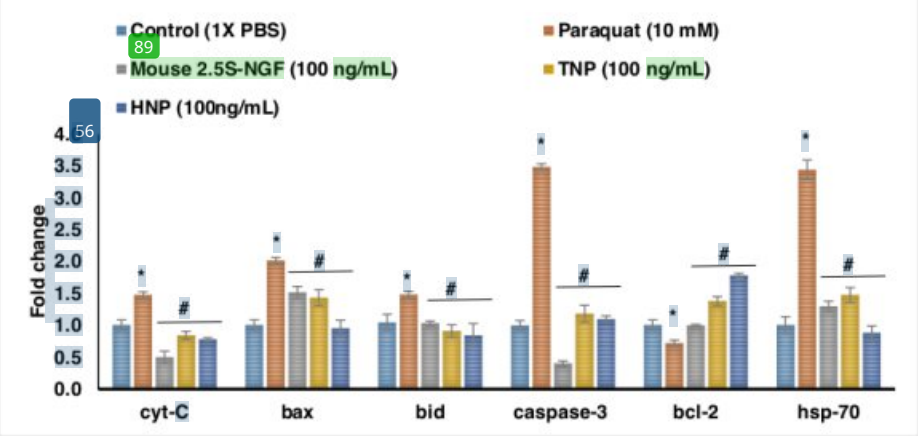

Fig 4.17 The qRT-PCR analysis to show the expression of key pro-/anti-apoptotic genes in PC-12 cells post-treatment with paraquat (10 mM) for 12 h, and comparison with the

custom peptides (100 ng/mL, ~71 nM) /mouse 2.5S-NGF (positive control, 100 ng/mL) pre-treatment for 1 h followed by the PT treatment for 12 h at 37°C in a CO_2 incubator. The expression of mRNA was normalized using the housekeeping gene GAPDH. $^{*}p \leq 0.05$, a significant difference between untreated (control) and PT-treated cells; $^{\#}p \leq 0.05$, a significant difference of PT-treated cells with respect to custom peptides (TNP and HNP)/mouse 2.5S-NGF pre-treated cells. Values are mean ± SD of triplicate determinations.

4.1.11 Comparing the differential expression of cellular proteins in the PT-treated PC-12 cells and the cells pre-treated with custom peptides by quantitative mass spectrometry

LC-MS/MS analysis unambiguously identified 207 non-redundant proteins from the four groups of PC-12 cells (PT, PHNP, CT, and HNP). Based on their intracellular locations and biological processes, the proteins were classified into nine distinct categories, among which three major cellular proteins were present in high relative abundances compared to the other proteins (Table 4.4).

Table 4.4 The quantitative proteomics data shows the relative abundance of the intracellular proteins in the different treatment groups. The relative abundance of the proteins was calculated by the MS2-based spectral count method. For comparison of differential expression of the cellular proteins, the PC-12 cells were subjected to the following treatments at 37°C: (a) 1X PBS (control) treated PC-12 cells (CT), (b) 10 mM paraquat (PT) treatment for 24 h, (c) pre-treatment with 100 ng/mL (~71 nM) custom peptide for 1 h followed by 10 mM paraquat treatment (PHNP) for 24 h, and (d) treatment with 100 ng/mL (~71 nM) of custom peptide (HNP) for 1 h.

Accession No	**Relative abundance of 1X PBS (control) treated PC-12 cells (CT)**	**Relative abundance of PC-12 cells pre-treated with 100 ng/mL (~71 nM) custom peptide for 1 h followed by 10 mM paraquat treatment (PHNP) for 24 h**	**Relative abundance of PC-12 cells treated with 10 mM paraquat (PT) for 24 h**	**Relative abundance of PC-12 cells treated with 100 ng/mL (~71 nM) of custom peptide (HNP) for 1 h**
Antioxidant/Stress response				
P06761|BIP_RAT	0.51	0.93	3.08	0.63
P63018|HSP7C_RAT	0.51	0.80	2.51	0.62
Q07936|ANXA2_RAT	0.51	0.62	2.51	0.58
Q66HD0|ENPL_RAT	0.51	0.97	2.76	0.67
P34058|HS90B_RAT	0.51	1.02	2.51	0.60
P48679|LMNA_RAT	0.51	0.88	2.92	0.60

Q00715|H2B1_RAT	0.51	0.75	4.18	0.72
Q9Z0V5|PRDX4_RAT	0.51	0.99	2.51	0.67
Binding protein				
tr|G3V6P7|G3V6P7_RAT	0.68	0.79	2.51	0.72
P68035|ACTC_RAT	0.51	0.88	2.76	0.73
tr|Q5RJR9|Q5RJR9_RAT	0.51	0.68	2.51	0.49
P13832|MRLCA_RAT	0.51	0.87	3.34	0.67
P62804|H4_RAT	0.51	0.85	3.01	0.53
P00507|AATM_RAT	0.51	0.99	2.51	0.49
Apoptotic protein				
P63039|CH60_RAT	0.51	0.92	2.51	0.63
P62630|EF1A1_RAT	0.51	0.62	2.51	0.80
P11240|COX5A_RAT	0.51	0.99	2.51	0.49
P62898| Cycs_RAT	0.51	0.99	2.51	0.50
P00787|CATB_RAT	0.51	0.99	2.51	0.48

Mitochondrial protein				
P10860|DHE3_RAT	0.51	0.90	2.51	0.49
P04636|MDHM_RAT	0.51	0.83	2.51	0.49
P32551|QCR2_RAT	0.51	0.99	2.51	0.49
P00507|AATM_RAT	0.51	0.99	2.51	0.49
ATP synthesis				
P10719|ATPB_RAT	0.51	2.73	0.90	3.61
P15999|ATPA_RAT	0.51	2.92	0.91	3.63
Neuronal development				
Q9JLT0|MYH10_RAT	0.51	2.51	0.69	3.57
P18418|CALR_RAT	0.51	2.51	0.79	3.69
P31000|VIME_RAT	0.51	3.01	0.93	
Innate immune response				
P07150|ANXA1_RAT	0.51	0.75	2.51	0.69
P11598|PDIA3_RAT	0.51	0.81	2.51	0.49

Structural protein				
Q64119|MYL6_RAT	0.51	0.76	2.51	0.63
Endoplasmic reticulum protein				
tr|D3ZH41|D3ZH41_RAT	0.51	0.80	2.51	0.49

The quantitative analysis showed differential expression of proteins in the PT group of PC-12 cells versus the CT group. A total of 130 intracellular proteins were identified in the PT group (Fig 4.18A), of which 118 proteins were differentially regulated compared to those in the CT group (Fig 4.18A). Among the 118 identified proteins, the PT-induced altered expression of 27 proteins was restored in PC-12 cells that had been pre-treated with HNP (Fig 4.18A). Notably, six intracellular proteins were regulated differently in the PHNP and PT groups (Fig 4.18A). Two proteins (keratin type 1 and type 2 cytoskeletal proteins) were uniquely expressed in the PHNP group.

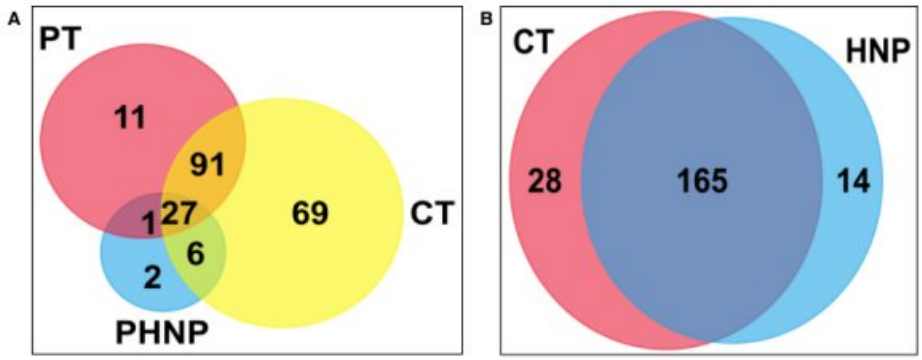

Fig 4.18 (A) Venn diagram showing the common intracellular proteins among untreated (control) (CT), PT (PT) treated, and HNP pre-treated followed by PT-treated (PHNP) groups of PC-12 cells determined by LC/MS-MS analysis. (B) Venn diagram showing common intracellular proteins among untreated (control) (CT) and only HNP-treated PC-12 cells determined by LC/MS-MS analysis.

Intracellular proteins in the PHNP group were also compared in the PT and CT groups to identify differentially expressed proteins involved in apoptosis (60 kDa heat shock protein (hsp-60), cytochrome C (cycs), Heat shock cognate 71 kDa (hspa8), the electron transport chain (cytochrome c oxidase subunit 5A; cox5a), cytochrome b-c1 complex subunit 2 (uqcrc2) stress response (heat shock protein (hsp 90-beta), antioxidant function (peroxiredoxin-4 (prdx-4), glutamate dehydrogenase 1 (glud-1), Wnt signaling (actin, (actc1), signal transduction (cytoskeleton-associated protein 4, (ckap4), the innate immune response annexin A2 (anaxa2), collagen biosynthesis (collagen-binding protein (serpinh1), and phagocytosis (cathepsin B (ctsb). PT treatment of the PC-12 cells caused the upregulation of some proteins involved in these pathways (Table 4.5A), and their

expression was restored in the PHNP treatment group. Their fold-change values are mentioned in Table 4.5A. In contrast, some proteins involved in neuronal development and ATP synthesis pathways were downregulated (Table 4.5B), though their expression was restored in the PHNP group (Table 4.5B).

Table 4.5 Comparison of the fold changes in differential expression of proteins in PT-treated PC-12 cells determined by proteomic analysis.

(A) List of up-regulated proteins in PT-treated PC-12 cells compared to untreated (control) PC-12 cells, and their downregulation in cells pre-treated with HNP.				
Accession	**PT treatment (fold change compared to control)**	**HNP pre-treatment, (fold change compared to control)**	**Pathway name**	**Description**
P06761|BIP_RAT	6.00	1.81	Apoptosis signaling pathway	Endoplasmic reticulum chaperone BiP OS=Rattus norvegicus OX=10116 GN=Hspa5 PE=1 SV=1
P63018|HSP7C_RAT	4.87	1.56	Apoptosis signaling pathway	Heat shock cognate 71 kDa protein OS=Rattus norvegicus OX=10116 GN=Hspa8 PE=1 SV=1
Q07936|ANXA2_RAT	4.87	1.21	Antioxidant pathway	Annexin A2 OS=Rattus norvegicus OX=10116 GN=Anxa2 PE=1 SV=2
Q66HD0|ENPL_RAT	5.36	1.88	Stress response pathway	Endoplasmin OS=Rattus norvegicus OX=10116 GN=Hsp90b1 PE=1 SV=2
P34058|HS90B_RAT	4.87	1.99	Stress response pathway	Heat shock protein HSP 90-beta OS=Rattus norvegicus OX=10116 GN=Hsp90ab1 PE=1 SV=4

P48679|LMNA_RAT	5.68	1.71	Apoptosis signaling pathway	Prelamin-A/C OS=Rattus norvegicus OX=10116 GN=Lmna PE=1 SV=1
Q00715|H2B1_RAT	8.12	1.46	Stress response pathway	Histone H2B type 1 OS=Rattus norvegicus OX=10116 PE=1 SV=2
Q9Z0V5|PRDX4_RAT	4.87	1.93	Stress response pathway	Peroxiredoxin-4 OS=Rattus norvegicus OX=10116 GN=Prdx4 PE=2 SV=1
tr|G3V6P7|G3V6P7_RAT	3.69	1.16	Phagocytosis	Myosin, heavy polypeptide 9, non-muscle OS=Rattus norvegicus OX=10116 GN=Myh9 PE=1 SV=1
P68035|ACTC_RAT	5.36	1.81	Wnt signalling pathway	Actin, alpha cardiac muscle 1 OS=Rattus norvegicus OX=10116 GN=Actc1 PE=2 SV=1
tr|Q5RJR9|Q5RJR9_RAT	4.87	1.71	Collagen biosynthesis	Collagen-binding protein OS=Rattus norvegicus OX=10116 GN=Serpinh1 PE=1 SV=1
P13832|MRLCA_RAT	6.50	1.33	Cell cycle	Myosin regulatory light chain RLC-A OS=Rattus norvegicus OX=10116 GN=Rlc-a PE=2 SV=2

P62804|H4_RAT	5.85	1.69	Transcription regulation	Histone H4 OS=Rattus norvegicus OX=10116 GN=H4c2 PE=1 SV=2
P00507|AATM_RAT	4.87	1.65	Asparagine and aspartate biosynthesis	Aspartate aminotransferase, mitochondrial OS=Rattus norvegicus OX=10116 GN=Got2 PE=1 SV=2
P63039|CH60_RAT	4.87	1.78	Apoptosis signaling pathway	60 kDa heat shock protein, mitochondrial OS=Rattus norvegicus OX=10116 GN=Hspd1 PE=1 SV=1
P62630|EF1A1_RAT	4.87	1.21	Protein biosynthesis	Elongation factor 1-alpha 1 OS=Rattus norvegicus OX=10116 GN=Eef1a1 PE=2 SV=1
P11240|COX5A_RAT	4.87	1.93	Electron transport chain	Cytochrome c oxidase subunit 5A, mitochondrial OS=Rattus norvegicus OX=10116 GN=Cox5a PE=1 SV=1
P62898| Cycs_RAT	4.87	1.93	Apoptosis signaling pathway	Cytochrome c OS=Rattus norvegicus OX=10116 GN= Cycs PE=3 SV=1
P00787|CATB_RAT	4.87	1.93	Phagocytosis	Cathepsin B OS=Rattus norvegicus OX=10116 GN=Ctsb PE=1 SV=2

P10860|DHE3_RAT	4.87	1.75	Antioxidant	Glutamate dehydrogenase 1, mitochondrial OS=Rattus norvegicus OX=10116 GN=Glud1 PE=1 SV=2
P04636|MDHM_RAT	4.87	1.61	Pyruvate metabolism	Malate dehydrogenase, mitochondrial OS=Rattus norvegicus OX=10116 GN=Mdh2 PE=1 SV=2
P32551|QCR2_RAT	4.87	1.93	Electron transport chain	Cytochrome b-c1 complex subunit 2, mitochondrial OS=Rattus norvegicus OX=10116 GN=Uqcrc2 PE=1 SV=2
P07150|ANXA1_RAT	4.87	1.45	Innate immune response	Annexin A1 OS=Rattus norvegicus OX=10116 GN=Anxa1 PE=1 SV=2
P11598|PDIA3_RAT	4.87	1.58	Vitamin D metabolism	Protein disulfide-isomerase A3 OS=Rattus norvegicus OX=10116 GN=Pdia3 PE=1 SV=2
Q64119|MYL6_RAT	4.87	1.48	Motor function	Myosin light polypeptide 6 OS=Rattus norvegicus OX=10116 GN=Myl6 PE=1 SV=3
tr|D3ZH41|D3ZH41_RAT	4.87	1.55	Signal transduction	Cytoskeleton-associated protein 4 OS=Rattus norvegicus OX=10116 GN=Ckap4 PE=1 SV=2

(B) List of down-regulated proteins in PT treated PC-12 cells compared to untreated (control) PC-12 cells and their upregulation in cells pre-treated with HNP.

Accession	Paraquat treatment (fold change with respect to control)	HG17 pre-treatment, (fold change with respect to control)	Pathway name	Description
P10719|ATPB_RAT	1.76	3.02	ATP synthesis	ATP synthase subunit beta, mitochondrial OS=Rattus norvegicus OX=10116 GN=Atp5f1b PE=1 SV=2
P15999|ATPA_RAT	1.77	3.22	ATP synthesis	ATP synthase subunit alpha, mitochondrial OS=Rattus norvegicus OX=10116 GN=Atp5f1a PE=1 SV=2
Q9JLT0|MYH10_RAT	1.34	3.63	Neuronal development	Myosin-10 OS=Rattus norvegicus OX=10116 GN=Myh10 PE=1 SV=1
P18418|CALR_RAT	1.54	3.17	Neuronal development	Calreticulin OS=Rattus norvegicus OX=10116 GN=Calr PE=1 SV=1
P31000|VIME_RAT	1.05	5.85	Neuronal development	Vimentin OS=Rattus norvegicus OX=10116 GN=Vim PE=1 SV=2
O08878|GPER1_RAT	1.20	3.40	Neuritogenesis	G-protein coupled estrogen receptor 1 OS=Rattus norvegicus OX=10116 GN= Gper1 (Cmkrl2, Gper, Gpr30, Gpr41) SV=2

When comparing the expression of intracellular proteins in the HNP to the CT group of cells, 14 proteins were found to be uniquely expressed in the former group (Fig 4.18B). Therefore, the proteomic analyses provide evidence of uniquely expressed proteins and their associated metabolic pathways in PC-12 cells treated with HNP, in comparison to untreated cells (Table 4.6).

Table 4.6 List of the uniquely expressed metabolic pathways in PC-12 cells treated with HNP when compared to untreated PC-12 cells. These pathways are determined by quantitative proteomic analyses.

Mapped IDs	**Pathway name**	**Protein**
RAT|RGD=71000|UniProtKB=Q9JLT0, RAT|RGD=1565476|UniProtKB=Q6P9V9	Cytoskeletal regulation by Rho GTPase	Tuba1b, Plec
RAT|RGD=2451|UniProtKB=P62898, RAT|RGD=621379|UniProtKB=Q06647, RAT|RGD=68374|UniProtKB=P10888	ATP synthesis	Cycs, Cox4i1, Atp5
RAT|RGD=71000|UniProtKB=Q9JLT0	Nicotinic acetylcholine receptor signalling pathway	Myh10
RAT|RGD=71000|UniProtKB=Q9JLT0	Inflammation mediated by chemokine and cytokine signaling pathway	Myh10
RAT|RGD=1565476|UniProtKB=Q6P9V9	Gonadotropin-releasing hormone receptor pathway	Tuba1b
RAT|RGD=71006|UniProtKB=Q63692, RAT|RGD=1305960|UniProtKB=Q498E0	Stress response antioxidant pathway	Txndc12, Plec

The PPI network revealed the functional significance of the intracellular proteins and their involvement in particular pathways (Fig 4.19). The cellular pathways governed by the 27 differentially regulated proteins in the CT, PT, and PHNP groups of PC-12 cells were curated manually and the interaction network was established to highlight the interconnected pathways (Fig 4.19).

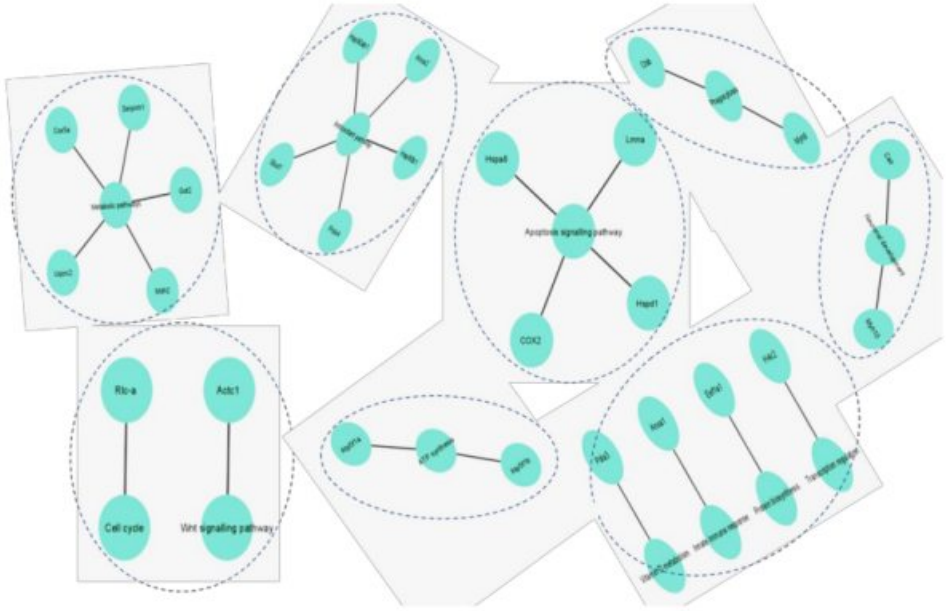

Fig 4.19 Molecular network of HNP-mediated neuroprotection drawn in Cytoscape (version 3.9.1). The molecular network shows the multiple pathways that are interconnected to each other and involved in the HNP-mediated neuroprotection. The proteins involved in the pathways were determined by LC/MS-MS analysis.

Based on the information on the neuritogenesis potency of the custom peptides, inhibition of downstream signaling pathways by specific inhibitors (MAPK-ERK, PI3K/AKT pathways), the neuroprotective potential of custom peptides (via different mechanisms such as inhibition of ROS generation, restoration of MMP, anti-apoptotic/necrotic potential), and the differential expression of proteins (determined by quantitative mass spectrometry analysis) involved in neuroprotective activities, the mechanism of action of HNP against PT-induced neuroprotective activity is shown in Fig 4.20.

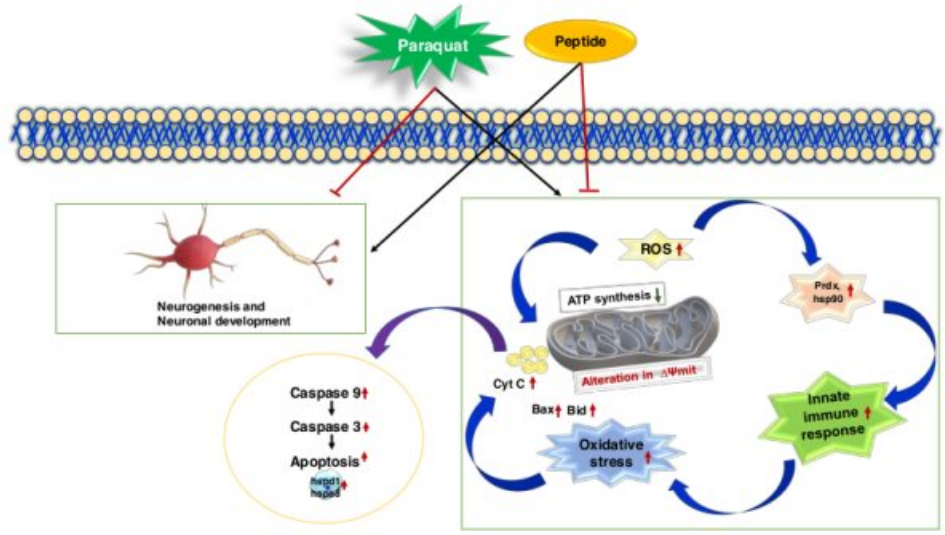

Fig 4.20 The proposed neuroprotection mechanism of custom peptides against PT-induced neurotoxicity in PC-12 cells.

4.2 Discussion

Neuronal differentiation is a vital physiological phenomenon, often associated with intellectual development in children and age-related neurodegenerative diseases such as PD, AD, and Huntington's disease (HD) [4]. Proposing a large neurotrophin polypeptide or a protein molecule as a drug candidate has several disadvantages including its undesired pleiotropic effect, short half-life, proteolytic degradation, and poor pharmacokinetics [5-8]. Therefore, in recent years, the development of small, peptide-based drugs has gained momentum and opened new avenues of research to overcome the limitations of parent molecules [9]. In any case, the peptide-based drugs must show improved neuroprotective effects, synaptic and neuronal plasticity, neuritogenesis, better pharmacokinetics than their larger, parent neurotrophin molecules, and easy penetration to cells via the BBB [8-11]. In this study, two small, water-soluble custom peptides (TNP and HNP, with masses of 1.2 kDa and 1.4 kDa, respectively) were designed from snake venom neurotrophin molecules to be developed as possible neuroprotective drug prototypes with improved neuritogenesis potency, compared to mouse 2.5S-NGF (positive control) for the restoration of neurons that have been degenerated by toxic chemicals.

Several studies have demonstrated that computational analysis (docking) is a powerful tool for identifying novel compounds of therapeutic interest with high probability and which can forecast ligand-target interactions at the molecular level with high efficiency [1-3,12-14]. The computational study can assist in screening many compounds (ligands) against specific targets (i.e., a receptor) to identify compounds that can bind efficiently with the target, though *in silico* findings must be confirmed by *in vitro* and *in vivo* studies [1-3,12-14]. The *in silico* analysis demonstrated that domain-3 of the TrkA receptor extracellular domain is the only region that binds with NGF and forms the NGF/TrkA domain-3 complex. Subsequently, the complex induces TrkA dimerization and transduces a signal to activate MAPK and the PI3K/Akt signaling pathways [15]. The docking analysis also demonstrated that, like human NGF molecules, the TNP and HNP custom peptides show high-affinity binding only with domain-3 of the human TrkA receptor. The binding site for the custom peptides was also shown to differ from that of the human NGF-TrkA binding site.

Since TrkA dimerization is important for activation of the signal transduction mechanism, dimerization of the TrkA receptors after binding to custom peptides needs to be explored. The docking scores of the docked complex (custom peptide and TrkA domain-3) indicate higher binding affinities of TNP towards the TrkA domain-3, compared to that of HNP. Since binding affinity does not always correlate with the stability of the binding, the stability of binding should also be evaluated by a molecular dynamic simulation study and computational analyses. In this study, our findings predicted that HNP (compared to TNP) would form a more stable complex with the TrkA receptor. Differences in the binding affinities and stability of the custom peptides and TrkA receptors can be attributed to the electrostatic interactions (hydrogen bonds) between the charged molecules of the HNP / TrkA domain-3 complex [1-3].

Since the custom peptides were designed to mimic the TrkA binding region of the snake venom neurotrophin molecule, the *in silico* analysis convincingly showed that the high-affinity binding of HNP or TNP to the TrkA receptor is primarily essential for inducing neuritogenesis. The spectrofluorometric binding assay showed high-affinity binding (low K_d value in picomolar range) to the TrkA receptor expressed in mammalian cell lines (PC-12, MDA-MB-231, MCF7) but not in L6 cells, which lack TrkA receptors, which was further validated by fluorescence microscopic study. In the presence of a

chemical inhibitor of the TrkA receptor (K252a), no binding was observed under a fluorescence microscope, confirming that the custom peptides bind with the TrkA receptor exclusively. These *in vitro* binding studies also validated the results of the *in silico* analysis. Further, studies have shown the Kd value of binding of mammalian NGF to TrKA receptor is also $1X10^{-11}M$ [16,17], indicating HNP and TNP are of equivalent potency with binding to the same receptor.

Because the *in silico* and *in vitro* binding of ligands to receptors does not necessarily assure their desired therapeutic effect, we also evaluated the neuritogenesis potency of these peptides in PC-12 cells, which is considered to be an appropriate *in vitro* model for neuronal differentiation, development, and neurological diseases [1-3,18,19]. PC-12 cell lines have advantages in being derived from neural crest cells with similar structures and functions, and they are easy to grow and maintain [18]. The induction of neuritogenesis is generally initiated after 4-6 h of incubation with NGF [20]; however; optimum neurite length and differentiation of PC-12 cells observed after 14 days of incubation with snake venom NGFs [1,2] TNP and HNP in this study showed the same result.

In evaluating the neuronal outgrowth-inducing properties of the custom peptides in PC-12 neuronal cells, we found that, as predicted, both peptides significantly increased the neurite length and percent differentiation of PC-12 cells measured simultaneously point, in comparison to the effect of mouse 2.5S-NGF treatment alone. No significant difference was observed between the two peptides. In previous studies, however, the neuritogenesis potency of TNP and HNP has been shown to surpass the potency of SV NGF in PC-12 cells [1-3] or natural polyphenols such as curcumin and resveratrol [21]. Compared to synthetic tripeptide (p-BTX-I) synthesized from *Bothrops atrox* venom [40], TNP and HNP were almost equal in their neuritogenesis potency. The reported differences in neuritogenesis potency may be due to the different experimental conditions (i.e., doses, incubation time, etc.). As mentioned, mammalian NGF and snake venom NGF-induced TrkA dimerization activate MAPK and PI3K/AKT pathway-dependent neuritogenesis [1-3,15]. The selective inhibition of the MAPK and PI3K/AKT pathways by U0126 and LY294002 inhibitors, respectively, provides convincing evidence of the similarity of the custom peptides to snake venom NGF molecules [1-3,11]. The custom peptides we developed also activate the MAPK and PI3K/AKT signalling pathways for

neuronal survival and differentiation in PC-12 cells [1-3,22,23]. In this study, we also reported that the custom peptides lacked cytotoxicity against different cell types and did not interfere with the mammalian blood coagulation cascade, indicating a lack of side effects based on *in vitro* experiments.

A plethora of studies have reported that the pathogenesis of PD is related to oxidative stress, resulting from a homeostatic imbalance in pro-oxidant and antioxidant genes that leads to the production of excessive ROS (free radicals), which ultimately triggers apoptotic cell death [24,25]. Some non-selective herbicides (such as PT) that are frequently used by farmers in agricultural practice, cause neurotoxicity and mitochondrial toxicity and can lead to the development of PD-like pathologies [26,27]. This study showed the neuroprotective potency of custom peptides TNP and HNP (pre-treatment conditions) in PC-12 cells by 15-20%. Further, their neuroprotective potency at a low concentration (100 ng/mL) and less incubation time (1h) suggest that these custom peptides may have a higher effect at low concentrations compared to other natural compounds [73, 77-79]. Our data also showed that both custom peptides possess similar neuroprotective effects but surpass the neuroprotective activity of mouse 2.5S-NGF (positive control) when tested at the same experimental conditions.

The antioxidant system against ROS is in dynamic balance under normal circumstances. PT induces an increase in ROS production, oxidative stress response, mitochondrial membrane potential, induction of apoptosis, and a reduced proliferation of PC-12 cells [28,29]. Studies have already reported that natural compounds such as naringin, curcumin, resveratrol, silymarin, pirfenidone, quercetin, selenium, bacosides, and Vitamin C have a significant therapeutic potential for treating PT-induced toxicity [21,30-32]. Like these natural compounds, the custom peptides that we tested in this study have profound neuroprotective activity, and we aimed to investigate their mechanism of action. Following the findings from previous studies [29], we showed that PT treatment increases ROS production, and the custom peptide pre-treatment significantly attenuated the PT-induced ROS production, at a concentration (100 ng/mL, equivalent to 71 nM) that was 1,000 times less than that of Vitamin C (positive control, 10000 ng/mL). Although Vitamin C in this study showed appreciable antioxidant activity, it did not offer protection against PT-induced neurotoxicity. This suggests that antioxidant property alone may not be sufficient to offer protection against PT-induced neuronal damage and

justifies the therapeutic application of the custom peptides under study. Additional quantitative proteomic analyses demonstrated the upregulation (fold-change increase) of antioxidant proteins such as heat shock protein 90 (hsp90), peroxiredoxin (prdx4), and glutamate dehydrogenase (glud1) in PT-treated PC-12 cells. These genes are reported to play an important role in the oxidative deamination and reduction of free radicals [33,34]. The increased ROS production in the PT group was validated by the upregulation of antioxidant proteins, and the activity of the custom peptides to attenuate the ROS production was confirmed by the downregulation of the same proteins in the PHNP group.

Mitochondrial dysfunction is another crucial phenomenon involved in the pathogenesis of PD, which is caused by oxidative stress [25,35]. Oxidative stress eventually leads to the loss of MMP, which results in the release of cytochrome C (pro-apoptotic protein) from the mitochondria and activation of the caspase cascade that induces cellular apoptosis [28,29,36,37]. Studies have shown that preventing mitochondrial dysfunction may be a therapeutic strategy for avoiding cell death [38]. In this study, we showed that pre-treatment of PC-12 cells with custom peptides significantly restored the depolarization of PT-induced MMP, which points to the neuroprotective property of custom peptides to maintain mitochondrial health and balance the expression of apoptotic proteins.

Due to the high energy demand of neuronal cells, they can be vulnerable to extensive mitochondrial damage, which can lead to nerve cell injury and death [38]. Different cellular pathways are involved in maintaining mitochondrial homeostasis and integrity, like the rapid translation of mitochondrial protein, pathways involved in autophagy, energy (ATP) production via oxidative phosphorylation, amino acid synthesis, fat metabolism, and other biochemical pathways [25,39]. Together, these pathways maintain mitochondrial homeostasis by replacing defective mitochondria with new organelles that subsequently prevent neurodegeneration and show neuroprotective effects [40].

The proteomic analyses indicated that HNP pre-treatment restored the PT-induced upregulated genes and proteins involved in mitochondrial stress response pathways, such as glutamate dehydrogenase 1 (glud1) and glutamic-oxaloacetic transaminase (got2) involved in the mitochondrial redox balance [34,41]. To help maintain cellular integrity,

HNP pre-treatment restored the upregulation of pro-apoptotic proteins in the PT group, such as cytochrome C (cyt-C), heat shock protein 60 (hspd1, GO:0043065), heat shock protein 70 (hspa5, GO:1903265). These proteins are reported to participate in the mitogen-activated protein kinase (p38/MAPK) signaling pathways, which are coupled to the oxidative stress response [42]. The global proteomic studies of snake venom NGF treated PC-12 cells had revealed about the oxidative stress-mediated apoptosis [1-3]. Moreover, the release of mitochondrial cyt-C into the cytoplasm in response to pro-apoptotic signals (bax, bid) and the activation of caspase-3 (cas-3) leads to apoptotic cell death [43-45]. In this study, the qRT-PCR analysis showed the downregulation of anti-apoptotic gene (bcl-2) expression and the upregulation of pro-apoptotic genes (cyt-C, bax, bid, hsp-70, and cas-3) in PT-treated PC-12 cells, which triggered cell death. The custom peptide pre-treatment restored the gene expression of the pro-/anti-apoptotic genes suggesting the therapeutic potency of the peptides to prevent PT-induced premature apoptosis in PC-12 cells.

The PT group of cells also showed upregulation of genes involved in detoxification (myh9 and ctsb) [46,47], the TCA cycle (cox5a and uqcrc2) [48,49] and the innate immune response (anxa1) [50], which were downregulated in the PHNP group of cells. As mentioned before, more energy is required to maintain mitochondria against oxidative stress, so the upregulation of these proteins is essential for the neuroprotective effect [38]. Our findings also suggest the upregulation of proteins involved in energy production by ATP synthesis via oxidative phosphorylation, such as the ATP synthase F1 subunit beta, alpha (atp5f1b and atp5f1a) [51] in HNP pre-treated cells, compared to the PT group of cells. In addition, HNP pre-treatment showed a neuroprotective effect by counteracting the PT-induced downregulation of proteins directly or indirectly involved in neural development (myh10 and vim) and neuritogenesis [52] (gper1, cmkrl2, gper, gpr30, and gpr41) [52] (GO:0007399, GO:0019228).

A molecular network was constructed to show the multiple pathways that are interconnected and involved in HNP-mediated neuroprotection. Based on our experimental results, an overall neuroprotective mechanism was proposed for the action of the custom peptides against PT-induced neuronal damage (Fig 4.20).

CHAPTER V

The *in vivo* neuroprotective mechanism of custom peptides in *C. elegans*

5.1 Results

5.1.1 *In silico* analysis of custom peptides binding in *C. elegans*

Among all the proteins analyzed, the custom peptides viz. TNP (left side) and HNP (right side) exhibited interaction in three main proteins of the *C. elegans* – CED-9 (Fig 5.1A), which functions as a programmed cell death activator; PMK-2 (Fig 5.1B) which is a mitogen-activated protein kinase; immunoglobulin (IG) (Fig 5.1C) and frizzled domain (FZ) of CAM-1 (Fig 5.1D) which is a tyrosine-protein kinase receptor.

The RMSD analysis of the trajectory demonstrated significant stable interaction for all these proteins (Figs 5.1E-H). The MM-GBSA binding free energies obtained for different complexes were between -40 and -51 kcal/mol. The root mean square deviation (RMSD) values exhibited variation up to 4.2 Å. For instance, the interaction with CED9 demonstrates that the peptides can interfere with the apoptosis pathway (KEGG map04215) in *C. elegans*. CED9 acts on a cell surface receptor EGL-1, which activates the programmed cell death in *C. elegans* (Figs 5.1A and 5.1D). Secondly, the peptides' ability to interact with MAP kinases revealed their diverse biological significance, especially for regulating the SKN-1 pathway. Various MAP kinases in *C. elegans* share a similar protein 3D structure. This study uses a type of MAP kinase PMK-2, which responds to environmental stress and pro-inflammatory cytokines and phosphorylates downstream protein targets. In our homology model, the PMK-2 model was relatively accurate compared to the homology model of similar proteins (Figs. 5.1B and 5.1F). MAPK has specific importance in the SKN-1 pathway (KEGG map04212) because it plays an essential role in phosphorylating SEK-1, which is a dual specificity mitogen-activated protein kinase and is a crucial component of the SKN-1 pathway and prevents oxidative stress in *C. elegans*.

Moreover, the custom peptide showed efficient binding with one of the tyrosine-protein kinase receptors CAM-1. Entries in the Reactome pathway browser database [1] suggest that CAM-1 is an essential component in the MAPK signaling pathway by playing multiple roles. Custom peptides TNP and HNP can form a complex with immunoglobulin (IG) (Figs. 5.1C and 5.1G) and frizzled domain (FZ) (Figs 5.1D and 5.1H) of CAM-1 exhibiting reasonable stability. Notably, BLAST sequence search

revealed that CAM-1 shares considerable homology (38.5%) with human NTRKA receptors and functions similarly.

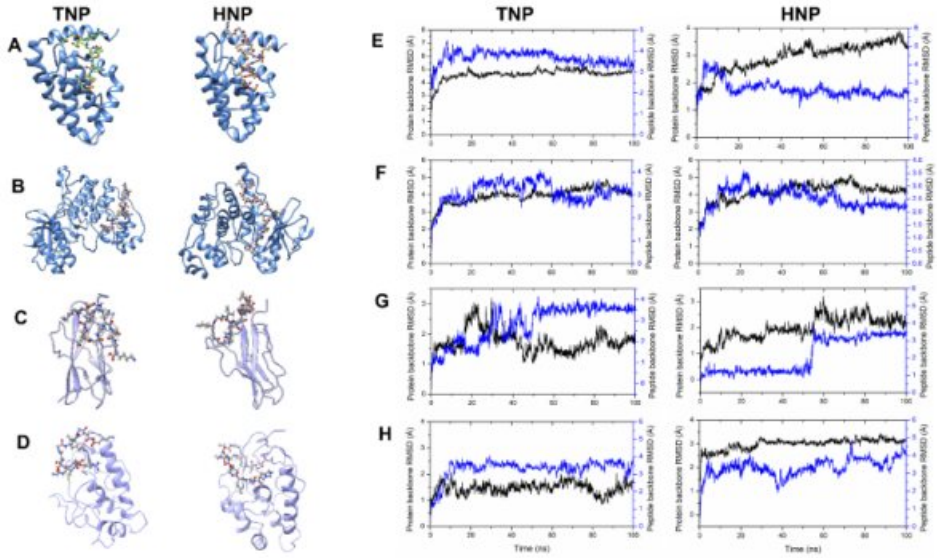

Fig. 5.1 Custom peptide interaction of TNP (left) and HNP (right) complex with (A) CED9, (B) PMK2, (C) CAM1-IG domain, and (D) CAM1-FZ domain shown in cartoon representation. Root mean square deviation (RMSD) plot of TNP (left) and HNP (right) complex with (E) CED9, (F) PMK2, (G) CAM1-IG domain, and (H) CAM1-FZ domain.

5.1.2 The confocal microscopic study shows *in vivo* binding of FITC–conjugated custom peptides to the nerve ring region of *C. elegans* N2 strain; however, an insignificant binding was observed with CAM-1 mutant strain of *C. elegans*

The confocal microscopic images of the dose-dependent (12.5 μg/mL to 100 μg/mL) and time-dependent (1h - 6 h) binding of the fluorescein isothiocyanate (FITC)-custom peptides (TNP and HNP) to *C. elegans* (L4 of N2 strain) are shown in Figs 5.2A-B and Figs 5.2C-D respectively. The FITC-custom peptides (TNP and HNP, 50 μg/mL) showed binding at 2 h of incubation at the nerve ring part and hypodermal syncytia covering the lips and head portion of the *C. elegans* (Figs 5.2C-D).

Pre-treatment of *C. elegans* with FITC-conjugated TNP and HNP showed optimum fluorescence intensity at the nerve ring region; nevertheless, only FITC-

treatment (control) did not show fluorescence signal at the nerve ring region of *C. elegans*, indicating binding of peptides to the nerve ring region of *C. elegans* (Figs 5.2E-F). However, the post-addition of peptides after PT treatment showed a significant decrease in fluorescence intensity at the nerve ring region compared to custom peptides pre-treated worms before adding PT (Figs 5.2E-F). Further, when a fixed concentration of peptides was co-treated with increasing concentrations of PT, a PT concentration-dependent reduction in the fluorescence intensity at nerve ring regions was observed, suggesting the competitive binding between PT and custom peptides to the nerve ring region of the *C.elegans* (Figs 5.2E-F).

Further, the binding efficiency of FITC-custom peptides (TNP and HNP) at their optimum dose (50 μg/mL) and time (2 h) in the N2 strain and CAM-1 mutant strain of *C. elegans* were compared in (Figs 5.3A-B). However, negligible binding was observed at the nerve ring region in the CAM-1 mutant strain of *C. elegnas*, compared to the binding of FITC-custom peptides in the N2 strain of *C. elegans* which is evident by a significant ($p \leq 0.05$) decrease in the fluorescence intensity (19-27 %) of FITC-custom peptides was observed in the CAM-1 mutant strain when compared to the N2 strain of *C. elegans* (Fig 5.3B).

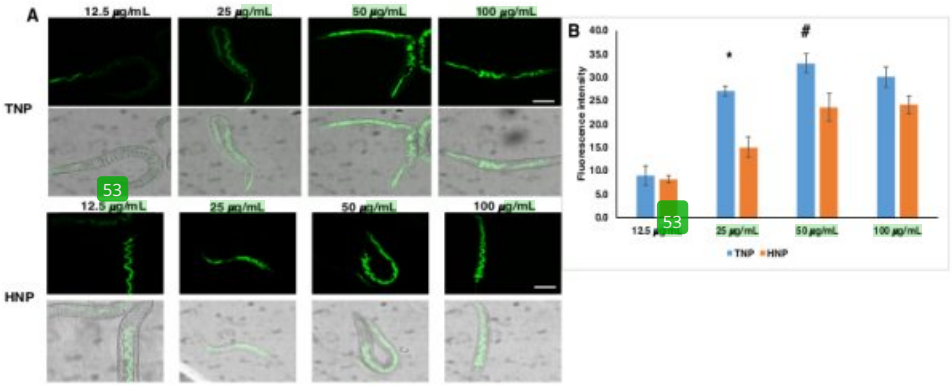

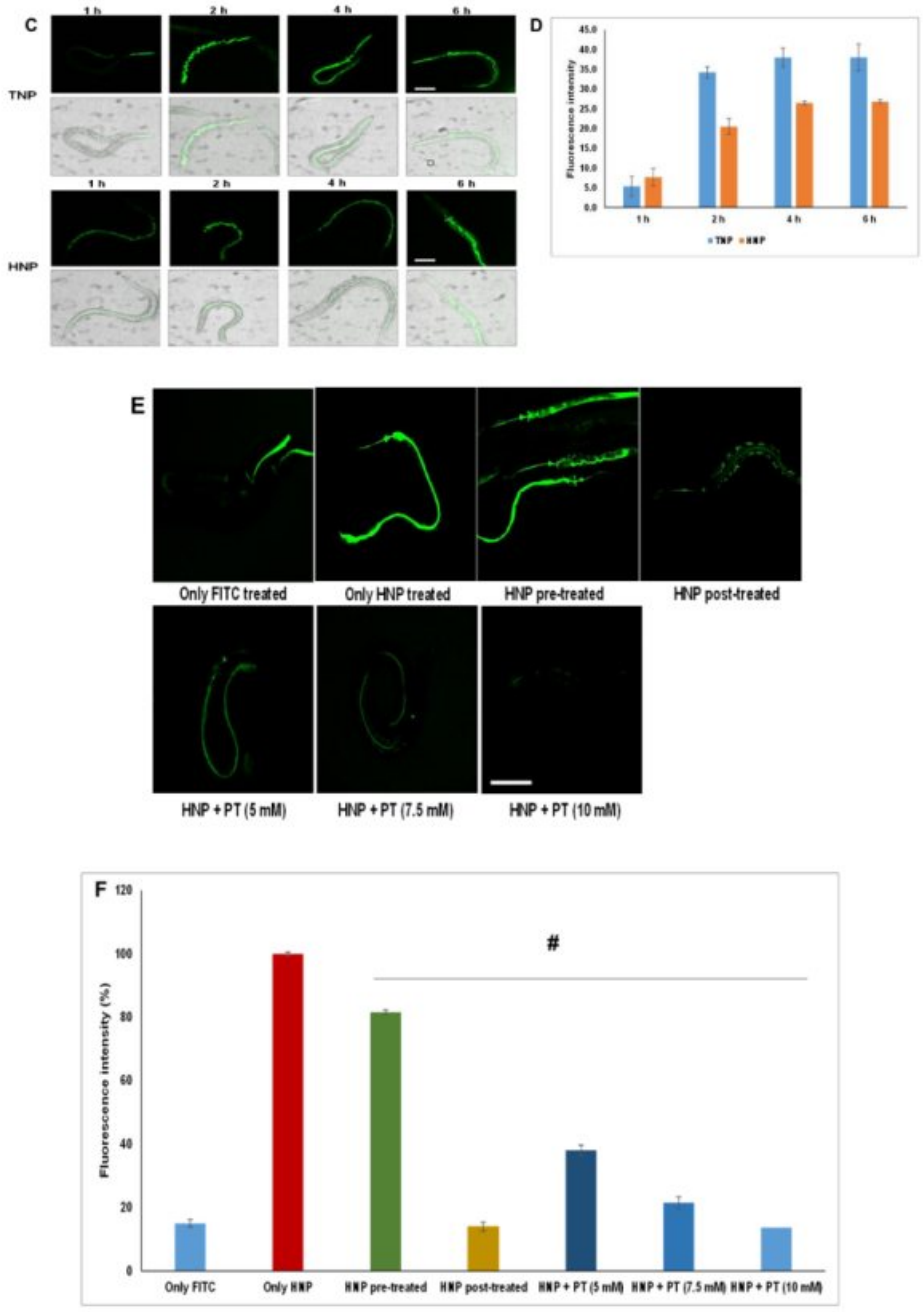

Fig. 5.2 Confocal microscopic (40 X) studies of the *in vivo* binding of FITC-custom peptides to *C. elegans* for 2h. (A) Dose-dependent (12.5 μg/mL – 100 μg/mL) binding of custom peptides to the *C. elegans*. The scale bar indicates the length as 100 μm. (B) Bar

graph representing fluorescence intensity between the treatment groups; *p < 0.05, a significant difference between 12.5 μg/mL and 25 μg/mL dose of FITC-conjugated peptides to *C. elegans*, #p < 0.05, a substantial difference between 25 μg/mL and 50 μg/mL dose of FITC-conjugated peptides to *C. elegans*. (C) Time-dependent (1 h – 4 h) binding of custom peptides (50 μg/mL) to the C. elegans. (D) Bar graph representing fluorescence intensity between the treatment groups (E) Microscopic image of the custom peptide binding to *C. elegans* in pre-treatment, post-treatment, and co-treatment conditions (with various concentrations of PT). The scale bar indicates the length as 100 μm. (F) Bar graph representing fluorescence intensity between the treatment groups; Significant difference between the pre-treatment, post-treatment, and co-treatment with FITC-custom peptide HNP compared to binding of only FITC-conjugated HNP to *C.elegans*, #p < 0.05.

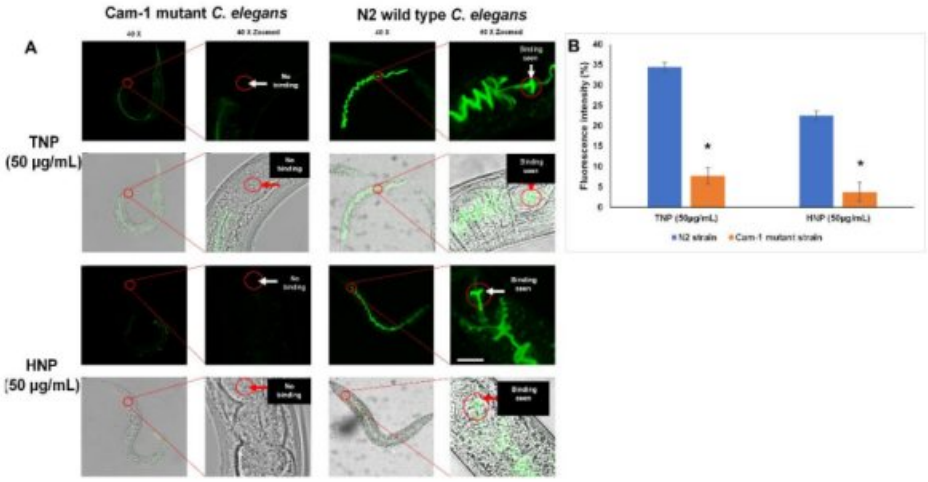

Fig. 5.3 (A) Confocal microscopic (40 X) studies of the *in vivo* binding of FITC-custom peptides (50 μg/mL, 2 h) to CAM-1 mutant and compared with wild-type N2 strain *C. elegans*. The scale bar indicates the length as 100 μm. (B) Bar graph representing fluorescence intensity between the CAM-1 mutant and N2 strains. *p < 0.05, a significant difference between CAM-1 mutant and N2 strain of *C. elegans*. Values are mean ± SD of triplicate determinations.

5.1.3 Pre-treatment with custom peptides reduced PT-induced worms' death and restored their chemotaxis dysfunction

Custom peptides pre-treatment demonstrated a concentration-dependent increase in the survivability of the N2 strain of *C. elegans* against PT (LC_{50} value)-induced death, and the optimum concentration was determined for both the peptides at 50 μg/mL (~38 μM) (Fig 5.4A). HNP showed a significant ($p \leq 0.05$) increase in survivability compared to TNP. The antioxidant vitamin C (positive control; 100 μg/mL) pre-treated group showed minimal protective effect from death (Fig 5.4A).

Custom peptide pre-treatment for two hours showed a significant ($p \leq 0.05$) increase (35-40%) in the survivability of the N2 strain of untreated (control) *C. elegans* compared to PT-treated *C. elegans*; however, 12 h pre-treatment compared to 2 h pre-treatment was found to be less effective in protecting the *C. elegans* against PT-induced toxicity and death. Nevertheless, 12 h pre-treatment with custom peptides followed by re-supplementation of custom peptides again for 12 h (total pre-incubation time 24 h) restored the survivability of *C. elegans* against PT, and this result was found to be similar as shown by pre-incubation with custom peptides for 2 h before addition of PT (Fig 5.4B). Pre-treatment with 50 µg/mL quercetin, a known neuroprotection compound, demonstrated much lower protection than custom peptides under similar experimental conditions (Fig 5.4B). Post-treatment with custom peptides, vitamin C (antioxidant), mouse 2.5 S NGF, and quercetin (after PT addition) did not reverse the PT-induced toxicity in *C. elegans* (Fig 5.4C). Also, a significant ($p \leq 0.05$) decrease in the neutralization (23-27%) against paraquat-induced toxicity by custom peptides pre-treatment in CAM-1 mutant strain was observed when compared to the N2 strain of *C. elegans* (Fig 5.4D).

No significant difference ($p \geq 0.05$) in the chemotaxis index (CI) between the peptide-treated and untreated (control) *C. elegans* was observed (Fig 5.4E). However, sensory neuron dysfunction was observed in PT-treated wild-type *C. elegans* (Fig 5.4E). Notably, a significant restoration ($p \leq 0.05$) of PT-induced sensory dysfunction was observed in pre- (CI = 0.43 $\pm$ 0.028 for TNP, and CI = 0.48 $\pm$ 0.024 for HNP) and post-peptide-treated worms (CI = 0.20 $\pm$ 0.014 for TNP, and CI = 0.24 $\pm$ 0.012 for TNP) compared to the worms treated with PT (Fig 5.4E). Further, pre- or post-treatment with

vitamin C (antioxidant) is ineffective in improving PT-induced sensory neuron dysfunction (Fig 5.4E). Peptides TNP and HNP demonstrated similar potency ($p \geq 0.5$) in the restoration of PT-induced sensory neuron dysfunction in *C. elegans* (Fig 5.4E).

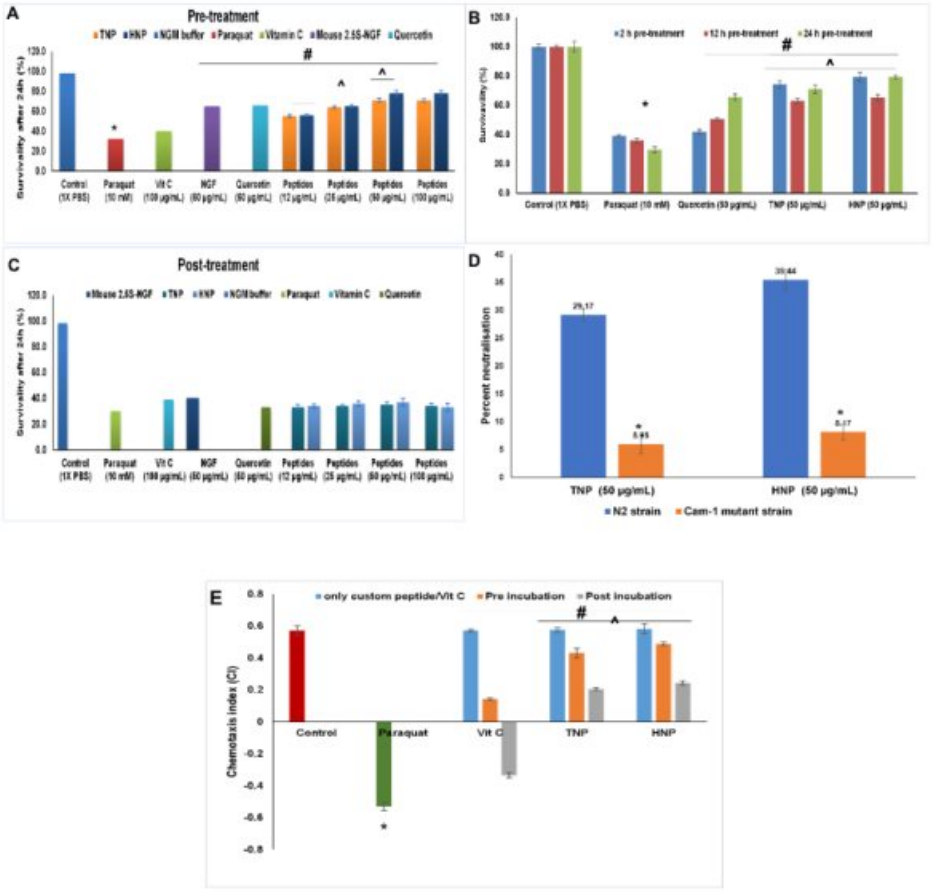

Fig. 5.4 Determination of the effect of the custom peptide on PT-induced death of *C.elegans*. (A) worms were pre-incubated with mouse 2.5S-NGF (50 μg/mL)/quercetin (50 μg/mL, positive control) / vitamin C (100 μg/mL, positive control) and progressive concentration of custom peptides (12 μg/mL - 100 μg/mL) followed by the PT (10 mM) treatment. $^{*}p \leq 0.05$, a significant difference between untreated (control) and PT-treated cells; $^{\#}p \leq 0.05$, a significant difference between PT-treated cells and quercetin/ mouse 2.5S-NGF/ vitamin C and custom peptide pre-treated *C. elegans*. $^{\wedge}p \leq 0.05$ Significance of difference in different concentrations for custom peptides. (B) worms were pre-

incubated with quercetin (50 μg/mL, positive control) and custom peptides (50 μg/mL) for 2 h, 12 h, and 24 h followed by the PT (10 mM) treatment. $^{*}p \leq 0.05$, a significant difference between untreated (control) and PT-treated cells; $^{\#}p \leq 0.05$, a significant difference between PT-treated cells and quercetin (positive control) and custom peptide pre-treated *C. elegans*. $^{\wedge}p \leq 0.05$, a significant difference between quercetin pre-treated *C. elegans* and the peptide (TNP and HNP) pre-treated *C. elegans*. (C) Worms were incubated with PT (10 mM) for 1 h and treated with custom peptides (12 μg/mL to 100 μg/mL). Freshly prepared custom peptides were added after 12 h of pre-incubation for 24 h pre-incubation condition. Worms were counted under a stereo zoom microscope for 30 s up to 24 h of treatments. Values are mean ± SD of triplicate determinations. (D) Determination of the effect of the custom peptides on PT-induced death of cam-1 mutant compared with wild type N2 strain of *C. elegans*. Worms were pre-incubated with custom peptides (50 μg/mL) followed by the PT (10 mM) treatment. Percent neutralization was calculated against only paraquat-treated worms. $^{*}p < 0.05$, a significant difference between wild-type and cam-1 mutant strain. (E) Restoration of chemosensory behavior in *C. elegans* pre-treated with custom peptides. Synchronized L4 stage *C. elegans* wide-type strain N2 was incubated with or without 50 μg/mL custom peptides. They were then subjected to PT-treatment (10 mM) and a chemosensory assay. $^{*}p \leq 0.05$, a significant difference between untreated (control) and PT-treated cells; $^{\#}p \leq 0.05$, a significant difference between PT-treated cells and quercetin (positive control) and custom peptide pre-treated *C. elegans*. $^{\wedge}p \leq 0.05$, a significant difference between quercetin pre-treated *C. elegans* and the peptide (TNP and HNP) pre-treated *C. elegans*. Values are means ± SD of triplicate determinations.

5.1.4 Custom peptides inhibit PT-induced reactive oxygen species (ROS) production and depolarization of mitochondrial membrane potential in *C. elegans* N2 strain but could not protect CAM-1 mutant strain

The spectrofluorometric determination of fluorescence intensity of DCF (2,7-dichlorofluorescein) confirmed a significant ($p \leq 0.05$) increase in the ROS level in PT (10 mM)-treated wild-type worms by 44% compared to control (untreated) worms. A significant reduction ($p \leq 0.05$) in ROS level was observed in wild-type worms pre-treated with HNP and TNP (68-70%) and vitamin C (35%), mouse 2.5S-NGF (33%) as compared to the PT-treated wild type worms (Fig 5.5A). The custom peptide HNP at a concentration

of 50 μg/mL (~38 μM) showed superior reduction (32-35%) ($p \leq 0.05$) in the ROS generation, compared to TNP and vitamin C (positive control) (Fig 5.5A).

The confocal microscopic analysis also determined the custom-peptides mediated reduction in intracellular ROS generation in wild-type N2 strain *C. elegans* (Figs 5.5B-C). The data showed a significant increase ($p \leq 0.05$) in intracellular ROS levels in PT-treated worms compared to control wild-type worms. Further, pre-treatment of worms with custom peptides (TNP and HNP, 50 μg/mL) and vitamin C (positive control, 100 μg/mL) /mouse 2.5S-NGF (50 μg/mL) significantly diminished the ROS production (Fig 5.5C); however, to a different extent. Custom peptide HNP, compared to TNP, showed superior activity in inhibiting PT-induced ROS production in wild-type worms (Fig 5.5C). No significant ($p \geq 0.05$) decrease in ROS production was observed in the custom peptides pre-treatment group compared to the PT-treated group in the CAM-1 mutant strain of *C. elegans* (Figs 5.5D-E).

The JC-1 staining procedure was used to study whether custom peptides can restore the loss of mitochondrial membrane potential (MMP) triggered by PT in *C. elegans* N2 and CAM-1 mutant strains. The effect of custom peptides on MMP using JC-1 dye (cyanin dye) (Fig 5.5D) was demonstrated. The red/green fluorescence ratio was quantified from the confocal images to monitor the MMP (Fig 5.5F). The fluorescence intensity of the red/green ratio was significantly reduced ($p \leq 0.05$) by 80% in 10 mM PT-treated worms compared to control (1X PBS-treated) worms (Fig 5.5F). However, the fluorescence intensity of the red/green ratio was significantly ($p \leq 0.05$) restored by 60 to 70% when worms were pre-treated with custom peptide (TNP / HNP) as compared to PT-treated worms (Figs 5.5F-G), indicating a reduction of PT-induced depolarization of MMP by custom peptides in *C. elegans*. HNP showed a significant ($p \leq 0.05$) 20% increase in the restoration of PT-induced mitochondrial depolarization as compared to TNP (Figs 5.5F-G). In contrast, vitamin C pre-treatment showed no significant difference in the restoration of PT-induced mitochondrial depolarisation (Figs 5.5F-G). Moreover, custom peptide pre-treatment did not show any considerable restoration of alteration of MMP in the CAM-1 mutant strain of *C. elegans* (Figs 5.5H-I).

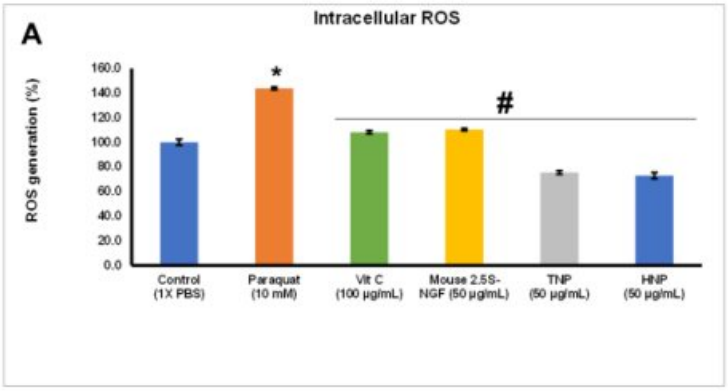
A
Intracellular ROS
ROS generation (%)
160.0
140.0
120.0
100.0
80.0
60.0
40.0
20.0
0.0
*
#
Control (1X PBS)
Paraquat (10 mM)
Vit C (100 µg/mL)
Mouse 2.5S-NGF (50 µg/mL)
TNP (50 µg/mL)
HNP (50 µg/mL)

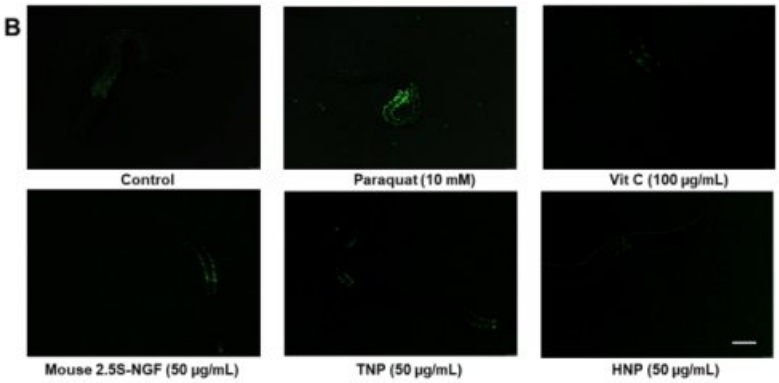
B
Control
Paraquat (10 mM)
Vit C (100 µg/mL)
Mouse 2.5S-NGF (50 µg/mL)
TNP (50 µg/mL)
HNP (50 µg/mL)

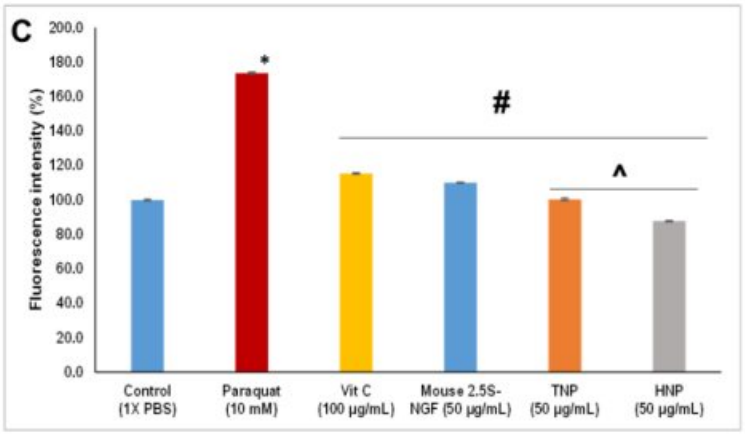
C
Fluorescence intensity (%)
200.0
180.0
160.0
140.0
120.0
100.0
80.0
60.0
40.0
20.0
0.0
*
#
^
Control (1X PBS)
Paraquat (10 mM)
Vit C (100 µg/mL)
Mouse 2.5S-NGF (50 µg/mL)
TNP (50 µg/mL)
HNP (50 µg/mL)

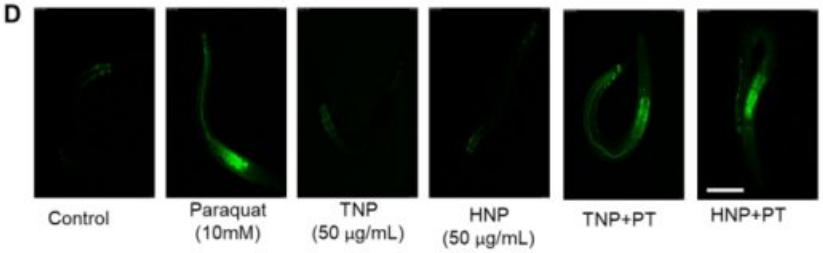
D
Control
Paraquat (10mM)
TNP (50 µg/mL)
HNP (50 µg/mL)
TNP+PT
HNP+PT

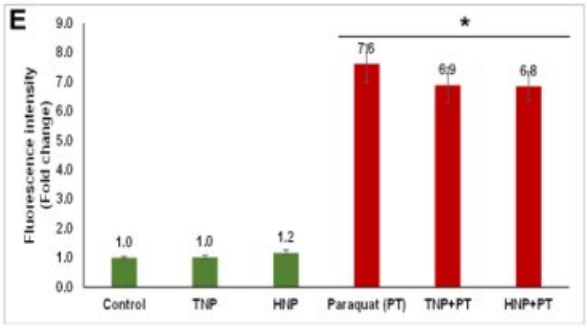
E
Fluorescence intensity (Fold change)
9.0
8.0
7.0
6.0
5.0
4.0
3.0
2.0
1.0
0.0
1.0
1.0
1.2
7.6
6.9
6.8
*
Control
TNP
HNP
Paraquat (PT)
TNP+PT
HNP+PT

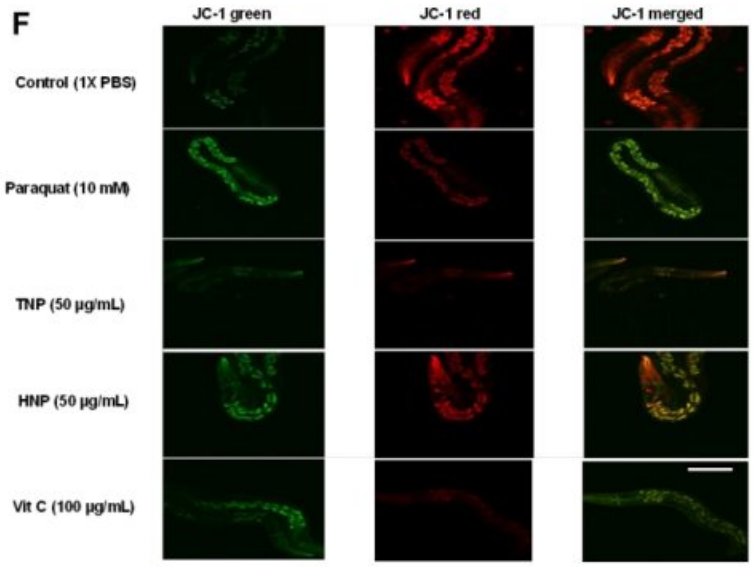
F
JC-1 green
JC-1 red
JC-1 merged
Control (1X PBS)
Paraquat (10 mM)
TNP (50 µg/mL)
HNP (50 µg/mL)
Vit C (100 µg/mL)

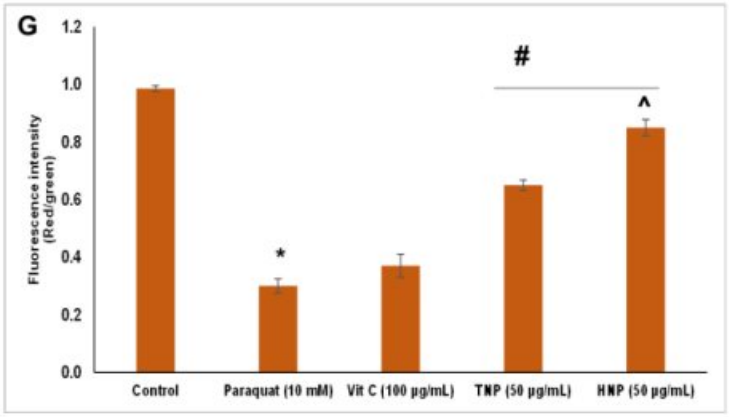

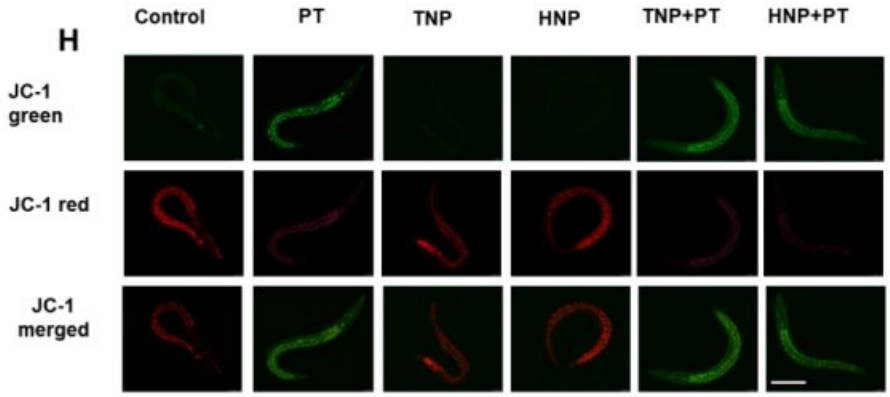

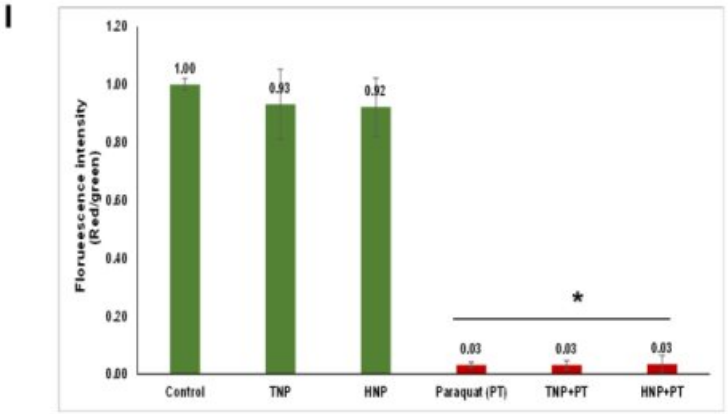

Fig. 5.5 Determination of PT-induced intracellular ROS generation and its reversal by pre-treatment with custom peptide in wild type N2 strains of *C. elegans*. The ROS generation was determined by using an H_2DCFDA fluorescence probe. (A)

spectrofluorometric determination of intracellular ROS. $^{*}p < 0.05$, the significant difference between untreated (control) and PT-treated worms; $^{\#}p < 0.05$, the significant difference between PT-treated and custom peptide-treated worms. (B) confocal microscope images of nematodes expressing ROS. The scale bar indicates the length as 100 μm. (C) Bar graph representing dosimetry analysis of confocal images to quantitate the intracellular ROS generation. Error bars indicating SD (n=3). $^{*}p < 0.05$, the significant difference between untreated (control) and PT-treated worms; $^{\#}p < 0.05$, the significant difference between PT-treated and custom peptide-treated worms. $^{\wedge}p \leq 0.05$, a significant difference between Vit C/ mouse 2.5 S-NGF pre-treated *C. elegans* and the peptides (TNP and HNP) pre-treated *C. elegans*. Values are means ± SD of triplicate determinations. (D) confocal microscope images of nematodes expressing ROS. The scale bar indicates the length as 100 μm. (E) Bar graph representing dosimetry analysis of confocal images to quantify intracellular ROS generation.

(F) Confocal images of *C. elegans* showing reversal of PT-induced disruption of mitochondrial membrane potential (MMP) of *C. elegans* pre-treated with custom peptides. The scale bar indicates the length as 100 μm. The scale bar indicates the size as 100 μm. The PT-treated (10 mM) N2 wild-type strain of nematodes pre-treated with or without custom peptide (50 μg/mL) was observed to measure the red/green fluorescence intensity ratio by JC-1 staining. (G) Bar diagram representing the red/green fluorescence intensity ratio quantified using Image J software. $^{*}p \leq 0.05$, a significant difference between untreated (control) and PT-treated worms; $^{\#}p \leq 0.05$, a significant difference between PT-treated and custom peptide pre-treated worms. $^{\wedge}p \leq 0.05$, a significant difference between the two peptides (TNP and HNP) pre-treated *C. elegans*. Values are means ± SD of triplicate determinations. (H) Confocal images of CAM-1 mutant strain of *C. elegans* showing reversal of PT-induced disruption of mitochondrial membrane potential (MMP) of *C. elegans* pre-treated with custom peptides. The scale bar indicates the length as 100 μm. The scale bar indicates the size as 100 μm. The PT-treated (10 mM) N2 wild-type strain of nematodes pre-treated with or without custom peptide (50 μg/mL) was observed to measure the red/green fluorescence intensity ratio by JC-1 staining. (I) Bar diagram representing the red/green fluorescence intensity ratio quantified using Image J software. $^{*}p \leq 0.05$, a significant difference between untreated (control)/only

custom peptide treated group and PT/custom peptide and PT-treated group of cam-1 mutant worms

5.1.5 Custom peptides restored PT-induced dopaminergic (DAergic) neurodegeneration and reduced α-synuclein accumulation in *C. elegans*

C. elegans BZ555 strain expresses a green fluorescent protein in all six intact DAergic neurons comprising two distal cephalic (CEPD), two ventral cephalic (CEPV), and two anterior deirid (ADE) (Fig 5.6A). Studies have shown that specific DAergic neuron degeneration is attained with 10 mM PT exposure [2-4], which showed impairment of CEPs and ADEs cell bodies (Fig 5.6B). The analysis showed a significant decrease ($p \leq 0.05$) in the fluorescence intensity with PT treatment by 54-58% for CEPs and 70-75% for ADEs neurons compared with the PBS-treated (control) worms (Fig 5.6B). The TNP and HNP peptides pre-treated groups showed a significant ($p \leq 0.05$) increase in fluorescence intensity for CEPs neurons and ADEs neurons (Figs 5.6A-B). This data suggests a considerable impairment of PT-induced neuronal degeneration and significantly higher activity of HNP as compared to TNP (Figs 5.6A-B). However, the vitamin C pre-treated group does not show a significant ($p > 0.05$) increase in fluorescence intensity for CEPs and ADEs neurons compared with the PT-treated worms (Figs 5.6A-B). Similarly, peptides TNP and HNP in post-treated worm groups showed a significant ($p \leq 0.05$) increase in GFP intensity by 57.5-59.3% and 60.3-63.7%, respectively, for CEPs neurons and 38.5% and 65%, for ADES neurons (Figs 5.6A-B).

The fluorescence intensity at the anterior part of the NL5901 strain of *C. elegans* showed aggregation of human α-synuclein (YFP tagged) in the body wall muscles (Fig 5.6C). The image analysis showed a significant decrease ($p \leq 0.05$) in the fluorescence intensity in the custom peptides-treated *C. elegans* as compared with the PBS-treated (control) *C. elegans* (Fig 5.6D). The TNP and HNP treatment showed a significant ($p \leq 0.05$) decrease in the fluorescence intensity by 37% and 60%, respectively, compared to the fluorescence intensity of the control (untreated) group of worms (Figs 5.6C-D). HNP treatment, compared to the TNP treatment, showed a significant ($p \leq 0.05$) 20% decrease in the α-synuclein accumulation in *C. elegans* (Figs 5.6C-D). However, vitamin C pre-treatment did not show a significant ($p > 0.05$) reduction in the α-synuclein accumulation, as compared to the PBS-treated (control) group of *C. elegans* (Figs 5.6C-D).

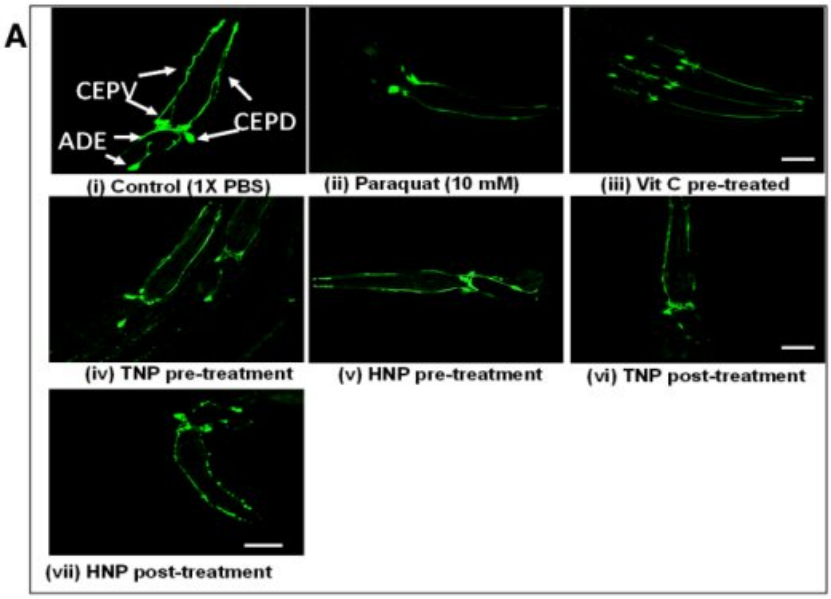
A
CEPV
CEPD
ADE
(i) Control (1X PBS)
(ii) Paraquat (10 mM)
(iii) Vit C pre-treated
(iv) TNP pre-treatment
(v) HNP pre-treatment
(vi) TNP post-treatment
(vii) HNP post-treatment

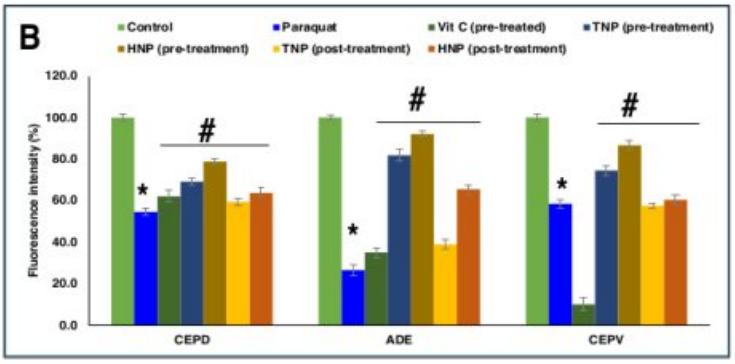
B
Control
Paraquat
Vit C (pre-treated)
TNP (pre-treatment)
HNP (pre-treatment)
TNP (post-treatment)
HNP (post-treatment)
Fluorescence Intensity (%)
120.0
100.0
80.0
60.0
40.0
20.0
0.0
CEPD
ADE
CEPV

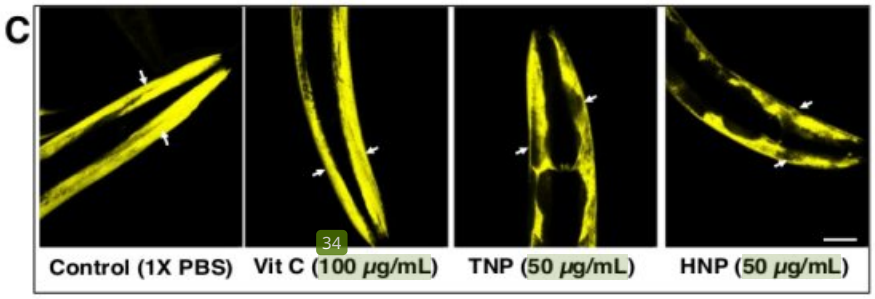
C
Control (1X PBS)
Vit C (100 µg/mL)
TNP (50 µg/mL)
HNP (50 µg/mL)

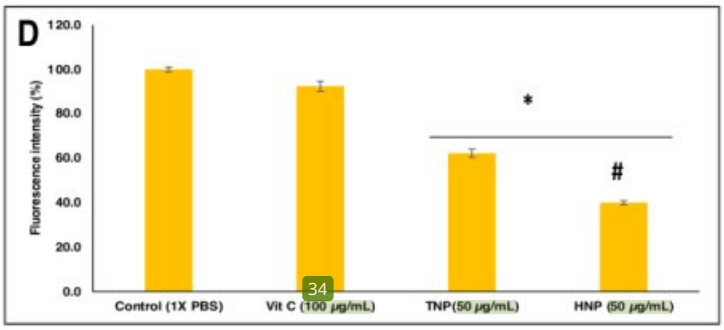

Fig. 5.6 Determination of dopaminergic neurodegeneration induced by PT in BZ555 *C. elegans*. (A) Confocal microscopic images (40 X) of DA neurons emerging GFP fluorescence signals in PT-treated BZ555 worms with or without pre-treated with custom peptides (50 μg/mL). The scale bar indicates the length as 100 μm. (B) The bar diagram shows the GFP fluorescence intensity indicating the content of DA neurons in BZ555 worms, quantified using the Image J software. $^{*}p \leq 0.05$, a significant difference between untreated (control) and PT-treated worms; $^{\#}p \leq 0.05$, a significant difference between PT-treated and custom peptide-treated worms. Custom peptides inhibit the aggregation of α-synuclein in transgenic NL5901 strains of *C. elegans*. (C) Confocal images of custom peptides (50 µg/mL)-treated NL5901 worms after 12 h of incubation. The scale bar indicates the length as 100 μm. (D) The bar chart shows the fluorescence intensity representing the α-synuclein protein accumulation in custom peptide-treated NL5901 worms for 12 h. * ($p \leq 0.05$) a significant difference between control (CT) and custom peptides-treated *C. elegans*, $^{\#}$ ($p \leq 0.05$) a significant difference between TNP and HNP treated *C. elegans*. Values are means ± SD of triplicate determinations.

5.1.6 The custom peptides pre-treatment restores the PT-induced upregulated antioxidant/heat shock response/ p38 mitogen-activated protein kinase (MAPK) genes and delayed PT-induced programmed cell death in *C. elegans*

The quantitative reverse transcription-polymerase chain reaction (qRT-PCR) analysis data demonstrated a significant increase ($p \leq 0.05$) in the expression of antioxidant genes (*sod-1*, *sod-3*, *cat-1*, *cat-3*, *trx-1*, *gst-4*, and *gst-6)*, heat shock gene *hsp-16.1*, and MAPK signaling pathways genes (*skn-1*, *sek-1*, and *pmk-1)* in PT-treated N2 worms compared to untreated worms (control). However, pre-treatment of worms with vitamin C (positive control) / custom peptides (HNP and TNP) resulted in a significant downregulation ($p \leq$

0.05) or restoration of the expression of those genes upregulated by PT treatment (Fig 5.7). Further, the qRT-PCR analysis also showed significant ($p \leq 0.05$) upregulation of pro-apoptotic genes (*ced-3* and *ced-4*) and significant downregulation ($p \leq 0.05$) of antiapoptotic genes (*ced-9*) in PT-treated *C. elegans* compared to untreated (control) *C. elegans*. Further, the pre-treatment of custom peptides (TNP and HNP) restores the upregulated (*ced-3* and *ced-4*) and downregulated (*ced-9*) pro-apoptotic and antiapoptotic genes, respectively, in PT-treated *C. elegans* (Fig 5.7). However, vitamin C (positive control) pre-treatment did not show significant down-regulation ($p \leq 0.05$) of MAPK signaling pathway genes (*skn-1*, *sek-1*, and *pmk-1*) and pro-apoptotic genes (*ced-3* and *ced-4*) compared to PT-treated worms (Fig 5.7). Further, the qRT-PCR analysis showed better activity of HNP compared with TNP. Therefore, HNP was selected for the transcriptomic and proteomics analyses to decipher the gene regulatory pathways for preventing PT-induced neuronal degradation.

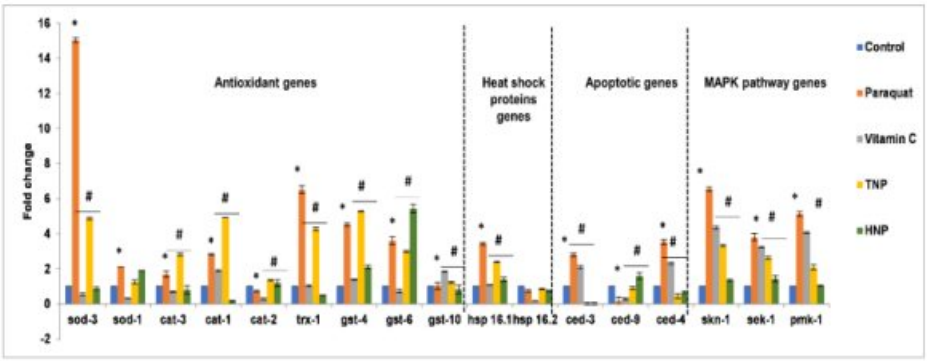

Fig. 5.7 The qRT-PCR analysis shows the genes' expression in stress resistance, innate immunity, and apoptotic pathways in the PT-treated *C. elegans*, compared with the vitamin C (positive control)/custom peptide pre-treated *C. elegans*. The expression of mRNA was normalized using the housekeeping gene act-1. * ($p \leq 0.05$) a significant difference between control (CT) and PT-treated *C. elegans*, # ($p \leq 0.05$) a significant difference between PT-treated and vitamin C/ custom peptide pre-treated worms. Values are means ± SD of triplicate determinations.

5.1.7 Transcriptomic analysis shows the differential expression of mRNA between PT-treated *C. elegans* and pre-treatment of *C. elegans* with custom peptides followed by PT-treatment

The cDNA libraries were prepared for the mRNA, isolated from each group of *C. elegans* (N2) treated with (a) 1X PBS (control) treated worms (CT group), (b) 10 mM PT treatment for 1 h (PT group), (c) pre-treatment with 50 μg/mL (~38 μM) custom peptide HNP for 2 h followed by 10 mM PT treatment for 1 h (PHNP group), and (d) treatment with 50 μg/mL of custom peptide HNP for 2 h (HNP group). The mRNAs were sequenced with the Illumina 150 bp PE platform. The average total number of reads aligned was found to be 16.7 million (CT), 15.3 million (HNP), 12.8 million (PHNP), and 20.2 million (PT) for the three corresponding cDNA libraries.

The transcriptomic analysis showed differential expression of 15,102 genes in *C. elegans* compared to the PT and CT group of worms and 701 genes when compared between the PT and PHNP group, in which 441 and 260 genes were found to be upregulated and downregulated, respectively.

The transcriptomic data's principal component analysis (PCA) revealed variance in the gene expression level between all four treatment groups (Fig 5.8A). The correlation plot (Fig 5.8B) shows clustering among different treated groups. Red indicates the positive, and blue indicates the negative correlation plot between the four treatment groups (Fig 5.8B). The volcano (p-values vs. fold change) and scatter plots display the (i) differential gene expression between PT and CT groups (Figs 5.8C-D) and (ii) differentially altered genes between PHNP and PT groups (Figs 5.8E-F). The Volcano plot and scatter plot analyses revealed significant downregulation (Fc < -1) of most of the genes in *C. elegans* in the PT group compared to the CT group. The pre-treatment of peptide (HNP) resulted in the upregulation of those 'genes' expression downregulated in the PT group of worms (Figs 5.8C-F). The heat map analysis displayed a disparity in gene expression between the PT and PHNP groups compared to the CT group (Fig 5.8G).

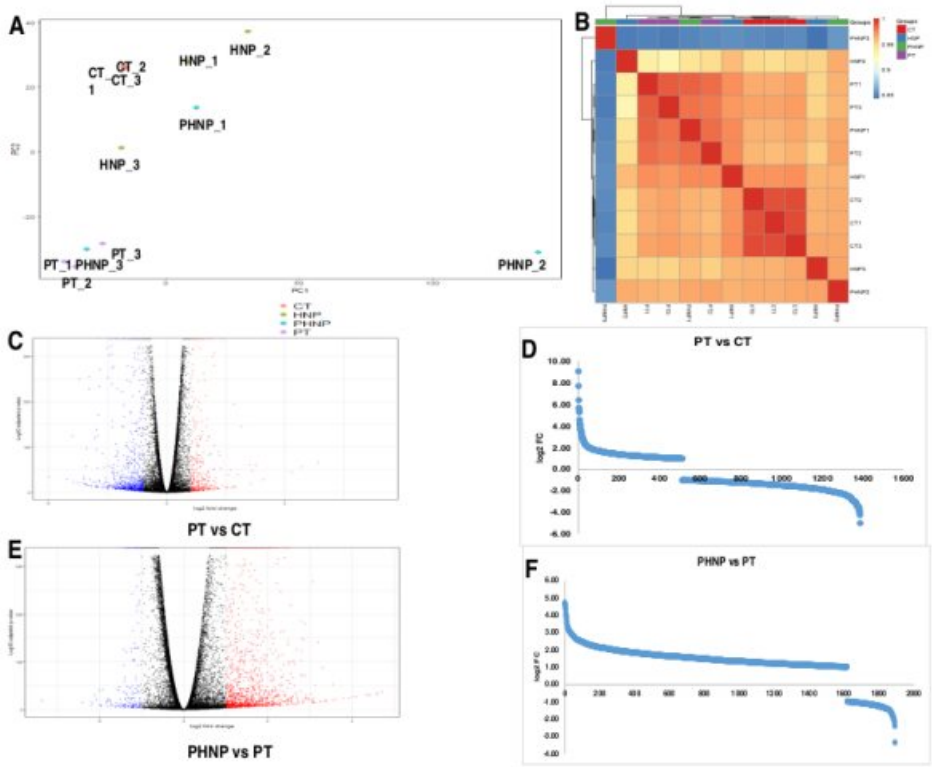
A
CT_1
CT_2
CT_3
HNP_1
HNP_2
PHNP_1
HNP_3
PT_1
PHNP_3
PT_3
PT_2
PHNP_2
CT
HNP
PHNP
PT
B
C
PT vs CT
D
PT vs CT
E
PHNP vs PT
F
PHNP vs PT

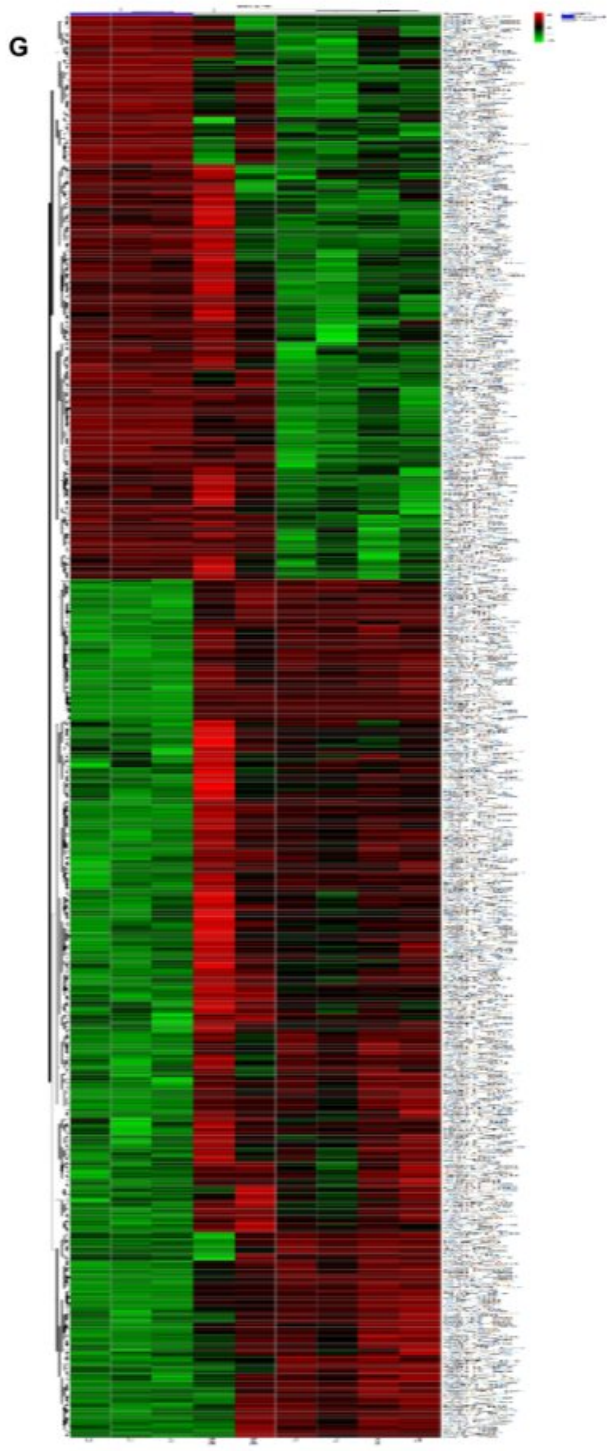
G

Fig. 5.8 Differential expression of genes between different treated groups of *C. elegans*. (A) PCA score plot showing the gene expression variability between the groups of *C. elegans* and within the biological replicates. (B) Correlation plot showing a correlation between treated groups of *C. elegans*. CT: untreated worms, PT: PT treated worms, PHNP: custom peptide HNP pre-treatment followed by PT treatment, HNP: custom peptide HNP treated worms. Plots showing differential expression of genes in PT-treated *C. elegans* and their restoration with peptide (HNP) pre-treatment. (C) Volcano plot (p-value v/s log Fc) for PT group versus CT group. (D) scatter plot displaying the statistically significant differentially altered genes between PT treatment and control group (PT vs. CT). (E) Volcano plot (p-value v/s log Fc) for PHNP group versus PT group (F) scatter plot displaying the statistically significant differentially altered genes between peptide HNP pre-treated *C. elegans* followed by PT treatment and PT-treated *C. elegans*. CT: untreated worms, PT: PT treated worms, PHNP: custom peptide HNP pre-treatment followed by PT treatment, HNP: custom peptide HNP treated worms. (G) Heat map showing the differential expression of the upregulated and downregulated genes among different groups of *C. elegans*. PT: PT treated, PHNP: peptide HNP pre-treatment followed by PT treatment, CT: untreated (control) worms.

5.1.8 Quantitative proteomic analysis demonstrated differential expression of cellular proteins between PT-treated and HNP peptide pre-treated followed by PT-treated *C. elegans*

A total number of 1026 non-redundant proteins were identified by the LC-MS/MS analysis from the different treatment groups of *C. elegans* (N2 strain). The identified proteins were classified into 20 discrete categories based on their cellular location and biological activity (Fig 5.9A, Appendix Table A1), of which 13 major cellular proteins were found with high relative abundance.

In the PT group, 991 proteins were identified, among which differential expression was observed in 689 proteins compared to the control, and the expression of 406 proteins was restored in the PHNP group (Fig 5.9A). Between the PHNP and PT groups, 49 proteins were uniquely expressed (Fig 5.9A).

The scatter plot shows the differential expression of proteins in the PT group of *C. elegans* compared to the CT group of worms (Fig 5.9B). Further, the intracellular

proteins of the PHNP group were compared with the PT and CT groups to identify the differentially expressed proteins involved in apoptosis, electron transport chain, stress response, antioxidant, and ubiquitin-proteasome pathways, which were restored in the PHNP group of worms (Appendix Table A1). The intracellular protein of HNP-treated *C. elegans* was compared with the CT group, of which 297 proteins were uniquely expressed (Fig 5.9C). Proteomics analysis provided evidence of uniquely defined protein-regulated pathways in neuronal growth and development (Table 5.1).

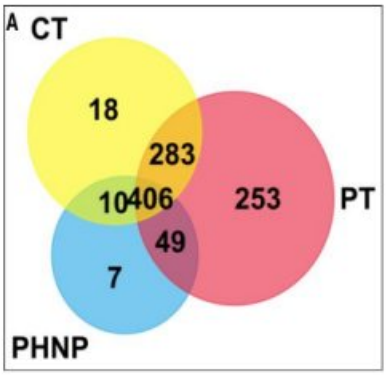

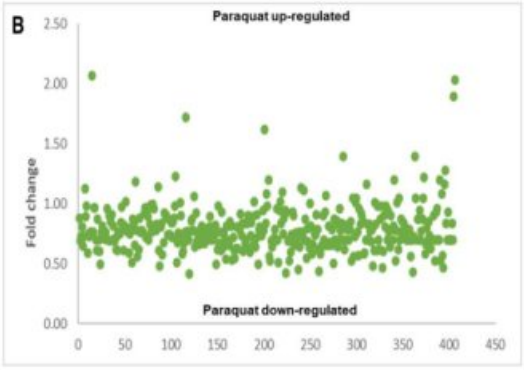

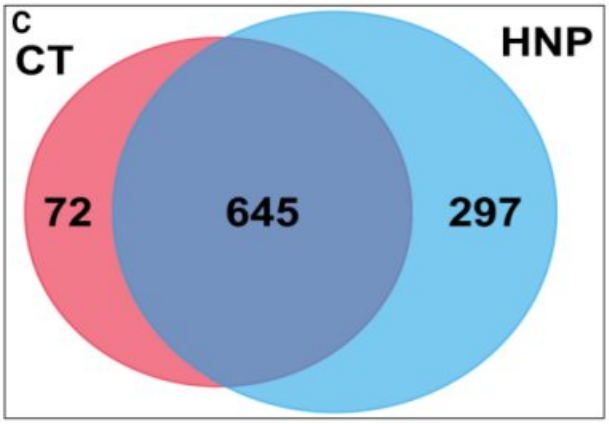

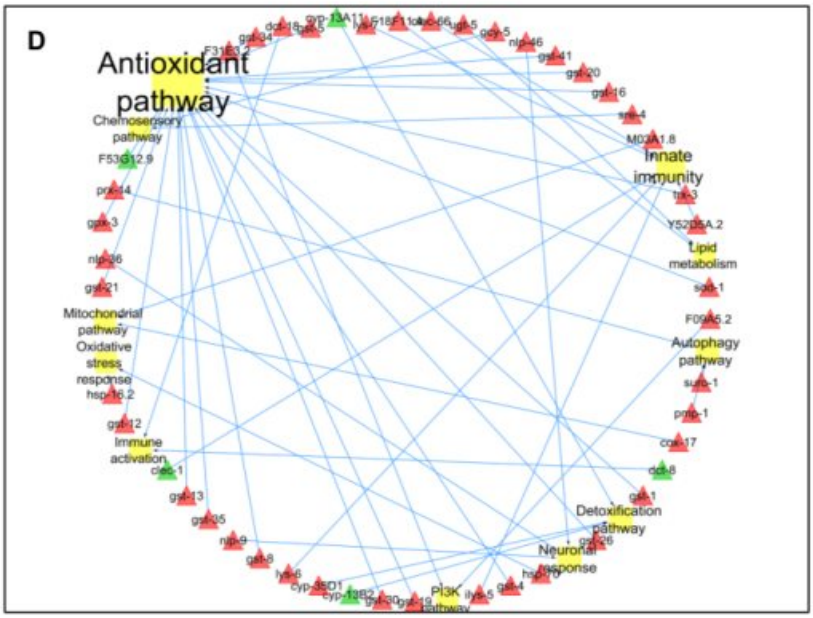

Fig. 5.9 Proteomics analysis to show the expression of common and intracellular proteins among the treated groups of *C. elegans*. (A) Venn diagram showing common intracellular proteins among untreated (control) (CT), PT (PT) treated, and HNP pre-treated followed by PT-treated (PHNP) groups of *C. elegans* determined by LC/MS-MS analysis. (B) Scatter plot showing significantly upregulated (fold change>1.25) and downregulated (fold change <0.80) proteins in PT-treated *C. elegans*. FC: fold-change in expression determined by LC/MS-MS analysis. (C) Venn diagram showing common intracellular proteins among untreated (control) (CT) and only HNP-treated *C. elegans* determined by LC/MS-MS analysis. (D) Molecular network of custom peptide HNP-mediated neuroprotection. The interaction network of peptide HNP-regulated genes/proteins and interlinking pathways as determined by both transcriptomic and proteomic analyses.

Table 5.1. List of the uniquely expressed metabolic pathways in *C. elegans* (N2) treated with HNP compared to untreated (control) *C. elegans*. Quantitative proteomic analyses determined these pathways.

Mapped ID/ Accession number	Pathways name	Proteins
CAEEL|WormBase=WBGene00006460|UniProtKB=Q19775	Activin beta signaling pathway	ppm-1.A
CAEEL|WormBase=WBGene00004307|UniProtKB=Q18246	Heterotrimeric G-protein signaling pathway-Gi alpha and Gs alpha-mediated pathways	rap-1
CAEEL|WormBase=WBGene00004357|UniProtKB=Q22038, CAEEL|WormBase=WBGene00000390|UniProtKB=Q05062	Axon guidance mediated by Slit/Robo	rho-1
CAEEL|WormBase=WBGene00001748|UniProtKB=P48727, CAEEL|WormBase=WBGene00001747|UniProtKB=Q27497	Nicotine pharmacodynamics pathway	gsp-2
CAEEL|WormBase=WBGene00003951|UniProtKB=Q9XUV0, CAEEL|WormBase=WBGene00003949|UniProtKB=Q23237	Proteasome pathway	pbs-5
CAEEL|WormBase=WBGene00021826|UniProtKB=G5EES9	Oxidative stress response	txl-1
CAEEL|WormBase=WBGene00006460|UniProtKB=Q19775	ALP23B_signaling_pathway	ppm-1.A
CAEEL|WormBase=WBGene00019599|UniProtKB=O01590	5-Hydroxytryptamine degradation	acds-10
CAEEL|WormBase=WBGene00004460|UniProtKB=Q04908	Cell cycle	rpn-3
CAEEL|WormBase=WBGene00015337|UniProtKB=P34277	Vitamin C metabolism	gsto-2
CAEEL|WormBase=WBGene00020146|UniProtKB=Q22067	Neurogenesis	maph-1.1,
CAEEL|WormBase=WBGene00001262|UniProtKB=Q09590	Vitamin D metabolism pathway	emb-8

CAEEL|WormBase=WBGene00001914|UniProtKB=K7ZUH9, CAEEL|WormBase=WBGene00003955|UniProtKB=O02115	DNA replication	pcn-1
CAEEL|WormBase=WBGene00006460|UniProtKB=Q19775	MYO_signaling_pathway	ppm-1.A
CAEEL|WormBase=WBGene00008809|UniProtKB=O17806, CAEEL|WormBase=WBGene00010606|UniProtKB=Q9XUT8	Detoxification pathways	cyp-13B2, cyp-13A11
CAEEL|WormBase=WBGene00000547|UniProtKB=Q9N4B1, CAEEL|WormBase=WBGene00000390|UniProtKB=Q05062, CAEEL|WormBase=WBGene00000161|UniProtKB=Q22601, CAEEL|WormBase=WBGene00003171|UniProtKB=P12456, CAEEL|WormBase=WBGene00006537|UniProtKB=P52275, CAEEL|WormBase=WBGene00000183|UniProtKB=G5EFK4, CAEEL|WormBase=WBGene00001683|UniProtKB=P04970	Huntington disease	clp-7, cdc-42, mec-7, arf-3, gpd-1
CAEEL|WormBase=WBGene00001683|UniProtKB=P04970	Glycolysis	gpd-1
CAEEL|WormBase=WBGene00020557|UniProtKB=P91455	Adenine and hypoxanthine salvage pathway	T19B4.3
CAEEL|WormBase=WBGene00007175|UniProtKB=Q17499	Nicotinic acetylcholine receptor signalling pathway	B0395.3
CAEEL|WormBase=WBGene00021286|UniProtKB=Q966C7	Pentose phosphate pathway	tald-1
CAEEL|WormBase=WBGene00004357|UniProtKB=Q22038, CAEEL|WormBase=WBGene00000390|UniProtKB=Q05062, CAEEL|WormBase=WBGene00003171|UniProtKB=P12456, CAEEL|WormBase=WBGene00006537|UniProtKB=P52275, CAEEL|WormBase=WBGene00006794|UniProtKB=Q07750	Cytoskeletal regulation by Rho GTPase	rho-1, cdc-42, tbb-2, unc-60

CAEEL|WormBase=WBGene00015064|UniProtKB=Q09438	Purine metabolism	B0228.7
CAEEL|WormBase=WBGene00012149|UniProtKB=G5EDW8	Allantoin degradation	CELE_VF13D12I
CAEEL|WormBase=WBGene00008654|UniProtKB=Q19311, CAEEL|WormBase=WBGene00011064|UniProtKB=Q21774	De novo purine biosynthesis	pfas-1, adsl-1
CAEEL|WormBase=WBGene00011745|UniProtKB=Q94048, CAEEL|WormBase=WBGene00001532|UniProtKB=Q23682, CAEEL|WormBase=WBGene00009306|UniProtKB=P91859	Chemosensory response	sre-4, gcy-5, got-1.2
CAEEL|WormBase=WBGene00017772|UniProtKB=Q22966,	Innate immune response pathways	clec-1
CAEEL|WormBase=WBGene00000390|UniProtKB=Q05062	TGF-beta signalling pathway	cdc-42
CAEEL|WormBase=WBGene00003951|UniProtKB=Q9XUV0, CAEEL|WormBase=WBGene00004505|UniProtKB=O76371, CAEEL|WormBase=WBGene00004501|UniProtKB=Q18787, CAEEL|WormBase=WBGene00004460|UniProtKB=Q04908	Ubiquitin proteasome pathway	pbs-5, rpt-5,
CAEEL|WormBase=WBGene00003747|UniProtKB=H2KZL2 CAEEL|WormBase=WBGene00012145|UniProtKB=Q7YTJ1 CAEEL|WormBase=WBGene00007185|UniProtKB=Q03561	Neuronal process	nlp-36 nlp-9 nlp-46
CAEEL|WormBase=WBGene00006460|UniProtKB=Q19775	GBB_signaling_pathway	ppm-1.A
CAEEL|WormBase=WBGene00012149|UniProtKB=G5EDW8	TCA cycle	CELE_VF13D12I
CAEEL|WormBase=WBGene00007175|UniProtKB=Q17499	Muscarinic acetylcholine receptor 1 and 3 signalling Pathway	B0395.3

CAEEL|WormBase=WBGene00012149|UniProtKB=G5EDW8, CAEEL|WormBase=WBGene00014001|UniProtKB=Q23539, CAEEL|WormBase=WBGene00020139|UniProtKB=P91408	Pyruvate metabolism	pyk-2, eppl-1

5.1.9 Transcriptomic and functional proteomics analyses in unison have elucidated the reversal of PT-induced upregulated and downregulated metabolic pathway genes by pre-treatment of *C. elegans* with neuroprotective peptide

The transcriptomic and quantitative proteomics data explicitly demonstrated the regulation of commonly upregulated and downregulated genes and their intracellular proteins in the PT and HNP groups compared to the CT group of *C. elegans* (N2 strain) The upregulated and downregulated proteins are involved in apoptosis, superoxide removal, lipid and protein metabolism, cellular differentiation, energy metabolism, mitochondrial function, axonal transport, autophagy, and neuronal development pathways in *C. elegans*. The analyses showed that the 15 upregulated (Table 5.2A) and 25 downregulated (Table 5.2B) signaling pathways in PT-treated *C. elegans* (N2 strain) were restored to an average level by the HNP peptide pre-treatment before the addition of PT (Tables 5.2A, B).

The comparative data obtained from transcriptomic, proteomics, and qRT-PCR studies suggest that PT treatment induced upregulation of apoptotic pathways, heterotrimeric G-protein signaling pathway-Gq alpha and Go alpha mediated pathway, ras pathway, p53 pathway, T-cell activation pathway, DA receptor-mediated signaling pathway, and hypoxia response via HIF activation in *C. elegans* (Table 5.2A). In contrast, the downregulation of essential pathways such as antioxidative, detoxification, chemosensory response, EGF receptor signaling, PI3K, ubiquitin-proteasome, neurogenesis, TGF-beta signaling, Axon guidance, FGF signaling, nicotinic acetylcholine receptor signaling, ATP synthesis, TCA cycle, DNA replication, oxidative stress response, glycolysis, and neuronal development was noted post-PT-treatment in *C. elegans* (Table 5.2B). Likewise, the collective analysis of transcriptomic and quantitative proteomics data showed that the HNP group, compared to the CT group, induced the expression of 33 unique signaling pathways (Table 5.1). Moreover, overexpression of the metabolic pathway genes (Table 5.2B) in the PHNP group explicitly validated the enhanced biosynthesis of biomolecules required for neurogenesis and neuroprotection mechanism against PT-induced toxicity in *C. elegans*.

Table 5.2A Transcriptomic and proteomic analyses to show the paraquat-induced upregulated metabolic pathways in wild type N2 strain of *C. elegans*. These pathways were restored to control (normal) level by pre-treatment of worms with neuroprotective custom peptide HNP.

Accession Numbe	Mapped ID	Metabolic pathway name
P02748	CAEEL|WormBase=WBGene00001149|UniProtKB=P54688, CAEEL|WormBase=WBGene00020831|UniProtKB=O61856	Isoleucine biosynthesis
P00027	CAEEL|WormBase=WBGene00001648|UniProtKB=P51875	Heterotrimeric G-protein signalling pathway-Gq alpha and Go alpha-mediated pathway
P06959	CAEEL|WormBase=WBGene00002183|UniProtKB=Q22100	CCKR signalling map
P00053	CAEEL|WormBase=WBGene00000552|UniProtKB=O16305	T cell activation
P00055	CAEEL|WormBase=WBGene00002190|UniProtKB=P30625	Transcription regulation by bZIP transcription factor
P00059	CAEEL|WormBase=WBGene00002363|UniProtKB=G5EGK8	p53 pathway
P02723	CAEEL|WormBase=WBGene00010083|UniProtKB=O17892	Adenine and hypoxanthine salvage pathway
P05912	CAEEL|WormBase=WBGene00002190|UniProtKB=P30625	Dopamine receptor-mediated signalling pathway
P00006	CAEEL|WormBase=WBGene00017121|UniProtKB=P19974	Apoptosis signalling pathway
P00021	CAEEL|WormBase=WBGene00002363|UniProtKB=G5EGK8	FGF signalling pathway
P00034	CAEEL|WormBase=WBGene00000942|UniProtKB=P19826, CAEEL|WormBase=WBGene00016913|UniProtKB=Q18823	Integrin signalling pathway
P02724	CAEEL|WormBase=WBGene00001149|UniProtKB=P54688	Alanine biosynthesis

P00030	CAEEL|WormBase=WBGene00006922|UniProtKB=Q19213	Hypoxia response via HIF activation
P04393	CAEEL|WormBase=WBGene00016236|UniProtKB=Q18313, CAEEL|WormBase=WBGene00021022|UniProtKB=Q9UA62	Ras Pathway
P02745	CAEEL|WormBase=WBGene00014095|UniProtKB=Q23621	Glutamine glutamate conversion

Table 5.2B Transcriptomic and proteomics analyses to show the paraquat-induced downregulated metabolic pathways in N2 strain *C. elegans*. These pathways were restored to normal (control) levels by pre-treatment of worms with neuroprotective custom peptide HNP.

Accession Number	**Mapped ID**	**Metabolic pathway name**
P00012	CAEEL|WormBase=WBGene00008809|UniProtKB=O17806, CAEEL|WormBase=WBGene00010606|UniProtKB=Q9XUT8	Detoxification pathways
P02746	CAEEL|WormBase=WBGene00010645|UniProtKB=G5EBW5, CAEEL|WormBase=WBGene00001337|UniProtKB=Q23315	Heme biosynthesis
P00018	CAEEL|WormBase=WBGene00001515|UniProtKB=Q22720, CAEEL|WormBase=WBGene00004287|UniProtKB=Q94124, CAEEL|WormBase=WBGene00002335|UniProtKB=P22981	EGF receptor signalling pathway
P00019	CAEEL|WormBase=WBGene00013785|UniProtKB=Q9U2T1, CAEEL|WormBase=WBGene00013786|UniProtKB=Q9U2T0	Endothelin signalling pathway
P02771	CAEEL|WormBase=WBGene00016103|UniProtKB=Q18164	Pyrimidine metabolism
P00004	CAEEL|WormBase=WBGene00011745|UniProtKB=Q94048, CAEEL|WormBase=WBGene00001532|UniProtKB=Q23682,	Chemosensory response

	CAEEL|WormBase=WBGene00009306|UniProtKB=P91859	
P00048	CAEEL|WormBase=WBGene00012816|UniProtKB=Q9XWX3, CAEEL|WormBase=WBGene00017183|UniProtKB=O16575, CAEEL|WormBase=WBGene00002335|UniProtKB=P22981	PI3 kinase pathway
P00060	CAEEL|WormBase=WBGene00004466|UniProtKB=O61742, CAEEL|WormBase=WBGene00004503|UniProtKB=P46502, CAEEL|WormBase=WBGene00004465|UniProtKB=Q22253	Ubiquitin proteasome pathway
P00052	CAEEL|WormBase=WBGene00002335|UniProtKB=P22981	TGF-beta signalling pathway
P00049	CAEEL|WormBase=WBGene00020146|UniProtKB=Q22067	Neurogenesis
P00013	CAEEL|WormBase=WBGene00004466|UniProtKB=O61742, CAEEL|WormBase=WBGene00004465|UniProtKB=Q22253	Cell cycle
P00031	CAEEL|WormBase=WBGene00003747|UniProtKB=H2KZL2 CAEEL|WormBase=WBGene00012145|UniProtKB=Q7YTJ1 CAEEL|WormBase=WBGene00007185|UniProtKB=Q03561	Neuronal process
P00016	CAEEL|WormBase=WBGene00003171|UniProtKB=P12456, CAEEL|WormBase=WBGene00004287|UniProtKB=Q94124	Cytoskeletal regulation by Rho GTPase
P00021	CAEEL|WormBase=WBGene00001515|UniProtKB=Q22720, CAEEL|WormBase=WBGene00004287|UniProtKB=Q94124, CAEEL|WormBase=WBGene00006352|UniProtKB=G5EDR3, CAEEL|WormBase=WBGene00002335|UniProtKB=P22981	FGF signalling pathway

P00044	CAEEL|WormBase=WBGene00012437|UniProtKB=Q9XWR0, CAEEL|WormBase=WBGene00002348|UniProtKB=P02567, CAEEL|WormBase=WBGene00003514|UniProtKB=P12845	Nicotinic acetylcholine receptor signalling pathway
P02721	CAEEL|WormBase=WBGene00010419|UniProtKB=Q9XXK1, CAEEL|WormBase=WBGene00000229|UniProtKB=P46561, CAEEL|WormBase=WBGene00022089|UniProtKB=Q95XJ0	ATP synthesis
P00009	CAEEL|WormBase=WBGene00004287|UniProtKB=Q94124	Axon guidance mediated by netrin
P00008	CAEEL|WormBase=WBGene00004287|UniProtKB=Q94124, CAEEL|WormBase=WBGene00004357|UniProtKB=Q22038, CAEEL|WormBase=WBGene00000390|UniProtKB=Q05062	Axon guidance mediated by Slit/Robo
P00045	CAEEL|WormBase=WBGene00000075|UniProtKB=Q94316	Notch signalling pathway
P00007	CAEEL|WormBase=WBGene00016104|UniProtKB=Q18163	Axon guidance mediated by semaphorins
P00051	CAEEL|WormBase=WBGene00018491|UniProtKB=Q9UAV5, CAEEL|WormBase=WBGene00001503|UniProtKB=O17214, CAEEL|WormBase=WBGene00007350|UniProtKB=P53596, CAEEL|WormBase=WBGene00020679|UniProtKB=O61199, CAEEL|WormBase=WBGene00000041|UniProtKB=P34455, CAEEL|WormBase=WBGene00000833|UniProtKB=P34575	TCA cycle
P00017	CAEEL|WormBase=WBGene00008645|UniProtKB=P90829, CAEEL|WormBase=WBGene00004340|UniProtKB=P53016	DNA replication
P00046	CAEEL|WormBase=WBGene00015879|UniProtKB=O45155	Oxidative stress response
P00009	CAEEL|WormBase=WBGene00000390|UniProtKB=Q05062	Axon guidance mediated by netrin

P00024	CAEEL|WormBase=WBGene00011884|UniProtKB=Q27527, CAEEL|WormBase=WBGene00011474|UniProtKB=P54216, CAEEL|WormBase=WBGene00006601|UniProtKB=Q10657, CAEEL|WormBase=WBGene00020185|UniProtKB=P91427	Glycolysis

5.1.10 The molecular network analysis demonstrates the neuroprotective functions of HNP against PT-induced toxicity and neuronal damage

Transcriptomic and proteomic analyses revealed different metabolic pathways involved in HNP-induced protection against PT-induced neuronal damage in N2 strain *C. elegans*. Based on these pieces of information, the molecular interactions, a network of gene expression profiles was constructed (Fig 5.9D). The mapping showed that the interconnected pathways of PT-induced knock-over genes leading to neuronal dysfunction were restored with the HNP pre-treatment in *C. elegans* (Fig 5.9D). In unison, transcriptomic and proteomic studies have identified 15 common upregulated pathways between the PHNP and PT groups of *C. elegans*. The molecular network displayed the snapshot of the genes regulating proteins and their biological functions, modulating the neurogenesis and neuroprotective function of HNP against PT-induced toxicity and neuronal dysfunction (Fig 5.9D, Table 5.1).

An overall neuroprotective mechanism against PT-induced neurotoxicity is proposed in Fig. 5.10.

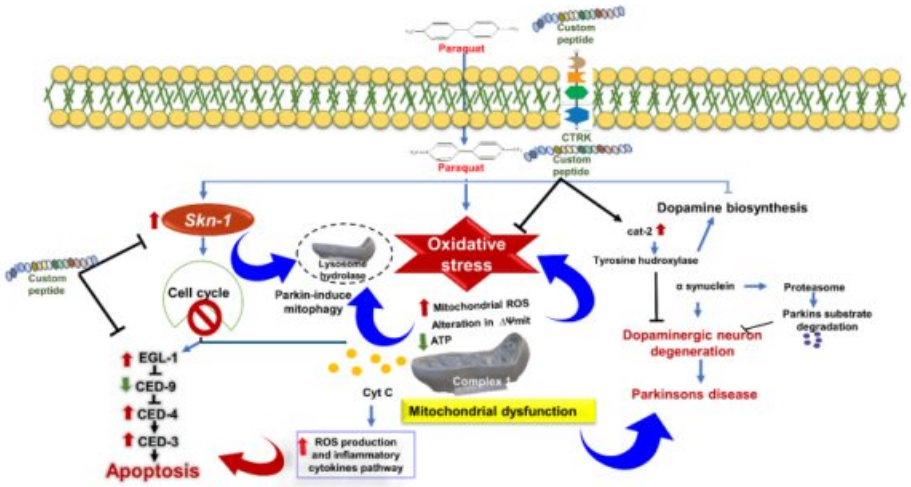

Fig. 5.10 The proposed neuroprotection mechanism pathways of custom peptide mediated protection against PT-induced neurotoxicity in *C. elegans* (N2 strain).

5.1.11 Custom peptides were non-toxic to mice and safe to administer

Custom peptides (TNP and HNP at the ratio 1:1, 10.0 mg/kg) were non-toxic to mice and did not show behavioral changes or adverse effects in treated mice. The serum profiles viz. serum glutamic oxaloacetic transaminase (SGOT), alkaline phosphatase (ALKP), serum glutamic pyruvic transaminase (SGPT), BUN (blood urea nitrogen), glucose content, creatinine, cholesterol, bilirubin and albumin of the custom peptide-treated mice (24 h post-treatment) did not show any significant ($p \geq 0.05$) deviation compared to the control (1X PBS treated) group of mice (Table 5.3). A minor increase in glucose level was measured in the blood of the treated mice compared to control mice, but it was within the normal range of blood glucose in mice (Table 5.3). Moreover, microscopic examination of the brain, heart, kidney, liver, lung, ovary, and testis of the custom peptide (HNP)-treated mice showed no morphological alterations (Fig 5.11). However, HNP treatment significantly ($p < 0.05$) reduced the production of pro-inflammatory cytokines viz. TNF-α, IL-6, IL-1β, compared to the control group of mice (Fig 5.12).

Table 5.3 Some biochemical properties of serum of control and custom peptides (TNP and HNP; 1:1)-treated (10 mg/kg) mice after 24 hours of *i.v.* injection. Values are mean ± SD of 6 mice. There was no significant difference in values ($p \geq 0.05$) between control and custom peptides-treated groups of mice.

	Values	
Parameters (Unit)	**Control**	**Custom peptides (TNP and HNP)-treated**
Glucose (mg/dL)	101.10 ± 1.27	160.0 ± 1.50
Billirubin (Direct) (mg/dL)	0.03 ± 0.00	0.08 ± 0.00
Billirubin (Total) (mg/dL)	0.05 ± 0.00	0.1 ± 0.00
BUN (mg/dL)	8 ± 0.05	10 ± 0.10
Creatinine(mg/dL)	0.18 ± 0.20	0.17 ± 0.20
Albumin (mg/dL)	1.98 ± 0.03	2.1 ± 0.05
ALKP(U/L)	81.85 ± 1.63	132 ± 1.70
SGPT(U/L)	33 ± 0.78	36 ± 0.70
SGOT(U/L)	62 ± 1.10	64 ± 1.13
Cholesterol (mg/dL)	66 ± 2.5	70 ± 3.0

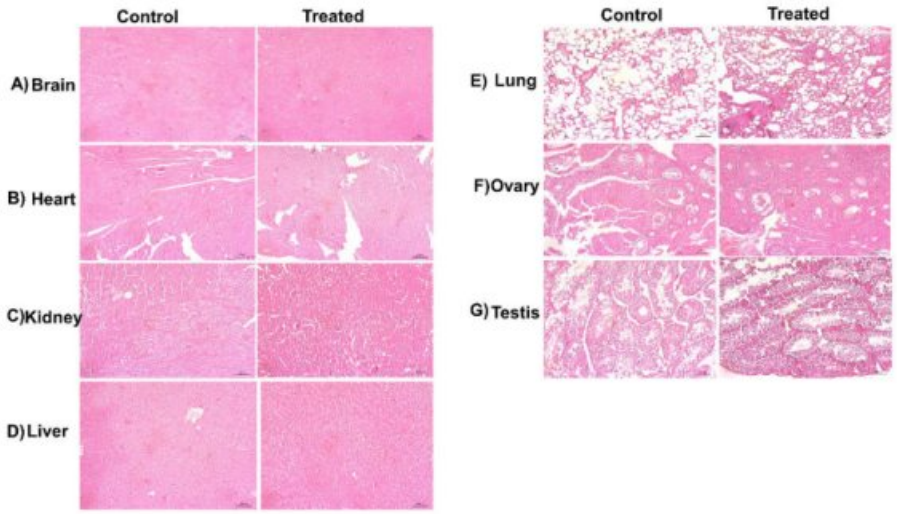

Fig 5.11 The effect of the custom peptides (TNP: HNP:: 1:1) treatment on histological changes in the tissues of Swiss albino mice. The H and E staining was employed to observe any morphological changes in the tissues compared to those of the control (untreated). Light microscopic observation of (A) Brain, (B) Heart, (C) Kidney, (D) Liver, (E) Lung, (F) Ovary, and (G) Testis for control and treated groups. Bar-100μM.

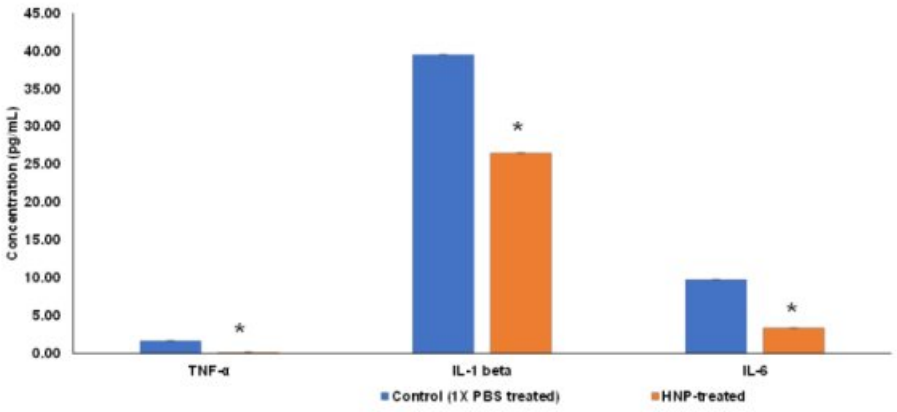

Fig 5.12 Determination of the concentration of pro-inflammatory cytokines in control (1X PBS treated)/ custom peptides-treated (10 mg/kg) group of mice plasma by Quantikine HS ELISA Kit. * A significant difference between control (1X PBS-treated) and custom peptide (TNP:HNP)-treated *C. elegans* ($p < 0.05$). Values are means ± SD of triplicate determinations.

5.2 Discussion

In recent years, the characterization of novel neurotrophic peptides has gained more focus in clinical trials against different NDs [5-9]. Neurotrophic peptides have several advantages over other neurotrophic drugs, such as improved neuroprotective effect, synaptic and neuronal plasticity, neurogenesis, better pharmacokinetics than the parent neurotrophin, and easy penetration [10,11].

Our previous study has demonstrated the exclusive binding of TNP and HNP to the TrkA receptor of PC-12 cells to induce neuritogenesis [12]; however, *C. elegans* possesses a simple nervous system and lacks Trk receptors [13]. Therefore, we were puzzled to understand the region of binding and mechanism of neuroprotective activity of custom peptides in *C. elegans*. To solve this issue, we investigated the presence of TrkA receptor homolog in the *C. elegans*. The presence of TrkA receptor homolog CAM-1 receptor in *C. elegans* was discovered by BLAST search.

Further *in silico* studies validated the binding of custom peptides to the CAM-1 receptor. The CAM-1 in *C. elegans* is a less functionally explored protein receptor. However, some reports suggest that CAM-1 is involved in essential functions, viz., the regulation of asymmetric division of V cells (seam cells), CA/CP neuroblast, and axon outgrowth [14,15] and the positioning of the nerve ring [16]. Further, the CAM-1 receptor is also responsible for the negative regulation of developmental neurite pruning of AIM neurons [17]. Moreover, Entries in the Reactome pathway browser database [1] demonstrated that the CAM-1 receptor is an essential component in the MAPK signaling pathway by playing multiple roles, such as the regulation and development of axons [14,15] and the positioning of the nerve ring [16].

Therefore, the CAM-1 receptor as a confirmed binding site for the custom peptides in this study was further validated by insignificant binding of FITC-custom peptides in the CAM-1 mutant strain of *C. elegans* at its nerve ring region. However, FITC-conjugated custom peptides showed binding to *C. elegans* at its nerve ring adjacent to the pharynx, which covers complex circuitry leading to most aspects of behaviors, such as chemosensation, locomotion, learning, memory, etc. [18]. The nerve ring of *C. elegans* adjacent to the pharynx functions similarly to a "brain' and most sensory neurons have endings organized around the mouth [18].

Moreover, wild-type *C. elegans* were treated under different experimental conditions with FITC-conjugated custom peptides. The binding of the PT for induction of PD in *C. elegans* and the binding of custom peptides were found to be competitive as co-treatment of peptides with increasing concentrations of PT showed a gradual decrease in the fluorescence intensity of the FITC-conjugated peptides in the nerve ring adjacent to the pharynx. This data indicates that the expression of the CAM-1 receptor may be downregulated by PT treatment, making it inaccessible for binding tested custom peptides. Therefore, pre-treatment with custom peptides protects this site from neuronal damage by PT.

PD is associated with multiple motor and non-motor symptoms developed due to elevated oxidative stress leading to mitochondrial membrane damage, which triggers DAergic neuron degeneration [19]. A plethora of reports support that oxidative stress is one of the essential factors associated with the progression of NDs such as PD, and evidence has been presented to show that antioxidant activity may prevent ND [20,21]. We have demonstrated the *in vitro* antioxidant properties of the TNP and HNP by their free radical scavenging activity [22]. Therefore, TNP and HNP *in vivo* conditions also prolong the lifespan by decreasing the oxidative stress in worms [23,24]. Antioxidants such as vitamin C and quercetin demonstrated neuroprotection properties in several *in vitro* and *in vivo* models of NDs viz. AD, PD, and Huntington's Disease (HD) [25-27]. Therefore, we considered quercetin and vitamin C a positive control for this study.

Since ASH sensory neurons of *C. elegans* play a pivotal role in the sensory response to aversive stimuli, PT treatment induces defective chemotaxis behavior in worms due to the loss of ASH neuronal function [3]. Therefore, the chemotaxis assay was performed in *C. elegans* to demonstrate the possibility of restoration of PT-induced chemotaxis dysfunction by pre-treatment with custom peptides. The pre-treatment of *C. elegans* with custom peptides before PT treatment has shown a superior protective effect by restoring the PT-induced chemotaxis defect and survivability, which may be correlated to the fact that these peptides bind to the same region (nerve ring adjacent to the pharynx) where PT binds to induce neurodegeneration in *C. elegans*. Therefore, post-administration of peptides after PT treatment, minimal protection was observed against PT-induced neurodegeneration when they already bind to neurons. Further, peptides' neuroprotective and neurotrophic effects were validated from the transcriptomic and proteomic analysis data. Both unambiguously showed that the proteins responsible for

chemosensory behavior, viz. sre-4, gcy-5, and got-1.2 were downregulated by PT, resulting in the loss of memory of *C. elegans*. In sharp contrast, pre-treatment with custom peptides upregulated these genes to increase the cellular proteins to an average level (untreated control worms).

The increased ROS content observed in the neurons of PD patients and PD-like model organisms triggers cellular damage and apoptosis [24,28,29]. Therefore, antioxidant compounds, for example, quercetin, curcumin, naringin, metformin, bacosides, hydralazine, and vitamin C, have found significant therapeutic potential to treat PT-induced toxicity [30-33]. For preventing cellular damage and neurodegeneration in a non-autonomous fashion, mitochondrial dysfunction triggers the upregulation of many stress response pathways, such as p38/MAPK innate immune pathways [34]. HNP and TNP (50 μg/mL, ~38 μM) pre-treatment for 2 h demonstrated appreciable potency to reduce the PT-mediated increase in cellular ROS level and mitochondrial membrane depolarization, subsequently enhancing survival rates in PT-treated *C. elegans*. Vitamin C pre-treatment for 24 h significantly attenuated the PT-induced ROS production but did not restore mitochondrial membrane depolarization at a concentration (100 μg/mL) two times higher than the concentration of custom peptides. Further, vitamin C could not offer protection against PT-induced neurotoxicity, thus implying that PT-induced neuronal damage may not be protected only by the antioxidant property of the peptides, which rationalizes the therapeutic potency of custom peptides under study.

In response to oxidative stress, the *skn-1* gene translocates and accumulates at the intestinal nuclei and induces transcription of genes such as SODs (*sod-1* and *sod-3*), catalases (*cat-1*, *cat-2* and *cat3*), thioredoxin-1 (*trx-1*), GSTs (*gst-4*, *gst-6* and *gst-10*), and heat-shock proteins HSPs (*hsp-16.1* and *hsp-16.2*) involved in phase 2 detoxification [35]. Accordingly, the MAPK genes *sek-1*, *pmk-1*, and *skn-1* were upregulated in *C. elegans* post-PT exposure. However, the qRT-PCR results have shown the overexpression of downstream genes of activated p38/MAPK pathways such as '*skn-1*' that regulates various detoxification processes (*sod*, *cat*, *trx*, *gst* series) and heat-shock proteins (HSPs) genes essential to abolish enhanced ROS production leading to cellular damage [34,36]. The expression level of SODs and other associated genes is low under normal conditions [36,37]. However, acute exposure to PT induces higher expression of such genes in mitochondria to withstand oxidative stress. The PT-mediated over-expression of HSPs prevents the protein from misfolding due to changes in the cellular

redox state [38]. The qRT-PCR result highlighted the significant downregulation of stress-related genes in custom peptide-treated wild-type N2 worms compared to the PT treatment, probably due to the enhanced transcription initiation or mRNA stability. Downregulation of these genes upon custom peptide pre-treatment is correlated with reduced oxidative stress and increased stress resistance in *C. elegans*, which concludes the antioxidant and neuroprotective potential of TNP and HNP.

DAergic neurons are vulnerable to PT-induced oxidative stress due to ROS generation, a principal neuronal death regulator [39]. DAergic neuronal degeneration and α-synuclein accumulation are two major hallmarks of PD [40]. The PT-induced overexpression of SKN-1 (p38/MAPK) induced response does not protect DAergic neurons from degeneration [34]. Upregulation of antioxidant enzymes (sods and catalases) and accumulation of ROS upon exposure to neurotoxins such as PT is one of the crucial factors in DAergic neuron degeneration and α-synuclein aggregation [41]. Custom peptides-mediated upregulation of the *cat-2* gene regulates tyrosine hydroxylase (TH) enzyme expression and restores the PT-induced DA deficiency [42].

The neurotransmitter DA availability to the striatum (brain structure) is essential for motor response and memory functions [43,44]. DA deficiency is another hallmark of PD, resulting in DAergic cell death and α-synuclein deposition [44,45]. The neuroprotective activity of custom peptides against PT-induced chemotaxis behavior defects, DAergic neurodegeneration, α-synuclein accumulation, and reduced life span may be correlated to their antioxidant and antiapoptotic properties [39]. However, vitamin C was ineffective in restoring chemotaxis behavior, DAergic neurodegeneration, and α-synuclein accumulation induced by the acute exposure of PT in C. elegans, so reinforcing antioxidation may not be the only property to offer protection against PT-induced neurodegeneration [22].

The custom peptide HNP surpassed TNP in preventing PT-induced toxicity; subsequently, it was selected for further studies. The cumulative data generated from *in silico*,qRT-PCR, transcriptomic, and proteomics analysis have unambiguously demonstrated that HNP pre-treatment resulted in the downregulation of PT-induced upregulated pro-apoptotic (cytochrome C, CED-4, and CED-3) genes expression. In contrast, it upregulated the expression of antiapoptotic genes (CED-9) in PT-treated *C. elegans*, thereby enhancing the survival rate of worms.

The transcriptomic and quantitative proteomic analyses have identified the molecular network of signaling pathways through which the peptide HNP blocked the PT-induced neurotoxicity in *C. elegans*. The findings aided that HNP pre-treatment restored the PT-induced altered genes and protein functions such as antioxidant pathways, mitochondrial stress response pathways, energy metabolism pathways, lipid and protein metabolism pathways, and programmed cell death in *C. elegans*.

The custom peptide also restored altered pathways induced by the PT treatment in the *C. elegans* PD model (N2 strain). PT causes its toxic effect by downregulating most of the antioxidant genes (sod, trx, gst), mitochondrial stress resistance gene (txl-1, cox-4), detoxification genes (cyp-13B2, cyp-13A11), TCA cycle (CELE_VF13D12L), genes involved in chemosensory response (sre-4, gcy-5, got-1.2), neurogenesis (maph-1.1), neuronal development (nlp-36, nlp-9, nlp-46) and upregulated apoptotic genes (cyt C, egl-1), MAPK genes involved in innate immune response (skn-1), and some of the stress response genes (hsp10) in *C. elegans*, which were counteracted by custom peptide (HNP) pre-treatment.

In a nutshell, the PT group of worms exhibited the maximal variation in differential gene expression compared with the CT group of *C. elegans*. In contrast, the custom peptides pre-treatment group showed a minimum variance compared to the CT group, signifying normalization or restoration of altered genes/proteins dynamics. This study highlights the therapeutic importance of custom peptides for attenuating neurodegeneration.

Using the tested custom peptides as a drug prototype exclusively depends upon their non-toxic nature in preclinical studies. The acute toxicity studies in mice models showed that the peptide is devoid of toxicity in mice at a dose that is 100 times higher than its therapeutic dose determined in *C. elegans*. Further, it has no detrimental effect on the biochemical parameters of blood parameters and vital organs, suggesting the safety of the peptides for the development of drug prototypes. Furthermore, the reduced concentration of inflammatory mediators (TNF-α, IL-6, IL-1β) in the HNP-treated mice, compared to control (1X PBS-treated) mice, diminished the risk of inflammatory response post-treatment with peptides. One of our future goals is to assess the neuroprotective effect and pharmacokinetics and pharmacodynamics properties of the custom peptides in rodent models.

CHAPTER VI

To study the microRNA expression profile in custom peptides-treated cultured *C. elegans*

Dev Madhubala

6.1 Results

6.1.1 Identification of mouse 2.5 S-NGF/custom peptide (HNP)-regulated miRNAs in *C. elegans* by miRNA sequencing analysis

The miRNA microarray analysis showed differential expression of twenty miRNAs in the NGF group of *C. elegans* (Table 6.1A). Among them, 10 miRNAs were upregulated, and 10 were downregulated in the NGF group of *C. elegans* compared to the CT group of *C. elegans*. Similarly, the microarray analysis revealed the differential regulation of 13 miRNAs in the HNP group of *C. elegans* (Table 6.1B); ten miRNAs were upregulated, whereas three miRNAs were downregulated compared to the CT group *C. elegans*. cel-miR-255-3p, cel-miR-1-3p, cel-miR-62, cel-miR-85-3p, cel-miR-71-3p, cel-miR-83-3p, cel-miR-84-5p, and cel-miR-4936 were found to be in common in mouse 2.5 S-NGF and HNP treated groups of *C. elegans*. Among them, the expressions of cel-miR-1-3p and cel-miR-255-3p were markedly increased in both the NGF and HNP groups of *C. elegans*. The annotated pathways of potential miRNA targets in the NGF and HNP groups of *C. elegans* are listed in Table 6.1C.

Table 6.1A. The miRNA microarray analysis data shows the fold changes of differentially regulated miRNA in the *C. elegans* treated with 50 μg/mL of mouse 2.5 S-NGF (NGF) for 2 h with respect to 1X PBS-treated *C. elegans* (CT) at 20°C.

Types of miRNA	logFC (CT vs NGF)
cel-miR-1-3p	2.69
cel-miR-255-3p	2.21
cel-miR-83-3p	1.93
cel-miR-85-3p	1.92
cel-miR-59-3p	1.87
cel-miR-62	1.72
cel-miR-84-5p	1.60
cel-miR-794-5p	1.54
cel-miR-795-3p	1.51
cel-miR-71-3p	1.30
cel-miR-4936	-3.08

cel-miR-67-3p	-3.14
cel-miR-41-5p	-3.27
cel-miR-5545-3p	-3.33
cel-miR-8211-5p	-3.79
cel-miR-8204-5p	-3.88
cel-miR-67-5p	-4.12
cel-miR-8205-3p	-4.81
cel-miR-2217b-3p	-5.04
cel-miR-8202-5p	-5.10

Table 6.1B. The miRNA microarray analysis data shows the fold changes of differentially regulated miRNA in the *C. elegans* treated with 50 µg/mL of custom peptide (HNP) for 2 h compared to 1X PBS-treated *C. elegans* (CT) at 20°C.

Types of miRNA	**logFC (CT vs HNP)**
cel-miR-255-3p	3.47
cel-miR-87-5p	3.13
cel-miR-1-3p	1.87
cel-miR-1820-5p	1.54
cel-miR-62	1.53
cel-miR-358-3p	1.50
cel-miR-85-3p	1.38
cel-miR-71-3p	1.30
cel-miR-83-3p	1.40
cel-miR-84-5p	1.55
cel-miR-791-3p	-1.36
cel-miR-789-5p	-1.44
cel-miR-4936	-1.55

Table 6.1C. Pathways annotation of potential miRNA target genes in only HNP/mouse 2.5 S-NGF-treated *C. elegans*.

Pathways of potential miRNA target genes	The p-Value of HNP-treated *C. elegans*	The p-Value of mouse 2.5 S-NGF treated *C. elegans*
BINDING: ATP		0.463
CARBOHYD: N-linked (GlcNAc) asparagine	0.183	0.239
cel01100: Metabolic pathways		0.000
cel01200: Carbon metabolism	0.006	0.004
cel01230: Biosynthesis of amino acids	0.001	0.000
GO:0000166~nucleotide binding	0.299	0.198
GO:0000287~magnesium ion binding	0.009	0.006
GO:0004888~transmembrane signaling receptor activity	0.255	0.209
GO:0005216~ion channel activity	0.367	0.321
GO:0005230~extracellular ligand-gated ion channel activity	0.249	0.214
GO:0005524~ATP binding	0.425	0.308
GO:0005739~mitochondrion	0.024	
GO:0005886~plasma membrane	0.226	0.055
GO:0006811~ion transport	0.055	0.039
GO:0006813~potassium ion transport	0.069	0.060
GO:0006937~regulation of muscle contraction	0.032	0.028
GO:0007165~signal transduction	0.070	0.109
GO:0007268~chemical synaptic transmission	0.348	0.314
KW-0407~Ion channel		0.481
GO:0016301~kinase activity	0.198	0.279
KW-0460~Magnesium		0.207
GO:0016310~phosphorylation	0.186	0.282
GO:0022848~acetylcholine-gated cation-selective channel activity	0.017	0.014
GO:0022857~transmembrane transporter activity	0.278	0.083
GO:0030054~cell junction	0.165	0.119
GO:0030594~neurotransmitter receptor activity	0.286	0.247

GO:0034220~ion transmembrane transport	0.146	0.123
GO:0040011~locomotion	0.039	0.154
GO:0042391~regulation of membrane potential	0.241	0.215
GO:0043005~neuron projection	0.254	0.189
GO:0045211~postsynaptic membrane	0.063	0.048
GO:0046662~regulation of oviposition	0.056	0.049
GO:0050877~neurological system process	0.226	0.201
GO:0055085~transmembrane transport	0.424	0.191
GO:0060078~regulation of postsynaptic membrane potential	0.002	0.001
GO:0060079~excitatory postsynaptic potential	0.021	0.018
GO:0090326~positive regulation of locomotion involved in locomotory behaviour	0.014	0.012
IPR002394: Nicotinic acetylcholine receptor	0.009	0.007
IPR006029: Neurotransmitter-gated ion-channel transmembrane domain	0.118	0.102
IPR006201: Neurotransmitter-gated ion-channel	0.172	0.149
IPR006202: Neurotransmitter-gated ion-channel ligand-binding	0.176	0.154
IPR011701: Major facilitator superfamily	0.157	0.137
IPR018000: Neurotransmitter-gated ion-channel, conserved site	0.116	0.100
KW-0067~ATP-binding	0.138	0.044
KW-0325~Glycoprotein	0.259	0.265
KW-0406~Ion transport	0.089	0.103
KW-0418~Kinase	0.063	0.119
KW-0443~Lipid metabolism	0.485	
KW-0472~Membrane	0.244	0.124
KW-0496~Mitochondrion	0.084	0.121
KW-0547~Nucleotide-binding	0.050	0.012
KW-0628~Postsynaptic cell membrane	0.031	0.021
KW-0770~Synapse	0.133	0.094

KW-0808~Transferase	0.132	0.153
KW-0809~Transit peptide	0.078	0.221
KW-0812~Transmembrane	0.066	0.177
KW-0813~Transport	0.419	0.472
KW-0965~Cell junction	0.098	0.060
KW-1003~Cell membrane	0.030	0.009
KW-1015~Disulfide bond	0.233	0.108
KW-1071~Ligand-gated ion channel	0.035	0.030
KW-1133~Transmembrane helix	0.233	
NP_BIND: ATP	0.375	0.146
R-CEL-112314~Neurotransmitter receptors and postsynaptic signal transmission	0.294	0.281
R-CEL-112316~Neuronal System	0.419	0.400
R-CEL-181431~Acetylcholine binding and downstream events	0.074	0.070
R-CEL-195721~Signaling by WNT		0.486
R-CEL-212436~Generic Transcription Pathway	0.224	0.425
R-CEL-3858494~Beta-catenin independent WNT signaling		0.143
R-CEL-556833~Metabolism of lipids	0.327	
R-CEL-622323~Presynaptic nicotinic acetylcholine receptors	0.011	0.010
R-CEL-622327~Postsynaptic nicotinic acetylcholine receptors	0.074	0.070
R-CEL-629594~Highly calcium permeable postsynaptic nicotinic acetylcholine receptors	0.074	0.070
R-CEL-629597~Highly calcium permeable nicotinic acetylcholine receptors	0.011	0.010
R-CEL-6798695~Neutrophil degranulation		0.493
R-CEL-71387~Metabolism of carbohydrates	0.031	0.112
R-CEL-73857~RNA Polymerase II Transcription	0.418	
R-CEL-74160~Gene expression (Transcription)	0.489	
R-CEL-8878171~Transcriptional regulation by RUNX1	0.196	

TOPO_DOM: Cytoplasmic	0.062	0.096
TOPO_DOM: Extracellular	0.103	0.072
TRANSIT: Mitochondrion	0.059	0.189

The volcano plot (p-values vs. fold change) displayed the differential gene expression between (i) NGF and CT groups (Fig. 6.1A) and (ii) HNP and CT groups (Fig. 6.1B). The heatmap analysis exhibited a disparity in gene expression between NGF and HNP groups compared to the CT group (Fig 6.1C-D). The list of possible targets of differentially expressed miRNAs was predicted. It was observed that probable target genes of upregulated miRNAs were involved in the PI3K pathway, Wnt/β-catenin signaling, TGF signaling, Axon development, transcriptional regulation, and cellular development in the NGF and HNP groups of *C. elegans*. The target genes of downregulated miRNAs were implicated in apoptotic pathways, p53 pathways, neurological diseases, Ras pathways, Innate immune response pathways, etc., in NGF and groups of *C. elegans* (data not shown). The role of some of the upregulated miRNAs in different stages of neuronal development in NGF and HNP groups of *C. elegans* is shown in Fig 6.2.

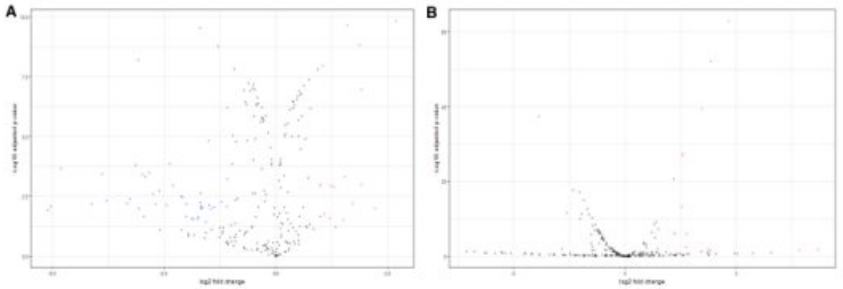

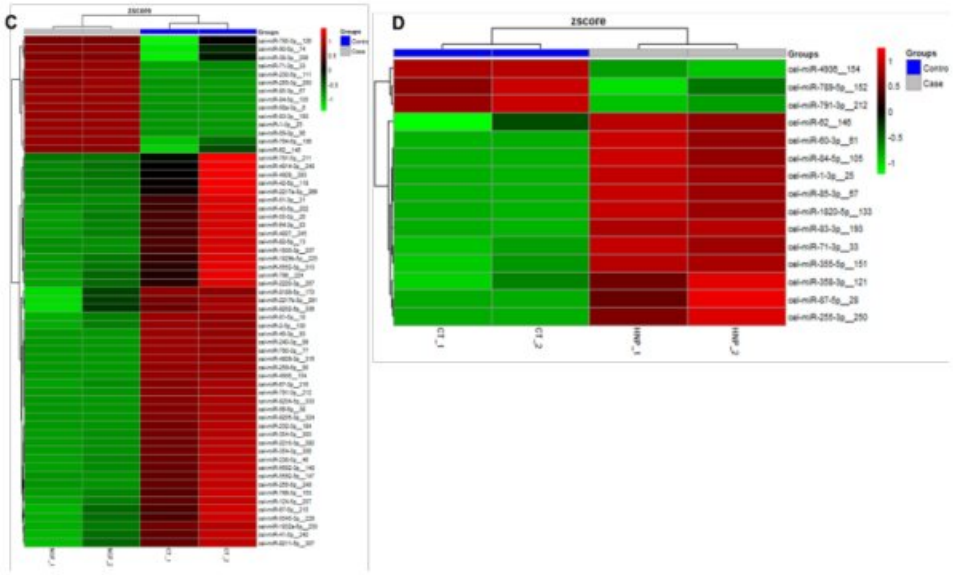

Fig 6.1 Differential expression of miRNAs between mouse 2.5S-NGF/peptide HNP-treated group of *C. elegans* and 1X PBS-treated (control) group of *C. elegans*. (A) Volcano plot (p-value v/s log Fc) for mouse 2.5S-NGF-treated (NGF group) versus 1X PBS-treated (CT group) *C. elegans*. (B) Volcano plot (p-value v/s log Fc) for custom peptide HNP-treated (HNP group) versus 1X PBS-treated (CT) *C. elegans*. Heat map showing the differential expression of the upregulated and downregulated genes among (C) mouse 2.5S-NGF-treated (NGF group) versus 1X PBS-treated (CT group) *C. elegans* and (D) custom peptide HNP-treated (HNP group) versus 1X PBS-treated (CT) *C. elegans*.

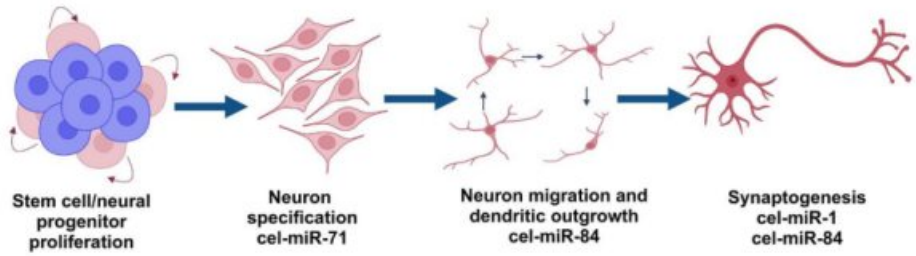

Fig 6.2 Roles of mouse 2.5S-NGF and HNP-induced miRNAs involved in different stages of neuronal development in *C. elegans*.

6.1.2 A comparison of the differential expression of global miRNA between paraquat-treated *C. elegans* and pre-treatment of *C. elegans* with mouse 2.5 S-NGF/ HNP followed by paraquat treatment

Novel miRNAs were identified in all the treated groups. The list of differentially expressed miRNAs with their respective logFC values in the PT group, compared to the CT group and their restoration with the treatment of mouse 2.5S-NGF and custom peptide HNP treatment in *C. elegans,* is shown in Table 6.2A and Table 6.2B, respectively. The principal component analysis (PCA) score plot showed the clustering between group 1 consisting of CT, PT, PNGF, and NGF groups of *C. elegans* (Fig 6.3A). The clustering between group 2, comprising CT, PT, PHNP, and HNP groups of *C. elegans* (Fig 6.3B), and the clustering between group 1 and group 2 is shown in Fig 6.3C. Similarly, the correlation plot (red indicates the positive, and blue indicates the negative correlation) was constructed within different groups as described previously (Fig 6.3D-F). The volcano plots (p-values vs. fold change) show the differential expression of the miRNAs in (i) PNGF vs. PT group of *C. elegans* (Fig 6.3G) and (ii) PHNP vs. PT group of *C. elegans* (Fig 6.3H).

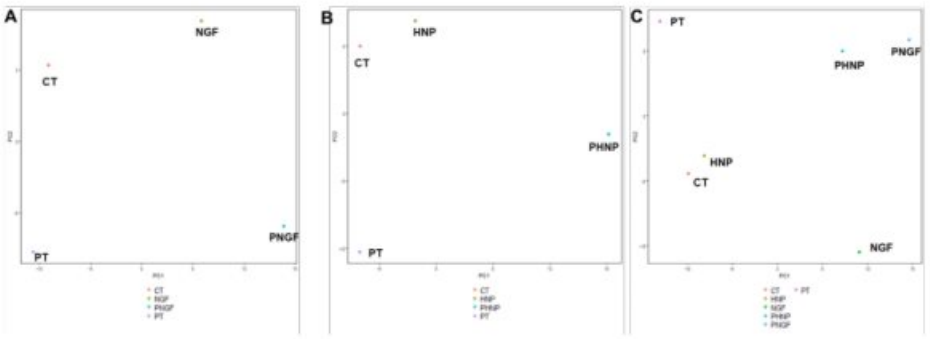

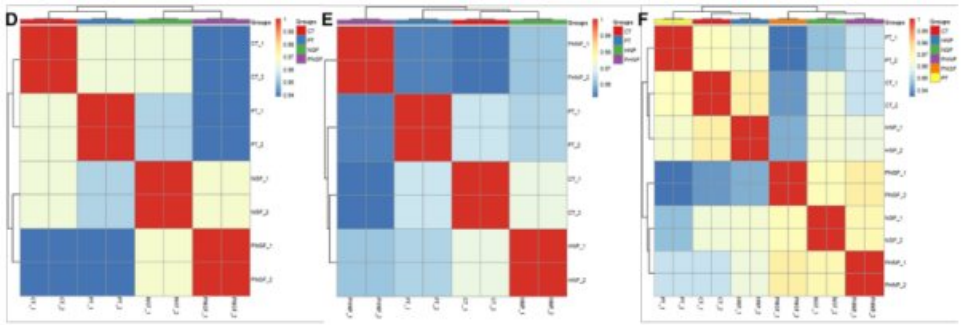

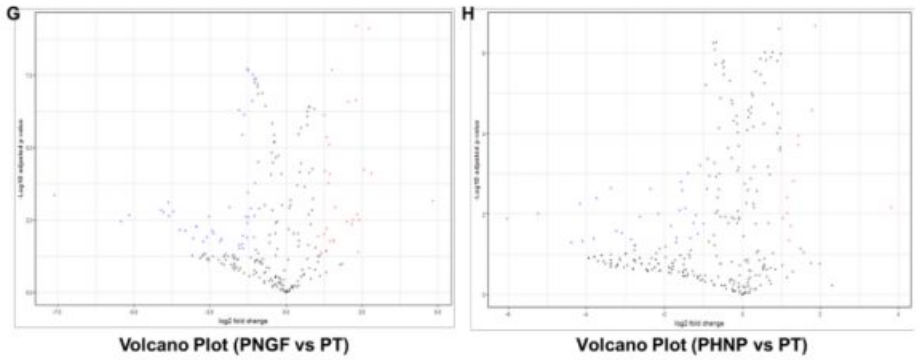

Fig 6.3 Differential expression of miRNAs between different treated groups of *C. elegans*. (A-C) PCA score plot showing the gene expression variability between the groups of *C. elegans* and within the biological replicates. (D-F) Correlation plot showing a correlation between treated groups of *C. elegans*. (G) Volcano plot (p-value v/s log Fc) for PNGF group versus PT group and (H) Volcano plot (p-value v/s log Fc) for PHNP group versus PT group of *C. elegans*. CT: untreated worms, PT: PT treated worms, PHNP: custom peptide HNP pre-treatment followed by PT treatment, PNGF: mouse 2.5S-NGF pre-treatment followed by PT treatment HNP: custom peptide HNP treated worms, NGF: mouse 2.5S-NGF treated worms.

Table 6.2A. The miRNA sequencing analysis data compares the fold changes in the differential expression of miRNA in the different treatment groups.

miRNA	Log FC (CT vs PT)	logFC (PNGF vs PT)	Function	References
cel-miR-77-5p	-3.17	1.32	Embryogenesis	[1]
cel-miR-4813-3p	-3.05	3.65	Degradation of alpha-synuclein	[2,3]
cel-miR-34-3p	-1.95	1.58	Increasing autophagic flux against oxidative stress	[4]
cel-miR-236-3p	-1.39	2.80	Phosphoinositide 3-kinase (PI3K) pathways for cell growth and development (promote longevity)	[5]

cel-miR-46-3p	-1.09	1.36	Development	[6,7]
cel-miR-786-3p	1.39	-1.16	Fatty acid metabolism	[8]
cel-miR-1820-5p	1.43	-1.54	Innate immune response	[9]
cel-miR-83-3p	1.75	1.35	Loss of miR-83 extends lifespan	[10]
cel-miR-795-3p	2.17	-1.44	Dauer formation	[11]
cel-miR-57-3p	3.23	-2.38		
cel-miR-8207-3p	4.31	-7.62		

Table 6.2B. The miRNA sequencing analysis data compares the fold changes in the differential expression of miRNA in the different treatment groups. For comparison of differential expression of the miRNA, the *C. elegans* were subjected to the following treatments at 20°C: (a) 1X PBS (control) treated *C. elegans* (CT), (b) 10 mM paraquat (PT) treatment for 1 h, (c) pre-treatment with 50 μg/mL custom peptide for 2 h followed by 10 mM paraquat treatment (PHNP) for 1 h.

miRNA	**logFC (CT vs PT)**	**logFC (PHNP vs PT)**	**Function**	**References**
cel-miR-77-5p	-3.17	1.18	Embryogenesis	[1]
cel-miR-62	-3.00	3.82	Regulate stress response and increase the lifespan	[5]
cel-miR-4813-3p	-3.05	1.20	Degradation of alpha-synuclein	[3]
cel-miR-4936	-2.59	1.57	Activation of heat shock factor-1 (HSF-1) to protect the cell from organelle dysfunction	[12]
cel-miR-236-3p	-1.39	1.77	Phosphoinositide 3-kinase (PI3K) pathways for cell growth and development (promote longevity)	[5]
cel-miR-83-3p	1.75	1.03	Loss of miR-83 extends lifespan	[10]

cel-miR-57-3p	3.23	-3.23	Unknown	
cel-miR-8207-3p	4.31	-6.03	Unknown	
cel-miR-354-5p	4.60	-5.24	The transforming growth factor beta (TGF -β) signaling pathway shows a protective response	[13]

The heat map analysis compared the expression profile of miRNA within different treatment groups (Figs 6.4A-B). Further, gene network analysis revealed the involvement of downstream mRNA targets, which modulate multiple classes of proteins (Appendix Table A2). The miRNA and the target mRNA networks for PNGF (Fig 6.5A) and PHNP (Fig 6.5B) groups of *C. elegans* were constructed.

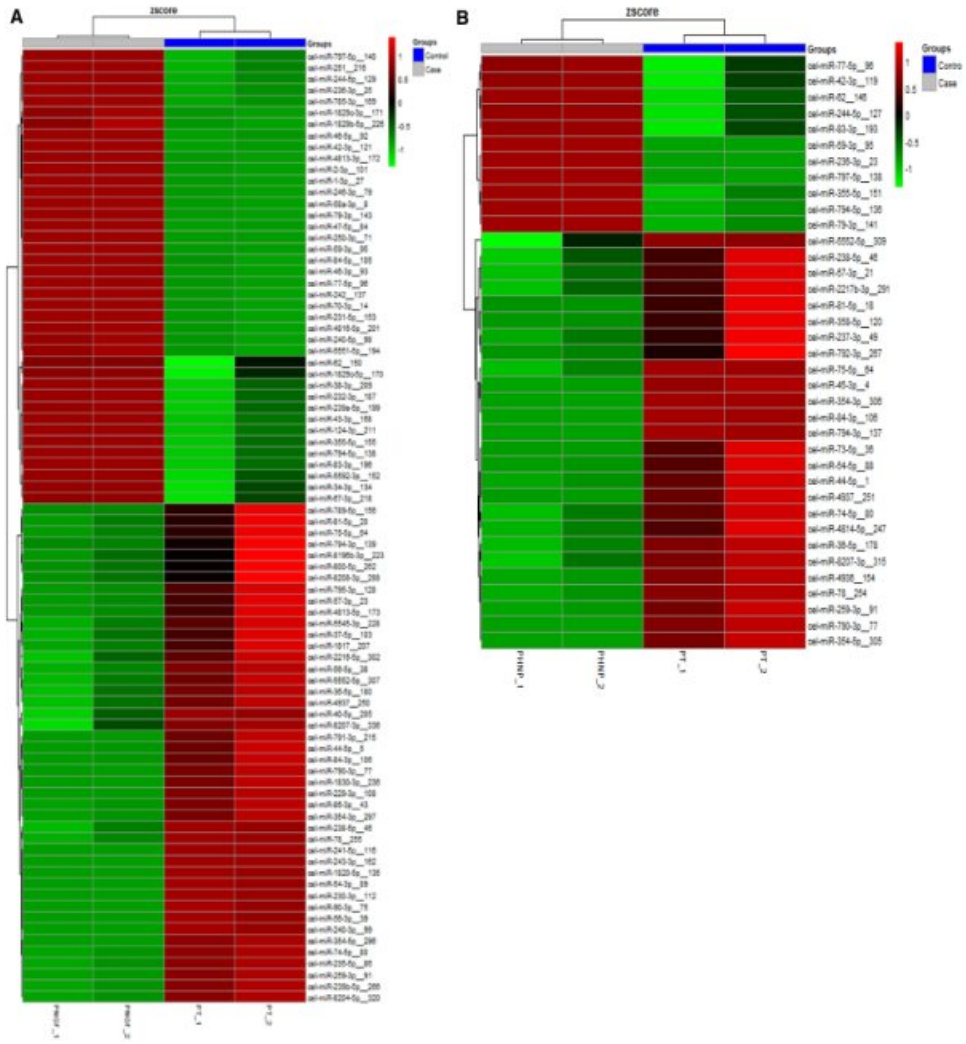

Fig 6.4 Heat map showing the differential expression of the upregulated and downregulated miRNAs among different groups of *C. elegans*. (A) PNGF group versus PT group (B) PHNP group versus PT group of *C. elegans*. CT: untreated worms, PT: PT treated worms, PHNP: custom peptide HNP pre-treatment followed by PT treatment, PNGF: mouse 2.5S-NGF pre-treatment followed by PT treatment HNP: custom peptide HNP treated worms, NGF: mouse 2.5S-NGF treated worms.

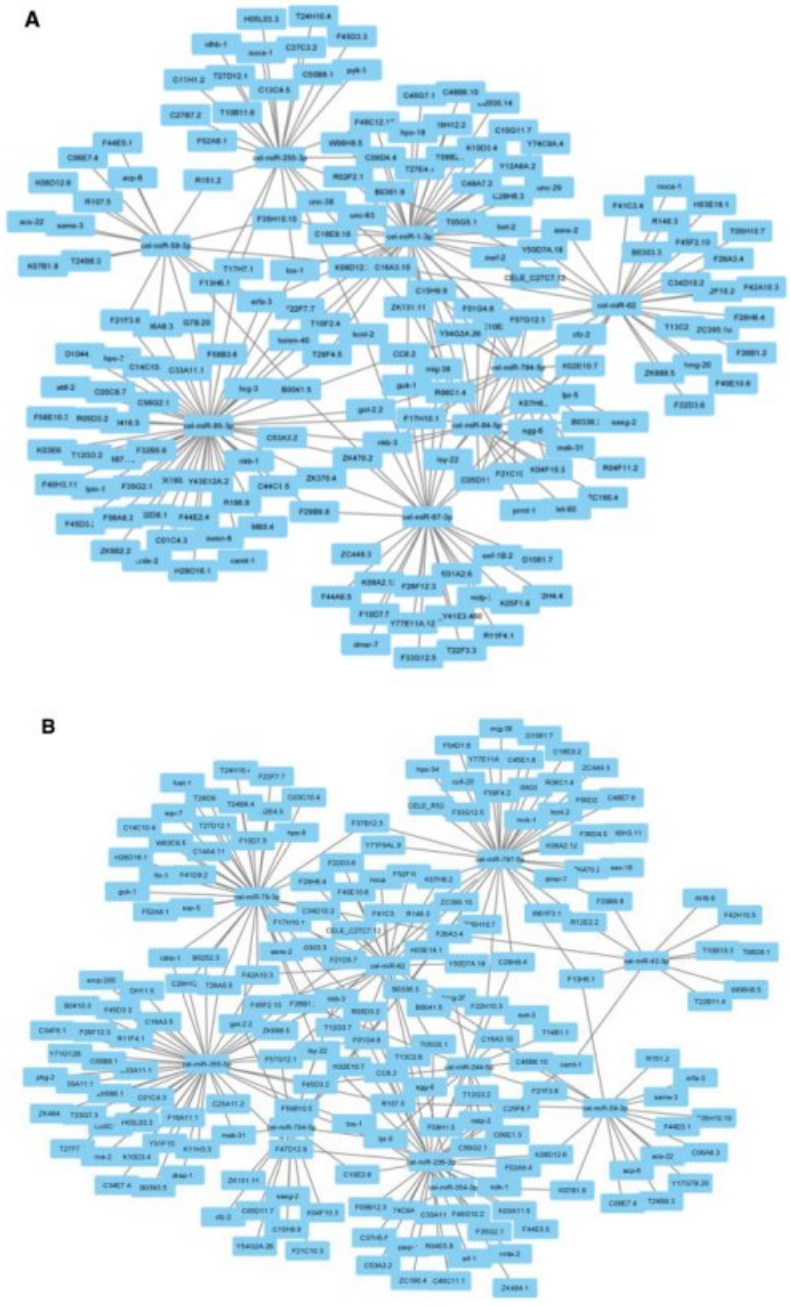

Fig 6.5 Network of miRNA and their target genes for (A) PNGF and (B) PHNP group of *C. elegans*. The interaction network miRNA and their target genes were drawn by using Cytoscape 3.9.1.

6.2. Discussion:

NDs are multifactorial diseases mainly associated with progressive loss of neuronal structure and function and neuronal cell death [14]. Since there is no effective therapy or treatment to prevent the progression of NDs such as AD and PD, which have emerged as a significant problem in neurobiology in recent years, more research efforts are being made to develop innovative neuroprotective therapeutics [14]. The potential role of miRNA in ND has encouraged finding novel therapeutic targets [15,16]. The miRNA was first discovered in *C. elegans*; fundamental research linking miRNA to crucial gene regulatory networks significant to neuronal development has been carried out using this model [13,17,18]. A clinical trial of NGF gene therapy was demonstrated because the function and degeneration of cholinergic neurons in the basal forebrain strongly depend on NGF activity. The therapeutic advantage of NGF administration to the basal forebrain has already been demonstrated [19].

Since neurotrophic factors cannot cross the blood-brain barrier (BBB) and must be administered intracerebrally, their use in treating central nervous system dysfunction is even more complicated. However, small synthetic peptides can be used as an alternative method with several advantages over large protein molecules in treating neuronal disease [20]. Some peptides named MIM-D3 (TrkA agonist) ameliorate corneal injury in rats with dry eye syndrome [21]. Similarly, GK-2 (NGF mimetics) improved neurological disorders such as AD, PD, and brain ischemia with zero side effects [22,23]. Our previous findings demonstrated the neuroprotective potential of synthetic custom peptides (TNP and HNP) in *in vitro* PC-12 cells and *in vivo C. elegans* PT-induced PD models. This study identified and compared the differential miRNA expression profile of mouse 2.5 S-NGF-treated *C. elegans* with the custom peptide HNP-treated *C. elegans,* where some miRNAs were common. The human brain is associated with a high degree of complexity, and working with the human brain requires ethical permission; therefore, *in vivo* model organisms such as *C. elegans* can be used for understanding the mechanism and function of the miRNAs in the neuronal developmental and functional processes [24].

Studies have reported that cel-miR-71, cel-miR-84, and cel-miR-1 are involved in the different stages of neuronal development [24]. In this study, these miRNAs' expression was highly upregulated in both the NGF and HNP groups of *C. elegans*. These results underlie that the custom peptides have neurorestorative and neurotrophic potential. The

potency of the peptides is found to be comparable with the mouse 2.5 S-NGF. The target genes of the cel-miR-1-3p and cel-miR-255-3p and their roles are further investigated due to their robust expression in response to mouse 2.5 S-NGF and custom peptide HNP treatment in *C. elegans*. The target genes of cel-miR-1-3p are mef-2, unc-63, unc-29, and unc-38, involved in the oxidative stress response pathways, mitogen-activated protein kinase (p38/MAPK) pathways, and nicotinic acetylcholine receptor signaling pathways (RefSeq, miRBase, ENA, WormBase). Similarly, the G protein signaling pathway, metabolic pathways (pyruvate metabolism), and integrin signaling pathways are regulated by cel-miR-255-3p target genes (kcnl-2, idhb-1, suca-1, pyk-1, and tos-1) (RefSeq, miRBase, ENA, WormBase). The p38/MAPK pathways play a crucial role in neuronal differentiation and it has been reported from our lab that the mouse 2.5 S-NGF induced these pathways for neuronal differentiation and growth [25-27]. Because the custom peptide in this study was developed from the TrkA binding region of snake venom NGF, it also retains the property of neuronal differentiation and growth [28]. This study shows that similar to mouse 2.5 S-NGF, the HNP also upregulates cel-miR-1-3p miRNA, eventually regulating p38/MAPK pathways for neuronal differentiation in *C. elegans*.

Aggregation of α-synuclein is a hallmark for the progression of PD, also observed in the PT-induced PD model [29]. Removal of aggregation of this protein is a required mechanism for improving PD [30]. Studies have reported that cel-miR-4813-3p regulates protein homeostasis, associated with the clearance of α-synuclein deposition in neuronal cells [2,3]. The neuroprotective potential of HNP has already been demonstrated in our lab [28]. cel-miR-4813-3p is downregulated in the PT-treated group of *C. elegans,* which results in the deposition of α-synuclein and the progression of PD. Further upregulation of the cel-miR-4813-3p in the PHNP and PNGF group of *C. elegans* univocally suggests the peptide's therapeutic role by regulating miRNAs.

The phosphoinositide 3-kinase (PI3K) pathway is reported to promote longevity, is responsible for growth and neuronal development, and is regulated by cel-miR-236-3p [5]. The PT treatment downregulates the expression of this miRNA, which is further upregulated in the PHNP and PNGF group of *C. elegans*, thus confirming the neuroprotective role of HNP via miRNA regulation. Two novel miRNAs, cel-miR-8207-3p and cel-miR-57-3p, are upregulated with the PT treatment and downregulated with the mouse 2.5 S-NGF and HNP pre-treatment. The function of these two miRNAs is unknown and needs to be explored.

6.3. Conclusion

In the PT group of *C. elegans*, the downregulated miRNAs target genes involved in the developmental process during embryogenesis; genes regulate the longevity of *C. elegans*, α-synuclein degradation, and oxidative stress response. Moreover, upregulated miRNAs target genes in the PT group involved in apoptotic pathways, decrease lifespan, innate immune response, and metabolic pathways are reported to increase the progression of NDs [3,13,31]. Pre-treatment with mouse 2.5 S-NGF and custom peptide HNP restored the expression of altered miRNAs induced by PT treatment and played a crucial role against NDs.

CHAPTER VII

CONCLUSION AND FUTURE PERSPECTIVES

7.1 Conclusion

This study showed that designed custom peptides derived from snake venom neurotrophin molecules can protect PC-12 cells (in vitro) and *C. elegans* (in vivo) from PT-induced neurotoxicity. The custom peptides counteract PT-induced neurotoxicity by thwarting excessive ROS production, oxidative stress, MMP, and premature apoptotic death. Our findings provide a greater understanding of the altered expression of proteins involved in the neurodegeneration pathways in the PT-induced PD model of PC-12 cells and *C. elegans* and how the expression of our custom peptides can be used in treatments.

The neuroprotective activity of custom peptides against PT-induced chemotaxis behavioral defects, DAergic neurodegeneration, α-synuclein accumulation, and reduced life span may be related to their antioxidant and antiapoptotic properties. The PT group of worms displayed maximum variation in differential gene expression compared to the untreated (control) group of C. elegans. In contrast, the custom peptides pre-treatment group showed minimal variation compared to the untreated (control) group, indicating normalization or restoration of altered gene/protein dynamics. This study highlights custom peptides' therapeutic importance in reducing neurodegeneration against toxic chemicals.

Further study shows that in the PT group of *C. elegans*, the downregulated miRNAs target genes involved in the developmental process during embryogenesis; genes regulate the longevity of *C. elegans*, α-synuclein degradation, and oxidative stress response. Moreover, upregulated miRNAs target genes in the PT group involved in apoptotic pathways, decreased lifespan, innate immune response, and metabolic pathways are reported to increase the progression of PD.

Using the tested custom peptides as a drug prototype exclusively depends upon their non-toxic nature in preclinical studies. The acute toxicity studies in mice models showed that the peptide is devoid of toxicity in mice at a dose that is 100 times higher than its therapeutic dose determined in *C. elegans*. Further, it has no detrimental effect on the biochemical parameters of blood parameters and vital organs, suggesting the safety of the peptides for the development of drug prototypes. Furthermore, the reduced concentration of inflammatory mediators (TNF-α, IL-6, IL-1β) in the CPs-treated mice, compared to

control (1X PBS-treated) mice, diminished the risk of inflammatory response post-treatment with peptides.

7.2 Future perspectives

The findings of the present study provide a fundamental basis for developing new agents that specifically target neurodegenerative diseases, especially PD, and for the successful development of safe drug prototypes through in vivo pharmacokinetics, and pharmacodynamics and encourage further in-depth investigation through bioavailability studies. Two uncharacterized miRNAs, cel-miR-8207-3p and cel-miR-57-3p, are upregulated with PT treatment and downregulated with mouse 2.5 S-NGF and custom peptides pre-treatment. The function of these two miRNAs is unknown and needs to be explored.

To study the snake venom nerve growth factor-derived custom peptides for their application in preventing Parkinson's disease

ORIGINALITY REPORT

9%	4%	7%	2%
SIMILARITY INDEX	INTERNET SOURCES	PUBLICATIONS	STUDENT PAPERS

PRIMARY SOURCES

1	ruor.uottawa.ca Internet Source	<1%
2	Elango, Bhakkiyalakshmi, Shalini Devibalan, Thillai Veerapazham Sekar, Rajaguru Palanisamy, Paulmurugan Ramasamy, and Ramkumar Kunka MohanRam. "Therapeutic potential of pterostilbene against pancreatic β-cell apoptosis through Nrf2 mechanism : Antiapoptotic mechanism of pterostilbene", British Journal of Pharmacology, 2014. Publication	<1%
3	Li Zhang, Min-Na Dong, Jun Deng, Chun-Hai Zhang, Ming-Wei Liu. "Resveratrol exhibits neuroprotection against paraquat-induced PC12 cells via heme oxygenase 1 upregulation by decreasing MiR-136-5p expression", Bioengineered, 2022 Publication	<1%
4	Submitted to CSU, Long Beach Student Paper	

<1%

Exclude quotes	On	Exclude matches	< 14 words
Exclude bibliography	On		